UNIVERSIDAD POLITÉCNICA DE MADRID

ESCUELA TÉCNICA SUPERIOR DE ARQUITECTURA

MODELO EMPÍRICO DE LA ISLA DE CALOR URBANA DE MADRID PARA SU INTEGRACIÓN EN LA SIMULACIÓN ENERGÉTICA DE EDIFICIOS

Tesis doctoral

Miguel Núñez Peiró

Arquitecto

2021

DEPARTAMENTO DE CONSTRUCCIÓN Y TECNOLOGÍA ARQUITECTÓNICAS

ESCUELA TÉCNICA SUPERIOR DE ARQUITECTURA

MODELO EMPÍRICO DE LA ISLA DE CALOR URBANA DE MADRID PARA SU INTEGRACIÓN EN LA SIMULACIÓN ENERGÉTICA DE EDIFICIOS

Miguel Núñez Peiró

Arquitecto

Director:

F. Javier Neila González

Doctor Arquitecto

2021

Tribunal nombrado por el Sr. Rector Magfco. de la Universidad Politécnica de Madrid, el día..... de.....de 20....

Presidente:_____

Vocal: _____

Vocal:_____

Vocal:_____

Secretario:_____

Suplente:_____

Suplente:_____

Realizado el acto de defensa y lectura de la Tesis el día.....de.....de 20…

en la E.T.S.I. /Facultad.....

Calificación …….

EL PRESIDENTE LOS VOCALES

EL SECRETARIO

Agradecimientos
Acknowledgements

He tenido la suerte de desarrollar mi tesis doctoral en un contexto excepcional. Se lo debo al extraordinario grupo de personas que me ha rodeado y apoyado durante todos estos años. Gracias a ellas, lo que podría haber sido un solitario y arduo camino en la academia, inherente en parte a la realización de una tesis doctoral, se ha convertido en una experiencia enriquecedora en muchos otros planos.

Comienzo agradeciendo a Javier Neila, mi director de tesis, la oportunidad de trabajar a su lado y la plena confianza depositada en mi durante todos estos años. Debo destacar su disponibilidad y paciencia a la hora de orientarme, así como para gestionar todos los trámites burocráticos, que no han sido pocos. También siento un profundo agradecimiento hacia Carmen Sánchez-Guevara, quien me abrió la puerta a este mundo y no ha dejado, desde entonces, de guiarme, acompañarme y enseñarme en todas y cada una de las etapas por las que he transitado. Esta tesis le debe mucho.

Gracias a todas las personas que integran y hacen posible la vida en nuestra Escuela, y en especial a todos los compañeros y compañeras del DCTA y del DUyOT. También a mis supervisores de la estancia, Anna Mavrogianni y Phil Symonds, y al resto del equipo del UCL IEDE, que con tanto cariño me recibieron y acogieron en Londres. Gracias también a Roberto González, que siempre ha estado atento y disponible. Y a la AEMET y a la Subdirección General de Energía y Cambio Climático del Ayuntamiento de Madrid, por su apoyo durante la etapa experimental.

Tampoco me olvido de todas mis compañeras de investigación, con quienes he compartido momentos muy divertidos tanto dentro como fuera de la Escuela, la mayoría alrededor de comida. Especial mención para Inês, quien con mucho mimo revisó el inglés de mis trabajos. Gracias también a Marta y a Camila, que han sufrido el final de esta tesis. Y a Ana, que me ha animado y apoyado tanto en el cierre de esta etapa. Muchísimas gracias a todas.

Por supuesto, muchas gracias también a todos mis amigos. A Alberto V y a Lizana, sin quienes nunca hubiese conocido ni explorado este mundo. A Sara, con quien no me lo podría haber pasado mejor durante la estancia. A Carlos y Juan, siempre atentos en la distancia. Y a Lidia y Cris, con quienes queda alguna celebración pendiente. También a Ce y Alberto B, con quienes he compartido tantos buenos momentos, incluso en los días más fríos y calurosos de Madrid.

Doy también las gracias a toda mi familia: tías y tíos, primas y primos, sobris... No es fácil acompañar a alguien en este camino, mucho menos hacerlo en la distancia, y aun así no recuerdo ninguna etapa en la que no estuvieran presentes. Agradezco a mis padres su fe ciega antes, incluso, de empezar. A mi hermano Luis, y a Alba, les agradezco su presencia, ya que actúan a modo de amplificador y me hacen sentir mucho más cerca a la familia. También les doy las gracias a mis abuelos, a quienes siempre he guardado con celo parte de mis vacaciones, ya que no hay mejor descanso que el tiempo que se pasa con ellos. Y a mi tía Montse, que siempre me recuerda que sea feliz.

Termino dando las gracias a Paula. Siempre en primera línea, ha creído en mí más que yo mismo. Le estoy especialmente agradecido por cómo ha llenado toda esta etapa de color, incluso en los momentos más grises. Al final, si bien son las luces y las sombras las que nos hacen ver la profundidad del camino, es el color el que nos permite disfrutarlo.

I was fortunate to carry out my PhD thesis in an exceptional context. I owe it to the extraordinary group of people who have surrounded and supported me over these years. Thanks to them, what could have been a lonesome and arduous journey in academia, in part inherent to the completion of a PhD thesis, has become an enriching experience on many other levels.

I would like to begin by thanking Javier Neila, my thesis supervisor, for the opportunity to work with him and for the trust he has placed in me over the years. I must highlight his availability and patience in guiding me, as well as in managing all the bureaucratic formalities, which have not been few. I am also deeply grateful to Carmen Sánchez-Guevara, who first introduced me to this world and has never failed, since then, to guide me, mentor and teach me in each and every one of the stages through which I have progressed. This thesis is very much indebted to her.

Thanks to all the people who are part of and make possible the life in our School, and especially to all the colleagues of the DCTA and DUyOT. Also to my supervisors, Anna Mavrogianni and Phil Symonds, and to the rest of the UCL IEDE team, who so warmly received and welcomed me in London. Thanks also to Roberto González, who has always been available and supportive. And to the AEMET and the General Subdirectorate of Energy and Climate Change of the Madrid City Council for their support during the experimental stage.

I cannot forget all my research partners, with whom I have shared many great moments, especially during our meals. A special mention goes to Inês, who carefully revised the English of my work. Thanks also to Marta and Camila, who have suffered the end of this thesis. And to Ana, who has encouraged and supported me so much in this last stage. Thank you all very much.

Of course, many thanks also to all my friends. To Alberto V and Lizana, without whom I would never have explored this world. To Sara, with whom I could not have had a better time during my research stay. To Carlos and Juan, always supportive in the distance. And to Lidia and Cris, with whom we still have some celebrations to do. Also to Ce and Alberto B, with whom I have shared so many good moments, even on the coldest and hottest days in Madrid.

I also thank all my family: aunts and uncles, cousins, nieces and nephews.... It is not easy to accompany someone on this journey, much less to do it in the distance, and yet I do not remember any stage in which they were not present. I thank my parents for their unconditional faith, even before I started. To my brother Luis, and to Alba, I simply thank them for their presence, since they act as an amplifier which makes me feel the family much closer. I also thank my grandparents, to whom I have always jealously saved part of my holidays, as there is no better rest than the time spent with them. And to my aunt Montse, who always reminds me to be happy.

I end by thanking Paula. Always in the front line, she has believed in me more than myself. I am especially grateful to her for the way she has filled this whole journey with colour, even in the dullest moments. In the end, the lights and shadows make us see the depth of the road, yet it is the colours that let us enjoy it.

Resumen
Abstract

La isla de calor es un fenómeno climático que modifica las condiciones térmicas de las ciudades. Los entornos urbanos registran, de media, temperaturas de entre 1 y 2 ºC por encima de su alrededores rurales, pudiendo superar los 10 ºC de intensidad durante algunas noches. El diferencial de temperatura debido a la isla de calor puede provocar desajustes en la evaluación energética de edificios, ya que rara vez es considerado en la generación de los archivos climáticos empleados en la simulación energética. Esto contribuye a la brecha del comportamiento energético (*energy performance gap*) característica de las herramientas de simulación, poniendo en entredicho su fiabilidad.

Estudios previos han demostrado la relevancia del impacto de la isla de calor en el comportamiento energético de los edificios. Algunos de ellos han ensayado distintas fórmulas para integrar la isla de calor en la evaluación energética de edificios, fundamentalmente a través de modelos numéricos. Sin embargo, existen limitaciones relativas a su coste computacional, precisión y representatividad, indicativo de que todavía existe un amplio margen de mejora.

Dado que los archivos climáticos son los responsables de contextualizar climáticamente la simulación energética, esta tesis doctoral propone desarrollar un modelo empírico de la isla de calor de Madrid con el que obtener archivos climáticos adaptados a la realidad climática urbana. Se parte del objetivo de que los archivos generados, además de ser precisos en su representación de las condiciones climáticas urbanas, sean representativos de todo el municipio en su conjunto. Esta tarea se aborda de forma integral, cubriendo todas las etapas desde la observación hasta la modelización, y pasando por una importante etapa analítica relacionada con el fenómeno de la isla de calor y su variabilidad intraurbana.

The urban heat island is a climatic phenomenon that modifies the thermal conditions in cities. Due to this phenomenon, urban environments are, on average, between 1 and 2 °C warmer than their rural surroundings, reaching over 10 °C on some nights. The temperature differential due to the urban heat island can cause mismatches in the energy evaluation of buildings, as it is rarely considered in the generation of the climate files used in the energy simulation. This contributes to the *energy performance gap* characteristic of simulation tools, calling into question their reliability and, in some cases, even their usefulness.

Since weather files are responsible for the climatic contextualisation of the energy simulation, this PhD thesis focuses on obtaining weather files adapted to the urban climatic reality. Previous studies have tested different formulas to carry out this task, mainly through numerical models. However, limitations related to their computational cost, accuracy and representativeness suggest that there is still room for improvement.

This research proposes an empirical model of the urban heat island of Madrid in order to obtain weather files adapted to the reality of urban climate. The aim is that the generated weather files, as well as being accurate in their representation of the urban climate conditions, should be representative of the entire municipality as a whole. This requires a comprehensive approach to this work, developing an important experimental dimension aimed at obtaining data, as well as an analytical dimension related to the phenomenon of the heat island.

The experimental part of this PhD thesis is based on the development of two monitoring campaigns, one using mobile stations and the other using fixed locations. From these campaigns, data on the hygrothermal conditions in different parts of the city have been obtained. These temperature and humidity records have been used, firstly, to analyse the annual behaviour of the heat island at an hourly and intra-urban level, something unprecedented for the municipality of Madrid. Secondly, the data collected have allowed the generation of the empirical model based on artificial neural networks, one of the most popular tools in machine learning, and with proven potential for modelling the characteristics of the urban climate.

With these artificial neural networks, the time series of climatic data from the reference meteorological observatories have been adapted (*data morphing*). Thus, these new time series are the basis on which the urban weather files have been built. Finally, the urban heating and cooling degree hours have been used to delimit a series of climate zones within the city of Madrid, to which the new urban weather files have been associated.

The findings show an intense and widespread urban heat island, with a weak annual seasonality, but with a strong daily variability. The differences between urban fabrics are, as expected, very accentuated during the night. During the day, the differences are dampened and are no longer so clearly associated with the type of urban fabric. In total, nine urban climate zones are distinguished, which are represented in association with their respective urban weather files. Tests carried out on a residential H-block typology point to increases in the cooling energy demand of more than 30% due to the urban heat island, while the reduction in the heating demand due to the heat island would, in some cases, be close to 20%.

This research work confirms the impact of the urban heat island on the energy performance of buildings, as well as the importance of weather files in the development of energy simulation. It is hoped that these findings will contribute to the improvement and accuracy of simulation tools, while encouraging a critical review of the current availability of weather files and their application in urban environments.

La parte experimental de esta tesis doctoral se apoya en el desarrollo de dos campañas de monitorización, una mediante puntos móviles, de carácter exploratorio, y otra mediante puntos fijos. A partir de esta última se han obtenido datos de las condiciones higrotérmicas en diversos puntos de la ciudad durante más de dos años en régimen horario. Estos registros de temperatura y humedad han servido, primero, para analizar el comportamiento anual de la isla de calor a nivel horario e intraurbano en el municipio de Madrid, obteniendo importantes conclusiones para su posterior modelización. En segundo lugar, estos datos han permitido la generación de un modelo empírico basado en redes neuronales artificiales, una de las herramientas más populares dentro del aprendizaje automático, y con potencial demostrado a la hora de modelar las características del clima urbano.

Con estas redes neuronales artificiales se ha trabajado en la adaptación de las series temporales de datos procedentes de los observatorios meteorológicos de referencia a las condiciones climáticas urbanas, siendo estas nuevas series temporales la base sobre la cual se han construido los archivos climáticos urbanos. Finalmente, se ha trabajado con los grados hora de calefacción y refrigeración urbanos, a partir de los cuales se han delimitado una serie de zonas climáticas dentro de la ciudad de Madrid, y a las que se han asociado los nuevos archivos climáticos urbanos.

Los resultados obtenidos muestran una isla de calor intensa y extensa, con una estacionalidad anual débil, pero con una fuerte variabilidad diaria. Las diferencias entre tejidos urbanos son, como cabía esperar, muy acentuadas durante la noche. Durante el día, las diferencias se amortiguan y dejan de asociarse tan claramente al tipo de tejido. En total, se distinguen nueve zonas climáticas urbanas, las cuales se representan asociadas a sus respectivos archivos climáticos urbanos. Los ensayos realizados sobre una tipología residencial de bloque en H apuntan a incrementos en la demanda energética de refrigeración debido a la isla de calor superiores al 30%, mientras que la reducción en la demanda de calefacción por este fenómeno rozaría, en algunos casos, el 20%.

Este trabajo de investigación viene a confirmar la relevancia de la isla de calor en el comportamiento energético de los edificios de la ciudad de Madrid, así como la importancia de la precisión de los archivos climáticos en el desarrollo de la simulación energética. Se espera que los resultados obtenidos contribuyan a mejorar las herramientas de evaluación energética de edificios, a la vez que fomenten una revisión crítica de los actuales archivos climáticos disponibles y de aplicación en entornos urbanos.

Prólogo
Foreword

Comencé a investigar sobre la isla de calor en la Universidad Politécnica de Madrid en el año 2015. Entonces surgió la oportunidad de participar en el Proyecto MODIFICA, un proyecto de investigación dirigido por F. Javier Neila, coordinado por Carmen Sánchez-Guevara, y financiado por el que fuera el Ministerio de Economía y Competitividad. Con este proyecto se iniciaba una nueva línea en el grupo de investigación ABIO vinculada con la isla de calor y su influencia en el comportamiento energético de edificios. De este proyecto se han derivado otros tantos, así como varias tesis doctorales relacionadas con el clima urbano. Una de ellas es la que aquí se presenta.

Además de la vinculación con el proyecto MODIFICA, esta tesis ha sido posible gracias al apoyo de un contrato de investigación FPU (Formación de Profesorado Universitario) del Ministerio de Educación, Cultura y Deporte, desarrollado entre los años 2016 y 2020 (FPU15/ 05052). Durante el transcurso de esta tesis también se ha podido realizar una estancia de investigación de 3 meses en el *Institute for Environmental Design and Engineering* de la University College London (Reino Unido), y cuyos supervisores fueron Anna Mavrogianni y Phil Symonds. Esta estancia fue posible gracias a las ayudas de movilidad para estancias breves y traslados temporales del Ministerio de Ciencia, Innovación y Universidades (EST17/00825).

También debe señalarse que esta tesis doctoral ha sido planteada por compendio de artículos. La memoria que aquí se presenta sigue las directrices de la Universidad Politécnica de Madrid para esta modalidad, aprobadas por Consejo de Gobierno de 30 de noviembre de 2017. Además de la colección de publicaciones, este documento incluye un resumen de toda la investigación que comienza con

My research on the urban heat island started at Universidad Politécnica de Madrid in 2015. At that time, the opportunity to participate in the MODIFICA Project arose. This was a research project led by F. Javier Neila, coordinated by Carmen Sánchez-Guevara, and financed by the former Ministry of Economy and Competitiveness (BIA2013-41732-R). It was the start of a new line of research in the ABIO research group, linked to the urban heat island and its influence on the energy performance of buildings. Since then, several other projects have been derived from it, as well as many PhD theses related to urban climate. Of these, one of them is the one I present here.

Along with the MODIFICA project, this thesis has been possible thanks to the support of a research contract of the Spanish Ministry of Education, Culture and Sport, developed between 2016 and 2020 (FPU15/ 05052). During the course of this thesis, it has also been possible to carry out a 3-month stay as a visiting researcher at the Institute for Environmental Design and Engineering of the University College London (UK), under the supervision of Anna Mavrogianni and Phil Symonds. This stay was possible thanks to the mobility grants for short stays of the Ministry of Science, Innovation and Universities (EST17/00825).

It should also be noted that this PhD thesis is presented in the modality of a *thesis by publication*. It is therefore based on the publication of several scientific papers in high impact journals, which constitute the central body of this research. Other publications, such as communications to conferences, a book chapter or a patent, complement

this work. To this end, this dissertation follows the guidelines of the Universidad Politécnica de Madrid for this modality, approved by the Governing Council on 30 November 2017.

In addition to the publications collection, this document includes a summary of all the research that begins with a general introduction, where the hypothesis and initial objectives are stated; a brief review of the methodology; an integrated description of the research, in which the contributions of each of the publications are detailed; and a final section where a general discussion is included, as well as the conclusions and future lines of research. This report closes with a bibliography and a complete list of the works published during the course of this research.

This thesis has been developed over five years, combining it with the preparation and development of other research projects, both national and international. All of them have led to several collaborations and research results that have shaped a total of 12 articles in indexed journals (8 JCR Q1), 8 communications to conferences, 3 book chapters, 2 reports for public institutions, and 1 patent. All of this has given feedback to this research and has shaped the future lines of research that open up after the conclusion of this thesis.

una introducción general, donde se recogen la hipótesis y objetivos de partida; una breve reseña sobre la metodología; una descripción integrada de la investigación, en la que se detallan las aportaciones de cada una de las publicaciones; y un último apartado donde se incluye una discusión general, además de las conclusiones y futuras líneas de investigación. Esta memoria se cierra con la bibliografía y una relación completa de los trabajos publicados durante el transcurso de esta investigación.

Esta tesis doctoral se ha desarrollado a lo largo de cinco años, compaginándola con la preparación y desarrollo de varios proyectos y redes de investigación, tanto nacionales como internacionales. De todos ellos han surgido diversas colaboraciones y resultados de investigación que han dado forma a un total de 12 artículos en revistas indexadas (8 JCR Q1), 8 comunicaciones a congresos, 3 capítulos de libro, 2 informes para instituciones públicas, y 1 patente. Todo ello ha retroalimentado a este trabajo de investigación y ha dado forma a las futuras líneas de investigación que se abren tras concluir esta tesis doctoral.

Índice
Contents

Índice de figuras
List of figures XXVII

Índice de tablas
List of tables XXXVII

Listado de abreviaturas
List of abbreviations XLIII

Parte I. Introducción, hipótesis y objetivos
Part I. Introduction, hypothesis and objectives 3

1. Introducción
Introduction 4

1.1. El clima en la ciudad
The climate in the city 4

1.2. Antecedentes e historia del clima urbano
Urban climate history and background 6

1.3. El clima urbano aplicado a la arquitectura y el diseño urbano
Application of urban climate knowledge to architecture and urban design 9

1.4. El cambio climático y la simulación energética de edificios
Climate change and building energy modelling 10

1.5. La isla de calor en la simulación energética de edificios
The urban heat island in building energy modelling 13

2. Hipótesis y objetivos
Hypothesis and objectives 18

2.1. Hipótesis
Hypothesis 18

2.2. Objetivos
Objectives 19

PARTE II. METODOLOGÍA
PART II. METHODOLOGY 23

3. Metodología
Methodology 24

PARTE III. PUBLICACIONES
PART III. PUBLICATIONS 29

4. Capítulo de libro Book chapter
Update of the urban heat island of Madrid and its influence on the building's energy simulation 31

5. Patente Patent
Abrigo meteorológico para sensores ambientales 47

6. Artículo 1 Research paper 1
Source area definition for local climate zones studies. A systematic review 67

7. Artículo 2 Research paper 2
Hourly evolution of intra-urban temperature variability across the local climate zones. The case of Madrid 99

8. Artículo 3 Research paper 3
Modelling long-term urban temperatures with less training data: A comparative study using neural networks in the city of Madrid 147

9. Comunicación en congreso internacional Presentation at an international conference
Two decades of weather files in Spain. A comparison of their reliability for building energy modelling using the BESTEST method 173

PARTE IV. RESUMEN Y ANÁLISIS DE RESULTADOS
PART IV. SUMMARY AND ANALYSIS OF RESULTS 179

10. Monitorización de la isla de calor urbana de Madrid
Monitoring the urban heat island of Madrid 180

10.1. Delimitación del ámbito de estudio: escala vertical y horizontal
Delimitation of the study area: vertical and horizontal scale 180

10.2. Análisis previo de la distribución espacial de la isla de calor
Preliminary analysis of the spatial distribution of the ICU 183

10.3. Diseño de la red y búsqueda de datos complementarios
Network design and search for complementary data 188

10.4. Situación y protección de los equipos de medición
Location and protection of monitoring equipment 191

10.5. Autorización, despliegue y mantenimiento de la red
Authorisation, deployment, and maintenance of the network 194

11. Contextualización de los datos procedentes de la monitorización
Contextualisation of monitoring data 198

11.1. Descripción de los metadatos empleados
Description of the metadata 198

11.2. Selección de un sistema para la clasificación climática de las mediciones en entornos urbanos
Selection of a climatic classification system for urban environments 201

11.3. Definición y relevancia del área fuente de los sensores
Definition and relevance of the sensor source area 206

11.4. Revisión bibliográfica sobre la aplicación del área fuente en entornos urbanos
Literature review on the application of the source area in urban settings 206

11.5. Estimación del área fuente de acuerdo con la escala de monitorización
Source area estimation according to monitoring scale 209

11.6. Contextualización climática mediante LCZ y generación de fichas descriptivas
Climatic contextualisation by LCZ and generation of descriptive data sheets 211

12. Análisis de la evolución horaria e intraurbana de la isla de calor
Analysis of the hourly and intra-urban evolution of the urban heat island 218

12.1. Aproximación al análisis de la isla de calor
Approach to the urban heat island analysis 218

12.2. Visión global y evolución anual de la isla de calor según LCZs
Overview and annual evolution of the urban heat island according to LCZs 220

12.3. Evolución horaria de la intensidad de la isla de calor según LCZs
Hourly evolution of the urban heat island intensity according to LCZs 227

12.4. Diferencias intraurbanas de temperatura entre LCZs
Intra-urban temperature differences between LCZs 230

12.5. Implicaciones para la modelización de la isla de calor y la generación de archivos climáticos
Consequences for urban heat island modelling and the generation of weather files 233

13. Modelización de la isla de calor mediante un enfoque basado en datos
Modelling the urban heat island using a data-driven approach 236

13.1. Aproximación a la modelización de temperaturas urbanas
Approach to urban temperature modelling 236

13.2. Búsqueda de un modelo óptimo basado en FNN
Finding an optimal model based on FNN 239

13.3. Evaluación de los modelos en contextos de baja disponibilidad de datos
Evaluating models in contexts of low data availability 243

13.4. Inclusión de la humedad relativa en la modelización
Including relative humidity in modelling 247

13.5. 'Data morphing': generación de series temporales artificiales en puntos urbanos.
'Data morphing': generation of artificial time series at urban points. 249

14. Creación de archivos climáticos urbanos para la ciudad de Madrid
Creation of urban weather files for the city of Madrid 254

14.1. Selección de una metodología para obtener años meteorológicos típicos.
14.1. Selection of a methodology to obtain typical meteorological years. 254

14.2. Obtención de un año meteorológico típico para cada punto urbano
Obtaining a typical meteorological year for each urban site 259

14.3. Delimitación de zonas climáticas urbanas y asignación de TMY
Delimitation of urban climatic zones and TMY designation 263

14.4. Generación de un nuevo archivo climático de referencia para Madrid
Generating a new reference weather file for Madrid 271

14.5. Creación de archivos climáticos urbanos y ensayo sobre caso de estudio
Creation of urban weather files and testing with a case study 274

PARTE V. DISCUSIÓN, CONCLUSIONES Y FUTURAS LÍNEAS DE INVESTIGACIÓN
PART V. DISCUSSION, CONCLUSSIONS AND FUTURE RESEARCH LINES 283

15. Discusión
Discussion 284

15.1. Sobre los sistemas de clasificación climática del espacio urbano
On the use of urban climate classification systems 284

15.2. Sobre los archivos climáticos urbanos y la escala local
On the urban weather files and the local scale 286

15.3. Sobre el modelo empírico de la isla de calor urbana de Madrid
On the empirical model of the urban heat island of Madrid 287

15.4. Sobre el efecto de la isla de calor en la demanda energética de edificios
On the effect of the urban heat island on buildings' energy demand 288

16. Conclusiones
Conclusions 290

17. Futuras líneas de investigación
Future research lines 292

ANEXO A: COLECCIÓN COMPLETA DE PUBLICACIONES Y OTROS TRABAJOS DE INVESTIGACIÓN
ANNEX A: COMPLETE COLLECTION OF PUBLICATIONS AND OTHER RESEARCH 297

BIBLIOGRAFÍA
REFERENCES 307

Índice de figuras
List of figures

Figura 1.1 Ciclo del carbono para un barrio de Vancouver, en Canadá (Kellett et al., 2013, encontrado en Oke et al., 2017a). Representa la densidad de los flujos (laterales y verticales) y los sumideros de carbono. Nótese cómo el ciclo sigue una lógica lineal lateral-vertical, en lugar de circular vertical-vertical (esta última propia de los sistemas naturales, y que puede observarse a pequeña escala en los flujos de carbono de la vegetación urbana).....5

Figura 1.2 Muertes por raquitismo en la ciudad preindustrial de Londres (Brimblecombe, 1987). La contaminación atmosférica bloqueaba la radiación solar y, con ello, la síntesis de la vitamina D. Se cree que ésta fue una de las primeras enfermedades infantiles vinculadas con la contaminación atmosférica en las ciudades (O'Riordan, 2006).....6

Figura 1.3 Número de estudios sobre el clima urbano durante el s. XX, y donde no se incluyen los relacionados con la contaminación atmosférica (Oke, 1979).....8

Figura 1.4 Causas de la formación de la isla de calor, de acuerdo con Kleerekoper (2012). (1) Absorción de radiación de onda corta por superficies y materiales urbanos; (2) Absorción de radiación de onda larga y reirradiación por contaminación; (3) Bloqueo de la irradiación de onda larga a la atmósfera por la estructura urbana;(4) Emisión de calor antropogénico; (5) Acumulación de calor por superficies urbanas artificiales, de mayor admitancia térmica; (6) Reducción de la evaporación por ausencia de vegetación y mayor cantidad de superficies impermeables; (7) Reducción de la disipación de calor por menor velocidad de viento.....9

Figura 1.5 Principales causas de la brecha del comportamiento energético (energy performance gap, EPG) en las herramientas de simulación energética de edificios, según Cozza et al. (2021).....11

Figura 1.6 Representación esquemática de los tres tipos de acoplamiento entre modelos BEM y modelos UCM, según Rodler et al. (2021), a su vez a partir de Lauzet et al. (2019). El más sencillo consiste en el encadenado de los modelos, donde la información fluye en unidireccionalmente, desde el UCM al BEM. En el acoplamiento débil, los modelos se retroalimentan mutuamente, pero afectando únicamente a las simulaciones subsiguientes. Por último, en el acoplamiento fuerte, la retroalimentación se produce dentro de la misma simulación, de forma iterativa.....14

Figura 1.7 Representación esquemática de los módulos que forman parte del modelo Urban Weather Generator (Bueno et al., 2013). La entrada de datos se realiza a través de la Rural Station Model (RSM) a partir de un archivo climático. En este modelo se asume que el archivo climático proviene de un observatorio meteorológico rural. Según Mao y Norford (2021). 16

Figura 3.1. Etapas de esta tesis doctoral. 24

Figura 10.1 Capas atmosféricas contenidas en la capa límite urbana, durante el día. 181

Figura 10.3 Representación de los pasos realizados para adaptar los recorridos desarrollados entre 1984 y 1987 por López Gómez et al. (1988) a la estructura viaria actual. Se recreó la estructura viaria actual en un Sistema de Información Geográfica (GIS) (a), donde se configuró su conectividad y se asignó reglas para la circulación (b). Con ello se generaron nuevos recorridos óptimos, coincidentes con los puntos de medición del estudio previo de 1988 (c), y que se integraron en dispositivos móviles para poder seguir y registrar las rutas por GPS (d). 186

Figura 10.4 Mapas exploratorios de la isla de calor, ordenados por orden cronológico: (a) 15 de julio de 2015, (b) 28 de octubre de 2015, (c) 16 de febrero de 2016 y (d) 25 de abril de 2016. 187

Figura 10.5 Principales aproximaciones a la hora de diseñar una red urbana de medición (Muller et al., 2013; a partir de Robinson, 2010). 188

Figura 10.6 Localización de los equipos de monitorización empleados en este estudio. Incluye los equipos desplegados durante la campaña MODIFICA, así como los cinco observatorio meteorológicos de la AEMET situados en el municipio de Madrid. 190

Figura 10.7 Prueba piloto realizada con un prototipo en entorno ventilado. Se comparan las temperaturas obtenidas dentro del prototipo con las de una protección estándar ventilada de forma natural, considerada de referencia..... 191

Figura 10.8 Imágenes del proceso de fabricación de la protección de los sensores. 192

Figura 10.9 A la izquierda, ilustración de la posición de los equipos de medición. A la derecha, extracto de las figuras que forman parte de la patente (ES2642617-B2). 193

Figura 10.10 Distintivo identificativo único con el que contaron todos los equipos. Estos facilitaron el seguimiento de los equipos durante las tareas de mantenimiento y su retirada. 194

Figura 10.11 Instalación del primer equipo de monitorización en el espacio público. Las imágenes corresponden con la ubicación Aravaca, el punto de medición número 12. 194

Figura 10.12 Momento en el que se procede a la retirada del equipo de medición de Embajadores, situado en la calle Atocha, por motivo de la sustitución de los postes de alumbrado público. Imagen captada por el servicio Street View de Google. 195

Figura 11.1 Esquema en perspectiva que ilustra el concepto del área fuente y de la función de huella de flujos turbulentos. Nótese que el área fuente tiende a distribuirse en forma de elipse, con una contribución máxima a cierta distancia del sensor, en dirección contraria al viento. Representación en perspectiva realizada por Schmid (1994). 207

Figura 11.2 Organigrama del proceso llevado a cabo para realizar la revisión sistemática de la bibliografía..... 208

Figura 11.3 Distancia máxima desde el sensor hasta el límite exterior del área fuente. Incluye todos los estudios de relevancia alta. Se emplea la relación entre la altura de la medición (zm) y la altura de mezcla (zR) para delimitar las tres capas atmosféricas: el palio urbano (UCL), la subcapa de rugosidad (RSL) y la subcapa inercial (ISL). Nótese que ambos ejes presentan una escala logarítmica..... 210

Figura 11.4 Ilustración en planta mostrando la superposición del área fuente en diferentes instantes. (a) Para un instante i, el área fuente tendería a una elipse. (b) Sin embargo, la dirección del viento es cambiante para cada instante y, por lo tanto, el área fuente podría situarse en cualquier punto alrededor del sensor. (c) La superposición de áreas fuentes muestra, entonces, una tendencia teórica hacia la distribución concéntrica en forma de circunferencia, y donde el sensor se situaría en el centro..... 211

Figura 11.5 Correlación entre la temperatura del aire y tres indicadores de cobertura superficial durante el día 16 de abril de 2016. Incluye todos los puntos de medición contenidos dentro de un radio de 5 kilómetros desde el centro de la ciudad. Arriba, la figura (a) hace referencia al recorrido de ida del Transecto 1, (b) al recorrido de ida del transecto 2, y (c) al recorrido de ida del transecto 3. Se representan los ejes horizontales de forma logarítmica para facilitar la visualización de los datos. Abajo, un extracto de los puntos de medición del transecto 2 asociados a sus temperaturas y a su contexto urbano. 212

Figura 11.6 Situación de los puntos de medición del proyecto MODIFICA y de la AEMET, sobreimpresos sobre la clasificación del tejido urbano de Madrid según LCZ obtenido a partir del proyecto WUDAPT (Brousse et al., 2016)..... 213

Figura 11.7 Ejemplo de ficha resumen propuesta por la WMO para recopilar los metadatos más relevantes de observaciones desarrolladas en entornos urbanos. Obtenidas de WMO (2017b)..... 215

Figura 11.8 Ficha empleada en este estudio para recopilar los metadatos más relevantes asociados a cada punto de medición. En ella se incluye información tanto de la escala local como de la microescala, así como la clase LCZ asignada y el valor de los indicadores que lleva a su determinación. La ubicación se corresponde con el punto de medición 01 Embajadores. 216

Figura 11.9 Ficha empleada en este estudio para recopilar los metadatos más relevantes asociados a cada punto de medición. En ella se incluye información tanto de la escala local como de la microescala, así como la clase LCZ asignada y el valor de los indicadores que lleva a su determinación. La ubicación se corresponde con el punto de medición 15 San Diego. 217

Figura 12.1 Intensidad media diaria de la isla de calor durante la campaña de medición. Los valores se corresponden con el punto de medición 01 Embajadores, siendo este el más céntrico de la campaña de monitorización, y el que registró intensidades de isla de calor más elevadas. 222

Figura 12.2 Intensidad mínima diaria de la isla de calor durante la campaña de medición. Los valores se corresponden con el punto de medición 01 Embajadores, siendo este el más céntrico de la campaña de monitorización, y el que registró intensidades de isla de calor más elevadas. 223

Figura 12.3 Intensidad máxima diaria de la isla de calor durante la campaña de medición. Los valores se corresponden con el punto de medición 01 Embajadores, siendo este el más céntrico de la campaña de monitorización, y el que registró intensidades de isla de calor más elevadas. 224

Figura 12.4 Velocidad de viento media diaria. Nótese que los días con mayor velocidad de viento suelen corresponderse con días con picos de intensidad de isla de calor muy bajos (véase Figura 12.3). 225

Figura 12.5 Precipitaciones acumuladas durante 24 horas. Nótese que los días con mayor cantidad de precipitaciones suelen corresponderse con días con picos de intensidad de isla de calor muy bajos (véase Figura 12.3). 226

Figura 12.6 Evolución de la intensidad de la isla de calor a lo largo de las horas, en cada LCZ y para cada mes. Los valores se corresponden con la media de los registros horarios. 228

Figura 12.7 Valores medios horarios de la temperatura (arriba), intensidad de la isla de calor (centro) y ratio de enfriamiento (abajo) para dos meses del año: enero de 2017 (izquierda) y julio de 2017 (derecha). De fondo, en gris, se muestran los rangos para todos los puntos de medición, mientras que en color se resaltan las medias para cada LCZ. 229

Figura 13.1 Representación esquemática de las dos aproximaciones estudiadas para la modelización de la temperatura del aire exterior. 239

Figura 13.2 Mapa del municipio de Madrid donde se destacan los puntos de medición de los que se extraen los datos para la modelización. En el fondo se muestran las LCZs extraídas del proyecto WUDAPT (Brousse et al., 2016) 240

Figura 13.3 Comparativa del error acumulado de diversas configuraciones donde se itera un único parámetro. Se muestran los resultados para el enfoque UHII (izquierda) y el enfoque TEMP (derecha). El error se presenta como la raíz del error cuadrático medio (RMSE). 242

Figura 13.4 Resultados del análisis de sensibilidad de los parámetros de entrada en los modelos cuando la hora se fija a las 00:00 UTC (medianoche). Se muestran los resultados obtenidos siguiendo el enfoque TEMP (arriba) y el enfoque UHII (abajo). 243

Figura 13.5 Resultados obtenidos de la modelización de las temperaturas urbanas utilizando los enfoques UHII (línea negra discontinua) y TEMP (línea negra continua). Se presentan en tres escenarios de estabilidad atmosférica, lo que se traslada en un escenario con una alta intensidad de isla de calor (arriba), otro con una intensidad moderada (centro) y otro con una intensidad baja (abajo). El sombreado de fondo representa la intensidad de la isla de calor. 244

Figura 13.6 Distribución del error acumulado por los modelos cuando estos son entrenados bajo diferentes contextos de disponibilidad de datos. Se presentan los resultados para los dos enfoques (UHII y TEMP) y para dos métricas de error diferentes: la raíz del error cuadrático medio (RMSE, izquierda) y la mediana de la desviación absoluta (MAD, derecha). 245

Figura 13.7 Error adicional arrojado por los modelos entrenados con sólo 3 meses de datos. El nivel de referencia lo establecen los mismos modelos, pero entrenados con 12 meses de datos. Se comparan los resultados obtenidos con el enfoque TEMP (izquierda) y el enfoque UHII (derecha). 246

Figura 13.8 Resultados de la modelización para una semana de junio (arriba) y febrero (abajo). Para cada una de estas semanas se presentan los resultados de los modelos entrenados con 12 y 3 meses de datos, tanto con el enfoque UHII (línea negra discontinua) como con el enfoque TEMP (línea negra continua). 247

Figura 13.9 Error acumulado por los modelos de salida única (single output) y los modelos de salida múltiple (multi-output). Se muestran los resultados para la modelización de la temperatura (arriba) y la humedad relativa (abajo). 248

Figura 13.10 Series temporales artificiales de temperatura del aire generadas para el año 2008 en tres puntos urbanos. Nótese que corresponden con ubicaciones caracterizadas por una alta (arriba), media (centro) y baja (abajo) intensidad de isla de calor. En todas ellas se muestran los datos de temperatura del aire del observatorio de Barajas a modo de referencia. 252

Figura 13.11 Series temporales artificiales de humedad relativa generadas para el año 2008 en tres puntos urbanos. Nótese que corresponden con ubicaciones caracterizadas por una alta (arriba), media (centro) y baja (abajo) intensidad de isla de calor. En todas ellas se muestran los datos de humedad relativa del observatorio de Barajas a modo de referencia. 253

Figura 14.1 Ejemplo de representación de la función de distribución conjunta (CDF, por sus siglas en inglés) para un parámetro dado (p. ej., temperatura) y durante un mes concreto (p. ej., febrero). Las líneas de puntos se corresponden con la CFD de cada uno de los años contenidos en la serie, mientras que la línea continua representa la CFD de todos los años en conjunto. Se destaca en amarillo la CFD del año que mejor se corresponde con la del conjunto de la serie. Elaborada a partir de un ejemplo de Hall et al. (1978). 257

Figura 14.2 Grados día de refrigeración (CDD, izquierda) y de calefacción (HDD, derecha) obtenidos para cada ubicación. De fondo se muestran las LCZs de WUDAPT (Brousse et al., 2016). Nótese cómo los HDD siguen una distribución concéntrica y asociada a las LCZs, mientras que los CDD no tienen un patrón tan claro (p.ej., puntos 18 Canillas y 20 Canillejas)..... 264

Figura 14.3 Procedimiento para delimitar las zonas climáticas de invierno (arriba) y verano (abajo) a partir de los grados día de calefacción (HDD) y de refrigeración (CDD), respectivamente. Primero (a) se geolocalizan los HDD y los CDD para, posteriormente, (b) realizar una interpolación espacial dentro del municipio de Madrid. Por último, (c) se estiman los valores medios dentro de la delimitación administrativa barrio y se agrupan mediante el método de optimización de Jenks (Jenks, 1967)..... 266

Figura 14.4 Propuesta de zonificación climática para la ciudad de Madrid. Se divide a la ciudad en función de la severidad climática de invierno (a – d) y la severidad climática de verano (I – III). El resultado son 9 zonas climáticas urbanas (UCZ). Cada UCZ lleva asociado un año meteorológico típico procedente de un punto de medición. 268

Figura 14.5 Archivos climáticos urbanos para la ciudad de Madrid, ordenados de acuerdo a su severidad climática de invierno (a - d) y de verano (I - III). Nótese que el archivo climático asignado a la zona dI no se considera suficientemente representativo de su zona climática. 270

Figura 14.6 Geometría del módulo BESTEST 600 de la Agencia Internacional de la Energía. Fuente: Campana y Morini (2019) 271

Figura 14.7 Comparación de la demanda energética de calefacción y refrigeración obtenida para el módulo BESTEST 600 con diferentes archivos climáticos. El archivo ISO10 se corresponde con el archivo climático de referencia desarrollado en este trabajo siguiendo la norma ISO 15927-4 (ISO, 2005). 272

Figura 14.8 Ubicación del barrio de San Cristóbal de los Ángeles en Madrid, y los bloques en H que forman parte de este análisis. 274

Figura 14.9 Planimetría del bloque en H situado en el barrio de San Cristóbal de los Ángeles de Madrid. Alzado y secciones. Fuente: Sánchez-Guevara (2015) 275

Figura 14.10 Planimetría del bloque en H situado en el barrio de San Cristóbal de los Ángeles de Madrid. Plantas. Fuente: Sánchez-Guevara (2015) 276

Figura 14.11 Esquema de selección de viviendas tipo dentro de tipología de bloque en H. Fuente: Sánchez-Guevara (2015). 277

Figura 14.12 Comparativa entre zonas climáticas. En verano (a), las zonas climáticas más extremas se corresponderían con la zona aIII (verano más intenso) y la zona cI (verano menos intenso). En invierno (b), las zonas climáticas más extremas serían la zona dII (invierno más intenso) y la zona aIII (invierno menos intenso). 277

Figura 14.13 Demanda energética de refrigeración para el total del edificio (izquierda) y desagregada por plantas (derecha). Para el total del edificio se incluye el valor medio obtenido para cada clúster de verano (III, II, I). Los valores de la zona climática dI se representan, aunque no se consideran en el cómputo de los valores medios debido a su falta de representatividad. 278

Figura 14.14 Demanda energética de calefacción para el total del edificio (izquierda) y desagregada por plantas (derecha). Para el total del edificio se incluye el valor medio obtenido para cada clúster de invierno (a, b, c, d). Los valores de la zona climática dI se representan, aunque no se consideran en el cómputo de los valores medios debido a su falta de representatividad. 278

Figure 1.1 Carbon cycle for a neighbourhood in Vancouver, Canada (Kellett et al., 2013, found in Oke et al., 2017a). It depicts the density of carbon fluxes (lateral and vertical) and sinks. Note how the cycle follows a linear lateral-vertical logic, rather than a circular vertical-vertical one (the latter being typical of natural systems, and which can be observed on a smaller scale in the carbon fluxes of urban vegetation)..... 5

Figure 1.2 Deaths from rickets in pre-industrial London (Brimblecombe, 1987). Air pollution blocked solar radiation and thus the synthesis of vitamin D. This is thought to be one of the first childhood diseases linked to air pollution in cities (O'Riordan, 2006). 6

Figure 1.4 Causes of urban heat island formation, according to Kleerekoper et al. (2012). (1) Absorption of shortwave radiation by urban surfaces and materials; (2) Absorption of longwave radiation and re-radiation by pollution; (3) Blocking of longwave irradiation to the atmosphere by the urban structure; (4) Anthropogenic heat emission; (5) Heat accumulation by artificial urban surfaces with higher thermal admittance; (6) Reduced evaporation due to the absence of vegetation and more impervious surfaces; (7) Reduced heat dissipation due to lower wind speed. After Kleerekoper et al. (2012) 9

Figure 1.5 Main drivers of the energy performance gap (EPG) in building energy simulation tools, according to Cozza et al. (2021) 11

Figure 1.6 Schematic representation of the three types of coupling between BEM models and UCM models (after Rodler et al., 2021, following Lauzet et al., 2019). The simplest is the chaining of the models, where information flows unidirectionally from the UCM to the BEM. In weak coupling, the models feed back to each other, but only affecting subsequent simulations. Finally, in strong coupling, the feedback occurs within the same simulation, iteratively..... 14

Figure 1.7 Schematic representation of the modules that are part of the Urban Weather Generator model (Bueno et al., 2013). The data input is done through the Rural Station Model (RSM) from a weather file. In this model it is assumed that the climate file comes from a rural weather observatory. After Mao and Nordford (2021) 16

Figure 3.1 Stages of this PhD thesis. 24

Figure 10.1 Atmospheric layers contained in the urban boundary layer, during the day. 181

Figure 10.2a Urban transects carried out during the first measurement campaign, between July 2015 and July 2016. Available data from AEMET observatories and air quality stations are also included. 184

Figure 10.2b Urban transects carried out during the first measurement campaign, between July 2015 and July 2016. From top to bottom, the north - south route (Alcobendas - Getafe), northwest - southeast route (Aravaca - Vallecas) and southwest - northeast route (Alcorcón - Jarama). Based on López Gómez et al. (1988). 185

Figure 10.3 Representation of the steps taken to adapt the routes developed between 1984 and 1987 by López Gómez et al. (1988) to the current road structure. The current road structure was recreated in a Geographic Information System (GIS) (a), where its connectivity was configured and rules for circulation were assigned (b). This generated new optimal routes, coinciding with the measurement points of the previous study of 1988 (c), which were integrated into mobile devices to track and record the routes by GPS (d). 186

Figure 10.4 Exploratory maps of the urban heat island, arranged in chronological order: (a) 15 July 2015, (b) 28 October 2015, (c) 16 February 2016 and (d) 25 April 2016. 187

Figure 10.5 Main approaches to designing an urban monitoring network (Muller et al., 2013, based on Robinson, 2010). 188

Figura 10.6 Location of the monitoring equipment used in this study. It includes the equipment deployed during the MODIFICA campaign, as well as the five AEMET meteorological observatories located in the municipality of Madrid. 190

Figure 10.7 Pilot testing carried out with a prototype in a ventilated environment. The temperatures obtained inside the prototype were compared with those of a standard naturally ventilated protection, considered as a reference. 191

Figure 10.8 Images of the manufacturing process of the sensor protection. 192

Figure 10.9 On the left, illustration of the position of the measuring equipment. On the right, extract of the figures included in the patent (ES2642617-B2). 193

Figure 10.10 A unique identification tag was used for all the equipment. These made it easier to track the equipment during maintenance work and its removal. 194

Figure 10.11 Installation of the first monitoring unit in the public space. The images correspond to the Aravaca location, measuring point number 12. 194

Figure 10.12 The Embajadores metering equipment, located in Atocha street, is being removed as a result of the replacement of the street lighting poles. Image captured by Google's Street View service. 195

Figure 11.1 Diagrams illustrating the concept of a turbulent source area and its footprint function. Notice that the source are tends to an ellipse, with a maximum contribution at a certain distance from the sensor, upwind. Representation in perspective by Schmid (1994). 207

Figure 11.2 Flowchart of the process carried out for the systematic literature review. 208

Figure 11.3 Maximum distance from the sensor to the outer boundary of the source area. Includes all studies of high relevance. The ratio of the measurement height (zm) to the mixing height (zR) is used to delimit the three atmospheric layers: the urban canopy (UCL), the roughness sublayer (RSL) and the inertial sublayer (ISL). Note that both axes are presented on a logarithmic scale. 210

Figure 11.4 Illustration in plan showing the superposition of the source area for different instants. (a) For instant i, the source area would tend to an ellipse. (b) However, the wind direction varies for each instant and, therefore, the source area could be located at any point around the sensor. (c) The superposition of source areas shows, then, a theoretical tendency towards concentric distribution in the form of a circumference, and where the sensor would be located at the centre. 211

Figure 11.5 Correlation between air temperature and three indicators of surface coverage on 16 April 2016. Includes all measurement points contained within a radius of 5 kilometres from the city centre. Above, figure (a) refers to the outgoing path of Transect 1, (b) to the outgoing path of Transect 2, and (c) to the outgoing path of Transect 3. The horizontal axes are plotted logarithmically to facilitate the visualisation of the data. Below, an extract of the measurement points of transect 2 associated with their temperatures and urban context. 212

Figure 11.6 Location of the MODIFICA and AEMET measurement sites, superimposed on the classification of the Madrid urban fabric according to LCZ and obtained from the WUDAPT project (Brousse et al., 2016). 213

Figure 11.7 Example of a data sheet proposed by WMO to compile the most relevant metadata of observations carried out in urban environments. Retrieved from WMO (2017b). 215

Figure 11.8 Data sheet used to compile the most relevant metadata associated with each measurement point in this study. It includes information on both the local scale and the microscale, as well as the LCZ class assigned and the value of the indicators that lead to its determination. This example corresponds to the site 01 Embajadores. 216

Figure 11.9 Data sheet used to compile the most relevant metadata associated with each measurement point in this study. It includes information on both the local scale and the microscale, as well as the LCZ class assigned and the value of the indicators that lead to its determination. This example corresponds to the site 15 San Diego. 217

Figure 12.1 Mean daily UHI intensity during the measurement campaign. The values correspond to measurement site 01 Embajadores, being the most centric location of the monitoring campaign, and the one with the highest heat island intensities. 222

Figure 12.2 Minimum daily UHI intensity during the measurement campaign. The values correspond to measurement site 01 Embajadores, being the most centric location of the monitoring campaign, and the one with the highest heat island intensities. 223

Figure 12.3 Maximum daily UHI intensity during the measurement campaign. The values correspond to measurement site 01 Embajadores, being the most centric location of the monitoring campaign, and the one with the highest heat island intensities. 224

Figure 12.4 Mean daily wind speed. Note that days with higher wind speeds tend to correspond with days with very low peaks of UHI intensity (see Figure 12.3) 225

Figure 12.5 Accumulated precipitations during 24 hours. Note that days with higher accumulated precipitations tend to correspond with days with very low peaks of UHI intensity (see Figure 12.3) 226

Figure 12.6 Evolution of the urban heat island intensity over the hours, in each LCZ and for each month. The values correspond to the mean of the hourly records. 228

Figure 12.7 Hourly mean values of temperature (top), urban heat island intensity (centre) and cooling ratio (bottom) for two months of the year: January 2017 (left) and July 2017 (right). In the background, in grey, the ranges for all measurement points are shown, while in colour the means for each LCZ are highlighted. 229

Figure 13.1 Schematic representation of the two approaches studied for outdoor air temperature modelling. 239

Figure 13.2 Map of the municipality of Madrid showing the measurement points from which the data for the modelling are extracted. The LCZs extracted from the WUDAPT project (Brousse et al., 2016) are shown in the background. 240

Figure 13.3 Comparison of the cumulative error of various configurations where a single parameter is iterated. Results are shown for the UHII approach (left) and the TEMP approach (right). The error is presented as the root mean square error (RMSE). 242

Figure 13.4 Results of the sensitivity analysis of the input parameters in the models when the time is set at 00:00 UTC (midnight). The results obtained following the TEMP approach (top) and the UHII approach (bottom) are shown. 243

Figure 13.5 Results obtained from modelling urban temperatures using the UHII (black dashed line) and TEMP (black solid line) approaches. They are presented in three scenarios of atmospheric stability, which is translated into a scenario with high urban heat island intensity (top), a scenario with moderate intensity (centre) and a scenario with low intensity (bottom). The background shading represents the urban heat island intensity. 244

Figure 13.6 Distribution of the models' cumulative error when they are trained under different contexts of data availability. Results are given for the two approaches (UHII and TEMP) and for two different error metrics: the root mean square error (RMSE, left) and the median absolute deviation (MAD, right).....245

Figure 13.7 Additional error yielded by models trained with only 3 months of data. The reference level is set by the same models, but trained with 12 months of data. The results obtained with the TEMP approach (left) and the UHII approach (right) are compared. 246

Figure 13.8 Modelling results for one week in June (top) and February (bottom). For each of these weeks, results are presented for the models trained with 12 and 3 months of data, both with the UHII approach (dashed black line) and the TEMP approach (solid black line).....247

Figure 13.9 Accumulated error for single output and multi-output models. Results are shown for the modelling of temperature (top) and relative humidity (bottom). 248

Figure 13.10 Artificial air temperature time series generated for the year 2008 at three urban locations. Note that they correspond to locations characterised by high (top), medium (middle) and low (bottom) urban heat island intensity. In all of them, air temperature data from the Barajas observatory are shown for reference. 252

Figure 13.11 Artificial time series of relative humidity generated for the year 2008 at three urban locations. Note that they correspond to locations characterised by high (top), medium (middle) and low (bottom) urban heat island intensity. In all of them, relative humidity data from the Barajas observatory are shown for reference.....253

Figure 14.1 Example of a representation of the Cummulative Distribution Function (CDF) for a given parameter (e.g. temperature) and for a given month (e.g. February). The dotted lines correspond to the CFD for each of the years contained in the series, while the solid line represents the CFD for all years combined. The CFD of the year that best matches the combined CFD of the series is highlighted in yellow. Based on an example found in Hall et al. (1978). 257

Figure 14.2 Cooling degree days (CDD, left) and heating degree days (HDD, right) obtained for each location. WUDAPT LCZs are shown in the background (Brousse et al., 2016). Note how the HDDs follow a concentric distribution associated to the LCZs, while the CDDs do not have such a clear pattern (e.g., points 18 Canillas and 20 Canillejas).....264

Figure 14.3 Procedure to delimit winter (top) and summer (bottom) climate zones based on heating degree days (HDD) and cooling degree days (CDD), respectively. First (a) the HDD and CDD are geolocated and then (b) a spatial interpolation is performed within the municipality of Madrid. Finally, (c) the mean values within the administrative delimitation of the neighbourhood are estimated and clustered using the Jenks optimisation method (Jenks, 1967). 266

Figure 14.4 Proposed climate zoning for the city of Madrid. The city is divided according to winter climate severity (a - d) and summer climate severity (I - III). This results in 9 urban climatic zones (UCZ). Each UCZ is associated with a typical meteorological year from a measurement site. 268

Figure 14.5 Urban weather files for the city of Madrid, ordered according to their winter (a - d) and summer (I - III) climate severity. Note that the weather file asigned to zone dI is not considered sufficiently representative of its climate zone.....270

Figure 14.6 Geometry of the International Energy Agency's BESTEST 600 module. Source: Campana and Morini (2019) 271

Figure 14.7 Comparison of the heating and cooling energy demand obtained for the BESTEST 600 module with different weather files. The ISO10 file corresponds to the reference weather file developed in this work following the ISO 15927-4 standard (ISO, 2005).....272

Figure 14.8 Location of the San Cristóbal de los Ángeles neighbourhood in Madrid, and the H-blocks that form part of this analysis. 274

Figure 14.9 Planimetry of the H-block located in the neighbourhood of San Cristóbal de los Ángeles, in Madrid. Elevation and sections. Source: Sánchez-Guevara (2015) 275

Figure 14.10 Planimetry of the H-block located in the neighbourhood of San Cristóbal de los Ángeles, in Madrid. Floorplans. Source: Sánchez-Guevara (2015) 276

Figure 14.11 Scheme for the selection of typical dwellings within the H-block typology:. After Sánchez-Guevara (2015). 277

Figure 14.12 Comparison between urban climate zones. In summer (a), the most extreme climate zones would correspond to zone aIII (most intense summer) and zone cI (least intense summer). In winter (b), the most extreme climate zones would correspond to zone dII (most intense winter) and zone aIII (least intense winter) 277

Figure 14.13 Cooling energy demand for the total building (left) and disaggregated by floors (right). For the total building, the average value obtained for each summer cluster (III, II, I) is included. The values of the climate zone dI are represented, although they are not considered in the computation of the average values due to their lack of representativeness. 278

Figure 14.14 Heating energy demand for the total building (left) and disaggregated by storey (right). For the total building the average value obtained for each winter cluster (a, b, c, d) is included. The values of the climate zone dI are represented, although they are not considered in the computation of the average values due to their lack of representativeness..... 278

Índice de tablas
List of tables

Tabla 10.1 Resumen de los datos obtenidos a partir de la campaña de monitorización MODIFICA y de los observatorios de la AEMET. Los registros fueron señalados como correctos (correct), erróneos (erroneous), sospechosos (suspect) o perdidos (missing) de acuerdo con el protocolo de control de calidad de datos empleado. 197

Tabla 11.1 Metadatos empleados para describir las mediciones de este trabajo de investigación. 200

Tabla 11.2 Principales sistemas de clasificación climática para entornos urbanos. 202

Tabla 11.3 Definición de las clases que componen las Local Climate Zones. Traducido de la versión original de Stewart y Oke (2012). 203

Tabla 11.4 Valores de los indicadores geométricos y superficiales asociados a las Local Climate Zones. Traducido de la versión original de Stewart y Oke (2012). 204

Tabla 11.5 Valores de los indicadores térmicos, metabólicos y de radiación asociados a las Local Climate Zones. Traducido de la versión original de Stewart y Oke (2012). 205

Tabla 11.6 Relevancia de los resultados obtenidos durante la revisión sistemática de la bibliografía sobre el área fuente de sensores en entornos urbanos. 209

Tabla 11.7 Clasificación de los puntos de medición a partir del cálculo manual de los indicadores y a través de la cartografía del proyecto WUDAPT. 214

Tabla 12.1 Valores medios diarios de la temperatura y la intensidad de la isla de calor observada en cada punto de medición. Las cifras destacadas en negrita representan los valores más altos, mientras que los que se encuentran sobreimpresos sobre fondo gris representan los mínimos. 221

Tabla 12.2 Identificación de horas en las que las diferencias entre pares de LCZs son más significativas. Se muestran los resultados para enero y julio de 2017, analizándose para el conjunto de los días y para la selección de días ideales. La prueba post-hoc de Games Howell evalúa la significancia estadística.Table 12.2 Identification of hours where differences between pairs of LCZs are most significant. Results are shown for January and July 2017, analysed for all days and for the selection of ideal days. The Games Howell post-hoc test assesses statistical significance. ... 231

Tabla 12.3 Correlación entre indicadores LCZ y la temperatura del aire, por horas y para dos meses concretos. Se incluye la distancia al centro de la ciudad como indicador adicional. Se utiliza el coeficiente de correlación de Pearson (rp) ... 232

Table 12.3 Correlation between LCZ indicators and air temperature, on an hourly basis and for two specific months. The distance to the city centre is included as an additional indicator. Pearson's correlation coefficient (rp) is used. ... 232

Tabla 13.1 Estudios previos que han empleado redes neuronales artificiales (ANN) para la modelización de la temperatura del aire exterior. ... 238

Tabla 13.2 Parámetros iterados durante la búsqueda de una configuración y estructura óptima para la modelización. Se incluye la selección final de parámetros. ... 241

Tabla 13.3 Medidas del error arrojado por los modelos FNN desarrollados para cada punto de medición. Los valores más altos se resaltan en negrita, mientras que los más bajos se muestran sobre fondo gris. ... 249

Tabla 13.4 Datos ausentes detectados para cada uno de los parámetros empleados en la generación de las series temporales. ... 250

Tabla 14.1 Selección de algunos de los archivos climáticos más conocidos a nivel global. Cada uno de ellos se relaciona con la metodología empleada para la selección de un año meteorológico típico, ya sea la original (■) o una modificación de ésta (□) ... 256

Tabla 14.2 Distribución de pesos para la suma ponderada de los estadísticos de Finkelstein-Schafer, según distintas adaptaciones del método Sandia y el método ISO. ... 258

Tabla 14.3 Valores medios de temperatura y humedad relativa correspondientes al año meteorológico tipo seleccionado para cada ubicación. ... 261

Tabla 14.4 Grados día de calefacción (HDD) y refrigeración (CDD) correspondientes a las distintas zonas climáticas de España, según el CTE (Villar Burke et al., 2020) ... 262

Tabla 14.5 Grados hora de refrigeración (base 25 ºC) y de calefacción (base 18 ºC) obtenidos a partir del año meteorológico tipo seleccionado para cada ubicación. ... 262

Tabla 14.6 Clústeres de invierno y verano definidas para la ciudad de Madrid. Se recogen sus límites en grados día de calefacción (HDD) y de refrigeración (CDD). En la matriz se señalan los cruces entre clústeres, y que dan lugar a las zonas climáticas existentes en el municipio. ... 268

Tabla 14.7 Selección de año meteorológico típico correspondiente con un punto de medición dentro de cada zona climática urbana (UCZ). Se incluyen los rangos de grados día de calefacción (HDD18) y refrigeración (CDD25), así como sus valores correspondientes para cada punto de ubicación. También se incluye el error relativo medio (ε). 269

Tabla 14.8 Archivos climáticos preexistentes para la ciudad de Madrid. Únicamente se incluyen aquellos específicos para la ciudad o región de Madrid, excluyéndose específicamente los archivos de los climas de referencia del CTE (2014). 270

Tabla 14.9 Temperaturas medias, máximas y mínimas diarias de cada archivo climático preexistente para Madrid, así como para el nuevo archivo climático de referencia. Se incluyen los datos desagregados para los meses sobrecalentados (junio – septiembre) e infracalentados (octubre – mayo). 273

Tabla 14.10 Demanda energética de refrigeración asociada a cada zona climática urbana, desagregada por vivienda. En negrita se destacan los valores más elevados, mientras que los registros más bajos se sobreimprimen en gris. Los valores de la zona dI aparecen atenuados por su falta de representatividad..... 280

Tabla 14.11 Demanda energética de calefacción asociada a cada zona climática urbana, desagregada por vivienda. En negrita se destacan los valores más elevados, mientras que los registros más bajos se sobreimprimen en gris. Los valores de la zona dI aparecen atenuados por su falta de representatividad..... 281

Table 10.1 Summary of the data obtained from the MODIFICA monitoring campaign and the AEMET observatories. Records were marked as correct, erroneous, suspect or missing according to the data quality control protocol. 197

Table 11.1 Metadata used to describe the measurements in this research work. 200

Table 11.2 Main climate classification systems for urban environments. 202

Table 11.3 Definition of the classes that comprise the Local Climate Zones. Translated into Spanish from the original version by Stewart and Oke (2012) 203

Table 11.4 Geometric and surface parameter values associated with the Local Climate Zones. Translated into Spanish from the original version by Stewart and Oke (2012). 204

Table 11.5 Thermal, metabolic and radiation parameter values associated with the Local Climate Zones. Translated into Spanish from the original version by Stewart and Oke (2012). 205

Table 11.6 Relevance of the obtained results during the systematic literature review on the sensors source area in urban environments. 209

Table 11.7 Classification of the measurement points based on the manual calculation of the indicators and through the mapping of the WUDAPT project. 214

Table 12.1 Daily average values of temperature and urban heat island intensity observed at each measurement point. Figures highlighted in bold represent the highest values, while those overprinted on a grey background represent the lowest values. 221

Table 13.1 Previous studies using artificial neural networks (ANNs) for outdoor air temperature modelling. 238

Table 13.2 Iterated parameters during the search for an optimal modelling configuration and structure. The final selection of parameters is included. 241

Table 13.3 FNN models' error yielded at each measurement site. Higher values are highlighted in bold, while lower values are shown on a grey background. 249

Table 13.4 Missing data detected for each of the parameters used in the generation of the time series. 250

Table 14.1 A selection of some of the best known global weather files. Each of them is related to the methodology used for the selection of a typical meteorological year, either the original one (■) or a modified version of it (□). 256

Table 14.2 Distribution of weights for the weighted sum of the Finkelstein-Schafer statistics, according to different adaptations of the Sandia method and the ISO method. 258

Table 14.3 Average values of temperature and relative humidity for the selected typical meteorological year for each location. 261

Table 14.4 Heating (HDD) and cooling (CDD) degrees days corresponding to the different climatic zones of Spain, according to the CTE (Villar Burke et al., 2020) 262

Table 14.5 Cooling (base 25 ºC) and heating (base 18 ºC) degree hours obtained from the selected typical meteorological year for each location. 262

Table 14.6 Winter and summer clusters defined for the city of Madrid. Their limits are shown in heating degree days (HDD) and cooling degree days (CDD). The matrix shows the crossings between clusters, which lead to the existing climatic zones in the municipality. 268

Table 14.7 Typical meteorological year selection corresponding to a measurement point within each urban climatic zone (UCZ). Heating (HDD18) and cooling (CDD25) degree day ranges and their corresponding values for each location point are included. The mean relative error (ε) is also included. 269

Table 14.8 Pre-existing weather files for the city of Madrid. Only those specific to the city or region of Madrid are included, specifically excluding the reference climate files of the CTE (2014). 270

Table 14.9 Daily mean, maximum and minimum temperatures for each pre-existing weather file for Madrid, as well as for the new reference weather file. Disaggregated data for the overheated (June – September) and underheated (October – May) months are included 273

Table 14.10 Cooling energy demand associated with each urban climatic zone, disaggregated by dwelling. Higher values are highlighted in bold, while lower values are overprinted in grey. Values for zone dI are attenuated due to their lack of representativeness. 280

Table 14.11 Heating energy demand associated with each urban climatic zone, disaggregated by dwelling. Higher values are highlighted in bold, while lower values are overprinted in grey. Values for zone dI are attenuated due to their lack of representativeness. 281

Listado de abreviaturas
List of abbreviations

ABL	Atmospheric boundary layer	*Capa límite atmosférica*
AEMET	(Spanish) State Meteorological Agency	*Agencia Estatal de Meteorología*
ANN	Artificial neural network	*Red neuronal artificial*
ANOVA	Analysis of variance	*Análisis de varianza*
AR	Aspect ratio	*Relación de aspecto*
ASHRAE	American Society of Heating, Refrigerating and Air-Conditioning Engineers	*Sociedad Estadounidense de Ingenieros de Calefacción, Refrigeración y Aire Acondicionado*
BEM	Building energy modeling	*Modelización energética de edificios*
BSF	Building surface fraction	*Fracción de la superficie cubierta por edificación*
CDD	Cooling degree days	*Grados día de refrigeración*
CDF	Cumulative distribution function	*Función de distribución conjunta*
CDH	Cooling degree hours	*Grados hora de refrigeración*
CFD	Computational fluid dynamics	*Mecánica de fluidos computacional*
CIBSE	Chartered Institution of Building Services Engineers	-
CNN	Convolutional neural network	*Red neuronal convolucional*
CTE	(Spanish) technical building code	*Código Técnico de la Edificación*
CWS	Citizen weather stations	*"Estaciones meteorológicas ciudadanas"*
D. b. temp.	Dry bulb temperature	*Temperatura de bulbo seco*
DIST	Distance to the urban centroid	*Distancia al centroide urbano*
Dist.	Distance	*Distancia*
DRY	Design Reference Year	-
dT	Cooling rate	*Tasa de enfriamiento*
ELU	Exponential linear unit activation function	*Función de activación de la unidad lineal exponencial*
ENN	Elman recurrent neural network	*Red neuronal recurrente Elman*
EPG	Energy performance gap	*Brecha del comportamiento energético*
EU	European Union	*Unión Europea*
FCCC	Framework Convention on Climate Change	*Convención Marco sobre el Cambio Climático*

f_{max}	Footprint function maximum	*Máximo de la función de huella*
FNN	Feed-forward neural network	*Red neuronal prealimentada*
FS	Finkelstein-Schafer statistic	*prueba de Finkelstein-Schafer*
GF	Ground floor	*Planta baja*
GIS	Geographic information system	*Sistema de información geográfica*
GPS	Global positioning system	*Sistema de posicionamiento global*
HDD	Heating degree days	*Grados día de calefacción*
HDH	Heating degree hours	*Grados hora de calefacción*
HRE	Height of roughness elements	*Altura de los obstáculos*
IDW	Inverse distance weighting interpolation	*Interpolación mediante distancia inversa*
IEA	International Energy Agency	*Agencia Internacional de la Energía*
IF	Intermediate floor	*Planta intermedia*
IPCC	Intergovernmental Panel on Climate Change	*Panel Intergubernamental del Cambio Climático*
ISF	Impervious surface fraction	*Fracción de la superficie cubierta por superficies impermeables*
ISL	Inertial sublayer	*Subcapa inercial*
ISO	International Organization for Standardization	*Organización Internacional de Normalización*
IWEC	International Weather for Energy Calculations	-
JCR	Journal Citations Report	*"Informe sobre citas en revistas científicas"*
JIF	Journal Impact Factor	*Factor de Impacto de la Revista*
KS	Kolmogorov-Smirnov statistic	*prueba de Kolmogorov-Smirnov*
LCZ	Local Climate Zone	*"Zona Climática Local"*
LF	Last floor	*Planta última*
m a.s.l.	Meters above sea level	*Metros por encima del nivel del mar*
MAD	Median absolute deviation	*Mediana de la desviación absoluta*
MAE	Mean absolute error	*Error absoluto medio*
MITECO	(Spanish) Ministry for the Ecological Transition and the Demographic Challenge	*Ministerio para la Transición Ecológica y el Reto Demográfico*
ML	Mixed layer	*Capa de mezcla*
MSE	Mean-square error	*Error cuadrático medio*
NNARMAX	Neural nonlinear autoregressive moving average model with exogenous inputs	*Red neuronal de media móvil autorregresiva no lineal con entradas exógenas*
NNARX	Neural nonlinear autoregressive model with exogenous inputs	*Red neuronal autorregresiva no lineal con entradas exógenas*
OSCAR	Observing System Capability Analysis and Review Tool	*Herramienta de Análisis y Examen de Capacidad de los Sistemas de Observación*
PRIMA	Preferred Reporting Items for Systematic Reviews and Meta-Analyses	*"Elementos de Información Preferidos para las Revisiones Sistemáticas y los Meta-Análisis"*
PSF	Pervious surface fraction	*Fracción de la superficie cubierta por superficies permeables*
QC	Quality control	*Control de calidad*
R^2	Coefficient of determination	*Coeficiente de determinación*
ReLU	Rectified linear unit activation function	*Función de activación de la unidad lineal rectificada*
RMSE	Root-mean-square error	*Raíz del error cuadrático medio*

RNN	Recurrent neural network	*Red neuronal recurrente*
rp	Pearson correlation coefficient	*Coeficiente de correlación de Pearson*
r_s	Spearman correlation coefficient	*Coeficiente de correlación de Spearman*
RSL	Roughness sublayer	*Subcapa de rugosidad*
s. f.	Surface fraction	*Fracción de la superficie cubierta*
SELU	Scaled exponential linear unit activation function	*Función de activación de la unidad lineal exponencial escalada*
SGD	Stochastic gradient descent	*Descenso de gradiente estocástico*
SJR	Scimago Journal Rank	*Ranking de Revistas Scimago*
SL	Surface layer	*Capa límite superficial*
SVF	Sky view factor	*Factor de visión de cielo*
SVF_S	Sky view factor in summer	*Factor de visión de cielo durante el verano*
SVF_w	Sky view factor in winter	*Factor de visión de cielo durante el invierno*
SWEC	Spanish Weather for Energy Calculations	-
TAK	Title, abstract and keywords	*Título, resumen y palabras claves*
TEMP	Temperature	*Temperatura*
TMY	Typical Meteorological Yyear	-
TRY	Test Reference Year	-
UBEM	Urban building energy modeling	*Modelización energética de edificios a escala urbana*
UBL	Urban boundary layer	*Capa límite urbana*
UCL	Urban canopy layer	*Palio urbano*
UCM	Urban climate model	*Modelo climático urbano*
UCZ	Urban climatic zones	*Zonas climáticas urbanas*
UHI	Urban heat island	*Isla de calor urbana*
UHII	Urban heat island intensity	*Intensidad de la isla de calor urbana*
UTC	Coordinated universal time	*Tiempo universal coordinado*
UWG	Urban Weather Generator	-
VOC	Volatile organic compounds	*Compuestos orgánicos volátiles*
WIGOS	WMO Integrated Global Observing System	*Sistema Mundial Integrado de Observación de la WMO*
WMO	World Meteorological Organization	*Organización Mundial de la Meteorología*
WUDAPT	World Urban Database and Access Portal Tools	-
WYEC	Weather Year for Energy Calculations	-
z_m	Measurement height	*Altura de observación*
z_R	Mixing height	*Altura de mezcla*
ΔT	Diference of temperature	*Diferencia de temperatura*
ε	Mean average error	*Error relativo medio*
Φw	Weather factor	*Factor meteorológico*

« John, cuando la gente pensaba que la tierra era plana, se equivocaba. Cuando la gente pensaba que la tierra era esférica, se equivocaba. Pero si crees que pensar que la tierra es esférica es tan erróneo como pensar que la tierra es plana, entonces tu punto de vista es más erróneo que el de las dos ideas anteriores juntas.

Asimov, I. (1996)
The Relativity of Wrong

Parte I. Introducción, hipótesis y objetivos
Part I. Introduction, hypothesis and objectives

1. **Introducción**
   Introduction
2. **Hipótesis y objetivos**
   Hypothesis and objectives

En esta primera parte del documento se presenta una introducción sobre la relación entre el clima y la ciudad, los antecedentes del clima urbano y de las herramientas de simulación energética, y los diferentes métodos que se han utilizado para integrar el efecto de la isla de calor en la evaluación energética de edificios. Esta revisión del conocimiento previo conduce a la formulación de la hipótesis y los objetivos (principal y específicos) de esta tesis doctoral.

This first part of the document presents an introduction on the relationship between the climate and the city, the state of the art of urban climate and energy simulation tools, and the different methods that have been used to integrate the urban heat island effect into building energy modelling. This review of previous knowledge leads to the formulation of the hypothesis and the main and specific objectives of this PhD thesis.

1. Introducción

1.1. El clima en la ciudad

Escribía Rafael Serra que *si la arquitectura es clima, también es verdad que son muchos los climas que en ella intervienen* (Serra, 1999, p.7). Señalaba que la arquitectura se ve influenciada por una gran cantidad de *climas*, incluyendo los que no son propiamente climas (p.ej., clima sonoro). Y que, a partir de estos climas (o con estos climas), se generaba *la infinita variedad de los espacios arquitectónicos*.

Todos los climas son contexto; y la arquitectura y nuestras ciudades, el reflejo de cómo respondemos a este contexto. Si acotamos la definición de clima al conjunto de variables meteorológicas, queda claro que nuestra manera de responder a este contexto ha venido de la mano de la adaptación.

Como ejemplo de esta adaptación tenemos el mismo origen de las ciudades. El cambio climático del final de las últimas glaciaciones del Pleistoceno propició las migraciones y desertificaciones que, a su vez, favorecieron la aparición de las primeras aldeas humanas permanentes (Childe, 1950). Parece ser que la incertidumbre en la búsqueda de alimento, desencadenada por el aumento de las temperaturas, fue uno de los factores más relevantes que incentivaron el abandono de la vida nómada (Richards, 2002).

Este proceso de adaptación al nuevo contexto climático lo conocemos como *revolución neolítica*. Ocurrió hace 10,000 años, en los albores del Holoceno, periodo geológico ya coetáneo al desarrollo de la civilización humana, y que hoy subdividimos en tres edades igualmente determinadas por eventos climáticos globales (*Groenlandiense*, *Norgripiense* y *Megalayense*; Walker et al., 2019).

Desde sus inicios, nuestra civilización ha venido adaptando su arquitectura y urbanismo a las condiciones climáticas de los lugares en las que se emplazaban. Aunque muchas de las primeras ciudades no han llegado a nuestros días, sí que hemos conservado gran parte de su legado en forma de tradición arquitectónica. Una parte importante de la arquitectura que hoy admiramos, y de los entornos urbanos que habitamos, han evolucionado desde entonces, adoptando y adaptando estrategias para mejorar las condiciones climáticas de sus espacios (Neila González, 2004). En este sentido, la arquitectura popular, a menudo relegada a un segundo plano, ha supuesto una fuente inagotable de aprendizaje para la arquitectura contemporánea, hoy bioclimática, pasiva y neutra en carbono.

Actualmente transitamos hacia un nuevo periodo geológico, el *Antropoceno* (Crutzen, 2002; Syvitski et al., 2020; Waters et al., 2016, 2015; Zalasiewicz et al., 2015). El Antropoceno se diferencia de los anteriores periodos en que es la acción humana, y no un fenómeno climático natural, la que actúa como fuerza motora del cambio geológico (Silva et al., 2018). Esta fuerza se encuentra estrechamen-

1. Introduction

1.1. The climate in the city

Rafael Serra once wrote that *if we accept that architecture is climate, then it is also true that there are many climates that influence it* (Serra, 1999, p.7). He pointed out that architecture is shaped by a large number of climates, including those that are not properly climates (e.g., the sound). And that, from these climates (or with these climates), the *infinite variety of architectural spaces* are generated.

All climates are, in the end, context; and the architecture and our cities, the reflection of how we respond to this context. If we restrict the definition of the climate to the set of meteorological variables, it is clear that we respond to this context through adaptation.

An example of this adaptation is the origin of cities themselves. The climate change that occurred at the end of the last Pleistocene ice ages led to migrations and desertifications which, in turn, favoured the advent of the first permanent human villages (Childe, 1950). It seems that uncertainty in food provision, triggered by rising temperatures, was one of the most important factors that encouraged the end of nomadic life (Richards, 2002).

This adaptation process to the new climatic context is known as the Neolithic revolution. It occurred 10,000 years ago, during the early Holocene, a geological period coetaneous to human development, and which we now subdivide into three ages equally determined by global climatic events (*Greenlandian*, *Northgrippian* and *Meghalayan*; Walker et al., 2019).

Since its beginnings, our civilisation has adapted its architecture and urban planning to the climatic conditions of the places where it was located. Although many of the first cities have not survived to our times, we have preserved a large part of their legacy in the form of architectural tradition. An important part of the architecture we admire today, and of the urban environments we inhabit, have evolved since then, adopting and adapting strategies to improve the climatic conditions of their spaces (Neila González, 2004). In this sense, popular architecture, often relegated to a second plane, has been an endless source of inspiration for contemporary architecture, which today is bioclimatic, passive and carbon neutral.

We are now moving into a new geological period, the Anthropocene (Crutzen, 2002; Syvitski et al., 2020; Waters et al., 2016, 2015; Zalasiewicz et al., 2015). The Anthropocene differs from previous periods in that it is human action, rather than a natural climatic phenomenon, that acts as a driving force for geological change (Silva et al., 2018). This force is closely linked to the development and activity of

te vinculada con el desarrollo y actividad de las ciudades, que tienen un papel central tanto en términos absolutos (la mayoría de la población global habita en entornos urbanos) como en términos relativos (actúan como centros de desarrollo económico y cultural). Tanto es así, que incluso se ha propuesto rebautizar este nuevo periodo geológico como *Urbanoceno* (Chwałczyk, 2020; Palme and Salvati, 2021a).

cities, which play a central role both in absolute terms (the majority of the global population lives in urban environments) and in relative terms (they act as centres of economic and cultural development). So much so that it was even proposed to rename this new geological period as the Urbanocene (Chwałczyk, 2020; Palme and Salvati, 2021a).

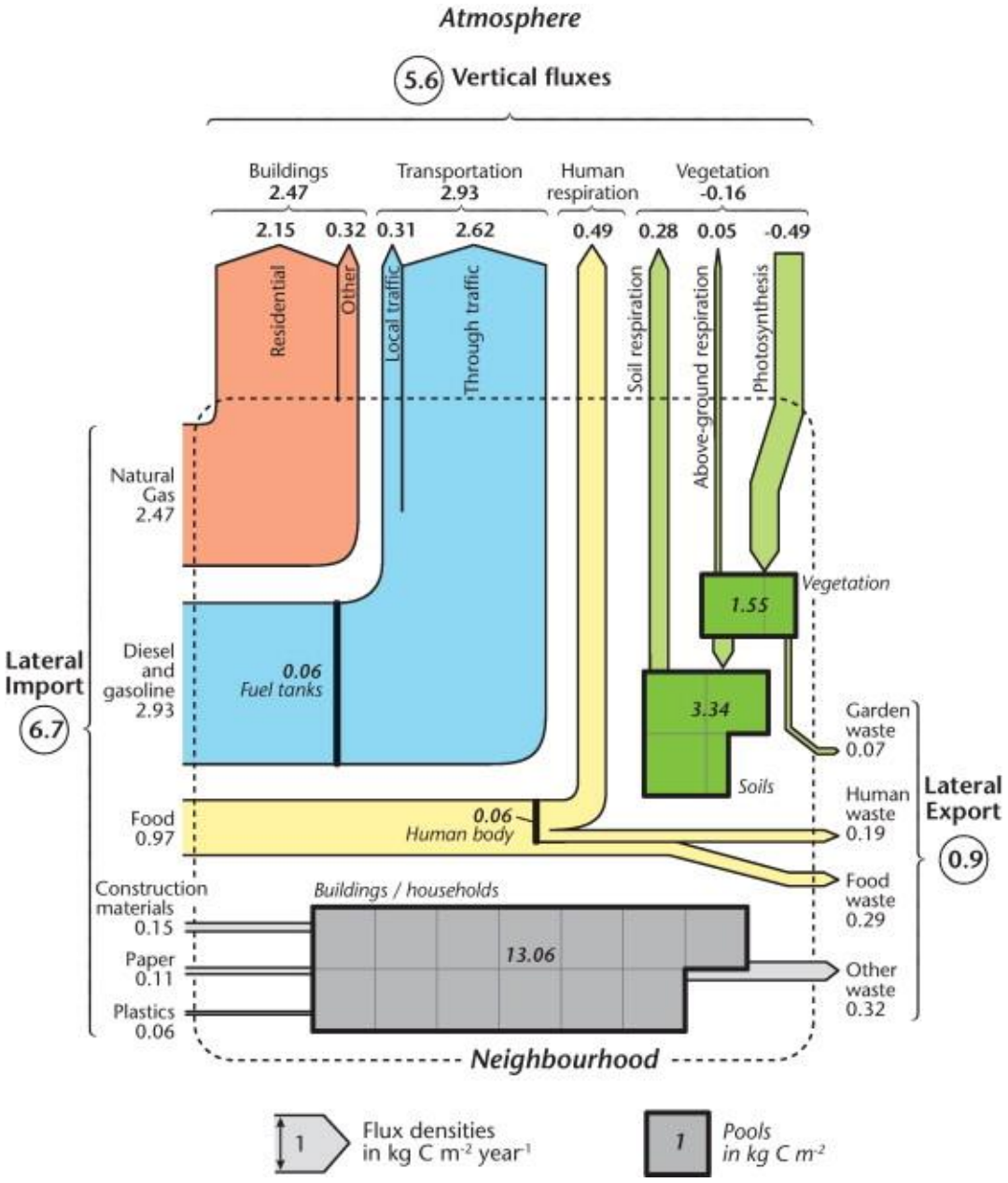

Figura 1.1 Ciclo del carbono para un barrio de Vancouver, en Canadá (Kellett et al., 2013*, encontrado en* Oke et al., 2017a). *Representa la densidad de los flujos (laterales y verticales) y los sumideros de carbono. Nótese cómo el ciclo sigue una lógica lineal lateral-vertical, en lugar de circular vertical-vertical (esta última propia de los sistemas naturales, y que puede observarse a pequeña escala en los flujos de carbono de la vegetación urbana).*

Figure 1.1 Carbon cycle for a neighbourhood in Vancouver, Canada (Kellett et al., 2013, found in Oke et al., 2017a). It depicts the density of carbon fluxes (lateral and vertical) and sinks. Note how the cycle follows a linear lateral-vertical logic, rather than a circular vertical-vertical one (the latter being typical of natural systems, and which can be observed on a smaller scale in the carbon fluxes of urban vegetation).

Cities are no longer only adapting to the climate, they are also modifying it. It is well known that, in the current context of climate change, cities play a very important role in the emission of greenhouse gases (Moran et al., 2018; Oke et al., 2017a). It is also clear that the changes they introduce in the climatic conditions of the territories where they are located exacerbate the impact of climate change (IPCC, 2021). Their structure and shape modify the conditions of the atmospheric boundary layer, the friction zone between the earth's surface and the free atmosphere; the metabolism of cities generates a large amount of waste in the form of heat that alters energy flows; and their artificial surfaces lead to the accumulation of infrared radiation that is perceptible, even in the subsoil of cities. All these phenomena combined give rise to climatic conditions characteristic of cities, which we know as the *urban climate*.

Y es que las ciudades ya no sólo se adaptan al clima, sino que también lo modifican. Es conocido que, en el actual contexto de cambio climático, las ciudades tienen un peso muy relevante en la emisión de gases de efecto invernadero (Moran et al., 2018; Oke et al., 2017a). También, que los cambios que introducen en las condiciones climáticas de los territorios donde se sitúan agudizan el impacto del cambio climático (IPCC, 2021). Su estructura y forma modifican las condiciones de la capa límite atmosférica, zona de fricción entre la superficie terrestre y la atmósfera libre; el metabolismo de las ciudades genera una gran cantidad de residuos en forma de calor que altera los flujos energéticos; y sus superficies artificiales propician la acumulación de radiación infrarroja que es perceptible, incluso, en el subsuelo de las ciudades. Todos estos fenómenos combinados dan lugar a unas condiciones climáticas características de las ciudades, y que conocemos como el *clima urbano*.

1.2. Urban climate history and background

According to Yoshino (1990), the awareness that cities modify atmospheric conditions dates back at least to the late 12th and early 13th century. This would be related to the rapid increase in population in some urban centres during the pre-industrial era and, in this context, London stood out from the rest. There, population growth and the greater coal burning led to an ever-increasing concentration of pollutant emissions. This resulted, in turn, in significant and continuing pollution episodes. Such was the problem that, in 1285, a commission was established under royal command to investigate the problem of urban pollution caused by coal burning and, a couple of decades later, to abolish the practice (Brake, 1975; Brimblecombe, 1987). The ban, although temporary, is considered the first air quality regulation in history. Centuries later, but still before the Industrial Revolution, John Evelyn' s *Fumifugium* (Evelyn, 1661), one of the first studies on urban air pollution, was published in London.

1.2. Antecedentes e historia del clima urbano

De acuerdo con Yoshino (1990), la conciencia de que las ciudades modifican las condiciones atmosféricas se remonta, al menos, hasta finales del siglo XII y comienzos del siglo XIII. Ésta estaría relacionada con el rápido aumento de la población de algunos centros urbanos durante la era preindustrial y, en este contexto, Londres destacaba sobre las demás. Allí, el crecimiento demográfico y el uso del carbón llevó a una cada vez mayor concentración de emisiones contaminantes. Ello condujo, a su vez, a importantes y continuados episodios de contaminación. Tal era el problema que, en 1285, se estableció una comisión bajo mandado real con el objetivo de investigar el problema de la contaminación urbana producida por la quema de carbón y, un par de décadas más tarde, a abolir esta práctica (Brake, 1975; Brimblecombe, 1987). La prohibición, aunque fue de carácter temporal, se considera la primera regulación en materia de calidad del aire de la historia. Siglos más tarde, pero todavía antes de la Revolución Industrial, se publicaría en Londres el trabajo de John Evelyn *Fumifugium* (Evelyn, 1661), uno de los primeros estudios sobre contaminación atmosférica urbana.

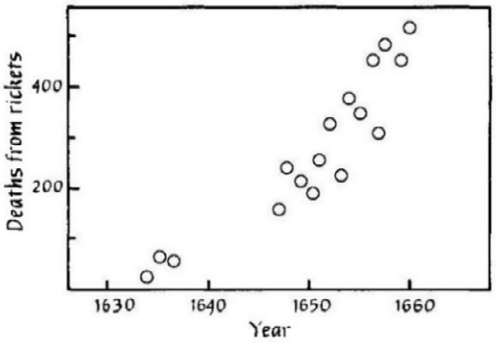

Figura 1.2 Muertes por raquitismo en la ciudad preindustrial de Londres (Brimblecombe, 1987). *La contaminación atmosférica bloqueaba la radiación solar y, con ello, la síntesis de la vitamina D. Se cree que ésta fue una de las primeras enfermedades infantiles vinculadas con la contaminación atmosférica en las ciudades* (O'Riordan, 2006).

Figure 1.2 Deaths from rickets in pre-industrial London (Brimblecombe, 1987). Air pollution blocked solar radiation and thus the synthesis of vitamin D. This is thought to be one of the first childhood diseases linked to air pollution in cities (O'Riordan, 2006).

La sociedad preindustrial era consciente, por lo tanto, de que la actividad urbana podía alterar significativamente las condiciones atmosféricas. Sin embargo, no fue hasta bien entrada la Revolución Industrial cuando se extendió el estudio a otros parámetros que no fuera la contaminación. La creciente disponibilidad de equipamiento para realizar mediciones meteorológicas, así como la estandarización, debieron posibilitar la comparación de mediciones entre distintos puntos (Stewart, 2019). Así surgió el primer antecedente en el estudio del clima urbano, *The Climate of London,* publicado a comienzos del s. XIX por Luke Howard (1833). Este trabajo se centraría en cinco parámetros atmosféricos: la temperatura, humedad y presión atmosféricas, el viento, y las precipitaciones.

La historia del clima urbano se puede agrupar en tres etapas (Stewart, 2019; Yoshino, 1990): nacimiento (s. XIX y comienzos del XX), innovación metodológica (1920 – 1950), y aumento de la experimentación (1950 – 1980). De la primera etapa, y además del trabajo pionero de Howard, también son conocidas las investigaciones de Hann en Austria (Hann, 1898, 1885, según recogen Kratzer, 1937; ZAMG, 1901), y de Renou en Francia (Renou, 1868, 1855). Ambos dedicaron un gran esfuerzo al estudio de las diferencias de temperatura entre la ciudad y sus alrededores. Los análisis y descripciones que se encuentran en sus trabajos dan cuenta de la relevancia de estas diferencias de temperatura, incluso en municipios de pequeño tamaño. Así, Renou destacaba que *"el valle de Huchigny, tan cercano a Vendôme, se diferencia a veces de éste de la misma manera que un clima continental se diferencia de uno marino"* (Renou, 1855, p.57). Se comenzaba, por tanto, a tener conciencia de que las diferencias de temperatura entre puntos urbanos y no urbanos podían llegar a ser notables.

Durante la segunda etapa de desarrollo del clima urbano, entre las décadas de los años 20 y 40, se ponen en práctica innovaciones metodológicas que permiten profundizar en el conocimiento de esta materia. La popularización de los automóviles posibilitó que tanto Schmidt (1927) en Viena como Peppler (1929) en Karlsruhe desarrollaran las primeras mediciones de temperatura mediante puntos móviles, introduciendo la técnica de los *transectos urbanos*. Estos consisten en recorridos transversales a la ciudad, predefinidos y con una duración determinada, a través de los cuales se realizan mediciones cuasi simultáneas en múltiples puntos de la ciudad.

Gracias al desarrollo de los transectos urbanos se pudo pasar de comparaciones estáticas, generalmente entre dos puntos, a un estudio basado en decenas e incluso cientos de puntos. Esto permitió estudiar la distribución de temperaturas urbanas con una elevada resolución y, por lo tanto, conocer con mayor grado de detalle sus límites y relaciones con la ciudad. De este modo se llegó a la concepción de la *isla de calor urbana*, término que hace referencia al gradiente térmico de forma concéntrica que se produce en las ciudades. De acuerdo con Stewart (2019), este término lo plantea por primera vez Peppler (1929) como la *städtlische Wärmeinsel* (lite-

Pre-industrial society was therefore aware that urban activity could significantly alter atmospheric conditions. However, it was not until well into the Industrial Revolution that the study was extended to parameters other than pollution. The increasing availability of equipment for meteorological measurements, as well as standardisation, facilitated the comparison of measurements between different points (Stewart, 2019). This led to the first precedent in the study of urban climate, *The Climate of London*, published in the early 19th century by Luke Howard (1833). This work focused on five atmospheric parameters: temperature, atmospheric humidity and pressure, wind, and precipitation.

The history of urban climate can be grouped into three stages (Stewart, 2019; Yoshino, 1990): birth (19th and early 20th century), methodological innovation (1920s – 1950s), and increased experimentation (1950s – 1980s). From the first stage, and in addition to Howard's pioneering work, the research of Hann in Austria (Hann, 1898, 1885, as reported by Kratzer, 1937; ZAMG, 1901), and Renou in France (Renou, 1868, 1855) are also well known. Both devoted a great deal of effort to the study of temperature differences between the city and its surroundings. The analyses and descriptions found in their works show the relevance of these temperature differences, even in small municipalities. Thus, Renou pointed out that "*the valley of Huchigny, so close to Vendôme, sometimes differs from Vendôme in the same way that a continental climate differs from a marine climate"* (Renou, 1855, p.57). It was therefore starting to be recognised that the differences in temperature between urban and non-urban areas could be considerable.

During the second stage of urban climate development, between the 1920s and 1940s, methodological innovations were put into practice that allowed for a deeper understanding of the subject. The popularisation of automobiles made it possible for both Schmidt (1927) in Vienna and Peppler (1929) in Karlsruhe to develop the first temperature measurements using mobile points, introducing the technique of *urban transects*. These are predefined, time-limited transects through which quasi-simultaneous measurements are taken at multiple points in the city.

The development of urban transects made it possible to move from static comparisons, usually between two points, to a study based on tens or even hundreds of points. This made it possible to study the distribution of urban temperatures with a high resolution and, therefore, to know in greater detail their limits and relationships with the city. This led to the conception of the urban heat island, a term that refers to the concentric thermal gradient that occurs in cities. According to Stewart (2019), this term was first proposed by Peppler (1929) as

the *städtlische Wärmeinsel* (literally, "urban heat island"), although the better-known term is its English equivalent *urban heat island*, first mentioned by Matthews (1937) and later popularised by Manley (1958).

During these years, several studies on urban climate were carried out. Kratzer (1937) presents an extensive bibliographical review on the subject, structured in the different parameters of urban climate, and where, as a novelty, he included the composition of the air and solar radiation. On the latter, Geiger (1950, although his first version is from 1927, and the latest from 1995), who is best known for his world climate classification (*Köppen-Geiger,* Geiger, 1954; Köppen, 1936), contributed with his studies on solar radiation and energy exchange to the development of the concept of the energy balance of the city (Oke, 1988).

The increase in experimentation was consolidated during the second half of the 20th century. The frequent bibliographical reviews that appeared in this period on urban climate provide evidence of this. In this sense, Mc Boyle (1968) shows the explosion of studies that emerged in the 1950s by means of several graphs. Later, Oke complemented this chronological approach with reviews of the periods 1968 - 1973 (Oke, 1974) and 1973 - 1976 (Oke, 1979). Also well recognised is the literature review by Landsberg (1981), who years earlier had developed a well-known report on climate and meteorology in urban environments (Landsberg, 1976). Both this work and Oke's reviews were developed for the World Meteorological Organization (WMO), promoters of a joint congress on urban climate and climatology applied to building design and construction (WMO, 1970a, 1970b).

ralmente, "isla de calor urbana"), aunque el término que más conocido es su equivalente en inglés *urban heat island*, mencionado por primera vez por Matthews (1937) y popularizado posteriormente por Manley (1958).

Durante estos años se llevaron a cabo diversos estudios sobre el clima urbano. Kratzer (1937) presenta una amplia revisión bibliográfica sobre el tema, estructurada en los diferentes parámetros del clima urbano, y donde como novedad incluyó la composición del aire y la radiación solar. Sobre esto último se centra más en detalle Geiger (1950, aunque su primera versión es de 1927, y la última de 1995), más conocido por su clasificación climática mundial (*Köppen-Geiger*, Geiger, 1954; Köppen, 1936), pero quien muy probablemente contribuyó con sus estudios sobre la radiación solar y el intercambio energético al desarrollo del concepto del balance energético de la ciudad (Oke, 1988).

El aumento de la experimentación se consolida durante la segunda mitad del s. XX. Las frecuentes revisiones bibliográficas aparecidas en este periodo sobre el clima urbano dan cuenta de ello. En este sentido, Mc Boyle (1968) muestra mediante varias gráficas la explosión de estudios surgidos en la década de 1950. Más adelante, Oke complementaría este enfoque cronológico con sendas revisiones sobre los periodos 1968 – 1973 (Oke, 1974) y 1973 – 1976 (Oke, 1979). También es muy reconocida la revisión bibliográfica de Landsberg (1981), quien años antes había desarrollado un conocido informe sobre el clima y la meteorología en entornos urbanos (Landsberg, 1976). Tanto este trabajo como las revisiones de Oke mencionadas anteriormente fueron desarrollados para la Organización Mundial de la Meteorología (WMO), promovedores de la celebración de un congreso conjunto sobre el clima urbano y la climatología aplicada al diseño y construcción de edificios (WMO, 1970a, 1970b).

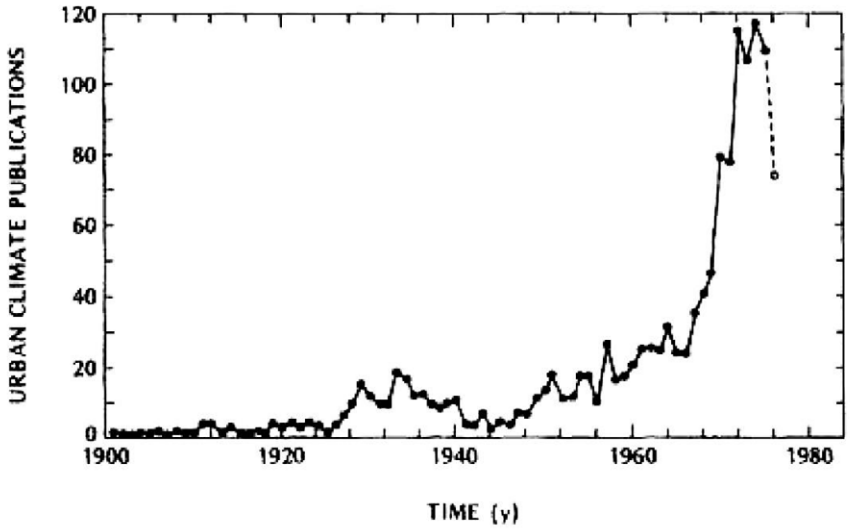

Figura 1.3 Número de estudios sobre el clima urbano durante el s. XX, y donde no se incluyen los relacionados con la contaminación atmosférica (Oke, 1979).
Figure 1.3 Number of studies on urban climate during the 20th century, not including those related to air pollution (Oke, 1979).

1.3. El clima urbano aplicado a la arquitectura y el diseño urbano

El interés de la WMO por la climatología urbana es un claro ejemplo de la creciente influencia que este campo de investigación comenzaba a ejercer sobre otras áreas. En este sentido, su influencia sobre la arquitectura y el planeamiento urbano comienza a ser visible en los años 70. Uno de los primeros antecedentes sobre este tema lo encontramos en Landsberg (1973), quien presenta *Metutopia*: la ciudad meteorológicamente utópica. En este escrito, Landsberg aboga por una mayor penetración de los principios meteorológicos en el diseño urbano.

También son destacables los trabajos de Lacy (1972) o de Chandler (1976), quien, de nuevo de la mano de la WMO, desarrollaría un informe sobre la relevancia del clima urbano en el diseño de las ciudades. Ese mismo año, Page (1976) publicaría otro trabajo sobre la importancia del clima para el diseño de edificios, y donde incorpora la perspectiva del clima urbano. En 1980, Page reflexionaría sobre cómo debería abordarse el diseño urbano y de edificios, argumentando que *el urbanismo necesita una base energética más sólida, animada por una adecuada conciencia climatológica* (Page, 1980, pág. 73).

Sin embargo, la transferencia de conocimiento climático al desarrollo de las ciudades no se ha producido al ritmo que hubiese sido deseable. El mismo Page mencionaba la *brecha educativa en arquitectura* (architectural educational gap; Page, 1980, pág. 84). Otros investigadores de prestigio también advirtieron sobre esta falta de transferencia de conocimiento a profesionales de la arquitectura y el urbanismo (i.e., Oke, 1984). Y, aunque la publicación de estudios sobre este tema ha sido relativamente constante y existen estrategias y

1.3. Application of urban climate knowledge to architecture and urban design

The WMO's interest in urban climatology is a clear example of the growing influence that this research field was beginning to exert on other areas. In this sense, its influence on architecture and urban planning began to be noticeable in the 1970s. One of the first examples of this is Landsberg (1973), who presents *Metutopia: the meteorologically utopian city*. In this paper, Landsberg argues for a greater penetration of meteorological principles in urban design.

Also noteworthy is the work of Lacy (1972) and Chandler (1976), who, again alongside the WMO, developed a report on the relevance of urban climate in the design of cities. In the same year, Page (1976) published another work on the importance of climate for building design, incorporating the urban climate perspective. In 1980, Page would elaborate on how urban and building design should be approached, arguing that *Urbanism needs a sounder energy base, enlivened by proper climatological awareness (Page, 1980, p. 73).*

However, the transfer of climate knowledge to the urban development has not happened at the pace that would have been desirable. Page himself mentioned the *architectural educational gap* (Page, 1980, p. 84). Other leading researchers also warned about this lack of knowledge transfer to architecture and urban planning professionals (e.g., Oke, 1984). And, although the publication of studies on this topic has been relatively constant and there are strategies and tools already known and applied (e.g., Barlag and Kuttler, 1990; Cartalis, 2014; Eliasson, 2000; Erell, 2008; Kleerekoper et al., 2012; Lenzholzer et al., 2020), today there are still certain barriers that limit the knowledge transfer.

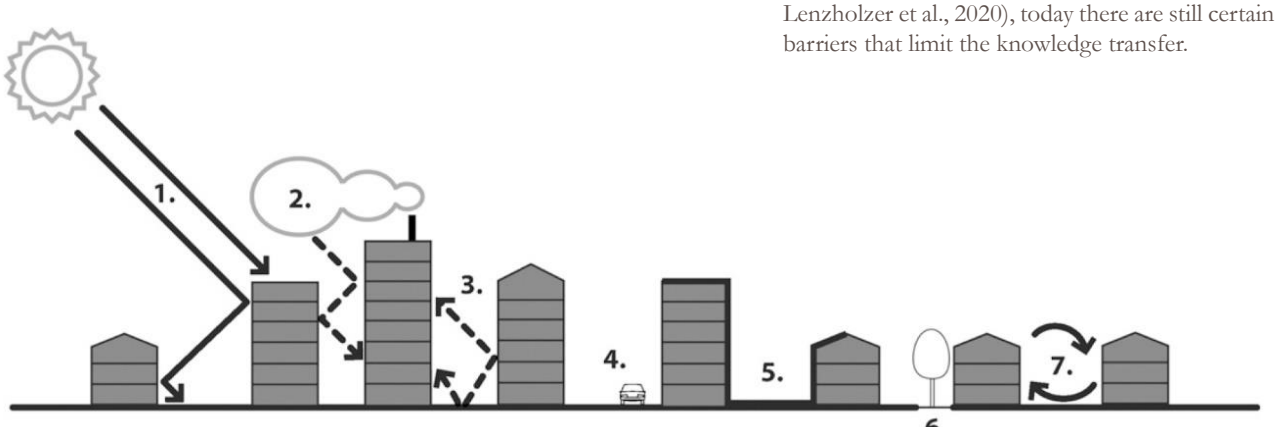

Figura 1.4 Causas de la formación de la isla de calor, de acuerdo con Kleerekoper (2012). *(1) Absorción de radiación de onda corta por superficies y materiales urbanos; (2) Absorción de radiación de onda larga y reirradiación por contaminación; (3) Bloqueo de la irradiación de onda larga a la atmósfera por la estructura urbana;(4) Emisión de calor antropogénico; (5) Acumulación de calor por superficies urbanas artificiales, de mayor admitancia térmica; (6) Reducción de la evaporación por ausencia de vegetación y mayor cantidad de superficies impermeables; (7) Reducción de la disipación de calor por menor velocidad de viento.*

Figure 1.4 Causes of urban heat island formation, according to Kleerekoper et al. (2012). (1) Absorption of shortwave radiation by urban surfaces and materials; (2) Absorption of longwave radiation and re-radiation by pollution; (3) Blocking of longwave irradiation to the atmosphere by the urban structure; (4) Anthropogenic heat emission; (5) Heat accumulation by artificial urban surfaces with higher thermal admittance; (6) Reduced evaporation due to the absence of vegetation and more impervious surfaces; (7) Reduced heat dissipation due to lower wind speed. After Kleerekoper et al. (2012)

In this regard, De Schiller and Evans (1996) pointed out a long time ago that there is a clear limitation in the degree of detail and complexity that the architect and planner can (and need to) assimilate as input to the design process. They noted that they are *not likely to wait for data that takes time to collect or process. They will only take into account data that is clearly presented* (De Schiller and Evans, 1996, p. 452). This must now also be understood in the context of the computational tools that are used in both disciplines, which allow, among other things, both the modelling of the urban climate and the assessment of the buildings' energy performance.

1.4. Climate change and building energy modelling

In June 2021, the European Union adopted the *European Climate Law* (Regulation (EU) 2021/1119). This law follows on from a long series of European policies and initiatives that have been accelerating since the *Paris Agreement* was adopted (FCCC/CP/2015/L.9/ Rev.1), such as the *European Green Pact* (COM(2019) 640) or the *European Climate Pact* (COM(2020) 788), and which are an example of the European Union's commitment to climate neutrality in the fight against climate change. In this sense, the European Climate Law establishes that, by mid-century, net greenhouse gas emissions must be equal to zero; and, by 2030, these must be reduced by 55% compared to 1990.

The building sector plays a central role in fulfilling this commitment, which is binding for all EU countries. 35% of European buildings are more than 50 years old, and it is estimated that 75% are inefficient. There is great potential for improvement, which is why energy renovation has become one of the major objectives in the fight against climate change. The recent European initiative known as the *renovation wave* (COM(2020) 662) is a clear example of this.

It should be noted that a focus on improving the buildings' energy performance not only has potential for reducing greenhouse gas emissions. It also has the potential to ensure minimum living conditions, which are increasingly difficult to achieve for the most vulnerable people, who face increasingly variable and rising energy prices. Mitigating energy poverty is also one of the *raisons d'être* of this trend towards more efficient buildings (Recommendation (EU) 2020/1563).

Among the tools available for assessing the energy performance of buildings, energy simulation is one of the most widespread and versatile (BEM, for Building Energy Modelling). These emerged during the 1960s (Brown, 1990; Kusuda, 1999), although it was not until the 1970s that they began to become popular. Shearer & Bromberg (1977), for example, compiled up to 16 alternatives in

herramientas ya conocidas y aplicadas (véase, p. ej., Barlag and Kuttler, 1990; Cartalis, 2014; Eliasson, 2000; Erell, 2008; Kleerekoper et al., 2012; Lenzholzer et al., 2020), hoy en día siguen existiendo ciertas barreras que limitan la transferencia de este conocimiento.

En este sentido, De Schiller y Evans (1996) apuntaban hace tiempo a que existen limitaciones en el grado de detalle y complejidad que profesionales de la arquitectura y el urbanismo pueden utilizar como 'inputs'. Señalaban que *no es probable que esperen a recibir datos que tardan en ser recogidos o procesados. Sólo tendrán en cuenta los datos que se presenten claramente* (De Schiller and Evans, 1996, pág. 452). Esto debe hoy entenderse, además, en el contexto de las herramientas informáticas que se utilizan en ambas disciplinas, y que permiten, entre otras cosas, evaluar el comportamiento energético de los edificios.

1.4. El cambio climático y la simulación energética de edificios

En junio de 2021, la Unión Europea aprobó la Ley Europea del Clima (Reglamento (UE) 2021/1119). Esta ley da continuidad a una larga serie de políticas e iniciativas europeas que se han venido acelerando desde que se aprobara el Acuerdo de París (Resolución FCCC/CP/2015/L.9/Rev.1), tales como el Pacto Verde Europeo (COM(2019) 640) o el Pacto Europeo por el Clima (COM(2020) 788), y que son un ejemplo del compromiso con la neutralidad climática de la Unión Europea en la lucha contra el cambio climático. En este sentido, la Ley Europea del Clima establece que, para mediados de siglo, las emisiones netas de gases de efecto invernadero deben ser iguales a cero; y, para 2030, éstas deberán haberse reducido un 55% con respecto a 1990.

En el cumplimiento de este compromiso, vinculante para todos los países de la Unión, el sector de la edificación tiene un papel central. El 35% de los edificios europeos tienen más de 50 años, y se estima que el 75% son ineficientes. Existe un gran potencial de mejora, motivo por el cual la rehabilitación energética se ha convertido en uno de los grandes caballos de batalla contra el cambio climático. La reciente iniciativa europea llamada *oleada de renovación* (*renovation wave*, COM(2020) 662) es un claro ejemplo de ello.

Debe señalarse que poner el foco en la mejora del comportamiento energético de los edificios no sólo tiene potencial como medida para reducir las emisiones de gases de efecto invernadero. También lo es como garante de unas condiciones de habitabilidad mínimas, cada vez más difíciles de conseguir para la población más vulnerable, la cual se enfrenta a unos precios de la energía más volátiles y en continuo ascenso. Mitigar la pobreza energética es, también, una de las razones de ser de esta tendencia hacia una edificación más eficiente (Recomendación (UE) 2020/1563).

De entre las herramientas disponibles para evaluar el comportamiento energético de la edificación, la simulación energética es de

las más extendidas y versátiles (BEM, por *Building Energy Modeling*). Estas surgieron durante los años 60 (Brown, 1990; Kusuda, 1999), aunque no fue hasta los años 70 cuando comenzaron a popularizarse. Shearer & Bromberg (1977), por ejemplo, recopilaron hasta 16 alternativas en los Estados Unidos. En esa década se gestaron tres de las herramientas BEM más conocidas hoy en día: TRNSYS (Klein et al., 1976, 1975), BLAST (Hittle, 1979) y DOE-2 (York and Tucker, 1980). Estas dos últimas se unificaron posteriormente en EnergyPlus (Crawley et al., 2001, 2000, 1999b, 1998) y, al igual que TRNSYS, se ha convertido prácticamente en la herramienta estándar a la hora de realizar simulaciones energéticas. Otras alternativas menos conocidas son HTB2 (Lewis and Alexander, 1990), PLEIADES (Peuportier and Sommereux, 1990) o el más reciente BuildSysPro (Plessis et al., 2014).

Aunque las herramientas BEM han progresado enormemente desde que se plantearan por primera vez, mejorando los algoritmos de cálculo y extendiéndolos a ámbitos como la mecánica de fluidos computacional (CFD, Foucquier et al., 2013), los resultados obtenidos de la simulación a menudo se alejan de los valores observados. Esta brecha del comportamiento energético (*energy performance gap*) entre realidad y simulación es uno de los temas más tratados de los últimos años (Coakley et al., 2014; Cuerda et al., 2020; De Wilde, 2014; Fumo, 2014; Gram-Hanssen and Georg, 2018; Johnston et al., 2015; Palma et al., 2019; van den Brom et al., 2018). En este sentido, Cozza et al. (2021) distingue entre las desviaciones reales (debidas, por ejemplo, al mal funcionamiento de los sistemas o un uso poco óptimo por parte de los usuarios) y las desviaciones teóricas (debidas a imprecisiones en la simulación energética). Éstas quedan resumidas en la **Figura 1.5** y, entre las desviaciones teóricas, destacan tres causas fundamentales: las suposiciones adoptadas durante la modelización del edificio, la imprecisa definición del perfil de los usuarios, y la incorrecta contextualización climática.

the United States. In that decade, three of today's best-known BEM tools were developed: TRNSYS (Klein et al., 1976, 1975), BLAST (Hittle, 1979) and DOE-2 (York and Tucker, 1980). The latter two were later merged into EnergyPlus (Crawley et al., 2001, 2000, 1999b, 1998) and, like TRNSYS, have become almost the standard tool for energy simulations. Less well-known alternatives are HTB2 (Lewis and Alexander, 1990), PLEIADES (Peuportier and Sommereux, 1990) or the more recent BuildSysPro (Plessis et al., 2014).

Although BEM tools have made great progress since they were first proposed, improving calculation algorithms and extending them to areas such as computational fluid dynamics (CFD, Foucquier et al., 2013), the results obtained from simulation are often far from the observed values. This energy performance gap between reality and simulation is one of the most discussed topics in recent years (Coakley et al., 2014; Cuerda et al., 2020; De Wilde, 2014; Fumo, 2014; Gram-Hanssen and Georg, 2018; Johnston et al., 2015; Palma et al., 2019; van den Brom et al., 2018). In this regard, Cozza et al. (2021) distinguish between real (actual) deviations (due to, for example, malfunctioning systems or sub-optimal use by users) and theoretical deviations (due to inaccuracies in the energy simulation). These are summarised in **Figure 1.5** and, among the theoretical deviations, three main causes stand out: assumptions made during the modelling of the building, inaccurate definition of the user profile, and incorrect climate contextualisation.

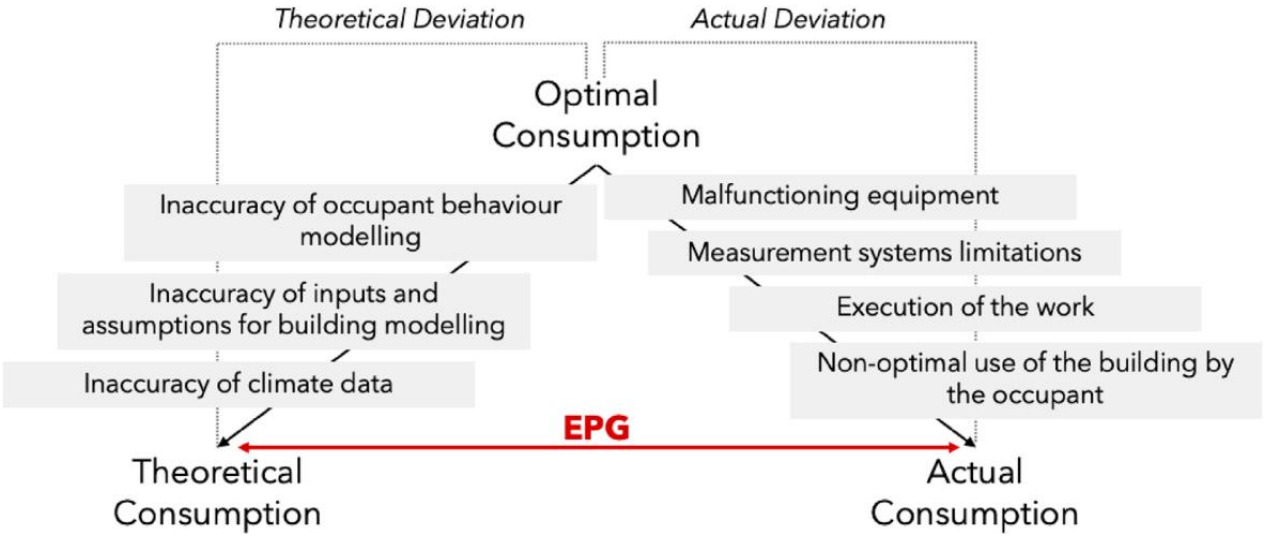

Figura 1.5 Principales causas de la brecha del comportamiento energético (energy performance gap, EPG) en las herramientas de simulación energética de edificios, según Cozza et al. (2021).

Figure 1.5 Main drivers of the energy performance gap (EPG) in building energy simulation tools, according to Cozza et al. (2021)

In building energy simulation, the climate contextualisation is carried out by means of a weather file. This contains all (or most) of the climate information relevant for the energy assessment, from outdoor air temperature to solar radiation, wind speed, cloud cover or atmospheric pressure. They usually contain hourly weather information for a meteorologically typical year, but are also developed for extreme weather conditions (e.g., design summer years (Eames, 2016) or extreme weather files (Crawley and Lawrie, 2019, 2015)). Today, there are several databases of weather files, most of them with records for thousands of locations around the globe (see, for example, the databases of OneBuilding (2018) or EnergyPlus (U.S. Department of Energy, 2003)).

There are, however, some problems with these files. One of the most obvious is that their development is based on the assumption of a stationary climate: they synthesise a representative year from a period that usually covers several decades in the past. In the current context of climate change, this can introduce a large mismatch between the conditions represented in the weather file and those observed in the present, feeding directly into the energy simulation, and contributing to the energy performance gap (Crawley and Lawrie, 2021; Erba et al., 2017; Kočí et al., 2019).

In addition, the energy assessment is carried out at the beginning of a building's lifetime (whether refurbished or newly constructed) and is expected to last for several decades. The energy assessment of buildings should perhaps include a prospective view, anticipating the future climate context of this building. To this end, work has been carried out in recent years on the generation of future *weather files,* mainly through morphing: the adaptation of existing weather files using global climate models that predict future climate conditions (Belcher et al., 2005; Herrera et al., 2017; Jentsch et al., 2013, 2008).

Finally, another source of uncertainty lies in the origin of the data used to generate the weather files. The vast majority of these data come from meteorological observatories. And while the quality of these data is undisputed, their representativeness could be questioned, especially when it comes to analysing the energy performance of buildings in urban environments. It should be noted that, in general, the weather observatories closest to cities are located at their airports. They tend to be located on the outskirts of cities and therefore avoid the climatic particularities of an urban climate. This has been found in numerous studies to date, especially with regard to the heat island effect (e.g., Akbari and Konopacki, 2005; Allegrini et al., 2012; Kolokotroni et al., 2012, 2010; Mavrogianni et al., 2011; Salvati et al., 2017; Skelhorn et al., 2016; Yang et al., 2020b).

En la simulación energética de edificios, la contextualización climática se realiza a través de un archivo climático. Éste contiene toda (o gran parte) de la información climática relevante para la evaluación energética, desde la temperatura del aire exterior hasta la radiación solar, pasando por la velocidad del viento, la nubosidad o la presión atmosférica. Acostumbran a contener información climática horaria para un año meteorológicamente típico, aunque también se desarrollan para condiciones climáticas extremas (p. ej., los *design summer years* (Eames, 2016) o los *extreme weather files* (Crawley and Lawrie, 2019, 2015)). Hoy en día existen diversas bases de datos de archivos climáticos, la mayoría con registros para miles de ubicaciones distribuidas por todo el planeta (véanse, por ejemplo, las bases de datos de OneBuilding (2018) o de EnergyPlus (U.S. Department of Energy, 2003)).

Estos archivos presentan, sin embargo, algunos problemas. Uno de los más evidentes es que su desarrollo se sustenta en la premisa de un clima estacionario: sintetizan un año representativo a partir de un periodo que, por lo general, suele cubrir varias décadas pasadas. En el contexto actual de cambio climático, esto puede introducir un gran desfase entre las condiciones representadas en el archivo climático y las observadas en el presente, trasladándose de forma directa a la simulación energética, y contribuyendo a la brecha del comportamiento energético (Crawley and Lawrie, 2021; Erba et al., 2017; Kočí et al., 2019).

A esto hay que sumar que la evaluación energética se realiza al inicio de la vida útil de un edificio (ya sea este rehabilitado o de nueva construcción), y que se espera que ésta se extienda durante varias décadas más. La evaluación energética de los edificios quizás debería incluir una mirada prospectiva, anticipándose al contexto climático futuro de esta edificación. Para ello, en los últimos años se viene trabajando en la generación de archivos climáticos futuros (*future weather files*), principalmente a través de la técnica del *morphing*: la adaptación de los archivos climáticos existentes mediante modelos climáticos globales que predicen las condiciones climáticas futuras (Belcher et al., 2005; Herrera et al., 2017; Jentsch et al., 2013, 2008).

Por último, otra fuente de incertidumbre se encuentra en el origen de los datos empleados para la generación de los archivos climáticos. Estos proceden, en su gran mayoría, de observatorios meteorológicos. Y, si bien la calidad de estos datos es indiscutible, su representatividad podría ser cuestionada, especialmente cuando se trata de analizar el comportamiento energético de los edificios en entornos urbanos. Debe tenerse en cuenta que, por lo general, los observatorios meteorológicos más próximos a las ciudades se sitúan en sus aeropuertos. Estos tienden a situarse en las afueras de las ciudades y, por lo tanto, esquivan las particularidades climáticas propias del clima urbano. Así lo han constatado numerosos estudios hasta la fecha, especialmente en cuanto al efecto de la isla de calor se refiere (p. ej., Akbari and Konopacki, 2005; Allegrini et al., 2012; Kolokotroni et al., 2012, 2010; Mavrogianni et al., 2011; Salvati et al., 2017; Skelhorn et al., 2016; Yang et al., 2020b).

1.5. La isla de calor en la simulación energética de edificios

La isla de calor, al igual que las otras componentes del clima urbano, ha sido constante y sistemáticamente obviada en la simulación energética de edificios. Dado que el interés por estudiar su efecto sobre la edificación es relativamente reciente y posterior, por tanto, al desarrollo de las herramientas de simulación, su integración no resulta en ningún caso directa ni sencilla. Los trabajos de Rodler et al. (2021) y Lauzet et al. (2019) dan cuenta de los últimos esfuerzos realizados para evaluar la influencia del contexto urbano en el comportamiento energético de edificios, algunos de los cuales se detallan a continuación.

La primera aproximación podría consistir en ampliar la escala de la simulación energética para que esta incluya una parte del contexto urbano, pasando así del BEM (*Building Energy Modelling*) al UBEM (*Urban Building Energy Modelling*; Lauzet et al., 2019; Reinhart and Cerezo Davila, 2016). En el UBEM existen diferentes formas de modelar el intercambio energético, generalmente diferenciadas entre aproximaciones *top-down* y *bottom-up* (Li et al., 2017). Estas últimas son las más populares y las que más fácilmente puede compararse con el BEM. Entre las opciones más conocidas se encuentran SimStadt (Nouvel et al., 2015), CityBES (Hong et al., 2016), UMI (Reinhart et al., 2013), TEASER (Remmen et al., 2018), OpenIDEAS (Baetens et al., 2015) o UrbanOPT (Polly et al., 2016). Así, si en el BEM se puede modelar el consumo energético de un único edificio de forma aislada, en el UBEM se puede modelar el consumo de un conjunto de edificios teniendo en cuenta las interacciones entre ellos y su entorno inmediato.

El UBEM, sin embargo, resulta más complejo que el BEM durante la fase de modelización, lo que puede constituir una barrera para algunos profesionales. Además, dado que el enfoque del UBEM es urbano, el grado de detalle con el que se suele caracterizar a los edificios es menor que en el BEM. Esto puede llegar a ser problemático si se busca tener en cuenta las diferencias intra-edificio, ya que su precisión en esta escala puede no ser suficiente. Por último, aunque muchos UBEM son capaces de modelar parte del intercambio energético entre los edificios y su entorno inmediato, esto no parece ser suficiente para capturar el efecto de la isla de calor (Hong et al., 2020). De hecho, en el UBEM, al igual que en el BEM, también se utiliza un archivo climático para la contextualización.

Una forma de superar esta limitación consiste en sustituir la información de los archivos climáticos por la procedente de modelos climáticos urbanos (*Urban Climate Models,* UCMs; (Best and Grimmmmond, 2015; Grimmond et al., 2011, 2010)). De entre los UCMs, algunas de las opciones más conocidas son el modelo *Building Effect Parameterisation* (BEP, Martilli et al., 2002), el *Town Energy Balance* (TEB, Masson, 2000), o el *Single-Layer Canopy Model* (SLCM, Kondo and Liu, 1998) los cuales son capaces de modelar el balance energético de las ciudades a partir de los datos procedentes de los modelos mesoclimáticos

1.5. The urban heat island in building energy simulation

The urban heat island, like the other components of the urban climate, has been consistently and systematically ignored in building energy simulation. Given that the interest in studying its impact on buildings is relatively recent and, therefore, subsequent to the development of simulation tools, its integration is by no means straightforward or simple. The works of Rodler et al. (2021) and Lauzet et al. (2019) report on recent efforts to assess the influence of the urban context on the energy performance of buildings, some of which are detailed below.

The first approach could be to scale up the energy simulation to include part of the urban context, thus moving from BEM (*Building Energy Modelling*) to UBEM (*Urban Building Energy Modelling*; Lauzet et al., 2019; Reinhart and Cerezo Davila, 2016). In UBEM, there are different ways of modelling energy exchange, generally differentiated between *top-down* and *bottom-up* approaches (Li et al., 2017). The latter are the most popular and can be most easily compared to BEM. Among the best known options are SimStadt (Nouvel et al., 2015), CityBES (Hong et al., 2016), UMI (Reinhart et al., 2013), TEASER (Remmen et al., 2018), OpenIDEAS (Baetens et al., 2015) or UrbanOPT (Polly et al., 2016). Thus, if in BEM it is possible to model the energy consumption of a single building in isolation, in UBEM it is possible to model the consumption of a set of buildings considering the interactions between them and their immediate environment.

UBEM, however, is more complex than BEM during the modelling phase, which can be a barrier for some practitioners. In addition, as the focus of UBEM is urban, the level of detail with which buildings are often characterised is less detailed than in BEM. This can become problematic if intra-building differences are to be taken into account, as their accuracy at this scale may not be sufficient. Finally, although many UBEMs are able to model part of the energy exchange between buildings and their immediate surroundings, this does not seem to be sufficient to capture the urban heat island effect (Hong et al., 2020). In fact, in UBEM, as in BEM, a climate file is also used for contextualisation.

One way to overcome this limitation is to replace the data from weather files with data from *Urban Climate Models* (UCMs; Best and Grimmmmond, 2015; Grimmond et al., 2011, 2010). Among the UCMs, some of the best known options are the *Building Effect* Parameterisation (BEP, Martilli et al., 2002), the *Town Energy Balance* (TEB, Masson, 2000), or the *Single-Layer Canopy Model* (SLCM, Kondo and Liu, 1998) which are able to model the energy balance of cities based on data from the mesoclimatic models *Weather Research and Fore-*

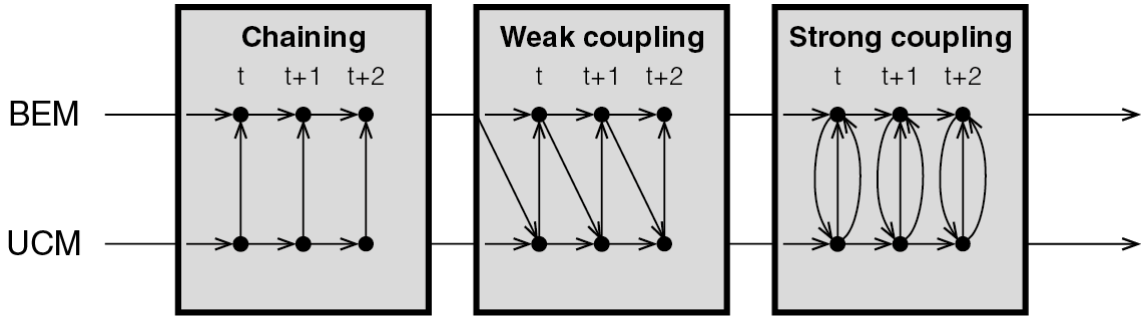

Figura 1.6 Representación esquemática de los tres tipos de acoplamiento entre modelos BEM y modelos UCM, según Rodler et al. (2021), a su vez a partir de Lauzet et al. (2019). El más sencillo consiste en el encadenado de los modelos, donde la información fluye en unidireccionalmente, desde el UCM al BEM. En el acoplamiento débil, los modelos se retroalimentan mutuamente, pero afectando únicamente a las simulaciones subsiguientes. Por último, en el acoplamiento fuerte, la retroalimentación se produce dentro de la misma simulación, de forma iterativa.

Figure 1.6 Schematic representation of the three types of coupling between BEM models and UCM models (after Rodler et al., 2021, following Lauzet et al., 2019). The simplest is the chaining of the models, where information flows unidirectionally from the UCM to the BEM. In weak coupling, the models feed back to each other, but only affecting subsequent simulations. Finally, in strong coupling, the feedback occurs within the same simulation, iteratively.

casting (WRF, Skamarock et al., 2019, 2008, 2005), Meso-NH (Lac et al., 2018; Lafore et al., 1998), or NIRE-MM (Kondo, 1995), respectively. In this way, the coupling or chaining of several models at different levels takes place, converting the outputs of some models into the inputs of others.

Examples of this second approach are the WRF+BEP+BEM08 coupling proposed by Salamanca et al. (2010a; 2010b), the NIRE-MM+SLCM+BEM developed by Kikegawa (2003), or the CCLM+DCEP+BEM recently introduced by Jin et al. (2021). In these, a specific BEM was developed for its integration in this type of chained modelling, and it is, in fact, a simplification of the BEM models typically used for the energy assessment of buildings. Other studies have attempted to couple detailed BEM models, such as Bueno et al. (2011), where a model developed in EnergyPlus is used. However, the limitations of this approach are related to the high computationa l cost, which reduces its technical feasibility to carry out hourly simulations over a year (Mao and Norford, 2021).

Technical limitations are also the main problem that the research community has faced when trying to couple BEMs to CFD-based microclimatic models, such as ENVI-met (Bruse and Fleer, 1998), FLUENT (Boysan et al., 1982) or SOLENE-Microclimat (Musy et al., 2015). Thus, there are examples coupling FLUENT with EnergyPlus (Zhang et al., 2013) or with TRNSYS (Barbason and Reiter, 2014); coupling ENVI-met with EnergyPlus (Yang et al., 2012) or with HTB2 (Deng et al., 2016); or also coupling SOLENE-Microclimat with DANA (Rodler et al., 2018) or with BuildSysPro (Merlier et al., 2019a, 2019b). However, none of them carry out simulations lasting longer than several days, which is a clear limitation for the building energy evaluation.

Weather Research and Forecasting (WRF, Skamarock et al., 2019, 2008, 2005), *Meso-NH* (Lac et al., 2018; Lafore et al., 1998), o *NIRE-MM* (Kondo, 1995), respectivamente. De este modo, se produce el acople o encadenamiento de varios modelos a distinto nivel, convirtiendo las salidas de unos en las entradas de otros.

Un ejemplo de esta segunda aproximación son el acoplamiento WRF+BEP+BEM08 planteado por Salamanca et al. (2010a; 2010b), el NIRE-MM+SLCM+BEM desarrollado por Kikegawa (2003), o el CCLM+DCEP+BEM recientemente introducido por Jin et al. (2021). En ellos, el BEM utilizado se ha desarrollado para su integración en este tipo de modelización encadenada y es, en realidad, una simplificación de los modelos BEM típicamente empleados para la evaluación energética de edificios. Otros estudios han intentado acoplar modelos BEM detallados, como Bueno et al. (2011), donde se utiliza un modelo desarrollado en EnergyPlus. Sin embargo, las limitaciones de este enfoque residen en que tiene un coste computacional demasiado elevado, lo que reduce su viabilidad técnica para llevar a cabo simulaciones horarias a lo largo de un año (Mao and Norford, 2021).

Las limitaciones técnicas son también el principal problema al que se ha enfrentado la comunidad investigadora al tratar de acoplar BEMs a modelos microclimáticos basados en CFD, como ENVI-met (Bruse and Fleer, 1998), FLUENT (Boysan et al., 1982) o SOLENE-Microclimat (Musy et al., 2015). Así, existen ejemplos acoplando FLUENT con EnergyPlus (Zhang et al., 2013) o con TRNSYS (Barbason and Reiter, 2014); acoplando ENVI-met con EnergyPlus (Yang et al., 2012) o con HTB2 (Deng et al., 2016); o también acoplando SOLENE-Microclimat con DANA (Rodler et al., 2018) o con BuildSysPro (Merlier et al., 2019a, 2019b). Sin embargo, ninguno de ellos lleva a cabo simulaciones con una duración superior a varios días, lo que supone una clara limitación para la evaluación energética de edificios.

Si las necesidades de computación dificultan la interrelación entre UCMs y BEMs detallados, la solución puede pasar por una integración menos directa. De este modo surgen los enfoques orientados hacia el desarrollo de modelos UCM para la adaptación de los archivos climáticos al contexto urbano, los cuales son posteriormente empleados en la simulación energética de edificios. Se trata de aplicar la técnica del *morphing* descrita en el apartado anterior, aunque cambiando el objetivo: en lugar de adaptar archivos climáticos a las condiciones climáticas futuras, estos se ajustan a las condiciones climáticas urbanas.

Por un lado, *Meteonorm* (Remund et al., 2020a, 2020b), un programa ampliamente utilizado para la obtención de información climática alrededor del mundo, incluye en sus últimas versiones el modelo *UrbClim* (De Ridder et al., 2015). Este ofrece la opción de adaptar los archivos climáticos al contexto urbano, aunque sólo para algunas zonas urbanas. Por otro lado, el *Urban Weather Generator* (UWG, Bueno et al., 2013; véase la **Figura 1.7**) plantea un modelo UCM parametrizado que adapta los valores de temperatura, humedad y viento a las condiciones urbanas. Éste sí que se puede emplear en cualquier ciudad y ha sido testeado tanto con TRNSYS (Palme et al., 2017) como con EnergyPlus (Salvati et al., 2017). Otro ejemplo parecido de modelo que aplique la técnica del *morphing* es el *Canyon Air Temperature* (CAT, Erell and Williamson, 2006), aunque este únicamente se centra en la adaptación de la temperatura.

Desarrollar modelos para aplicar la técnica del morphing y así generar archivos climáticos ajustados a las condiciones climáticas urbanas parece, a día de hoy, la opción más realista para trasladar el efecto de la isla de calor a la simulación energética (Evola et al., 2018; Palme and Salvati, 2021b). Sin embargo, trabajar con modelos numéricos como los descritos en el párrafo anterior podría presentar algunas limitaciones.

Quizás la más relevante tiene que ver con la definición del punto de referencia. Estos modelos utilizan los datos del archivo climático como referencia, asumiendo que estos proceden de un punto rural (no urbano), situado fuera de la ciudad. Esto les permite generar las condiciones de contorno para su modelo climático. Aunque ya se ha señalado que la mayoría de los archivos climáticos proceden de observatorios meteorológicos situados en las afueras de la ciudad, esto no significa que éstos puedan ser considerados rurales. La propia definición como *rural* de muchos observatorios es cuestionable, tal y como señala Stewart (2011). En Madrid, por ejemplo, los registros de temperatura obtenidos en tres observatorios situados en las afueras (Barajas, Cuatro Vientos y Ciudad Universitaria) son muy diferentes entre sí, lo que podría originar diferencias significativas en la modelización de archivos climáticos urbanos.

Determinar los valores de los parámetros característicos que permiten inicializar el modelo también parece ser una barrera para su aplicación. No sólo porque, con alrededor de 50 variables (como en

If computational requirements make the interrelation between UCMs and detailed BEMs difficult, a less direct integration may be the solution. This led to the development of UCM models for the adaptation of weather files to the urban context, which are then used in building energy simulation. This involves applying the *morphing* technique described in the previous section, but changing the objective: instead of adapting weather files to future climatic conditions, they are adjusted to urban climatic conditions.

On the one hand, *Meteonorm* (Remund et al., 2020a, 2020b), a widely used programme for obtaining climate information around the world, includes in its latest versions the UrbClim model (De Ridder et al., 2015). It offers the option to adapt the weather files to the urban context, although only for some urban areas. On the other hand, the *Urban Weather Generator* (UWG, Bueno et al., 2013; see Figure 19.6) provides a parameterised UCM model that adapts temperature, humidity and wind values to urban conditions. This model can be used in any city and has been tested with both TRNSYS (Palme et al., 2017) and EnergyPlus (Salvati et al., 2017). Another similar example of a model using *morphing* is *Canyon Air Temperature* (CAT, Erell and Williamson, 2006), although this one only focuses on temperature adaptation.

Developing models to *morph* weather files adjusted to urban climate conditions seems, at present, the most realistic option to translate the urban heat island effect into energy simulation (Evola et al., 2018; Palme and Salvati, 2021b). However, working with numerical models as described in the previous paragraph might have some limitations.

Perhaps the most relevant has to do with the definition of the reference point. These models use the data from the weather file as a reference, assuming that the data comes from a rural (non-urban) point outside the city. This allows them to generate the boundary conditions for their climate model. Although it has already been pointed out that most weather files come from weather observatories located outside the city, this does not mean that they can be considered rural. The very definition of many observatories as rural is questionable, as Stewart (2011) points out. In Madrid, for example, the temperature records obtained in three observatories located in the outskirts (Barajas, Cuatro Vientos and Ciudad Universitaria) are very different from each other, which could lead to significant differences in the modelling of urban weather files.

Determining the characteristic parameter values to initialise the model also seems to be a barrier to its implementation. Not only because, with around 50 variables (as in the case of the UWG), setting

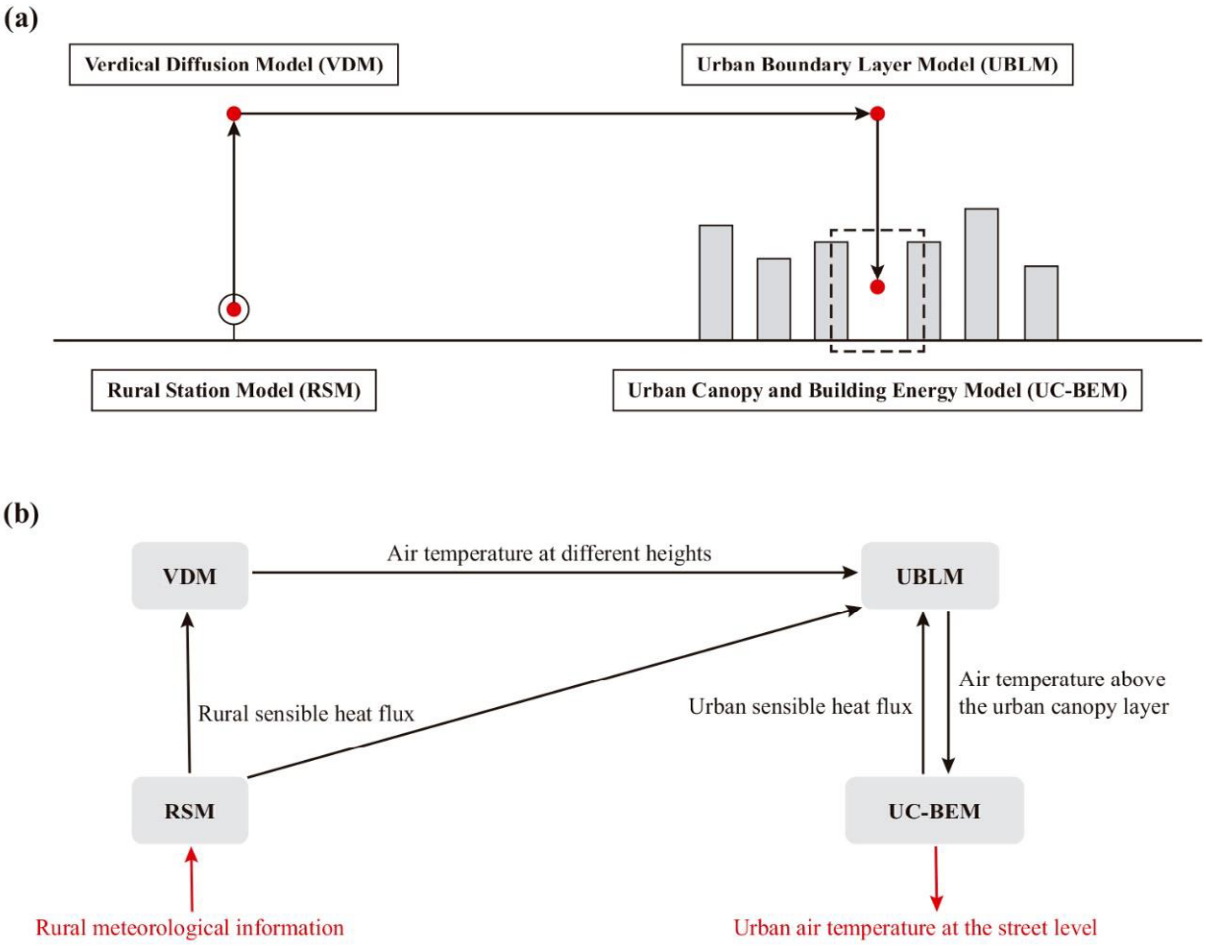

Figura 1.7 Representación esquemática de los módulos que forman parte del modelo Urban Weather Generator (Bueno et al., 2013). *La entrada de datos se realiza a través de la* Rural Station Model *(RSM) a partir de un archivo climático. En este modelo se asume que el archivo climático proviene de un observatorio meteorológico rural. Según Mao y Norford (2021).*

Figure 1.7 Schematic representation of the modules that are part of the Urban Weather Generator model (Bueno et al., 2013). The data input is done through the Rural Station Model (RSM) from a weather file. In this model it is assumed that the climate file comes from a rural weather observatory. After Mao and Nordford (2021)

it up correctly can be challenging. Also because it is complicated to decide which characteristic parameters should be adopted as representative for each urban area that make up the city, as well as how many of them should be distinguished. In this regard, previous studies seem to have focused on obtaining a single urban weather file, adjusted to a specific context, and not on obtaining a battery of weather files, representative of the entire urban context.

One last alternative are empirical models. These differ from numerical models since, instead of modelling the physical processes that determine the energy exchange to obtain a certain value (*bottom-up* approach), they approximate it through the generalisation of the existing statistical correlations between the available data (*top-down* ap-

el caso del UWG), configurarlo correctamente pueda ser un reto. También porque resulta complicado decidir los valores que tomarían los parámetros característicos de las distintas zonas urbanas que componen la ciudad, así como cuántas de ellas deberían distinguirse. En este sentido, parece que los estudios previos consultados se han centrado en la obtención de un único archivo climático urbano, ajustado a un contexto específico, y no en la obtención de una batería de archivos climáticos que sean representativos de todo el contexto urbano.

Como última alternativa se presentan los modelos empíricos. Éstos se diferencian de los modelos numéricos en que, en lugar de modelar los procesos físicos que determinan el intercambio energético para obtener un determinado valor (aproximación *bottom-up*), consiguen aproximarlo a través de la generalización de las correlaciones estadísticas existentes entre los datos disponibles (aproximación *top-down*, también

conocido como *data-driven approach*). Una regresión lineal representaría el ejemplo más sencillo de este tipo de modelos. Hoy en día, sin embargo, el desarrollo de la inteligencia artificial es el que ha motivado el desarrollo y adopción de este tipo de modelos con el fin de modelar el efecto de la isla de calor (e.g., (Cellura et al., 2011; Kolokotroni et al., 2010, 2009, 2007; Lee et al., 2016; Mihalakakou et al., 2002, 1998; Papantoniou and Kolokotsa, 2016; Schuch et al., 2017)

Utilizar este tipo de modelos para la obtención de archivos climáticos urbanos parece ser algo todavía por explorar. En esta línea únicamente se ha podido encontrar una investigación, publicada muy recientemente (Han et al., 2021), en la que se plantea la utilización de redes neuronales artificiales para este fin. Si bien este trabajo representa un ejemplo del potencial de este tipo de aproximaciones, se centra en la modelización del archivo climático en un único punto. Siguen pendientes, por tanto, cuestiones relativas a la representatividad del archivo climático desarrollado, así como a la misma viabilidad de utilizar este tipo de enfoques de forma sistemática para incorporar, de forma efectiva e integral, el efecto de la isla de calor en la simulación energética de edificios.

proach, also known as *data-driven approach*). A linear regression would represent the simplest example of this type of model. Nowadays, however, it is the development of artificial intelligence that has motivated the adoption of this type of approach for modelling the urban heat island effect (e.g., (Cellura et al., 2011; Kolokotroni et al., 2010, 2009, 2007; Lee et al., 2016; Mihalakakou et al., 2002, 1998; Papantoniou and Kolokotsa, 2016; Schuch et al., 2017).

Using this type of models to obtain urban weather files seems to be yet to be explored. In this regard, only one recently published study (Han et al., 2021) considering the use of artificial neural networks was found. Although this work represents an example of the potential of this type of approach, it focuses on morphing a weather file at a single point. Questions remain regarding the representativeness of the developed weather file, as well as the feasibility of systematically using such approaches to effectively and comprehensively incorporate the urban heat island effect into building energy simulation.

2. Hypothesis and objectives

2.1. Hypothesis

In the introduction, several aspects were highlighted regarding the relationship between climate and the city, the dimension of the urban heat island phenomenon, and the uncertainty that it may be introducing in the building energy evaluation. From this point it is formulated the hypothesis that **it is possible to empirically and comprehensively characterise the urban heat island effect by generating weather files in order to improve the building energy evaluation in urban environments**.

The stated hypothesis includes two relevant aspects regarding the characterisation. First, it is intended to be empirical. That is, based on real data derived from a monitoring campaign. This entails a series of challenges different from those that could be encountered when using numerical models, based on the formulation of the physical processes that govern urban energy exchanges, the development of which seems to be more advanced. It is understood that an empirical approach, even if it results in a less universal application, is a more realistic approximation to the traditional procedures for generating weather files. Furthermore, this approach can contribute to greater precision and certainty when linking the weather files to the different urban realities existing in the city.

The second claim of this hypothesis is that the characterisation of the urban heat island through weather files must be comprehensive. This means that, to fulfil this hypothesis, the proposed solution must consider the municipality as a whole. Thus, it cannot focus exclusively on the areas where the intensity of the heat island is highest, nor can it be limited exclusively to the hours when the intensity of the heat island is highest. The urban heat island is understood as a continuous phenomenon between urban and non-urban environments; the urban heat island is understood as a dynamic phenomenon that encompasses all dimensions of urban heat.

2. Hipótesis y objetivos

2.1. Hipótesis

En la introducción se han destacado varios aspectos relativos a la relación entre el clima y la ciudad, la dimensión del fenómeno de la isla de calor, y la incertidumbre que ésta puede estar introduciendo en la evaluación energética de edificios. A partir de este punto se formula la hipótesis de que **es posible caracterizar empírica e integralmente el efecto de la isla de calor mediante la generación de archivos climáticos con el fin de mejorar la evaluación energética de edificios en entornos urbanos.**

La hipótesis enunciada incluye dos aspectos relevantes sobre la caracterización. Primero, se pretende que ésta sea empírica. Es decir, basada en datos reales derivados de una campaña de monitorización. Esto conlleva asociados una serie de retos distintos de los que podrían encontrarse al emplear modelos numéricos, basados en la formulación de los procesos físicos que gobiernan los intercambios energéticos urbanos, y cuyo desarrollo parece estar más avanzado. Se entiende que una aproximación empírica, aunque resulte en una aplicación menos universalizable, se aproxima de una forma más realista a los procedimientos tradicionales de generación de archivos climáticos. También, que este enfoque puede contribuir a una mayor precisión y certeza a la hora de vincular los archivos climáticos con las distintas realidades urbanas existentes en la ciudad.

La segunda pretensión de esta hipótesis es que la caracterización de la isla de calor a través de archivos climáticos debe ser integral. Esto significa que la solución planteada que dé cumplimiento a esta hipótesis debe contemplar el municipio en su conjunto. Así, ésta no puede centrarse exclusivamente en las zonas donde se registra la mayor intensidad de la isla de calor, del mismo modo que tampoco puede limitarse exclusivamente a los momentos donde se registra su mayor intensidad. Se entiende la isla de calor como un fenómeno continuo entre el espacio urbano y el no urbano; se entiende la isla de calor como un fenómeno dinámico que engloba todas las dimensiones del calor urbano.

2.2. Objetivos

En coherencia con la hipótesis enunciada, el objetivo principal de esta tesis queda definido como **el desarrollo un modelo empírico de la isla de calor urbana de la ciudad de Madrid, adaptado al régimen dinámico de los procesos de simulación energética de edificios, y cuyo propósito es la generación de archivos climáticos basados en la realidad climática de las diferentes zonas urbanas de la ciudad de Madrid.**

El modelo resultado de esta tesis doctoral deberá servir, por tanto, para obtener series temporales de registros horarios de temperatura y humedad relativa en la escala urbana mediante una aproximación basada en datos (*data driven-approach*). Estas series temporales servirán de base para la construcción de los archivos climáticos urbanos mediante la técnica del *morphing*. También serán empleadas para vincular la realidad física con los datos climáticos, permitiendo la comparación entre las distintas partes de la ciudad, y proveyendo una base objetiva sobre la que evaluar el impacto de este fenómeno sobre el comportamiento energético de los edificios.

Debe destacarse que el objetivo de esta tesis doctoral no es llevar a cabo una evaluación del impacto de la isla de calor sobre el comportamiento energético de los edificios, sino el de proveer herramientas (en forma de archivos climáticos y conocimiento sobre las dinámicas del fenómeno) que permitan llevar a cabo este tipo de evaluación en futuros trabajos de investigación. En este sentido, y con el fin de cumplir con el objetivo principal de esta tesis doctoral, se hace necesario enunciar una serie de objetivos específicos que permitan estructurar las distintas etapas de esta investigación. Son los siguientes:

1. **Desarrollar una campaña de monitorización en la ciudad de Madrid cuya resolución espacial y temporal sea acorde al régimen dinámico de la simulación energética.** Este objetivo tiene como fin la obtención de datos empíricos con los que generar el modelo, dará lugar a la primera etapa de esta investigación: *Monitorización de la isla de calor urbana de Madrid.*

2. **Recabar los metadatos necesarios para poder procesar y contextualizar adecuadamente los datos procedentes de la campaña de monitorización**. Dado que la isla de calor tiene una fuerte vinculación con el entorno urbano, es necesario recabar toda aquella información que permita describir los datos obtenidos. Esto permitirá evaluar su representatividad y vincularlos con un contexto específico. Este segundo objetivo se traslada a la segunda etapa de esta tesis doctoral: *Contextualización de los datos procedentes de la monitorización.*

2.2. Objectives

In coherence with the stated hypothesis, the main objective of this thesis is defined as **the creation of an empirical model of the urban heat island of the city of Madrid, adapted to the dynamic regime of building energy simulation tools, and whose purpose is the generation of weather files based on the climatic reality of the different urban areas of the city of Madrid.**

The model resulting from this thesis should therefore lead to obtaining time series of hourly temperature and relative humidity records at the urban scale by means of a data-driven approach. These *morphed* time series will serve as the basis for the construction of urban weather files. They will also be used to link physical reality with climate data, allowing comparison between different parts of the city, and providing an objective basis on which to assess the impact of this phenomenon on the energy performance of buildings.

It should be noted that the aim of this thesis is not to carry out an exhaustive evaluation of the impact of the urban heat island on the energy performance of buildings, but to provide tools (in the form of weather files and knowledge about the dynamics of the phenomenon) that will enable this type of evaluation to be carried out in future research work. In this sense, and to fulfil the main objective of this thesis, it is necessary to set out a series of specific objectives to structure the different stages of this research. They are the following:

1. **To carry out a monitoring campaign in the city of Madrid whose spatial and temporal resolution is in accordance with the dynamic regime of the energy simulation**. This objective aims at obtaining empirical data with which to generate the model, and it will lead to the first stage of this research: *Monitoring of the urban heat island of Madrid.*

2. **To collect the metadata needed to adequately process and contextualise the data from the monitoring campaign**. Given that the urban heat island is strongly linked to the urban environment, it is necessary to collect all the information required to describe the measured data. This will enable the assessment of their representativeness and will facilitate their linkage to a specific urban context. This second objective will be fulfilled during the second stage of this thesis: *Contextualisation of the monitoring data.*

3. **To study the dynamics of the urban heat island, both on a temporal and spatial scale, in the city of Madrid**. The aim of this objective is to analyse the hourly evolution of urban temperatures, comparing the different dynamics between urban areas and identifying their similarities and differences. It is expected this will help guide the modelling of the phenomenon. From this objective arises the third stage of the research: *Analysis of the hourly and intra-urban evolution of the heat island.*

4. **To morph artificial time series that will allow studies to be carried out with a broader time coverage than that obtained directly through measurements**. This objective will lead to the development of a model (or models) with which to obtain the necessary data for the creation of weather files. It will correspond to the fourth step of this study: *Modelling the urban heat island using a data-driven approach.*

5. **Generate a set of urban weather files that are representative of urban climate conditions**. The representativeness of these files will have to be adjusted, both in terms of coverage and variety, to the urban climate variability of the city of Madrid. This last objective will be the main focus of the last stage of this research: *Creating urban weather files and testing with a case study.*

3. **Evaluar el comportamiento dinámico de la isla de calor, tanto en su escala temporal como espacial, en la ciudad de Madrid**. Con este objetivo se pretende estudiar la evolución horaria de las temperaturas urbanas, comparando las distintas dinámicas entre zonas urbanas, e identificando sus similitudes y diferencias con el fin de orientar la modelización del fenómeno. A partir de este objetivo surge la tercera etapa de la investigación: *Análisis de la evolución horaria e intraurbana de la isla de calor.*

4. **Generar series temporales artificiales que permitan realizar estudios con una cobertura temporal más amplia que la obtenida directamente a través de las mediciones**. Este objetivo desembocará en el desarrollo de un modelo (o modelos) con el que obtener los datos necesarios para la creación de un archivo climático. Se corresponderá con la cuarta etapa de este estudio: *Modelización de la isla de calor mediante un enfoque basado en datos.*

5. **Obtener una batería de archivos climáticos urbanos que sean representativos de las condiciones climáticas urbanas**. La representatividad de estos archivos tendrá que ajustarse, tanto por su cobertura como por su diversidad, a la variabilidad climática urbana de la ciudad de Madrid. Este último objetivo centrará los esfuerzos de la última etapa de esta investigación: *Creación de archivos climáticos urbanos y ensayo sobre caso de estudio.*

Parte II. Metodología
Part II. Methodology

3. Metodología
Methodology

El desarrollo de esta tesis doctoral se ha planteado, desde un inicio, por compendio de artículos. Este trabajo se sustenta, por tanto, en la publicación de varios artículos científicos en revistas de alto impacto, y que constituyen el cuerpo central de esta investigación. Otras publicaciones, como son comunicaciones a congresos, un capítulo de libro o una patente, complementan este trabajo. A continuación, se detallan las etapas en las que se divide esta investigación, así como la relación con cada una de las publicaciones que se incluyen en la Parte III de este documento.

This PhD thesis was conceived, from the beginning, as a thesis by publication. This work is therefore based on the publication of several scientific papers in high impact journals, which constitute the central body of this research. Other publications, such as communications to conferences, a book chapter, and a patent, complement this work. The stages into which this research is divided, as well as the relationship with each of the publications included in Part III of this document, are outlined in this section.

3. Methodology

This PhD thesis is articulated in such a way that each of the specific objectives set out in the Introduction section shapes each of the stages of the research. Thus, the structure of this work comprises five stages which are summarised in the following diagram:

3. Metodología

Esta tesis doctoral se ha articulado de manera que cada uno de los objetivos específicos enunciados en el apartado anterior de forma a cada una de las etapas de la investigación. De este modo, la estructura de este trabajo se compone de cinco etapas que quedan resumidas a través del siguiente diagrama:

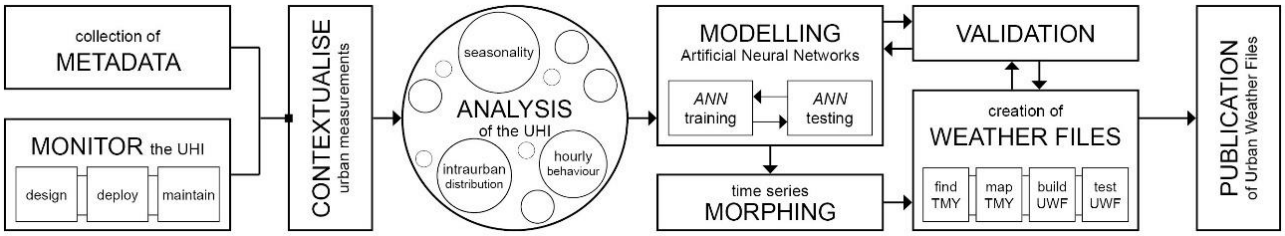

Figura 3.1. Etapas de esta tesis doctoral.

Figure 3.1 Stages of this PhD thesis.

The **first stage** of this research focused on the monitoring of the urban heat island (UHI) by means of fixed points distributed throughout the city of Madrid. To do this, it was necessary, firstly, to delimit both the scope of the study and the time frame of the monitoring. Secondly, the design of this campaign was informed by a previous analysis based on mobile measurements (through urban transects), the results of which provided a first updated image of the phenomenon. The monitoring campaign includes from the design and fabrication of the solar shielding to the deployment and maintenance tasks, as well as the selection of the exact locations for the subsequent review and approval by the urban authority.

Part of this first stage has been developed within the MODIFICA project (Universidad Politécnica de Madrid, 2014), where this research on the UHI of Madrid was initiated, and thanks to which the necessary financial resources and human support were made available for the implementation of the monitoring. Support was also provided by the General Subdirectorate for Energy and Climate Change of Madrid City Council, which funded the installation of the equipment.

La **primera etapa** de esta investigación se ha centrado en el desarrollo de una campaña de monitorización de la isla de calor a través de puntos fijos distribuidos por la ciudad de Madrid. Para ello ha sido necesario, primero, acotar tanto el ámbito de estudio como el recorrido temporal de la monitorización. En segundo lugar, el diseño de esta campaña vino informado por un estudio previo basado en mediciones móviles (a través de transectos urbanos), y cuyos resultados permitieron partir de una primera imagen actualizada del fenómeno. La campaña de monitorización se ha planteado a partir de estos trabajos previos, e incluye desde el diseño y fabricación de la protección solar de los equipos hasta el despliegue y las tareas de mantenimiento, pasando por la selección de las ubicaciones exactas para su posterior revisión y aprobación por parte de la autoridad urbana.

Parte de esta primera etapa se ha desarrollado en el seno del proyecto de investigación MODIFICA (Universidad Politécnica de Madrid, 2014), lugar donde se dio inicio a esta investigación sobre la isla de calor de Madrid, y gracias al cual se pudo disponer de los recursos económicos y el apoyo humano necesarios para la ejecución de la monitorización. También se ha contado con el apoyo de la Subdirección General de Energía y Cambio Climático del Ayuntamiento de Madrid, desde donde se sufragó la colocación de los equipos.

Universidad Politécnica de Madrid. (2014). *Proyecto MODIFICA: Modelo predictivo del comportamiento energético de edificios de viviendas bajo condiciones de isla de calor urbana*. Ministerio de Economía y Competitividad. BIA2013-41732-R

Los resultados de esta primera etapa de investigación han dado lugar a una comunicación en un congreso internacional (Núñez Peiró et al., 2017b), a una publicación de un capítulo de libro de la editorial *Springer* (Núñez Peiró et al., 2017, **capítulo 4**), y a la concesión de una patente con examen previo (Núñez Peiró et al., 2018, **capítulo 5**).

The results of this first stage of the research have led to a communication at an international conference (Núñez Peiró et al., 2017b) subsequently included in a book chapter published by *Springer* (Núñez Peiró et al., 2017, **chapter 4**), and the granting of a patent (Núñez Peiró et al., 2018, **chapter 5**).

Núñez Peiró, M., Sánchez-Guevara Sánchez, C., & Neila González, F. J. (2017). Update of the urban heat island of Madrid and its influence on the building's energy simulation. In P. Mercader-Moyano (Ed.), *Sustainable Development and Renovation in Architecture, Urbanism and Engineering*. Springer. https://doi.org/10.1007/978-3-319-51442-0_28

Núñez Peiró, M., Sánchez-Guevara Sánchez, C., & Neila González, F. J. (2018). *Abrigo meteorológico para sensores ambientales* (Patent No. ES-2642617-B2).

La **segunda etapa** de la investigación ha consistido en la contextualización de las mediciones desarrolladas en la etapa anterior. El objetivo ahora es, por tanto, la provisión de los metadatos necesarios para describir los datos procedentes de la monitorización. Además de identificar una batería de indicadores relevantes para describir el contexto de las mediciones, también se ha trabajado con un sistema de clasificación climática de entornos urbanos. Se ha hecho especial hincapié en la definición del área fuente de los sensores, esencial en entornos urbanos para poder delimitar correctamente la *zona de influencia* de cada medición. Esto último ha dado forma a una revisión bibliográfica que se ha publicado en la revista *Building and Environment* (Núñez Peiró et al., 2019, **capítulo 6**), la cual es la primera de las tres publicaciones de alto impacto que pertenecen a esta tesis por compendio.

The **second stage** of the research consisted of contextualising the measurements developed in the previous stage. The aim is therefore to provide the necessary metadata to describe the monitoring data. In addition to identifying a set of relevant indicators to describe the context of the measurements, a climate classification system for urban environments was also applied. Particular emphasis was placed on the definition of the sensor source area, which is essential in urban environments in order to correctly delimit the area affecting each measurement. The latter has resulted in a literature review published in the journal *Building and Environment* (Núñez Peiró et al., 2019, **chapter 6**), and which is the first of the three high impact publications that belong to this thesis by publications.

Núñez Peiró, M., Sánchez-Guevara Sánchez, C., & Neila González, F. J. (2019). Source area definition for local climate zones studies. A systematic review. *Building and Environment*, *148*, 258–285. https://doi.org/10.1016/j.buildenv.2018.10.050

Estas dos primeras etapas se han desarrollado en paralelo. A la vez que se han registrado la temperatura y humedad relativa en diversos puntos de la ciudad (los datos), se ha estudiado la mejor manera de relacionar estos datos con su realidad urbana, identificando tanto aquellos indicadores más relevantes para describir las condiciones higrotérmicas de un espacio, así como el área fuente de cada uno de los equipos de medición (los metadatos), y garantizando con ello su representatividad espacial.

These first two stages were carried out in parallel. While temperature and relative humidity were recorded at several points in the city (the data), it was studied the best way to relate these data to their urban reality, identifying both the most relevant indicators to describe the hygrothermal conditions of a space as well as the source area of each of the measuring devices (the metadata), and thus guaranteeing their spatial representativeness.

Tras compilar los datos y metadatos de cada uno de los puntos de medición en una base de datos georreferenciada, se ha procedido a iniciar la **tercera etapa** de esta tesis doctoral: el análisis de la isla de calor urbana de Madrid. Su finalidad es doble: en primer lugar, confirmar que los datos recabados permiten representar e identificar las diferencias térmicas entre distintas áreas de la ciudad de Madrid; en segundo lugar, ofrecer una visión más detallada del fenómeno que se

After compiling the data and metadata from each of the measurement points in a geo-referenced database, the **third stage** of this doctoral thesis began: the analysis of the urban heat island of Madrid. Its purpose is twofold: firstly, to confirm that the data represent and identify the thermal variations between different areas of the city of Madrid; secondly, to provide a more detailed view of the phenomenon to be modelled in the next stage,

specifically in terms of its hourly evolution and the intra-urban differences produced by the heat island. This will provide a basis for the decisions taken during the modelling of the heat island and the creation of the climate archives. This stage therefore acts as a necessary transition between observation (stages 1 and 2) and modelling (stages 4 and 5). The result of this stage has led to the second high-impact publication of this thesis by publication, published in the journal *Urban Climate* (Núñez-Peiró et al., 2021b, **chapter 7**).

pretende modelar en la siguiente etapa, en concreto en cuanto a su evolución horaria y las diferencias intraurbanas producidas por la isla de calor. Esto permitirá dotar de argumentos a las decisiones tomadas durante la modelización de la isla de calor y la creación de los archivos climáticos. Esta etapa actúa, por tanto, a modo de necesaria charnela entre la observación (etapas 1 y 2) y la modelización (etapas 4 y 5). El resultado de esta etapa ha dado forma a la segunda publicación de alto impacto de esta tesis por compendio, publicada en la revista *Urban Climate* (Núñez-Peiró et al., 2021b, **capítulo 7**).

Núñez-Peiró, M., Sánchez-Guevara Sánchez, C., & Neila González, F. J. (2021). Hourly evolution of intra-urban temperature variability across the local climate zones. The case of Madrid. *Urban Climate*, *39*, 100921. https://doi.org/10.1016/j.uclim.2021.100921

The **fourth stage**, the data-driven modelling of the heat island, responds to the fourth specific objective of this thesis: the generation of artificial time series to enable studies with a wider temporal coverage than that obtained directly through measurements. Following the success cases identified in the literature on the empirical modelling of temperatures in urban environments, the use of artificial neural networks (ANNs) has been proposed. Different structures and configurations of neural networks have been tested in order to detect those that could give better results and, finally, a ten-year time series for each of the monitoring points have been artificially reconstructed.

This stage of the research was initiated during a research stay at the Institute for Environmental Design and Engineering at University College London. Specifically, and under the supervision of Anna Mavrogianni and Phil Symonds, the entire code base needed to programme the neural networks, optimise their operation and process the results was developed there. The result has led to the third and final high-impact publication that forms part of this doctoral thesis, published in the journal *Sustainability* (Núñez-Peiró et al., 2021a, **chapter 8**).

La **cuarta etapa**, la modelización basada en datos de la isla de calor, responde al cuarto objetivo específico de esta tesis: la generación de series temporales artificiales que permitan realizar estudios con una cobertura temporal más amplia de la obtenida directamente a través de las mediciones. Siguiendo los casos de éxito identificados en la literatura sobre la modelización empírica de temperaturas en entornos urbanos, se ha planteado la utilización de redes neuronales artificiales. Se han ensayado distintas estructuras y configuraciones de redes neuronales con el fin de detectar aquellas que podían dar mejores resultados y, por último, se han reconstruido de forma artificial las series temporales de diez años para cada uno de los puntos de monitorización.

Esta etapa de la investigación fue iniciada durante la estancia de investigación llevada a cabo en el *Institute for Environmental Design and Engineering* de la *University College London*. En concreto, y bajo la supervisión de *Anna Mavrogianni* y *Phil Symonds*, allí se desarrolló toda la base de código necesaria para programar las redes neuronales, optimizar su funcionamiento y procesar los resultados. El resultado ha dado forma a la tercera y última publicación de alto impacto que forma parte de esta tesis doctoral, publicada en la revista *Sustainability* (Núñez-Peiró et al., 2021a, **capítulo 8**).

Núñez-Peiró, M., Mavrogianni, A., Symonds, P., Sánchez-Guevara Sánchez, C., & Neila González, F. J. (2021). Modelling Long-Term Urban Temperatures with Less Training Data: A Comparative Study Using Neural Networks in the City of Madrid. *Sustainability (Switzerland)*, *13*(15), 8143. https://doi.org/10.3390/su13158143

Once the artificial time series were obtained, it was possible to proceed to the **fifth and final stage** of this research work: the generation of urban weather files for the city of Madrid. The first step consisted of selecting a methodology for obtaining a typical meteorological year from an extended data series.

Una vez obtenidas las series temporales artificiales se pudo proceder a la **quinta y última etapa** de este trabajo de investigación: la generación de archivos climáticos urbanos para la ciudad de Madrid. El primer paso ha consistido en la selección de una metodología para la obtención de un año meteorológico tipo a partir de series de datos más amplias. A continuación, se han delimitado las zonas urbanas con unas

condiciones higrotérmicas homogéneas, a las que se les ha asociado un año meteorológico típico representativo.

Finalmente, y antes de construir los archivos climáticos correspondientes a cada una de estas zonas climáticas urbanas, se ha generado un nuevo archivo climático *de referencia* con el que comparar los resultados obtenidos a través de este procedimiento con los existentes previamente para la ciudad de Madrid. Esto último ha sido presentado en forma de comunicación a un congreso internacional (Núñez Peiró et al., 2021, **capítulo 9**).

Then, urban areas with similar hygrothermal conditions were delimited and a representative typical meteorological year was associated with them.

Finally, and before constructing the weather files corresponding to each of these urban climatic zones, a new reference weather file was generated with which to compare the results with those previously existing for the city of Madrid. The latter was presented in the form of a communication at an international congress (Núñez Peiró et al., 2021, **chapter 9**).

Núñez Peiró, M., Sánchez-Guevara Sánchez, C., & Neila González, F. J. (2021). Two decades of weather files in Spain. A comparison of their reliability for building energy modelling using the BESTEST method. *VI International Conference on Technological Innovation in Building*, 62–64.

El resultado final es una delimitación geográfica de las distintas zonas urbanas de Madrid que comparten unos perfiles de temperatura y humedad relativa similares, y a los que se les ha asociado un archivo climático urbano generado mediante la técnica del *morphing* a partir del modelo empírico creado. Esta parte de la investigación no se ha publicado todavía, por lo que se ha incluido en esta tesis una descripción detallada de todo el proceso que puede ser consultada en el **capítulo 14**.

The final result is a geographical delimitation of the different urban areas of Madrid that share similar temperature and relative humidity profiles. An urban weather file was associated to each one of these, generated using the morphing technique and based on the ANNs empirical model. This part of the research has not yet been published, so a detailed description of the whole process has been included in this thesis. This is available in **chapter 14**.

Parte III. Publicaciones
Part III. Publications

4. **Capítulo de libro**
   Book chapter
5. **Patente**
   Patent
6. **Artículo 1**
   Research paper 1
7. **Artículo 2**
   Research paper 2
8. **Artículo 3**
   Research paper 3
9. **Comunicación en congreso internacional**
   Communication at an international congress

En esta tercera parte se presenta la colección de publicaciones que dan forma a esta tesis por compendio, tal y como recoge la normativa aprobada por el Consejo de Gobierno de 30 de noviembre de 2017 de la Universidad Politécnica de Madrid. Entre ellas se incluyen tres artículos científicos de alto impacto en los que el autor de esta tesis figura en primer lugar, y que se encuentran indexados en el Journal Citations Report (JCR), dentro de su primer o segundo cuartil. Se presentan en orden cronológico, dada la correspondencia temporal entre la fecha de publicación y el desarrollo de las distintas etapas de esta tesis doctoral.

This third part presents the set of publications that shape this thesis by publication, as stated in the regulations approved by the Governing Council of 30 November 2017 of Universidad Politécnica de Madrid. These include three high-impact scientific papers in which the author of this thesis appears in first place, and which are indexed in the Journal Citations Report (JCR) within its first or second quartile. They are presented in chronological order, given the temporal correspondence between the date of publication and the development of the different stages of this PhD thesis.

4. Capítulo de libro Book chapter

Update of the urban heat island of Madrid and its influence on the building's energy simulation

Núñez Peiró, M., Sánchez-Guevara Sánchez, C., Neila González, F.J. (2017)

Sustainable Development and Renovation in Architecture, Urbanism and Engineering, 339-530. Springer Publishing.

doi: 10.1007/978-3-319-51442-0_28

PARTE III
PART III

Update of the Urban Heat Island of Madrid and Its Influence on the Building's Energy Simulation

Miguel Núñez Peiró, Carmen Sánchez-Guevara Sánchez and F. Javier Neila González

1 Introduction

Nowadays building energy evaluation tools play a key role in establishing the basic energy strategies in the building sector. They do not only help to improve the decision-making about building design and its inhabitants' comfort, but also to stablish the payback periods and select the best solution among all the possibilities in both new and renovated buildings.

Despite the last decades have witnessed great advances in building evaluation, there are still some disagreement between the simulation results and reality (Coakley et al. 2014). Several studies have addressed the issue, focusing on the models' calibration through the improvement of the thermodynamic algorithms, the user interaction profiles and the weather conditions (Evins 2013; Foucquier et al. 2013; Fumo 2014).

The Urban Heat Island (UHI) relates to the last one, and it consists in the temperature differences between the built (urban) and the unbuilt landscape (rural). Regardless the wide knowledge about the UHI, available climate data does not include its effects, as they undertake the regional scale. Previous studies in this research project have already anticipated the relevance of this phenomenon in the building energy evaluation (López Moreno et al. 2015), and so the significance of addressing the integration of the UHI effects in the buildings' energy simulations.

M. Núñez Peiró (✉) · C. Sánchez-Guevara Sánchez · F.J. Neila González
ABIO Research Group, Universidad Politécnica de Madrid, Madrid, Spain
e-mail: miguel.nunez@upm.es

P. Mercader-Moyano (ed.), *Sustainable Development and Renovation in Architecture, Urbanism and Engineering*, DOI 10.1007/978-3-319-51442-0_28

2 Background

Due to the sum of factors that influence the UHI formation, as well as its temporal and spatial variation, having an in-depth record of the phenomenon requires a large amount of measurements. While the first studies focused on detecting the existence of the UHI and identifying those areas with the greatest intensity (Arnfield 2003; Santamouris 2007, 2015), in recent years much of the research efforts have been linked to the development of numerical models, which allow to study the urban heat island dynamically (Mirzaei and Haghighat 2010).

The first UHI study in Spain was carried out in the city of Madrid (López Gómez et al. 1988, 1993), where the transects methodology[1] was used. It was followed by many other works related to specific questions of urban climate (Almendros and López Gómez 1995; Fernández García 2001; Sobrino et al. 2009), and even a numerical model that tried to explain the urban heat island's behaviour at both the mesoclimatic and microclimatic scale (Salamanca and Martilli 2010; Salamanca et al. 2011).

These studies, however, have not proven to be consistent with the objective of this research, given its age, their inability to generate hourly records, and their lack of accuracy at the microclimatic scale (Grimmond et al. 2010, 2011). Based on the recommendations that point towards the development of models built upon the target of the research (Mirzaei et al. 2015), this project aims to generate an empirical model from the collected data at multiple fixed urban locations (Kolokotroni et al. 2006, 2010; Mihalakakou et al. 2002).

This paper addresses the first phase of the development of the model, carrying out an update of the last surveys in the spatial distribution of the UHI, which dates back to the late 1980s.

3 Means and Methods

This research replicates the methodology used in the first study of Madrid's UHI (López Gómez et al. 1988), based on the development of proximity measurements through urban transects. In order to reckon the highest intensity of the urban heat island, the data gathering was performed under anticyclonic weather conditions with a cloudless sky, calm wind and few hours after the sunset (2100–2300 UTC). Three simultaneous transects configured a set of observations, conducting each of them twice on every set (return trip), and providing the temperature records used in the results section.

[1]The transects methodology refers to transversal itineraries through the city, commonly carried out simultaneously, and from which the air temperature at multiple points is obtained.

Needs to be mention that our study refines the process of planning, data gathering, and analysis. These improvements allowed for the reduction of the needed means, helped to automate the process, and to better the precision and the resolution of the results. In the next sections we explain its characteristics.

3.1 Itineraries and Geolocation

Since the original itineraries from the study of 1988 are not suited to the current road hierarchy of the city, new routes were created for each transect based on the original measuring points. It has been necessary to generate a digital transport network, continuous along the entire city, and able to emulate the current traffic restrictions. For its development it was used the *Network Analyst* extension of *ArcGis 10.3* as well as the *Openstreetmap* base map. Afterwards, the new routes were integrated into a mobile application to enable monitoring and geolocation at every single position of the vehicle.

3.2 Equipment and Data Gathering

Three temperature sensors and data loggers were used for the temperature record. Each sensor consisted on a NTC (N*egative Temperature Coefficient*) exposed thermistor, with an accuracy of ±0.2 °C and a response time of t_{90} = 60 s (Fig. 1). Virtually immediate response was guaranteed for the sensor at speeds above 30 km/h, and thus enabling to detect temperature differences in up to 10 s intervals.

Datalogger Testo 175 T2
Dimensions: 89x53x27 mm
Channels: 2 (int/ext)
Measuring rate: 10s – 24h
Measuring range: -35… +55ºC
Accuracy: ±0,5 ºC

Sensor NTC exposed thermistor
Dimensions: Ø 5 x 115 mm
Measuring range: -50… +125ºC
Accuracy: ±0,2 ºC
Response time: t_{90} = 60s

Fig. 1 Technical data of the equipment used in the measurements. *Source* Testo AG

The transects were carried out by car, with the sensor placed at the roof and distanced from the surface and the exhaust pipe. Since the measurements took place several hours after sunset, it was not necessary to protect the sensor from solar radiation.

3.3 *Analysis Tools, Interpolation Techniques and Maps Generation*

On the basis of the obtained data, a frequency distribution analysis of each data set was carried out in order to identify common patterns among them.

Also several isotherm maps were created for each set of observations. For that process a geostatistical analysis method called *cokriging* was used. The *kriging* is a technique that allows, by interpolating a particular batch of data, to predict the value on a given point:

$$\hat{Z}(s_0) = \sum_{i=1}^{n} \lambda_i Z(s_i) \tag{1}$$

The *variogram*, which is the function that describes the spatial correlation in the *kriging*, was set to be exponential (2), as it has been widely used in meteorology and contamination prediction (Palomino et al. 2015).

$$\gamma(h) = c_0 + c\left(1 - \exp\left(\frac{-h}{r}\right)\right); \quad h > 0 \tag{2}$$

Previous research have also pointed out that the stream beds influence the UHI distribution (Fernández García et al. 1996). Therefore, the model was completed with a *DTM* layer (Digital Terrain Model) in order to provide information on the altimetry. All the process was fulfilled with the *Geostatistical Analyst* package from *ArcGIS 10.3*.

In addition to the 101 points from the transects, collected data from six observatories of the National Meteorological Agency (AEMET) and from nine urban stations of the air quality system (SICAM) were added to the process, giving a total of 116 measuring locations (Fig. 2).

4 Results and Discussion

Four data sets were obtained from the measurements that were carried out between July 2015 and April 2016. Each data set corresponds to one season, as the measurements took place around one month after the solstices and equinoxes. As it is

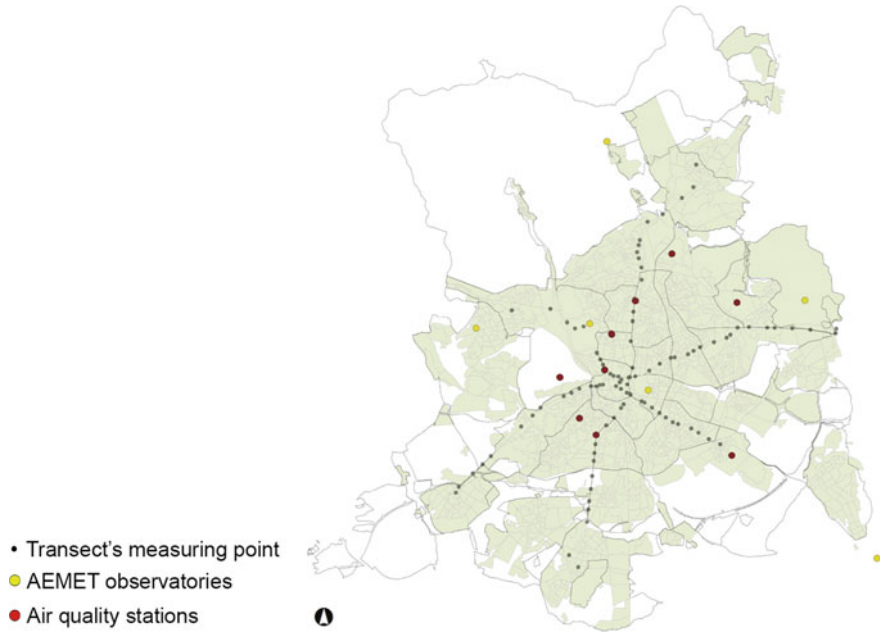

Fig. 2 Location of the observation points used in the map's generation

Table 1 Statistical parameters from each temperature data set

Parameter	July 15th, 2015	October 28th, 2015	February 16th, 2016	April 25th, 2016
Average	31.2	12.8	2.6	15.6
Minimum	27.3	11.2	−0.6	12.1
P_{10}	28.7	11.9	1.5	13.7
P_{50}	31.6	12.9	2.6	15.6
P_{90}	33.1	13.4	3.8	17.4
Maximum	33.7	13.8	5.9	18.0
Range	6.4	2.6	6.5	5.9
Standard deviation	1.6	0.6	1.0	1.3

explained in *3 Means and Methods*, all measurements were performed under the same atmospheric conditions, at the same time and following the identical itineraries.

Table 1 shows a summary of the most important statistical parameters that were used during the analysis of the frequency distribution and the isotherm maps' generation.

4.1 Frequency Distributions

The analysis of the frequency distribution (Fig. 3) shows that it can be inferred the intensity of the urban heat island from the data dispersion of each data set. Thus, it can be observed a decreasing pattern on the UHI intensity from summer to winter (*a–b–c*) and backwards (*c–d–a*), in line with the results of previous research (Núñez Peiró et al. 2016).

While confirming that the greater UHI intensity happens in the warmest month, the differences between the measurements from autumn (*b*) and spring (*d*) are remarkable, since both were performed at times of the year in which historical temperature records are very similar (Tmax = 16–20 °C; Tmin = 6–7 °C).

This can be explained by the fact that, at this latitude, the UHI intensity seems to have a high dependence upon solar radiation. It is noted, therefore, that the urban

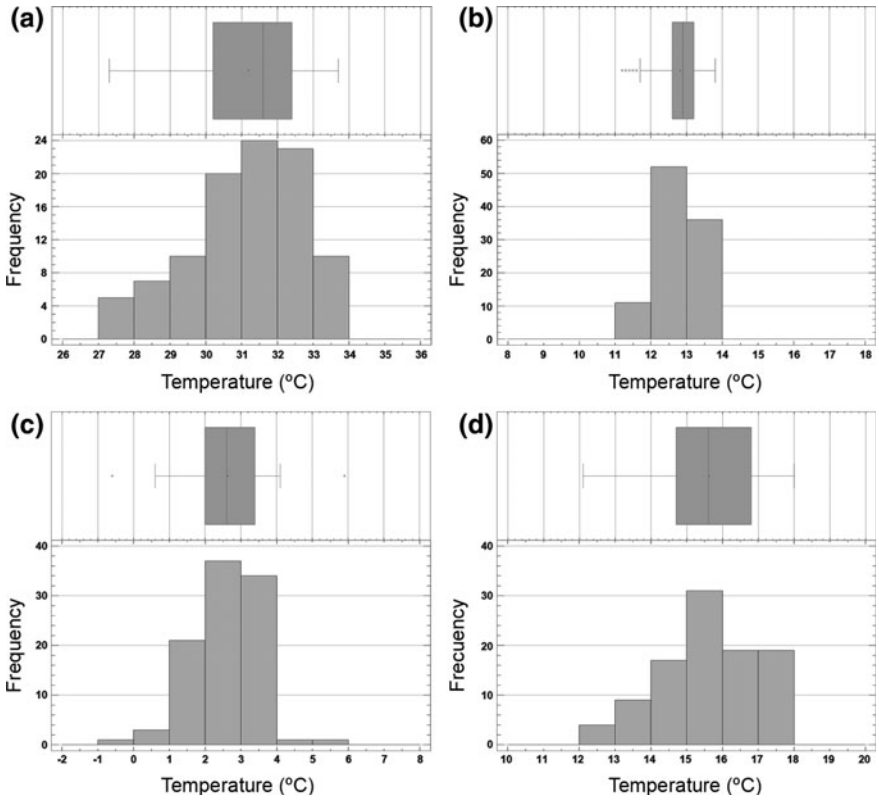

Fig. 3 Frequency distribution of temperature for each data set, presented in chronological order. **a** July 15th, 2015; **b** October 28th, 2015; **c** February 16th, 2016; **d** April 25th, 2016

heat island does not have a symmetrical behavior regarding the seasons but in relation to the solstices, intensifying or softening its effect depending on the proximity to them.

Consequently, the measurements could be presented from the highest to the lowest intensity: the data set *a* distances itself 24 days from the solstice, the *d* does 57 days, the *c* does 125 days and the *b* does 129 days. Moreover, it can be explained the resemblance between the autumn (*b*) and the winter (*c*) measurements, located symmetrically from the solstice and under the same solar radiation.

4.2 Isotherm Maps

Based on the temperature records collected during the measurements, and by following the methodology described in Sect. 3.3 *Analysis tools, interpolation techniques and maps generation*, there have been generated different maps of isotherms for each season (Fig. 4). These maps represent the temperature difference between each observation point and a reference value.

Usually the reference value is taken from a rural location placed in the surrounding of the city. It should be said that it is not an easy task to locate it, as there are consistent doubts about what can be considered a rural location, or how to ensure that the measurement of that particular point is truly representative of the surroundings of the city. Those doubts have led, among other things, to question the methodology and results from hundreds of UHI studies developed around the world (Stewart 2011).

Another approach to determine the reference temperature value consists, when developing urban transects, in taking the minimum temperature of the series. However, as it can be seen in Fig. 4c, there are cases where the minimum temperature corresponds to an atypical value. Although this does not mean that measurements are necessarily erroneous, using them as a reference value when generating a map could cause huge distortions and come to wrong conclusions. It should also be noted that in this study the coldest record was never found at the same location, moving from *Ciudad Universitaria* at the west (summer) to the exit of Madrid at the north (autumn), to the vicinity of the Jarama river at the east (winter) and to the entrance of Getafe in the south (spring).

This study, instead of setting a temperature value for the coldest point, it poses the use of the first decile of the data set as a reference value for the first isotherm. It was found that this process downplays the weight of any atypical and leads to a better and easier comparison between different maps of isotherms.

Figure 5 shows in more detail the spatial distribution of the UHI at its greatest intensity (July 15th, 2015). This has been compared with another isotherm map from the same time of the year, but using data from 30 years ago (July 11th, 1985; Fig. 6). The temperatures were obtained from the temperature profiles published in the first UHI study of Madrid (López Gómez et al. 1988).

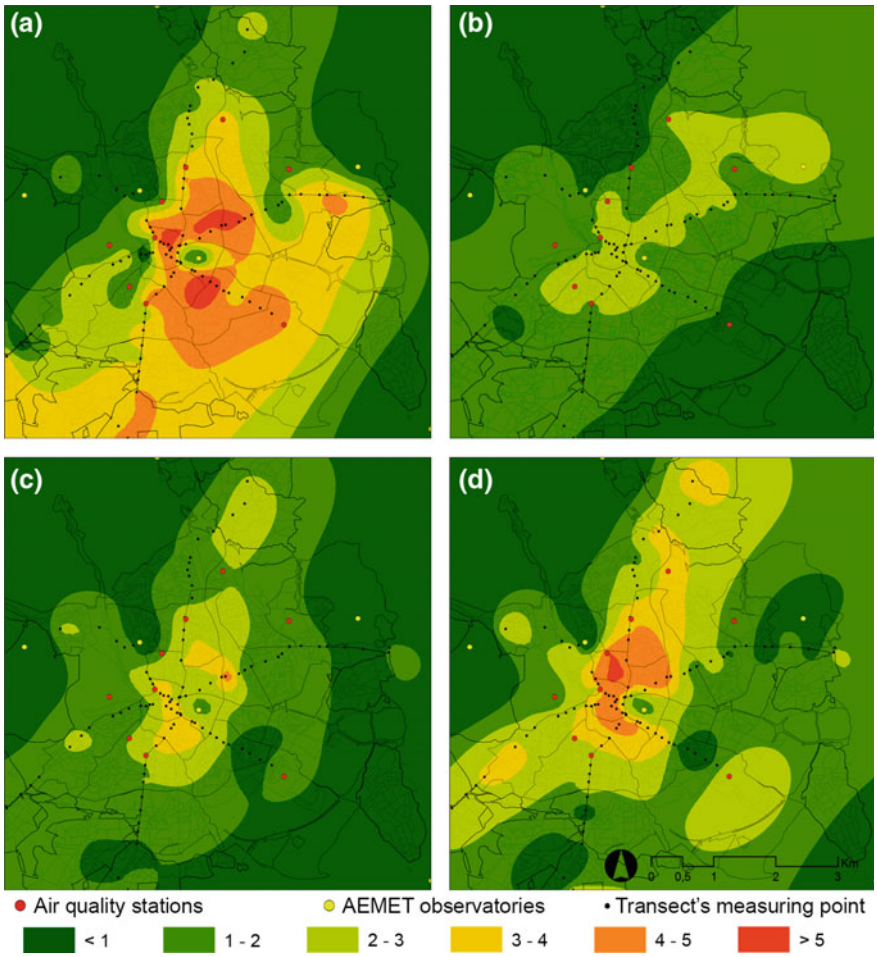

Fig. 4 Isotherm maps based on temperature variation for each data set, presented in chronological order. **a** July 15th, 2015; **b** October 28th, 2015; **c** February 16th, 2016; **d** April 25th, 2016

It is observed that the morphology of both of them is very similar. The concentric distribution of the urban heat island is tinged with a more intense development in the NE-SW axis, in line with the urbanization expansion. It is found a repeated pattern in *Ciudad Universitaria,* as it is in both cases the closest point to the city with the lowest temperature. The surroundings of the park *El Retiro,* with a cool island, show a similar behaviour too. Results confirm that the villages around the city of Madrid are under the effect of micro-heat islands, with an intensity of 1–3 °C. Confirming that there are some urban fabrics that cause either a rise or a fall in temperatures is worth of interest as well.

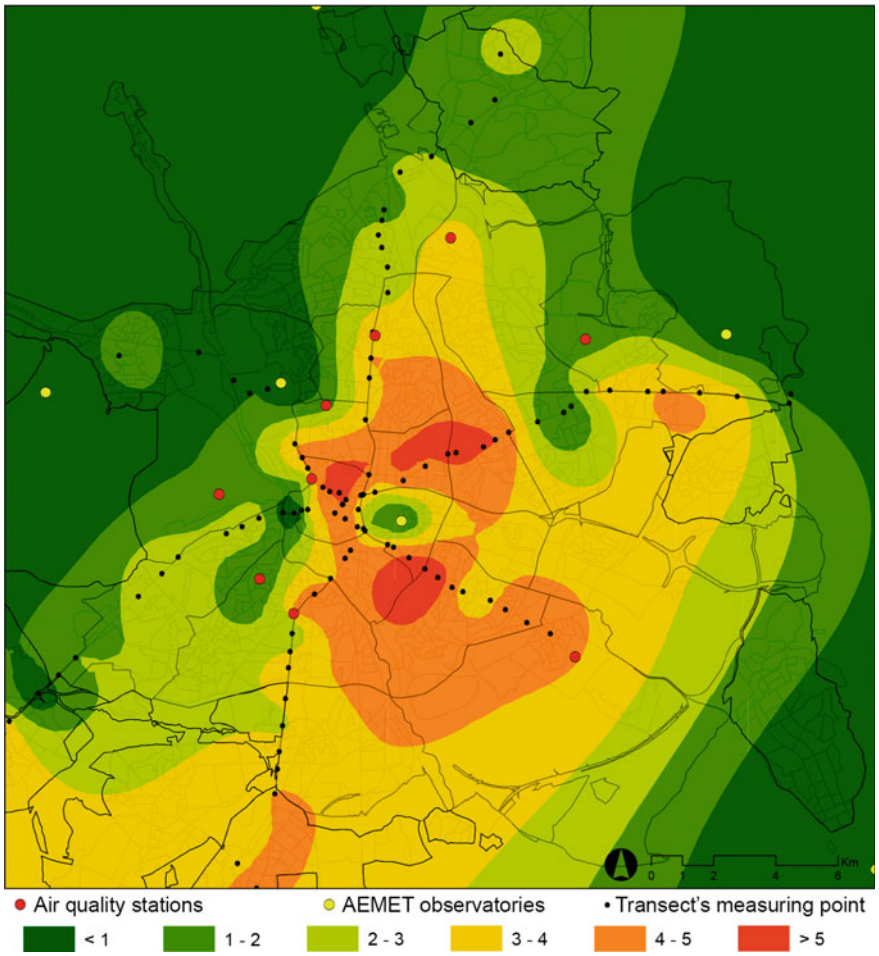

Fig. 5 Isotherm map based on temperature variation at midnight. July 15th, 2015

Regarding the evolution of the urban heat island during the last 30 years, it seems clear that the UHI has enlarged its size and increased the number of urban areas that bear the hottest temperature records (those where the intensity is over 4 °C). However, the UHI intensity does not seem to be increasing itself, as the maximum values are in both cases around 5–6 °C.

It appears that the growth of the city has effectively increased the domain of the urban heat island, spreading its higher effect over new areas. However, it does not seem enough to increase its intensity at the points where already had reached the maximum, probably because the urban fabric is consolidated and has changed little or nothing over the last three decades.

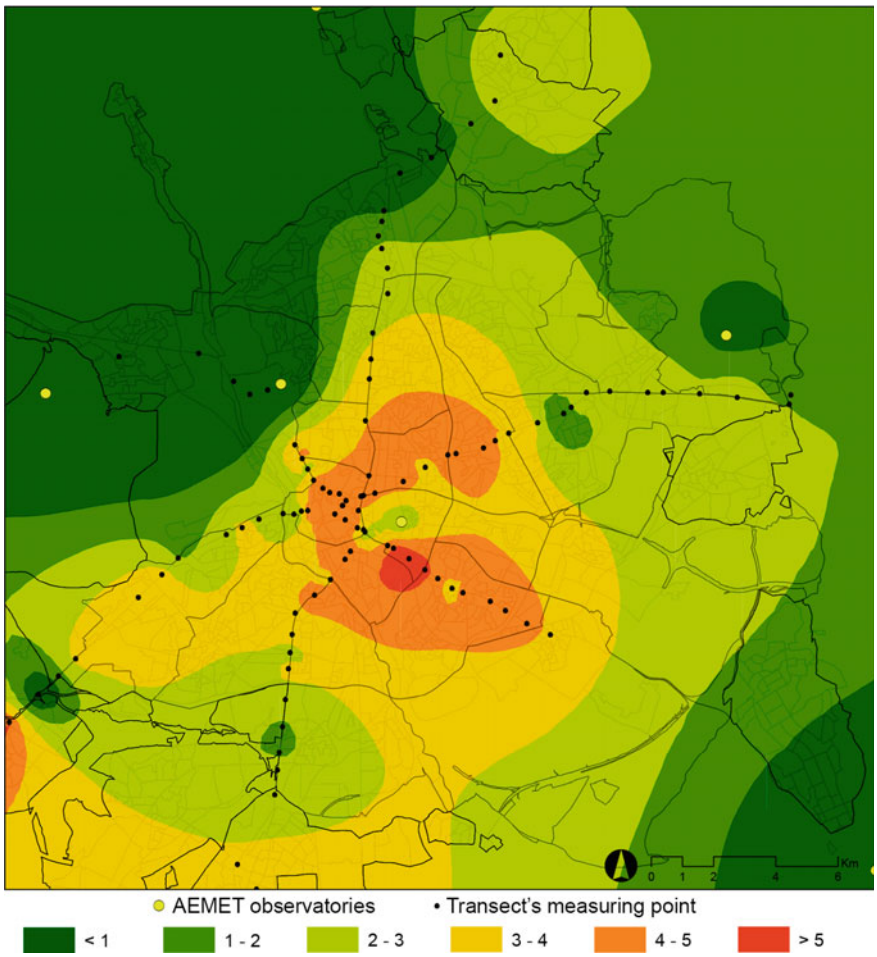

Fig. 6 Isotherm map based on temperature variation at midnight. July 11th, 1985. After López Gómez et al. (1988)

5 Conclusions

This research confirms that the urban heat island of Madrid has grown from the study that was firstly developed between 1984 and 1986 (López Gómez et al. 1988). It has been observed an increase in its area of influence, in particular on those parts with the highest temperatures.

Despite the significant human effort and the material means that were needed, the methodology that was used to carry out this updating of the UHI has turned out to be extremely useful. Due to the improvements that were implemented on the process, we expect to perform an urban climate analysis on a lower scale.

The comparison of the data sets from different times of the year suggests that the highest intensity happens around the summer solstice, mainly due to the greater amount of solar radiation that is received and accumulated by the urban fabric. Contrary to what is said in the study from 1988, the intensity of the UHI appears to reach its minimum around the winter solstice. The differences between both studies seems to be on the rural reference value.

In conclusion, the findings of this study have provided an updated base for the decision-making of UHI related aspects. These results could be used in many fields related to the urban climate, and it stands as an essential tool to select the most relevant locations of the urban microclimate. Ultimately, it completes the first stage of the dynamic model that will integrate the UHI effects into the building energy evaluation.

Acknowledgements This research is funded by *Programa de I+D+I orientada a los retos de la sociedad 'Retos In-vestigación'* of the Ministry of Economy and Competitiveness. Grant code BIA2013-41732-R, MODIFICA Project: Predictive Model For Dwellings Energy Performance Under The Urban Heat Island Effect.

Authors would also like to thank the State Meteorological Agency (AEMET) and Madrid Air Quality Integral System for weather data provided to carry out this research.

References

Almendros MÁ, López Gómez A (1995) La isla de calor en Madrid y las situaciones sinópticas. Estud Geogr 56(219):207–221

Arnfield AJ (2003) Two decades of urban climate research: a review of turbulence, exchanges of energy and water, and the urban heat island. Int J Climatol 23(1):1–26

Coakley D, Raftery P, Keane M (2014) A review of methods to match building energy simulation models to measured data. Renew Sustain Energy Rev 37:123–141

Evins R (2013) A review of computational optimisation methods applied to sustainable building design. Renew Sustain Energy Rev 22:230–245

Fernández García F (2001) El clima urbano de Madrid y su influencia sobre el confort térmico. Boletín de La Real Sociedad Geogr 137–138:12

Fernández García F, Almendros Coca MÁ, López Gómez A (1996) La influencia del relieve en la isla de calor de Madrid: las vaguadas del Manzanares y del Abroñigal. Estud Geogr 57 (224):473–494

Foucquier A, Robert S, Suard F, Stéphan L, Jay A (2013) State of the art in building modelling and energy performances prediction: a review. Renew Sustain Energy Rev 23:272–288

Fumo N (2014) A review on the basics of building energy estimation. Renew Sustain Energy Rev 31:53–60

Grimmond CSB, Blackett M, Best MJ, Baik J-J, Belcher SE, Beringer J, Zhang N (2011) Initial results from Phase 2 of the international urban energy balance model comparison. Int J Climatol 31(2):244–272

Grimmond CSB, Blackett M, Best MJ, Barlow J, Baik J-J, Belcher SE, Zhang N (2010) The international Urban energy balance models comparison project: first results from phase 1. J Appl Meteorol Climatol 49(6):1268–1292

Kolokotroni M, Davies M, Croxford B, Bhuiyan S, Mavrogianni A (2010) A validated methodology for the prediction of heating and cooling energy demand for buildings within the Urban Heat Island: case-study of London. Sol Energy 84(12):2246–2255

Kolokotroni M, Giannitsaris I, Watkins R (2006) The effect of the London urban heat island on building summer cooling demand and night ventilation strategies. Sol Energy 80(4):383–392
López Gómez A, López Gómez J, Fernández García F, Arroyo Ilera F (1988) El Clima urbano de Madrid: La isla de calor. CSIC, Madrid
López Gómez A, López Gómez J, Fernández García F, Moreno Jiménez A (1993) El Clima urbano: teledetección de la isla de calor en Madrid. MOPT, Madrid
López Moreno H, Sánchez-Guevara Sánchez C, Román López E, Neila González FJ (2015) Thermal characterization of urban heat island according to urban morphology of Madrid. In: Proceedings of the III International Congress on Construction and Building Research
Mihalakakou G, Flocas HA, Santamouris M, Helmis CG (2002) Application of neural networks to the simulation of the heat island over Athens, Greece, using synoptic types as a predictor. J Appl Meteorol 41(5):519–527
Mirzaei PA, Haghighat F (2010) Approaches to study urban heat island—abilities and limitations. Build Environ 45(10):2192–2201
Mirzaei PA, Olsthoorn D, Torjan M, Haghighat F (2015) Urban neighborhood characteristics influence on a building indoor environment. Sustain Cities Soc 19:403–413
Núñez Peiró M, Román López E, Sánchez-Guevara Sánchez C, Neila González FJ (2016) Hacia un modelo dinámico para la isla de calor urbana de Madrid = Towards a Dynamic Model for the Urban Heat Island of Madrid. Anales de Edificación 2(1):49–58
Palomino I, Vivanco MG, Theobald M, Garrido JL, Martín F (2015) Evaluación de la calidad del aire en España utilizando modelización combinada con mediciones. Preevaluación 2014. Madrid
Salamanca F, Martilli A (2010) A new building energy model coupled with an urban canopy parameterization for urban climate simulations-part II. Validation with one dimension off-line simulations. Theoret Appl Climatol 99(3–4):345–356
Salamanca F, Martilli A, Yagüe C (2011) A numerical study of the urban heat island over madrid during the DESIREX (2008) campaign with WRF and an evaluation of simple mitigation strategies. Int J Climatol 32(15):2372–2386
Santamouris M (2007) Heat island research in Europe: the state of the art. Adv Build Energy Res 1 (1):123–150
Santamouris M (2015) Analyzing the heat island magnitude and characteristics in one hundred Asian and Australian cities and regions. Sci Total Environ 512–513:582–598
Sobrino JA, Sòria G, Romaguera M, Cuenca J (2009) Desirex 2008: Estudio de la isla de calor en la Ciudad de Madrid. Revista de Teledetección 31:80–92
Stewart ID (2011) A systematic review and scientific critique of methodology in modern urban heat island literature. Int J Climatol 31(2):200–217

5. Patente Patent

Abrigo meteorológico para sensores ambientales

Núñez Peiró, M., Sánchez-Guevara Sánchez, C., Neila González, F.J. (2018)

Ref: ES 2642617 B2

PARTE III
PART III

(19) OFICINA ESPAÑOLA DE PATENTES Y MARCAS

ESPAÑA

(11) Número de publicación: **2 642 617**

(21) Número de solicitud: 201730698

(51) Int. CI.:

G01D 11/24 (2006.01)
G01K 1/08 (2006.01)
G01K 1/20 (2006.01)
E04H 1/12 (2006.01)

(12) PATENTE DE INVENCIÓN CON EXAMEN B2

(22) Fecha de presentación:

16.05.2017

(43) Fecha de publicación de la solicitud:

17.11.2017

Fecha de concesión:

20.09.2018

(45) Fecha de publicación de la concesión:

27.09.2018

(73) Titular/es:

UNIVERSIDAD POLITÉCNICA DE MADRID (100.0%)
Avda. Ramirez de Maeztu nº 7
28040 MADRID (Madrid) ES

(72) Inventor/es:

NUÑEZ PEIRO, Miguel;
SANCHEZ-GUEVARA SANCHEZ, Maria Del Carmen y
NEILA GONZALEZ, Francisco Javier

(74) Agente/Representante:

UNGRÍA LÓPEZ, Javier

(54) Título: **ABRIGO METEOROLÓGICO PARA SENSORES AMBIENTALES**

(57) Resumen:
La invención se refiere a un abrigo meteorológico para sensores ambientales formado por una unidad de extracción de aire (1), que comprende una cubierta transparente (4) incorporada en una carcasa exterior (11) para alimentar a una célula fotovoltaica (5) que activa un ventilador (10), un contenedor central (2), para la ubicación de al menos un sensor (7) ambiental ubicado en un soporte (18) fijado a unos vástagos (17) que atraviesan el contenedor central (2), y un soporte exterior (3), para la fijación del sistema a un elemento externo. El sistema comprende aberturas (8, 9, 10) para la circulación de aire por el interior del abrigo meteorológico.

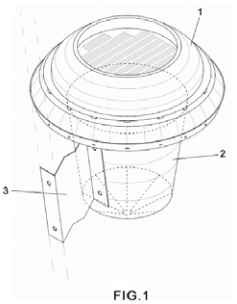

FIG.1

ES 2 642 617 B2

ES 2 642 617 B2

ABRIGO METEOROLÓGICO PARA SENSORES AMBIENTALES

DESCRIPCIÓN

OBJETO DE LA INVENCIÓN

La presente invención se refiere a un abrigo meteorológico, compacto y autónomo, que optimiza la protección de los sensores ambientales ubicados en entornos exteriores urbanos.

Encuentra especial aplicación en el ámbito de la industria relacionada con la monitorización de variables meteorológicas y el control de la calidad del aire, y en concreto a la protección de los sensores que realizan dichas funciones.

PROBLEMA TÉCNICO A RESOLVER Y ANTECEDENTES DE LA INVENCIÓN

La protección de los sensores ambientales no sólo es necesaria para evitar un prematuro deterioro de estos aparatos, sino también para mejorar su precisión y evitar que se registren datos erróneos. Debe garantizarse, además, una correcta circulación del aire a través de esta protección para evitar su sobrecalentamiento, con el fin de que las medidas registradas por los sensores sean realmente representativas del ambiente que les rodea. Por lo tanto, para poder proporcionar unas condiciones adecuadas para el registro de mediciones se deben controlar, al menos, tres parámetros: la ventilación, la radiación solar, y las precipitaciones.

Las garitas meteorológicas primigenias realizaban esta función de una forma sencilla, protegiendo los sensores en el interior de grandes recipientes de paredes opacas y ventiladas de forma natural a través de aperturas de dimensión variable, según se describe en el documento US2652722. Este sistema, que funciona mejor cuanto más reflectante sea su acabado exterior, ha contado con gran aceptación en entornos rurales, donde no existen limitaciones de espacio y donde el viento favorece la ventilación natural de su interior.

Sin embargo, estos sistemas pierden eficacia en entornos donde la velocidad del aire no es lo suficientemente elevada como para contrarrestar el sobrecalentamiento derivado de la radiación solar. A esto se le añade la aleatoriedad del viento, tanto en su dirección como

intensidad, por lo que confiar a este fenómeno la fiabilidad de los registros resulta poco adecuado y, en muchos casos, cuestionable.

En este sentido, los primeros esfuerzos realizados para superar esta problemática se orientaron hacia el diseño de protecciones que, por un lado, minimizasen las necesidades de la ventilación y, por otro, redujeran la dependencia de la ventilación respecto al viento. Estas medidas podrían encuadrarse en las consideradas como pasivas.

En el documento US2837916A se propone un diseño en el que un sistema de lamas horizontales circulares, y dispuestas de forma troncocónica, favorecen la reflexión de la radiación solar y evitan que la radiación reflejada por otras superficies pueda acceder al interior del sistema. Mejora así el diseño de las pantallas Stevenson, empleadas en las garitas meteorológicas tradicionales, e incrementa notablemente la precisión del sistema.

En el documento US2900821A se describe otro importante avance al proponerse un sistema que aprovecha la menor densidad del aire caliente para forzar la ventilación del interior del dispositivo. La ventilación por convección se logra al exponer la parte superior del sistema a la radiación solar y al proteger la inferior de ésta, logrando una diferencia de presión significativa que será más intensa cuanto mayor radiación solar exista. Además, para poder encauzar adecuadamente el circuito de aire, y con el fin de mejorar la durabilidad del sistema, éste abandona el sistema de lamas y opta por una superficie lisa reflectante.

Habiéndose encontrado otros mecanismos para favorecer la ventilación del interior de estos sistemas, los siguientes avances se enfocan en mejorar su envolvente. El documento US2900821A describe un dispositivo compuesto por una doble pared, reduciendo la re-emisión de radiación hacia el interior del sistema. El documento US3933037A describe un sistema de protección de sensores para globos meteorológicos con un encapsulado cilíndrico de doble pared, trasladando la filosofía del primero a un diseño más universal.

El documento GB2175693 implementa un gran avance en el sector al incorporar a la protección de sensores la ventilación mecánica, pasándose a trabajar con sistemas de protección activa. En este caso un ventilador alimentado por energía eléctrica fuerza la ventilación del sistema, permitiendo ajustar el flujo del aire a las necesidades específicas de los sensores. Incorpora, además, diversas mejoras propuestas por sus antecesores, como

una cubierta con voladizo para proteger de la lluvia y reducir el impacto de la radiación solar, o una doble pared para reducir la re-emisión de energía al interior.

Incorporar un ventilador eléctrico supone una mejora considerable en cuanto a la precisión del sistema, pero también implica una dependencia continua respecto a la red de suministro eléctrica, y por ello su ubicación se ve condicionada a la proximidad a dicha red. El desarrollo de las energías alternativas, y en concreto de la tecnología fotovoltaica, ha permitido que se sustituya el suministro eléctrico desde la red eléctrica convencional por otras fuentes alternativas. En este sentido, el documento US6247360B1 divulga un sistema que incorpora una célula fotovoltaica inclinada y una batería que acumula energía. Este dispositivo recupera las lamas horizontales para reducir el efecto de la radiación solar reflejada. El documento CN102200590 lo utiliza como base para describir un dispositivo en el que se mejora la conducción del aire hacia su interior.

Estos últimos avances, orientados hacia la autonomía y eficiencia del sistema, se encuentran con una importante limitación cuando se ubican en entornos urbanos. Por un lado, el régimen turbulento de las rachas de viento y la predominancia de calmas descartan el empleo de cualquier elemento pasivo. Por otro lado, la presencia de obstáculos tales como la edificación, la vegetación, o el mobiliario urbano, hacen muy complicada la tarea de orientar adecuadamente el panel fotovoltaico, siendo en muchos casos imposible captar radiación solar directa o procediendo ésta de ángulos opuestos. Por último, emplear la red eléctrica convencional tampoco resulta lo más apropiado, pues hacerlo requiere de una instalación más compleja y va en contra de la autonomía del sistema.

En este contexto, y dado el creciente interés por conocer la realidad ambiental de los entornos urbanos, resulta de interés desarrollar un sistema de protección autónomo y compacto para sensores ambientales, que sea operativo en condiciones de baja intensidad de viento, y con capacidad para alimentarse de la radiación solar, independientemente de que ésta sea directa o reflejada o de su ángulo de incidencia.

DESCRIPCIÓN DE LA INVENCIÓN

Con el fin de alcanzar los objetivos y evitar los inconvenientes mencionados anteriormente, la presente invención describe un abrigo meteorológico para sensores ambientales que comprende, como partes principales, una unidad de extracción de aire, cuya carcasa

exterior incorpora una cubierta transparente; un contenedor central, para la ubicación de al menos un sensor ambiental; y un soporte exterior, para la fijación del sistema a un elemento externo.

La unidad de extracción de aire incorpora una célula fotovoltaica, para la captación de energía solar a través de la cubierta transparente, y un ventilador conectado a la célula fotovoltaica. Funciona a modo de cubierta del contenedor central y se fija sobre él mediante fijaciones mecánicas que son removibles sin necesidad de herramientas. Para mejorar la captación de energía solar, la cubierta transparente puede ser una lente convergente.

El ventilador, por su parte, puede trabajar a velocidad variable, en función de la energía solar captada por la célula fotovoltaica. Además, puede estar conectado a la célula fotovoltaica mediante una batería recargable. De esta forma, la batería puede activar el ventilador cuando la energía captada por la célula fotovoltaica es menor de un valor predeterminado.

En cualquier caso, el sistema puede estar conectado a una fuente de energía externa, como puede ser la red eléctrica general, para suministro auxiliar.

Por su parte, el contenedor central comprende unos vástagos que sujetan a un soporte donde están fijados los sensores ambientales, de forma que se encuentren aislados. Además, está configurado en forma de cuerpo hueco troncocónico que comprende una carcasa exterior con un ala perimetral en uno de los extremos para la fijación de la unidad de extracción de aire, una capa intermedia de aislamiento de baja conductividad y una capa interna de aislamiento reflexivo.

El sistema puede incorporar un único sensor o varios, en función de las necesidades.

Los brazos del soporte pueden ser extensibles, de forma que sea válido para fijar sensores ambientales de diversos tamaños.

Para crear una circulación de aire en el interior del sistema, la unidad de extracción de aire incorpora unas primeras aberturas y el contenedor central incorpora, por un lado, unas

segundas aberturas en la zona de unión con la unidad de extracción de aire y una tercera abertura en el extremo libre.

BREVE DESCRIPCIÓN DE LAS FIGURAS

Para completar la descripción de la invención y con objeto de ayudar a una mejor comprensión de sus características, de acuerdo con un ejemplo preferente de realización de la misma, se acompaña un conjunto de dibujos en donde, con carácter ilustrativo y no limitativo, se han representado las siguientes figuras:

La figura 1 representa una perspectiva isométrica del abrigo meteorológico mejorado para sensores urbanos, objeto de esta invención, y donde se puede visualizar el volumen conjunto del sistema.

La figura 2 representa una vista frontal explosionada del dispositivo, pudiéndose identificar las tres partes elementales que conforman el conjunto de la invención.

La figura 3a representa una vista frontal del dispositivo, donde se hace referencia a los distintos elementos que lo componen.

La figura 3b representa una vista en planta del dispositivo, donde se hace referencia a los distintos elementos que lo componen.

La figura 4a representa una sección frontal del dispositivo, identificándose los elementos que lo componen.

La figura 4b representa una sección en planta del dispositivo, identificándose en cada una de ellas los elementos y capas que lo componen.

La figura 5 representa la figura 4a, indicándose los flujos de aire.

A continuación se facilita un listado de las referencias empleadas en las figuras:

1. Unidad de extracción de aire.
2. Contenedor central.
3. Soporte exterior.
4. Cubierta transparente.
5. Célula fotovoltaica.
6. Ventilador.
7. Sensor.
8. Primeras aberturas.
9. Segundas aberturas.

10. Tercera abertura.
11. Carcasa exterior.
12. Aislamiento de baja conductividad térmica.
13. Aislamiento reflexivo.
14. Primeras fijaciones.
15. Segundas fijaciones.
16. Terceras fijaciones.
17. Vástagos.
18. Soporte.

DESCRIPCIÓN DE UNA REALIZACIÓN PREFERENTE DE LA INVENCIÓN

Las figuras 1 y 2 permiten identificar las partes principales que conforman el sistema de la invención: la unidad de extracción de aire (1), situada en la parte superior, el contenedor central (2), donde se ubica el sensor (7) ambiental, y el soporte exterior (3), que es la parte mediante la que el sistema se fija en cualquier elemento externo. Estas tres partes del dispositivo pueden diferenciarse claramente por su función, y pueden ser ensambladas y reparadas de forma independiente.

La figura 3a muestra la unión de estas tres partes (1, 2, 3) del dispositivo. Así, unas primeras fijaciones (14) se encargan de unir la unidad de extracción de aire (1) con el contenedor central (2). Estas primeras fijaciones (14), preferentemente, llevan a cabo una unión de tipo mecánica, consistente en el acople de unas pestañas rígidas, ubicadas en la unidad de extracción de aire (1), en sendas muescas practicadas en el contenedor central (2). La ubicación de las pestañas y de las muescas puede encontrarse en posición inversa. Este tipo de unión permite el desmontaje manual de las dos partes (1, 2) sin necesidad de emplear herramientas. Para evitar el desmontaje accidental, las pestañas pueden tener forma de “L”, por ejemplo, de forma que para llevar a cabo la unión, sea preciso introducir las pestañas en las muescas y realizar un pequeño giro.

El soporte exterior (3) es la parte mediante la que se separa al sistema del elemento urbano al que se fija, evitando que el sobrecalentamiento de este elemento influya en las mediciones realizadas por el sensor (7).

Por otro lado, la unión del soporte (3) tanto al contenedor central (2) como al elemento urbano en el que se ubica se lleva a cabo mediante unas segundas fijaciones (15) que, preferentemente, también son mecánicas formadas, por ejemplo, por tornillos o pernos con arandelas y tuercas.

En cualquier caso, estas segundas fijaciones (15) pueden consistir en abrazaderas, tornillería, clavos o similares, sin que esta previsión suponga una limitación al uso de otros elementos de unión.

Por otro lado, las figuras 4a y 4b permiten identificar los distintos elementos que componen las partes principales (1, 2, 3) del sistema de la invención. Una carcasa exterior (11), presente en dos de las partes principales (1, 2, 3), estructura y protege al conjunto de la invención. Esta carcasa exterior (11) tiene un elevado coeficiente de reflexión y es opaca, impidiendo que la radiación solar penetre hacia el interior del sistema.

La unidad de extracción de aire (1) proporciona una protección activa al sistema, garantizando una ventilación suficiente del interior del contenedor para evitar su sobrecalentamiento. Para ello, la unidad de extracción (1) incorpora una cubierta transparente (4) montada directamente sobre una parte superior conformada por una carcasa exterior (11), de forma que permite la entrada de radiación solar para activar una célula fotovoltaica (5) ubicada sobre el chasis interior de la unidad de extracción de aire (1). En una forma de realización, la cubierta transparente (4) es una lente convergente y, gracias a las propiedades ópticas de esta lente, la luz se concentra en la célula fotovoltaica (5). Sobre este mismo chasis y conectada directamente a la célula fotovoltaica (5) se encuentra un ventilador (6), el cual se alimenta de la energía eléctrica proporcionada por la célula fotovoltaica (5). Una forma de realización alternativa incorpora una batería, situada entre la célula fotovoltaica (5) y el ventilador (6), con la misión de almacenar el excedente de energía captada por la célula fotovoltaica (5), y con el fin de extender el uso del ventilador (6) al horario nocturno.

Esta parte superior de la unidad de extracción de aire (1) se fija a una parte inferior, conformada también por una carcasa exterior (11) mediante unas terceras fijaciones (16). La razón de que la unidad de extracción de aire (1) no esté implementada en una única pieza es que entre la parte superior y la parte inferior existen unas primeras aberturas (8) por las

que puede circular el aire dirigido por el ventilador (6), creando una ventilación activa del sistema.

El contendor central (2) proporciona una protección pasiva al sistema, potenciando el aislamiento de las paredes exteriores, mejorando la protección frente a la radiación solar. Esta protección se compone de tres capas: la propia carcasa exterior (11) reflectante, un aislamiento de baja conductividad térmica (12), variable en espesor en función del clima, y un aislamiento reflexivo (13), cuyo cometido es reflejar la radiación que ha atravesado al aislamiento (12) hacia el interior. Las dos capas de aislamiento (12, 13) se encuentran adheridas entre sí mediante un adhesivo químico, mientras que la unión de estas dos a la carcasa exterior (11) no precisa de ningún elemento gracias a su forma troncocónica, que permite una fijación mecánica por rozamiento. La carcasa exterior (11) se extiende a modo de ala perimetral que termina en un reborde que contiene las muescas en las que se fija la unidad de extracción de aire (1). El ala perimetral incorpora unas segundas aberturas (9) para la circulación del aire del interior del sistema, provocando una ventilación pasiva del sistema.

En el interior del contenedor central (2) se sitúa el sensor (7), para lo que se ha provisto al sistema de una serie de elementos para su sujeción. La figura 4b muestra unos vástagos (17) que mantienen suspendido al sensor (7) en el centro del contendor central (2). Cada uno de los vástagos (17) atraviesa al contenedor central (2) por dos puntos, quedando fijado a él mediante fijaciones mecánicas. La fijación del sensor (7) se realiza mediante un soporte (18) que se fija a los vástagos (17). Además, para permitir que cualquier sensor (7) pueda ser empleado en este sistema, el soporte (18) incorpora brazos extensibles.

El contenedor central (2) incorpora una tercera abertura (10) por la zona más inferior. Esta tercera abertura (10) permite la entrada de aire para crear una circulación que se cierra por las primeras aberturas (8) y por las segundas aberturas (9).

Conviene señalar que, para aumentar la ligereza del sistema y su durabilidad en ambientes exteriores, tanto la carcasa exterior (11) como el chasis interior se conciben en un material termoplástico, como polipropileno o similar. Por otro lado, todas las fijaciones mecánicas y elementos de tornillería se conciben conjuntamente con elementos autoblocantes que impiden que puedan liberarse. No obstante, debe entenderse que los diversos elementos

aquí descritos pueden fabricarse de diferentes formas y empleando variados materiales, sin que esto repercuta en la utilidad o eficacia de la invención.

El soporte exterior (3) proporciona al sistema, además, una leve inclinación que facilita la limpieza por agua de lluvia, evitando que la cubierta transparente (4) acumule suciedad y pueda reducir la eficiencia del sistema.

De esta forma, el sistema de la invención cuenta con las siguientes ventajas:

1. El sistema es autónomo y no requiere acceso a un cuadro eléctrico o caja de registro para su instalación, lo que reduce tiempos de instalación y mantenimiento, además de costes eléctricos.
2. El sistema mejora la captación de energía solar, mediante el posicionamiento de la célula fotovoltaica (5) en la parte superior del sistema, en posición horizontal y protegida del exterior mediante una cubierta transparente en forma de lente convergente que tiende a concentrar en la célula fotovoltaica (5) la radiación solar incidente, ya sea directa o reflejada e independientemente de su procedencia, facilitando que el sistema de ventilación se active, optimizando el funcionamiento del proceso de extracción y aumentando la precisión de los registros de los sensores.
3. El sistema integra en una sola pieza todo el mecanismo de ventilación, reduciendo sus dimensiones y compactándolo de forma que es resistente a golpes y a las inclemencias meteorológicas, por lo que requiere de muy poco mantenimiento y facilita su instalación.

En definitiva, la presente invención no debe verse limitada a la forma de realización aquí descrita. Otras configuraciones pueden ser realizadas por los expertos en la materia a la vista de la presente descripción. En consecuencia, el ámbito de la invención queda definido por las siguientes reivindicaciones.

ES 2 642 617 B2

REIVINDICACIONES

1.- Abrigo meteorológico para sensores ambientales que comprende una unidad de extracción de aire (1), que incorpora una carcasa exterior (11) que se extiende a modo de ala perimetral, un contenedor central (2), para la ubicación de al menos un sensor (7) ambiental, y un soporte exterior (3), para la fijación del sistema a un elemento externo, estando el abrigo meteorológico **caracterizado** por que:

- la unidad de extracción de aire (1) comprende:
  - una cubierta transparente (4) incorporada en la carcasa exterior (11),
  - una célula fotovoltaica (5) para la captación de energía solar a través de la cubierta transparente (4),
  - un ventilador (6) conectado a la célula fotovoltaica (5), y
  - unas primeras aberturas (8),
- el contenedor central (2) comprende:
  - unos vástagos (17) para la fijación de un soporte (18) que sujeta a los sensores (7) ambientales,
  - unas segundas aberturas (9), ubicadas en el ala perimetral de la carcasa exterior (11), y
  - una tercera abertura (10) ubicada en un extremo libre del contenedor central (2)

de forma que:
se crea una circulación de aire entre la tercera abertura (10) y las primeras y segundas aberturas (8, 9).

2.- Abrigo meteorológico para sensores ambientales, según la reivindicación 1, **caracterizado** por que el contenedor central (2) está configurado por un cuerpo hueco troncocónico que comprende una capa intermedia de aislamiento de baja conductividad (12) y una capa interna de aislamiento reflexivo (13).

3.- Abrigo meteorológico para sensores ambientales, según cualquiera de las reivindicaciones 1 o 2, **caracterizado** por que la cubierta transparente (4) es una lente convergente.

4.- Abrigo meteorológico para sensores ambientales, según cualquiera de las reivindicaciones anteriores, **caracterizado** por que el ventilador (6) está configurado para regular la velocidad en función de la energía solar captada por la célula fotovoltaica (5).

5.- Abrigo meteorológico para sensores ambientales, según cualquiera de las reivindicaciones anteriores, **caracterizado** por que el ventilador (6) está conectado a la célula fotovoltaica (5) mediante una batería recargable.

6.- Abrigo meteorológico para sensores ambientales, según la reivindicación 5, **caracterizado** por que la batería está configurada para activar el ventilador (6) si la energía captada por la célula fotovoltaica (5) es menor de un valor predeterminado.

7.- Abrigo meteorológico para sensores ambientales, según la reivindicación 1, **caracterizado** por que está conectado a una fuente de energía externa con capacidad de suministrar energía al sistema de forma auxiliar.

8.- Abrigo meteorológico para sensores ambientales, según la reivindicación 1, **caracterizado** por que el soporte (18) incorpora brazos extensibles, de forma que sea válido para fijar sensores (7) ambientales de diversos tamaños.

ES 2 642 617 B2

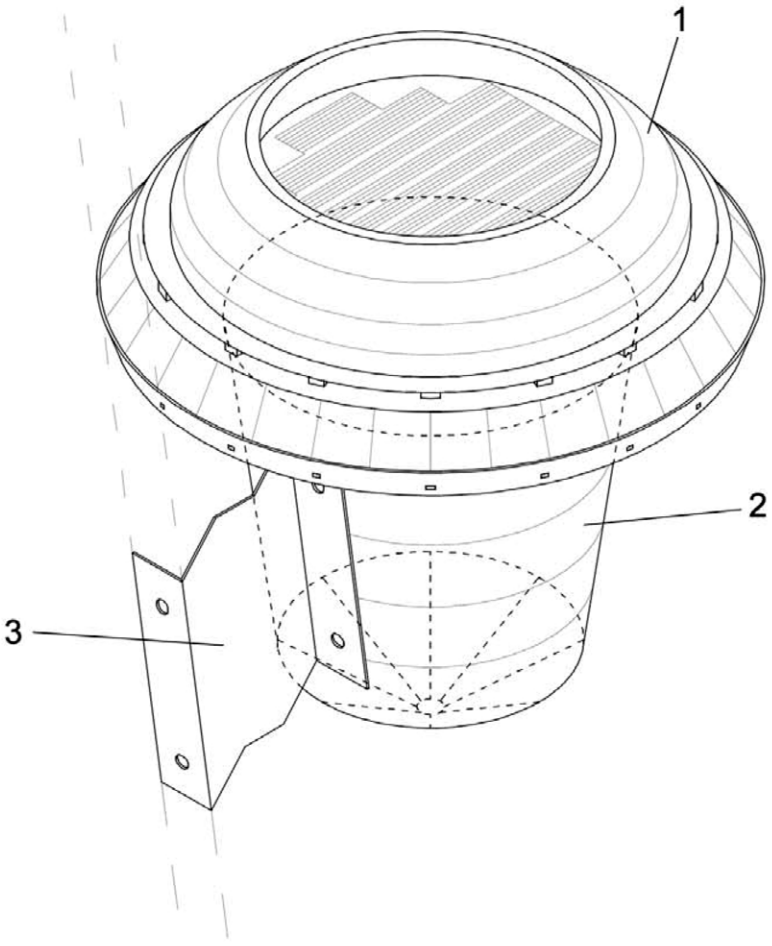

FIG.1

ES 2 642 617 B2

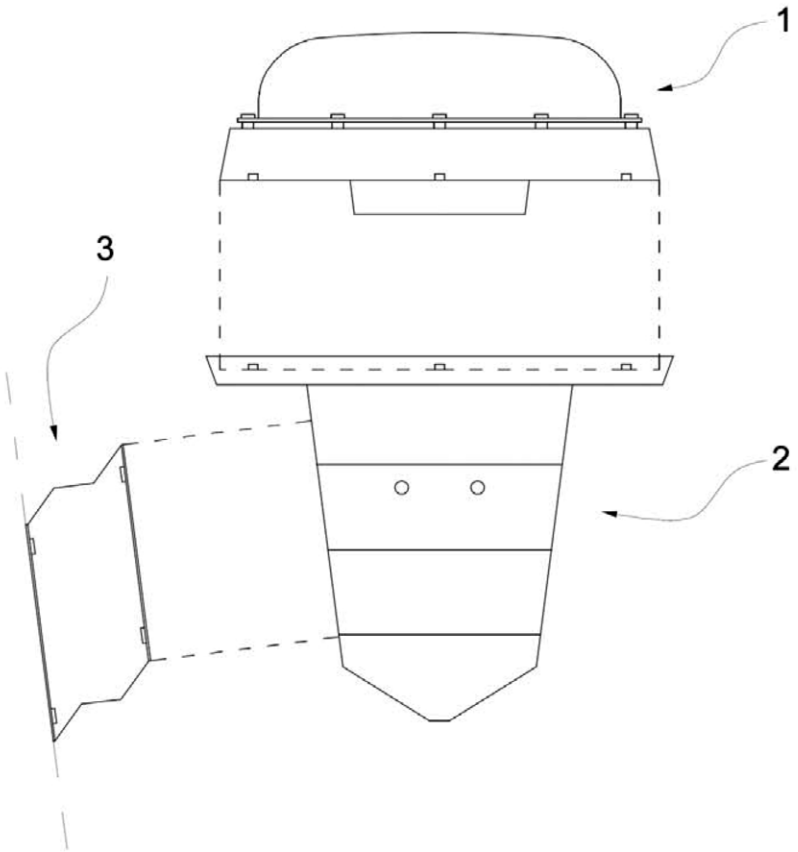

FIG.2

ES 2 642 617 B2

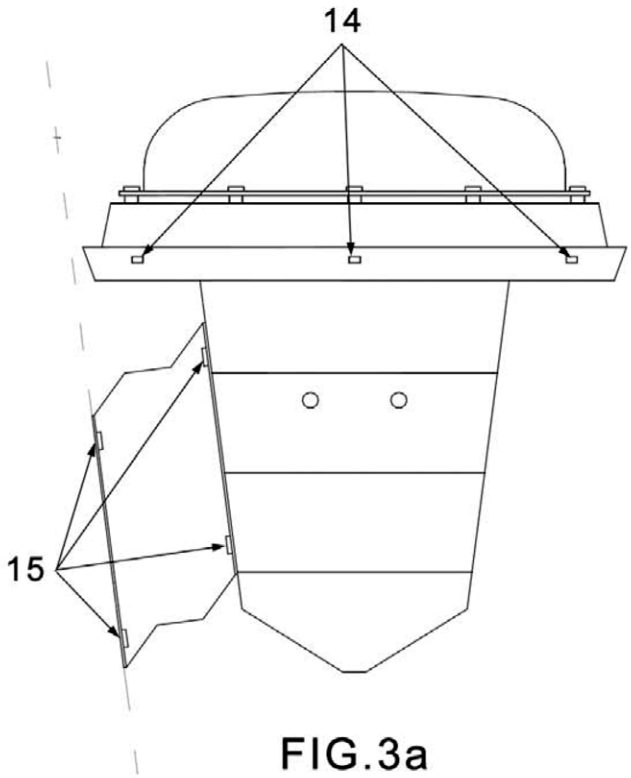

FIG.3a

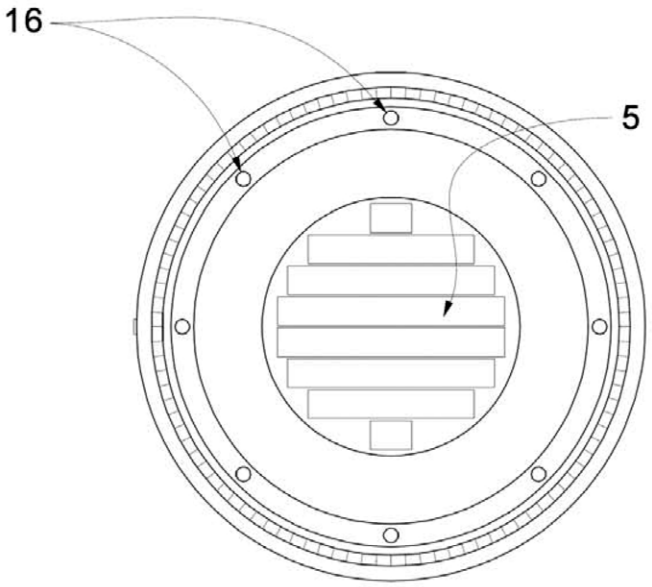

FIG.3b

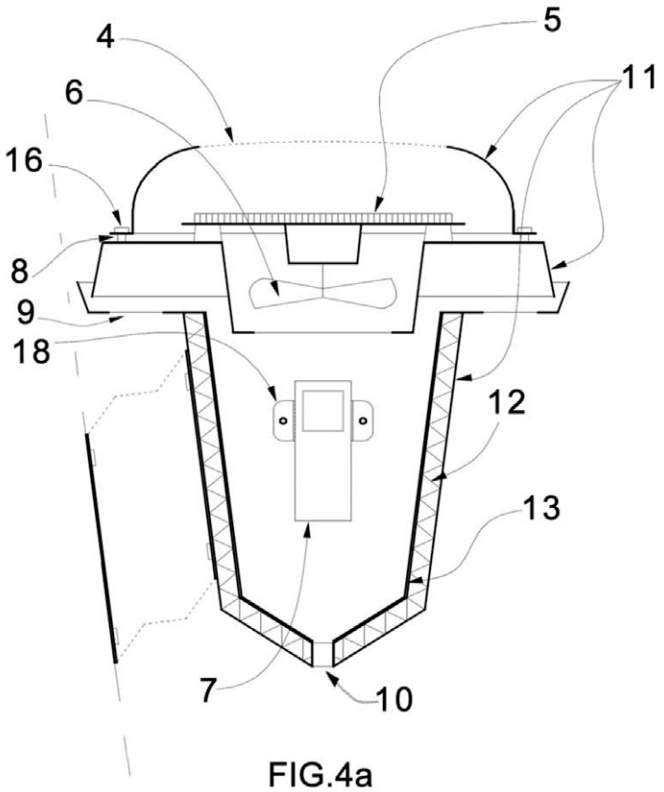

FIG.4a

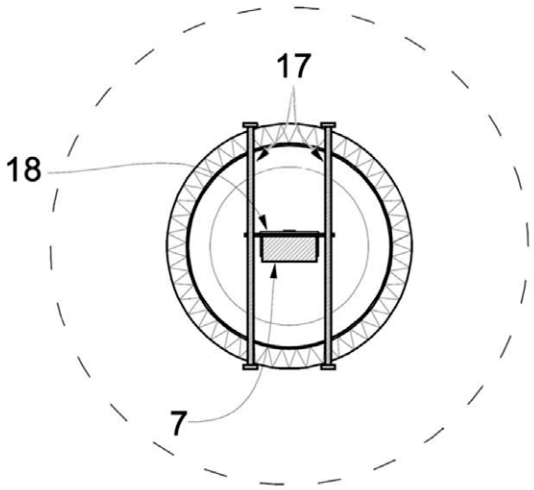

FIG.4b

ES 2 642 617 B2

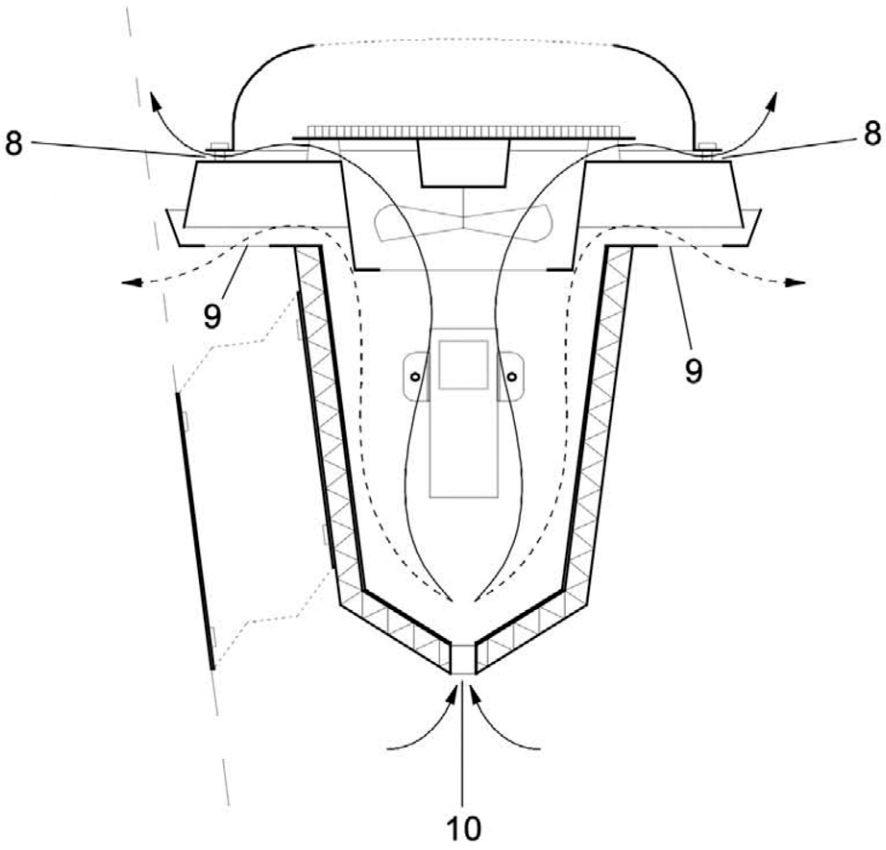

FIG.5

6. Artículo 1 Research paper 1

Source area definition for local climate zones studies. A systematic review

Núñez Peiró, M., Sánchez-Guevara Sánchez, C., Neila González, F.J. (2019)

Building and Environment, 148, 258-285.

doi: 10.1016/j.buildenv.2018.10.050

Índice de impacto:

JIF = 6.456 (**JCR Q1**, *Construction and Building Technology*)

SJR = 1.736 (**SJR Q1**, *Building and Construction*)

PARTE III
PART III

Building and Environment 148 (2019) 258–285

Contents lists available at ScienceDirect

Building and Environment

journal homepage: www.elsevier.com/locate/buildenv

Source area definition for local climate zones studies. A systematic review

M. Núñez Peiró*, C. Sánchez-Guevara Sánchez, F.J. Neila González

School of Architecture (ETSAM), Technical University of Madrid (UPM), Spain, Avda. Juan de Herrera 4, 28040, Madrid, Spain

ARTICLE INFO

Keywords:
Source area
Sensor footprint
Local climate zones
Heat island
Urban environment
Systematic review

ABSTRACT

The correct contextualisation of urban measurements is one of the challenges that urban climate researchers have been dealing with for decades. The Local Climate Zones scheme (LCZs) emerges as a system for characterising these measurements from the thermal perspective. The rapid embracing of the LCZs by researchers from many disciplines, altogether with its adoption for other purposes such as planning, has led to an inexistent or, at its best, flexible use of the source area definition. This practice might call into question the contextualisation of many measurements, highlighting the imperative need to shed light on the source area methods within the urban context. In this study, a systematic review is conducted to compile previous experiences in which the source area was applied in the built environment. Results obtained from the systematic search are summarized and presented according to three scales: the inertial sublayer, the roughness sublayer, and the urban canopy layer. These previous experiences are studied according to their methodological contribution to the source area definition, emphasizing those studies that have considered this concept altogether with the LCZ scheme. This review aims at promoting the knowledge about footprint methodologies and its correct application within the LCZs.

1. Introduction

Climate change and its related extreme events have led to an increasing interest for more precise and reliable temperature measurements. According to the IPCC [1], over the last few decades the number of climatic observations has increased by several orders of magnitude and has led to the reduction of short-term uncertainties. Hundreds of measuring stations have been deployed and provide continuous data on different atmospheric variables. FLUXNET [2], which collects several of those variables, is one of the most relevant networks and counts already with more than 800 in-situ measurement sites all around the world. Spatial agencies such as NASA and ESA have also developed strategies for increasing free public access to their remote-sensing products and findings [3,4]. Accessibility to climatic data has never been as wide and democratic as it is today.

The UN-dependent World Meteorological Organisation (WMO) periodically updates its guidelines regarding the contextualisation of measurements, the processing of metadata and its homogenisation [5,6]. The WMO has published a specific guideline for measuring in urban areas [7], where particular atmospheric characteristics might be found. The strong variability of the urban context, both horizontally and vertically, might generate strong variations among different measurements placed within few meters of each other. In that sense, the accuracy of many Urban Heat Island (UHI) studies were recently questioned due to the absence or incomplete definition of the measurement context, where the dual differentiation between urban-rural was traditionally accepted [8].

Understanding the city as a continuum from urban to rural and the standardisation of the process using specific metadata have been the keystones of many urban climatic classification systems [9–13]. All of them present an equivalent methodological approach, identifying and measuring similar parameters (*indicators*) on the horizontal scale and relating them with a set of uniform zones or *classes* (see Table 1).

The LCZ scheme [14] differentiates itself from the other systems in two ideas. In the first place, this scheme relies on two principles extracted from the classification theory: the *inductive generalisation* and the *logic division*. These are important as they give the structure to the system and contribute to keep it simple: a set of quantitative indicators relate to a set of qualitative urban classes (*inductive generalisation*), which at the same time keep a subclass-superclass relationship (*logic division*). The second idea is that the classification includes both urban and rural areas, in what is called *the landscape*. In this scheme, the gradient from urban to rural can be easily characterised and, therefore, easily compared with other cities or contexts.

Despite being a relative recent proposal, the LCZ has already gained a lot of recognition. Fig. 1 represents the citing evolution of the most

* Corresponding author.
E-mail address: miguel.nunez@upm.es (M. Núñez Peiró).

https://doi.org/10.1016/j.buildenv.2018.10.050
Received 14 August 2018; Received in revised form 15 October 2018; Accepted 24 October 2018
Available online 30 October 2018
0360-1323/

Table 1
Main schemes used as urban climate classification system.

Ref.	Scheme	Acronym	Authors	Indicators		Classification		Citations[1]		Standard. level[2]
				Type	Number of indicators	Type	Number of classes			
[9]	Urban Climatic Maps	UCMap	Knoch (1963)	Qualitative	12	*Undefined*	-	60[a]	(40)	●○○○
[10]	Urban Terrain Zones	UTZ	Ellefsen (1991)	Qualitative	7	Discrete	17	59	(7)	●●○○
[11]	Urban Climate Zones	UCZ	Oke (2004)	Qualitative	4 *(10)*	Discrete	7	-[b]	(6)	●●○○
[12]	Thermal Climate Zones	TCZ	Stewart & Oke (2009)	Quantitative	6	Discrete	20	15	(6)	●●●○
[13]	Urban Zones for Energy partitioning	UZE	Loridan & Grimmond (2012)	Quantitative	2 *(5)*	Continuous	*Not applicable*	42	(7)	●●●●
[14]	Local Climate Zones	LCZ	Stewart & Oke (2012)	Quantitative	10	Discrete	17	359	(91)	●●●○

[1] The metrics have been extracted with the Scopus search engine, looking for the direct citations of each document. In parenthesis appears the number of publications that have cited in their title, abstract or keywords the complete name of each system. Acronyms were not considered.
[2] The standardisation level is associated with the following description: *Low* (qualitative indicators without a specific classification system); *Medium* (qualitative indicators associated to discrete a classification); *High* (quantitative indicators associated to a discrete classification); *Complete* (quantitative indicators associated to a continuous classification).
[a] The UCMap classification was first suggested by Knoch [9], but the most cited document regarding this classification system is Ren et al. [15].
[b] The UCZ classification appears in a WMO report with a whole set of recommendations for carrying out precise measurements in an urban context. As the UCZ classification system represents only a small fraction of this document, the author has decided not to include the number of direct citations.

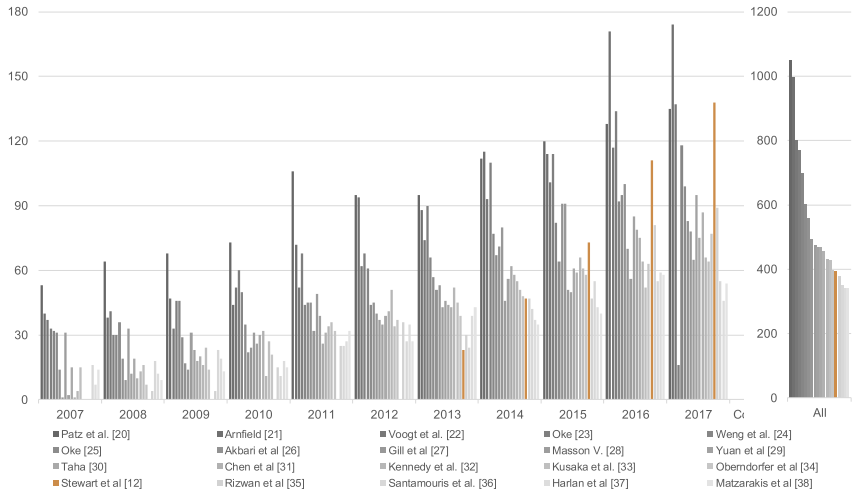

Fig. 1. Ten-years citing evolution of the 20 most cited documents under the "urban heat island" topic [12,20–38]. Source: Scopus.

relevant urban heat island studies between 2007 and 2017. It shows how the LCZ scheme has aroused an increasing interest since 2013, little after it was first published, becoming one of the most cited documents under the UHI topic of this decade. The explanation to such success might also be related to the wide range of applications that this classification system has. Urban climate researchers have used it not only for contextualising measurements, which was its original purpose, but as a classification of the urban fabric itself [16–18]. In that sense, the LCZ scheme has inspired many international initiatives, contributing to the expansion and awareness of the urban climate knowledge among researchers [16,19]. However, the adoption of the LCZs for a wide range of purposes has contributed to a flexible use of its original methodological approach. In that sense, and contrary to what can be done when classifying the urban fabric, the delimitation of the context of a measurement should not be settled arbitrary, but considering very specific parameters, like the height of the measurement or the roughness of the landscape. This concept, which has aroused little interest regarding the LCZ scheme, is called the *thermal source area*

1.1. The source area concept

The thermal source area could be defined as the total area that contributes to the thermal behaviour at a given point, hence outlining the limits of the context for any field observation. It should be noted that this term only refers to the temperature, while *source area*, or just *footprint*, refers to a more generic definition that would include any scalar measurement [39,40]. In fact, the first studies focused on the relationships between the surface properties inhomogeneities and the *flux-profiles* within the boundary layer, and regarding different parameters such as the energy flux, the water vapour, or diverse pollutants [41–43].

As it can be seen in Fig. 2, the extension of the source area usually spreads upwind, where its location and size depend on the sum of several factors. The source area increases its size and distance from the sensor while rising the height of the observation (z_m), the surface roughness, or weather stability. The *footprint function* represents the contribution that each point of the source area has to the total measurement. Over homogeneous surfaces, it reaches its peak (f_{max}) at certain distance, and then decreases logarithmically to the infinite [39]. Uncertainties arise when addressing near-the-ground measurements

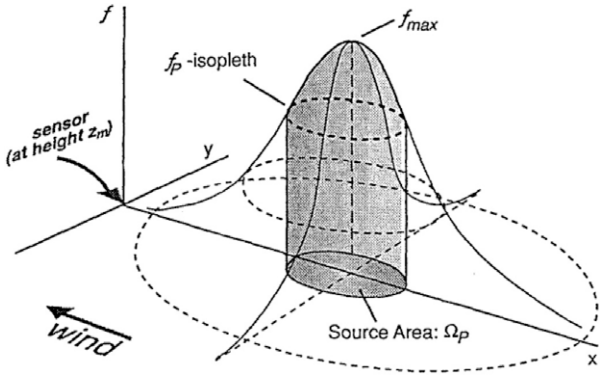

Fig. 2. Illustration of the source area and the footprint function. Source: Schmid [39].

within a heterogeneous context, where surface properties might vary within few hundred meters. This turns to be crucial in almost any urban context, where the source area might be very sensible to surface properties variations.

The source area definition is fundamental for the local climate zones application. According to the process stablished by Stewart & Oke [14], the thermal source area should be taken into account in phase two, right after the collection of metadata and before the local climate zone identification. The source area could be either computed with a footprint model or empirically approximated by field measurements [44]. Under stable atmospheric conditions, the thermal source area for a screen-height sensor might extend few hundred meters away, yet it needs to be further investigated within the urban context (see Fig. 3).

Regardless of that, many researchers have avoided to explore this concept within the LCZs, adopting the approximation given by Stewart & Oke [14] or just choosing a cell-size that would fit with their local climate analysis: the width of a block, the pixel size from a given remote sensor technique, or the emission inventories resolution [45–50]. In fact, there might be many advances in that field of knowledge that are not linked with the urban climate study, maybe due to the current use of scientific databases, where narrow searching might lead to strong barriers for interdisciplinarity and knowledge transfer. The present paper undertakes a *systematic review* of the current advances on the source area definition and its applications within urban areas.

1.2. Aims and objectives of the study

The aim of this work is to perform an organised search and synthesise all the available literature on the existing methodologies for estimating the source area of a sensor within an urban context, and to examine the uptake of these methodologies in the LCZ studies. For that purpose, three main objectives were settled:

- To identify the most appropriate approaches to estimate the source area within the urban context.
- To analyse the most relevant results, identifying the main methodologies, their strengths and weaknesses, and their applications and limitations.
- To determine the degree of embracement of these methods by the current LCZ studies.

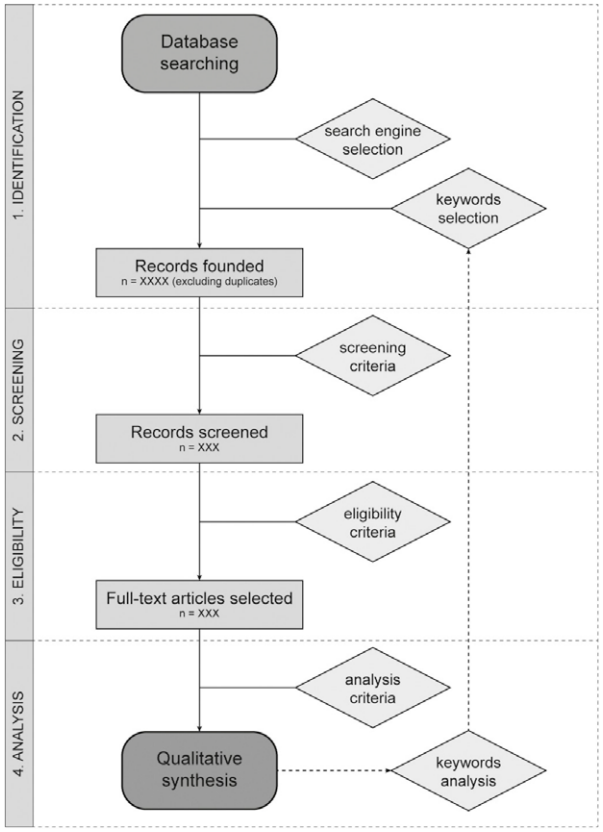

Fig. 4. Phases of the present review, based on the PRISMA flow methodology [63].

2. Means and methods

Systematic reviews are pointed out as the most efficient and less biased methodology for reviewing the existing scientific evidence [51–54]. Regarding urban climate studies, and despite traditional approaches such as narrative reviews [55–57] or critical reviews [58–60] are the most used ones, an increasing interest for systematic reviews is arising [8,61]. In that sense, this paper performs a qualitative systematic review on the source area concept regarding its degree of

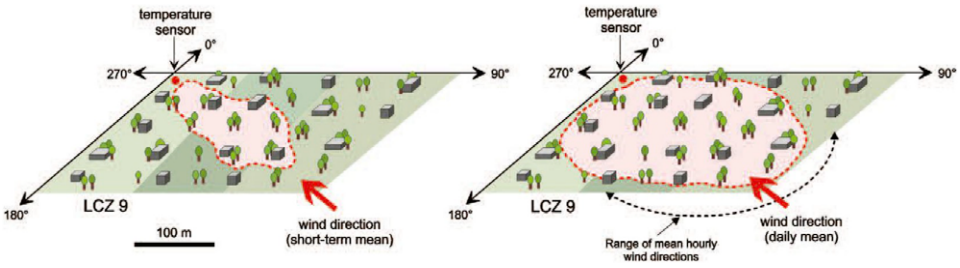

Fig. 3. Illustration of the thermal source area regarding the LCZ scheme. Source: Stewart & Oke [14].

development within the urban areas. For narrative purposes, though, this study will be referred to it as a systematic review.

Systematic reviews are usually conducted within a methodological framework [54,62,63], being available several guidelines from different renowned organisations [64–66]. In this paper we followed the PRISMA Statement from Moher et al. [63], which has been recently used in other urban studies [67–69]. Besides the well-known PRISMA flow diagram, the PRISMA Statement also provides a checklist with multiple items regarding the report of information across the whole review, which has also been used to validate the process. Fig. 4 shows an adapted PRISMA flow diagram, consisting of four phases: *Identification* (1), where a combination of keywords are used to explore scientific databases and find potential relevant results; *Screening* (2), in which non-related documents are discarded; *Eligibility* (3), consisted in ranking results and select the most relevant ones; and *Analysis* (4), in which relevant information is extracted, processed and synthesized.

To provide a clear framework for future systematic reviews on this topic and to facilitate the identification phase within search engines, this paper reviews literature up to 2017, which is the last whole year available. Search results were saved in the open-source *LaTeX* format for its processing and were analysed with the help of a spreadsheet software.

2.1. Identification

Scopus, ScienceDirect and Web Of Science (WOS) were selected as main search engines due to their focus on peer-reviewed research literature and wide range of multidisciplinary topics. Thus, the identification of relevant studies was carried out only among peer-reviewed literature. Interviews, reports, and non-indexed books related to the LCZ scheme were ruled out, as neither their quality nor their representativeness could be assessed.

Regarding the keywords selection, two parts should be differentiated. In the first place, every single search includes the words “source area” or “footprint” (keywords “A”) as, despite the fact that they represent slightly different concepts [40,70,71], many researchers use both in the literature indistinctly (e.g. Refs. [72–74]). Secondly, with the purpose of keeping results within the urban and LCZs scope, the two previous items were combined through Booleans operators with other keywords (keywords “B”). Keywords “B” were defined in two steps: first, keywords related to the urban climate were used (such as “heat island” or “local climate”). Results were then filtered to identify the most relevant records of this first search and keywords contained within these results were added to the identification process. To keep a balance and avoid narrow searching, six categories were stablished and no more than five concepts were considered within each one of them. 30 keywords “B” were then finally used and might be found in Table 2.

This exploration was carried out over the tittle, abstract and keywords (“TAK” search), and only in the case of ScienceDirect was extended to the whole document (“ALL” search). When the number of results were under 10, the “ALL search” included the keywords “B”. By contrast, when the outcomes were too many (above 100 in both “source area” and “footprint” searches), another keyword “C” was included to refine the search.

2.2. Screening

All the records obtained with the different keywords and search engines were screened to exclude repeated and non-related documents. Non-related documents were identified when the terms *footprint* or *source area* (keywords “A”) do not refer to the meaning given in this review, like *sediment source area*, *carbon footprint* or *building footprint*

Table 2
Summary of all the keywords used during the identification phase.

Keywords A			Keywords B		Keywords C
“source area” “footprint”	AND	CLIMATIC DEFINITION	“urban heat” OR “heat island” “local climate” OR “climate zone” “urban climate” “microclimate” “micrometeorology”		**“urban”**
		URBAN CONTEXT	“urban canyon” “heterogeneous” OR “heterogeneity” “spatial variability” “impervious surface” “urban landscape”	AND AND	
		TYPE OF MODELS	“analytical model” “stochastic model” “lagrangian model” “large-eddy simulation” “computational fluid” OR “fluid dynamics”	AND	
		FLUX CONCEPTS	“energy flux” “turbulent flux” “urban physics” “heat flux” “energy balance”	AND AND	
		ATMOSPHERIC SCALES	“surface layer” “inertial sublayer” “roughness sublayer” “urban canopy” OR “canopy layer” “urban boundary” OR “boundary layer”	AND	
		MEASURING CONCEPTS	“scintillometer” “eddy covariance” “temperature measurement” “air temperature” “flux measurement”	AND	

Table 3
Summary of non-related themes for the searched keywords identified during the screening phase.

Keywords	Non-related themes	Examples
"source area"	when referring to: - ecosystem sources - chemical processes - sediments motion	"supply source area", "potential source area", "dust source area", "source area soils", "pollen source area", "sediment source area", "valley-head source area"
"footprint"	When referring to: - greenhouse effect - measurement or size - chemical processes - remote sensing	"carbon footprint", "environmental footprint", "chemical footprint", "building footprint", "aerial footprint"

Table 4
Relevance criteria for classifying the screened records.

Level	Relevance	Description
1	High	**Addresses** the "source area"/"footprint" concept **within urban areas and the surface layer.**
2	Medium	**Mentions** the "source area"/"footprint" concept **within urban areas and the surface layer**.
3	Low	**Mentions** the "source area"/"footprint" concept **within homogeneous or rural areas**, or above the surface layer.

(see Table 3). Since it is relatively common to find more than one meaning for the same word in a single record, these non-related terms were not used as an exclusion criterion during the identification process. Instead, a manual identification of those words was performed in the screening phase. While the WOS and Scopus records were screened looking at their tittle, abstract and keywords, the ScienceDirect results were full-text screened.

2.3. Eligibility

At this stage, each record was evaluated according to its relevance level. Unlike the two previous phases (identification and screening), all

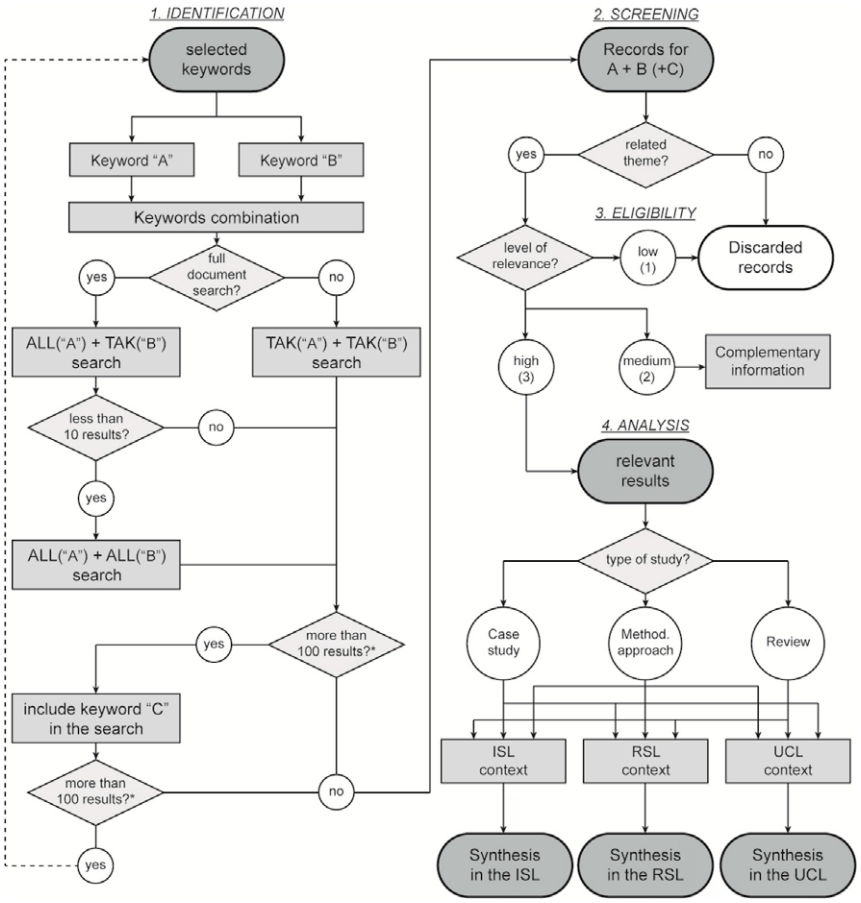

Fig. 5. Flowchart representing the identification, screening, eligibility and analysis phases of this systematic review.

records were examined completely, including the main body of the publication and its references. To this effect, three levels of relevance were used to classify every record. Table 4 recaps the classification criteria, which vary from *low* to *high* relevance. In case of doubt, records were placed in the highest considered level. This ensured that no record would be discarded accidentally when applying the eligible criteria. A level 2 *low relevance* was required to be eligible for the analysis phase.

2.4. Analysis

Results were analysed following a two-fold strategy. In the first place, highly relevant references were differentiated into *case studies*, *methodological approaches*, and *reviews*. Then, the most relevant findings were extracted following different approaches:

- *Case studies* were tabulated according to the measurement's location and atmospheric context, the size of the source area, and the application of the LCZ scheme (Table A.1).
- *Methodological approaches* were identified and related to case studies and were evaluated according to their use in the urban context (Table 6).
- *Reviews* were used to give complementary information regarding the *case studies* and the *methodological approaches and* reinforcing the structure of the analysis section. For that purpose, *reviews* were classified according to their main topic (Table 7).

After all relevant results were explored, an analysis of the source area definition was carried out differentiating three scales: the *inertial sublayer* (ISL), the *roughness sublayer* (RSL), and the *urban canopy layer* (UCL). The source area definition and its use within LCZ studies was addressed in each one of these contexts, particularly regarding the most common practices, remaining uncertainties, and future trends. Fig. 5 presents a flowchart diagram covering all the stages within this systematic search.

3. Results

3.1. Overview of the search results

This systematic review identified 3244 potential documents, while only 135 results were classified as *highly relevant* within this review. Barely 1% of results were not accessed, mainly due to language barriers. Table 5 shows the distribution of the literature results according to the search engine and the level of relevance.

Table 5
Relevance of the identified documents by search engine. The value in parenthesis gives the contribution of each search engine to the total amount of unique results (total results, excluding the repeated).

Level	Relevance	ScienceDirect	Scopus	Web of Science	Unique results
1	High	51 (37.8%)	75 (55.6%)	65 (48.1%)	**135**
2	Medium	71 (74.7%)	18 (18.9%)	17 (17.9%)	**95**
3	Low	307 (61.4%)	177 (35.4%)	200 (40%)	**500**
-	Not relevant	1399 (56.3%)	902 (36.3%)	689 (12.2%)	**2487**
-	No access/other	0 (0%)	27 (90%)	16 (53.3%)	**30**
TOTAL		**1828 (56.4%)**	**1189 (36.7%)**	**987 (30.4%)**	**3244**

All highly relevant results are next differentiated in three categories: *case studies*, where the authors present a field campaign in which measurements where contextualised using the source area concept; *methodological approaches*, in which a novel methodology for estimating the footprint is described; and *reviews*, which synthetize information regarding a specific topic related with the source area.

A total of 90 *case studies* were classified with a 3 *high relevance* level. Their methodological approach, measurement characteristics, atmospheric context and, in case the research was published after 2012, the application of the LCZs, was summarized in Table A.1 (Annex 1). These case studies constitute the core of this section, pointing towards differences in the methodological approach that were applied within the urban context.

Table 6 links most of the existing footprint models with all the urban case studies found within this systematic review. These models are summarized according to their methodological approach, which could be analytical dispersion solutions, lagrangian stochastic models, computational fluid dynamics such as Large-Eddy Simulations (LES) or Reynolds-Averaged Navier-Stokes equations (RANS), or an ensembled combination of different ones (LES-LS, RANS-LS). This table also includes the spatial dimensions each model might be able to reach, going from the most basic 1D analytical approaches to the most complex 3D LES-LS models. At this point it should be noted that, the simpler the methodology, the lesser resource intensive it normally is, and which certainly has an important weight when choosing for a method to estimate the source area.

Many reviews were also identified and used to articulate the results section. Table 7 presents some of the most relevant reviews according to their focus, which might be the atmospheric physics over urban or heterogeneous contexts, the footprint estimation, or the measurement techniques. Keywords given by the authors are also included to facilitate the identification of the main theme by the reader.

The source area size might range from few tens to thousands of meters away depending on a combination of multiple factors. Among all of these, there are some aspects that scientist cannot control when carrying out measurements, such as the wind direction and speed, or the atmospheric stability. These parameters introduce variations in the size and shape of the source area, thus requiring a continuous update along with their measurements. Authors normally report the average source area differentiating among wind sectors [99,130,138,145] and including a description of the weather conditions during the measurement campaign. In some cases, data is filtered to exclude measurements under certain stability conditions [128,132,148,175]. A description of other variables that influence the size of the footprint, and which are set by the authors, is also commonly reported. These include the height of the measurement and its surroundings, the measuring technique, the methodology used for modelling the footprint, and the land cover properties of its surroundings. Overall, and altogether with the information already mentioned, scientist report the size of the source area graphically including different percentages of the flux, typically 60, 70, 80 and 90%.

Fig. 6 summarises the maximum source area reported by all the case studies included in Table A.1, and according to some of the factors mentioned above. In most cases they are presented as a range of the maximum source areas for all wind sectors. There is a clear tendency for larger source areas when increasing the percentage of the considered flux or when increasing the relative height of the measurement. This tendency is faded out when looking at the season of the year, which correlates in many cases with atmospheric stability, and might be due to the filtering of measurements, the time of the day when measurements were carried out, or the latitude of the measurement site.

The absence of a common framework for the available results, as

Table 6
Overview of some of the most relevant footprint models, and its uptake by urban case studies. Adapted and updated from Foken [71], Leclerc [44], Vesala et al. [70] and Schmid [40].

Reference		Acron.	Model	Applicat.[a]	Case studies
[75]	Schuepp et al. (1990)	SP90	1D Analytical	Yes (3)	Dorsey et al. [76]; Jacobs et al. [77]; Stabler et al. [78]
[79]	Schmid and Oke (1990)	SO90	1D Analytical	Yes (7)	Grimmond et al. [80]; Grimmond [81]; Kaplan et al. [82]; Lemonsu et al. [83]; Rooney [84]; Rooney et al. [85]; Schmid et al. [86]
[87]	Leclerc and Thurtell (1990)	LT90	1D Lagrangian		
[88,89]	Horst and Weil (1992; 1994)	HW92/94	1D Analytical	Yes (3)	Jacobs et al. [77]; Järvi et al. [90]; Lee et al. [91]
[39,92]	Schmid (1994; 1997)	SD94/97	1D/2D Analytical	Yes (11)	Barlow et al. [93]; Contini et al. [94]; Häb et al. [95]; Kanda et al. [96]; Kordowski & Kuttler [48]; Liu & Sun [97]; Oke et al. [98]; Pawlak et al. [99]; Rooney et al. [85]; Weber & Kordowski [100]; Zielinski et al. [101]
[102]	Kaharabata et al. (1997)	KA97	2D Analytical		
[103]	Leclerc et al. (1997)	LC97	1D LES		
[104]	Baldocchi (1997)	BI97	1D Lagrangian		
[105,106]	Rannik et al. (2000; 2003)	RK00/03	2D Lagrangian		
[107]	Hsieh et al. (2000)	HH00	1D Analytical	Yes (11)	Contini et al. [94]; Gioli et al. [108]; Morin et al. [109]; Oliphant et al. [110]; Ramamurthy and Pardyjak (2011); Roth et al. [111]; Song & Wang [112]; Sparks and Toumi [113]; Velasco et al. [114–116]; Ward et al. [117]
[118]	Kormann and Meixner (2001)	KM01	1D Analytical	Yes (26)	Ando and Ueyama [119]; Auvinen et al. [120]; Björkegren and Grimmond [121]; Christen et al. [122]; Crawford et al. [123,124]; Feigenwinter et al. [125]; Helfter et al. [126]; Hellsten et al. [127]; Kent et al. [128]; Kota et al. [129]; Kotthaus and Grimmond [130,131]; Kurppa et al. [132]; Lee et al. [91]; Lietzke et al. [73]; Liu et al. [133]; Nordbo et al. [134]; Park et al. [135,136]; Rapsomanikis [137]; Salmond et al. [138]; Ueyama and Ando [139]; Valach et al. [140]; Wang et al. [141]; Zou et al. [142]
[143]	Kljun et al. (2002)	KN02	3D Lagrangian		
[144]	Kljun et al. (2004)	KN04	1D Analytical	Yes (8)	Bergeron and Strachan [145]; Guidolotti et al. [146]; Hiller et al. [147]; Langford et al. [148]; Mårtensson et al. [149]; Menzer and McFadden [150]; Park et al. [135,136]
[151]	Sogachev and Lloyd (2004)	SL04	2D/3D RANS (1.5-order)	Yes (2)	Järvi et al. [90]; Vesala et al. [152]
[153]	Cai and Leclerc (2007)	CL07	3D LES-LS		
[154]	Prabha et al. (2008)	PA08	3D LES		
[155]	Steinfeld et al. (2008)	ST08	3D LES-LS	Yes (2)	Auvinen et al. [120]; Hellsten et al. [127]
[156]	Hsieh and Katul (2009)	HK09	2D RANS-LS (2-order)		
[157]	Kljun et al. (2015)	KN15	2D Analytical	Yes (1)	Inagaki et al. [158]

[a] Application in an urban context.

Table 7
Overview of some of the most relevant reviews regarding urban atmospheric physics, footprint estimation or measuring techniques. Symbol (●) indicates the most relevant focus while (○) indicates a theme minorly addressed.

Reference		Focus			Keywords[a]
		Atmospheric physics	Footprint estimation	Measurement techniques	
[159]	Stull (1988)	●		○	boundary layer meteorology; turbulent flow; convective mixed layer; turbulent flux
[160]	Flesch (1996)		●		atmosphere; stochastic methods; Lagrangian model; atmospheric trajectory; boundary layer flux
[161]	Mahrt (1996)	●	○		bulk aerodynamic formulation; drag law; heat flux; surface fluxes
[162]	Aubinet (1997)	○		●	eddy covariance; temperature fluctuation; aerodynamic method; flux measurement
[163]	Roth (2000)	●		○	mixing-layer analogy; roughness sublayer; urban boundary layer; urban turbulence
[40]	Schmid (2002)		●		footprint; micrometeorology; atmosphere exchange; modelling; flux measurements
[164]	Arnfield (2003)	●			urban climate; energy budget; urban roughness; urban heat island; atmospheric turbulence
[22]	Voogt & Oke (2003)	○		●	remote sensing; urban climates; rural
[165]	Vesala et al. (2004)	○	●		boundary layer; footprint; heat flux
[166]	Göckede et al. (2007)		●	○	flow field; Lagrangian analysis; stochasticity; surface layer; turbulent boundary layer
[167]	Roth (2007)	●		○	tropical urban climatology; tropical urban heat island; tropical urban energy balance
[70]	Vesala et al. (2008)	○	●		footprint; source area; turbulent flux; atmospheric turbulence; atmospheric pollutants
[168]	Grimmond et al. (2010)	●		○	urban climate modelling; observations; adaptation; mitigation; built environment
[169]	Mahrt (2010)	○	○	●	eddy correlation; fluxes; turbulent transport; mesoscale flux; aircraft flux
[170]	Velasco & Roth (2010)		●		anthropogenic source; carbon flux; neighbourhood; eddy covariance; urban pollution
[171]	Vesala et al. (2010)	○		●	–
[172]	Feigenwinter et al. (2012)	○	●		urban heat island; street canyon; eddy covariance; urban ecosystem; urban surface
[173]	Rannik et al. (2012)	●		○	–
[164]	Barlow et al. (2014)	○		●	urban balance; boundary layer; roughness sublayer; surface heterogeneity; mesoscale circulations
[45]	Christen (2014)	○	●	○	atmospheric measurement; urban atmosphere; carbon dioxide; eddy covariance; greenhouse gases
[44]	Leclerc & Foken (2014)		●	○	–
[71]	Foken (2008; 2017)		●		atmospheric process; environmental meteorology; experimental methods; heterogeneous surface; measurement techniques
[174]	Toparlar et al. (2017)	●		○	Adaptation measures; building energy consumption; computational fluid dynamics; urban physics; sustainability

[a] Selection of the keywords given by the authors or proposed by the databases (five maximum).

well as the high number of influencing variables, makes very difficult when not impossible to carry out a meta-analysis, which would be the ideal scenario for a systematic review. However, and despite these uncertainties, about 75% of these studies place the source area from 100 to 1200 m away, which might be related with a common methodological framework for estimating the source area. In that sense, a meta-synthesis is more suitable for summarising scientist's common trends and shared assumptions regarding the estimation of the source area and its use within the LCZ scheme.

3.2. Detailed analysis of the results according to the three surface layer scales

As most of these authors agree, the concept of scale is fundamental for understanding the atmospheric processes that occur within the *surface layer* (SL) and, therefore, to determine the best methodological approach for estimating the source area. This section will be next presented according to these urban atmospheric scales. According to Fig. 7, three different contexts must be differentiated in the SL: the *inertial sublayer* (ISL), the *roughness sublayer* (RSL), and the *urban canopy layer* (UCL).

3.2.1. The inertial sublayer (ISL)

The ISL develops in the upper part of the surface layer, from the upper limit of the RSL, the so-called *blending height*, to the top of the SL. This part of the atmosphere links both the regional and the local scale, therefore reflecting the effects that the surface introduces in the atmospheric boundary layer structure [164]. Within this layer, and under neutral conditions, turbulent fluxes are mostly constant with height, so it can be assumed as a constant-flux layer with a homogeneous flow were the logarithmic wind laws apply [177]. With non-neutral condition, Monin-Obukhov Similarity theory might be used to explain turbulent fluxes near the ground (M − O theory [178]).

These two assumptions, which were ideally developed for flat and horizontally homogenous surfaces, were extensively accepted in rural areas [71]. These have been borrowed by urban climate studies, extending the wind log-profiles and M − O theory assumptions to measurements within the urban inertial sublayer; the main consensus is that, well above the blending height, turbulent fluxes might be already well mixed [164,170,172]. Despite that this principle might not be true for urban context [163,173], this simplification has allowed urban climate researchers to use analytical footprint models that easily delimit the most likely source area of their measurements.

The ISL has therefore become the most common scale for carrying out urban flux measurements (see Fig. 8). Schmid et al. [86] is one of the first known references that reported heat flux measurements over a city altogether with the use of the source area concept to contextualise it. Grimmond et al. [80,81] kept using the footprint to study energy flux measurements at the same location in Vancouver, while other studies started arising in other places: Mexico City [179], Christchurch [180], Tokyo [96], Marseille [83,181], Essen [100], Houston (TX) [135], Basel [125,138], Helsinki [134], Swindon [117,182], Gongju [91], London [124], Black Rock City (NV) [110], Łódź [101], and Nanjin [142].

Similar experiences can be found among gas measurements. Regarding the urban context, the most common ones are the CO_2 flux studies, which might be found in Mexico City [114,116], Helsinki [90,120,132,134,152], London [72,113,121,126,131,183], Vancouver [122,184], Montreal [145], Saint Lake City (UT) [185], Baltimore (MD) [123], Florence [108,186], Beijing [112,133], Basel [73], Minneapolis-Saint Paul (MN) [150], Singapore [187], Sakai [139], Black Rock City (NV) [110]. Other gas fluxes like CH_4 [99,108], VOCs [129,135,140,148], NO_x [188], water vapour [77] or aerosols [149] were also studied altogether with a previous footprint analysis.

Despite local climate zones were presented in the last decade [14], several studies have addressed them to describe the measurement context within the ISL. Its use has gone beyond the original *thermal* scope of the LCZ scheme, as it has been proven as a useful tool for many other parameters. Valach et al. [140] have recently used it when measuring the concentration of VOCs in London, while Pawlak et al. [99] have used it to compare methane fluxes in Łódź, and many other authors have also used it to contextualise CO_2 emissions [112,116,130–133,150,184,187,189]. In a recent review, GHG emissions were compared among different studies using the LCZ scheme [45,190]. As shown in Fig. 9, the LCZ seems to adapt in a good manner to other measurement parameters that also link with land cover properties.

Most of these studies used analytical footprint models, which might be differentiated between eulerian analytical models [39,75,79,88,89,92,118], and those that might be considered parameterisations of Lagrangian stochastic models [107,144,157]. According to results, Lagrangian stochastic approaches have not been applied within the urban context, probably due to the necessity of defining the wind field statistics. In few cases, the footprint has been directly derived from CFD techniques such as LES or RANS modelling, which require a 3D model and increase the resources needed for computing it.

The Kormann and Meixner [118,191] model is the most used one among analytical footprint models. Some of these methodologies might require different input parameters and assumptions, such as the Monin-Obukhov Similarity Theory (MOST) or logarithmic wind profiles already mentioned above (see Oke et al. [192] for a thoughtful explanation). Their performance mainly relies on the characterisation of the so-called *aerodynamic parameters*, which are the *zero-plane displacement* (z_d) and the *roughness length* (z_0). Kent et al. [128] have recently demonstrated their relevance among the footprint estimation, and which might in fact be higher than the footprint modelling itself (see Fig. 10). These values can be estimated using anemometer's observations, morphological information, or tabulated tables. One of the first and most used methodology is the height-based approach for urban areas proposed by Grimmond and Oke [193]:

$$z_d = f_d \bar{z}_H \tag{1}$$

$$z_0 = f_0 \bar{z}_H \tag{2}$$

where $\bar{z}_H$ is the mean height of the surrounding elements, and f_d and f_0 represent the empirical coefficients for each aerodynamic parameter, with a value of 0.7 and 0.1, respectively. Some examples found within this review are Velasco et al. [114,116], Roth et al. [187], Pawlak et al. [99], Crawford et al. [124], Zielinski et al. [101] and Ward et al. [117,182,194,195].

Among anemometric approaches in urban environments, the one derived from *Eddy Covariance* (EC) measurements [196] has been extensively used due to the prevalence of the EC technique for measuring energy fluxes [133,197]. Another interesting anemometric approach is the scintillometer heat flux method proposed by Kanda et al. [96], and which also uses a measurement equipment very extended among urban environments.

Other estimations of these parameters might be done with morphometric approaches. These might include the ratio of urban plan occupied by roughness elements (Mcdonald et al. [198], found in Refs. [134,180]) or the standard deviation of the roughness-element heights, as proposed by Millward-Hopkins et al. [199] and Kanda et al. [200], and which might be found in recent studies [125,158].

While the latter ones seem to better agree with in-situ measurements, anemometric tend to give higher z_d and lower z_0 than morphometric, resulting in differences up to and above 100% [128].

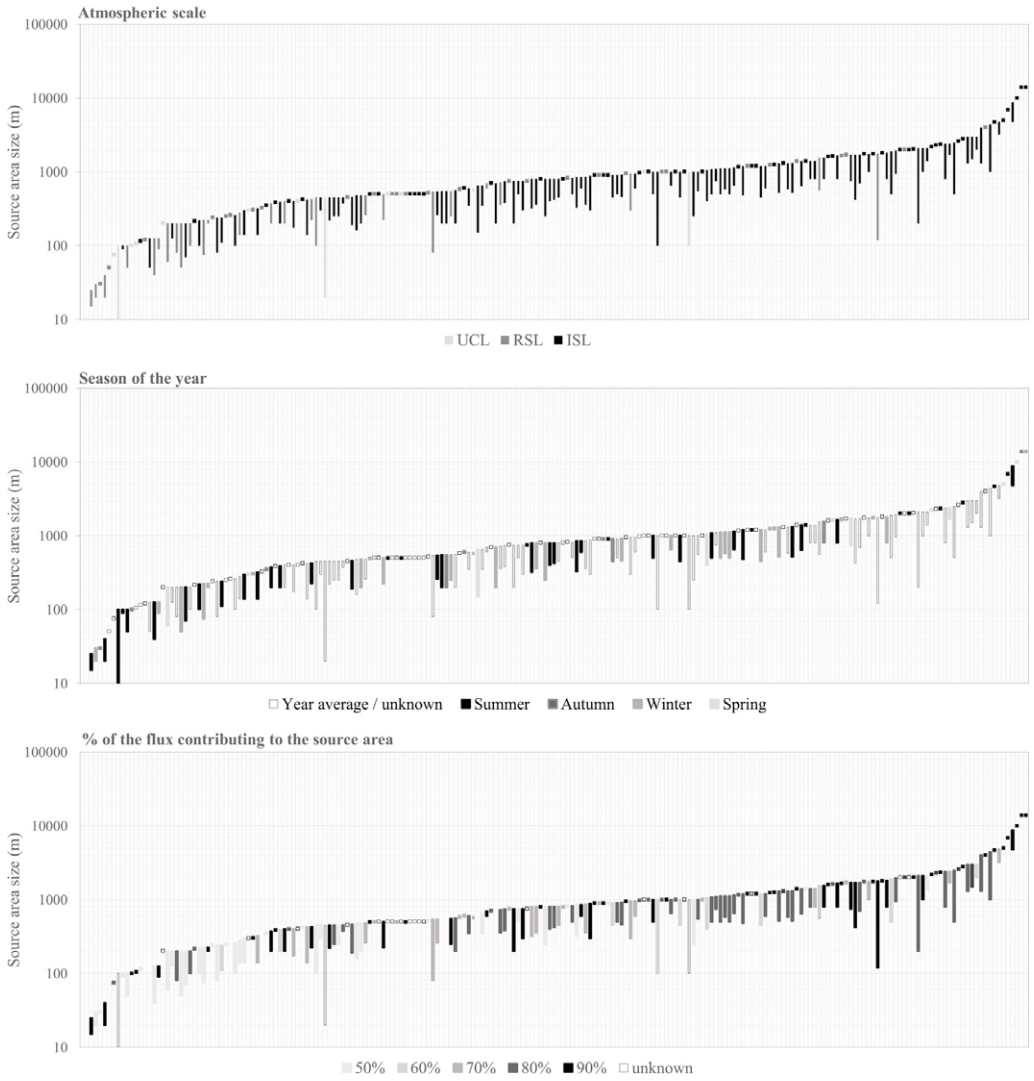

Fig. 6. Maximum source area distance for all case studies identified during the systematic review, and related with the considered atmospheric scale (top), the season of the year (middle), and the percentage of the flux contributing to the source area (bottom).

Therefore, although the use of analytical footprint models might be allowed within the ISL, urban climate researchers should account for the correct estimation of the aerodynamic parameters and the uncertainties derived from them.

Scientists measuring within the ISL should also take horizontal heterogeneities into consideration. Even though Hellsten et al. [127] have demonstrated that over relative homogeneous urban arrangements a constant-flux layer above the blending height could be expected, this principle does not hold when it comes to urban structures with strong roughness variations. At this point it should be underlined that, depending on the measurement height and weather conditions, the footprint fetch of a measurement within the ISL might extend from hundred meters to several kilometres, covering different types of urban fabric. Strong variations within the urban context '*seen*' by the sensor might introduce another degree of uncertainty among results from analytical footprint models.

In this direction, Vesala et al. [152] and Järvi et al. [90] have compared results within the ISL and over heterogeneous urban areas from an analytical and a more sophisticated model based in CFD (see section below for further information). They have corroborated that analytical models do not correctly reflect the contribution of each area to the overall flux. These models assume a horizontally homogeneous surface, and therefore produce a smooth footprint function where at certain distance the largest contribution is given, and from which it decays to the infinite. The CFD model identifies, on the contrary, different *high-contribution* distances, with a more reliable approach to the real urban structure (Fig. 11). The problem with CFD based models is that they are extremely resource demanding, and there is not yet an easy way to implement them.

Another problem with heterogeneous areas has to do with the local climate zone classification. This scheme was proposed for comparison purposes, but it is not prepared for heterogeneous-patchy areas.

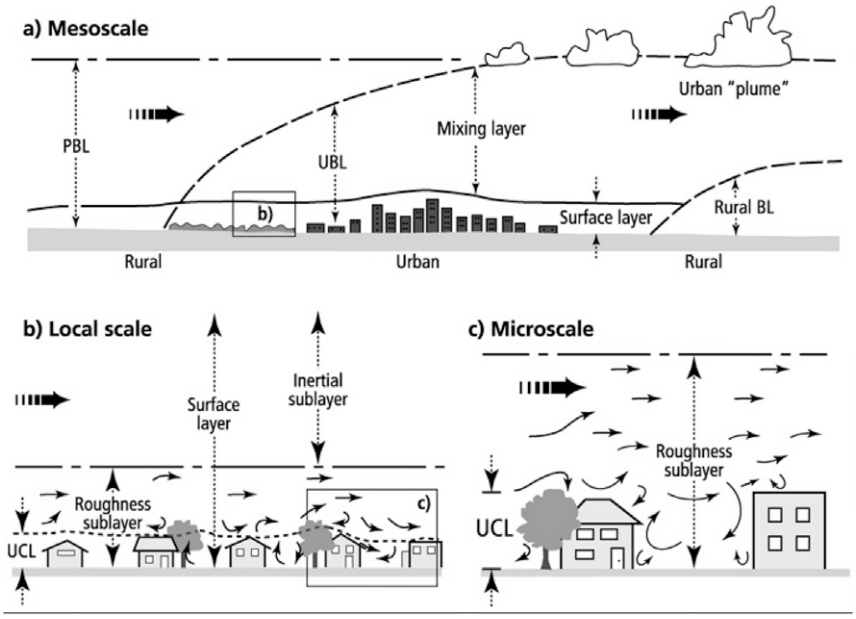

Fig. 7. Climatic scales and vertical layers found in urban areas. PBL: Planetary Boundary Layer. UBL: Urban Boundary Layer. UCL: Urban Canopy Layer. Source: Oke [176].

Heterogeneities should be kept within the described built and land cover types, or at least within a homogeneous mix of different ones. As stated by Stewart and Oke [14] (2012), transitional areas should be avoided when sitting the equipment. Otherwise, using the LCZ scheme might lead to similar problems as the ones identified by Stewart [8], who underlines the impossibility of comparing different measurements due to the poor definition of the context. In that sense, Alexander et al. [201] compared four measurement sites with its surroundings and decided to only consider the flux when the upwind LCZ was equivalent to the one at the measuring site (see Fig. 12).

For the sake of comparison, Fig. 13 represents the urban context of four other studies that were found within this systematic review [116,131,132,201]. Red circumferences with a radius of 500 and 1000 m are overlaid. In all cases, assuming a homogeneous urban context becomes more difficult as long the considered area increases. The Mexico City measurement site (upper-left image) contrasts with the one of London (lower-right one), where the Thames river covers almost half of the surface within the 500 m circumference. In the case of Dublin (top-right) and Helsinki (bottom-left), heterogeneities are more evident within the 1000 m circumference, where water bodies, parks or

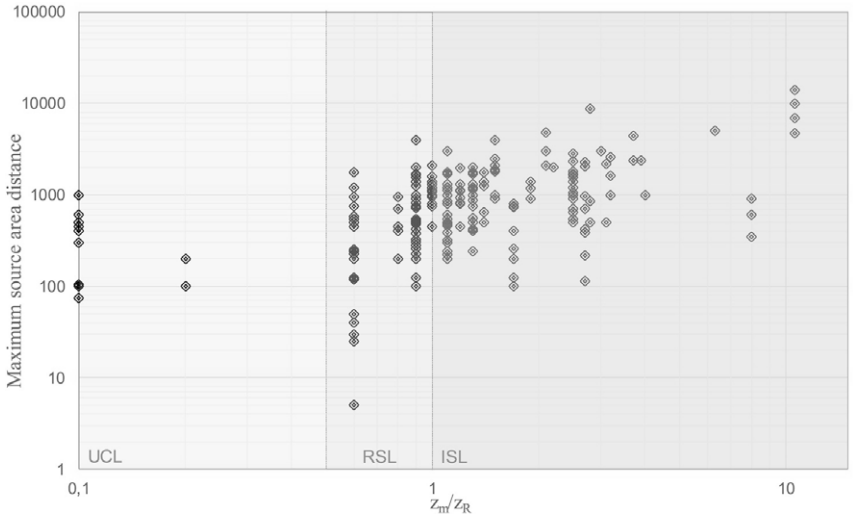

Fig. 8. Maximum footprint distance related with the atmospheric context, for all highly relevant case studies. UCL: Urban Canopy Layer; RSL: Roughness Sublayer; ISL: Inertial Sublayer; z_m: measurement height; z_R: blending height.

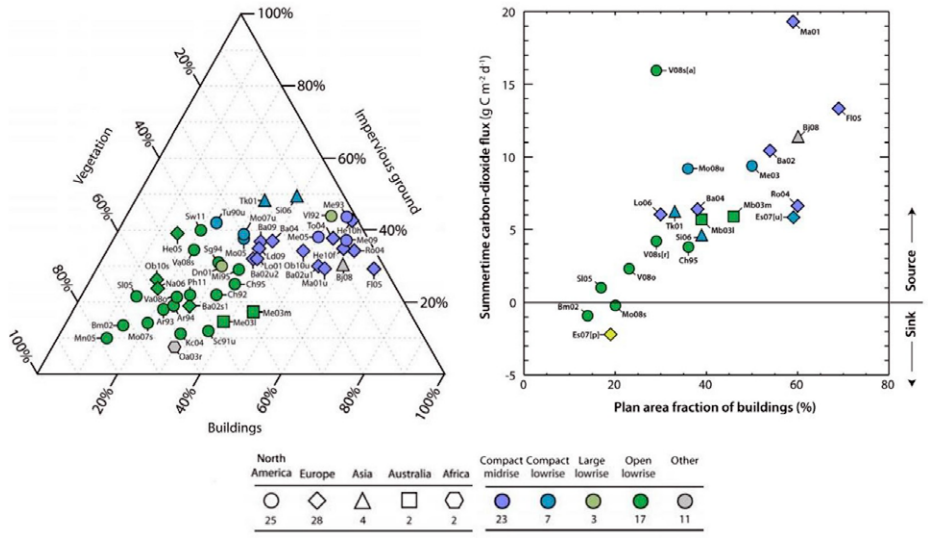

Fig. 9. (Left) Land cover percentages and LCZ classification for different GHG measurement sites. (Right) Correlation between CO_2 and the fraction of buildings, according to their LCZ class. Adapted from Grimmond and Christen [190].

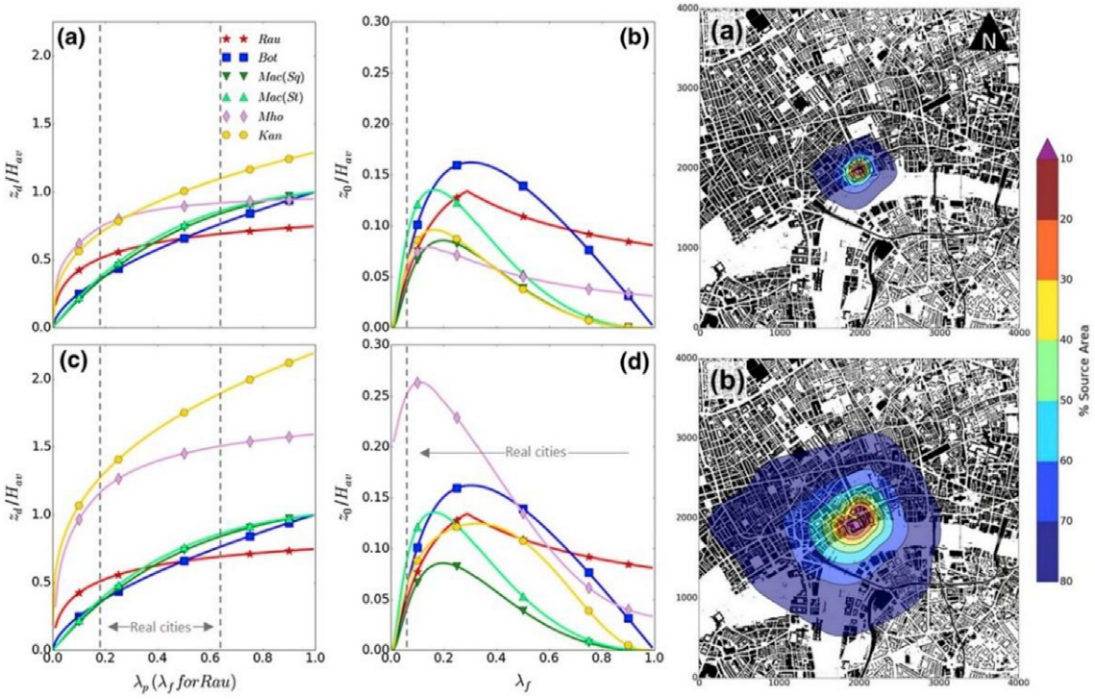

Fig. 10. In the left and the centre, the zero-plane displacement (z_d) and the roughness length (z_0) are estimated according to different methodologies. In the right side of the figure, source areas for the same location and time period are estimated with Kormann and Meixner [118] and using the aerodynamic parameters derived from the Mho (a) and Mac (b) morphometric methods. After Kent et al. [128].

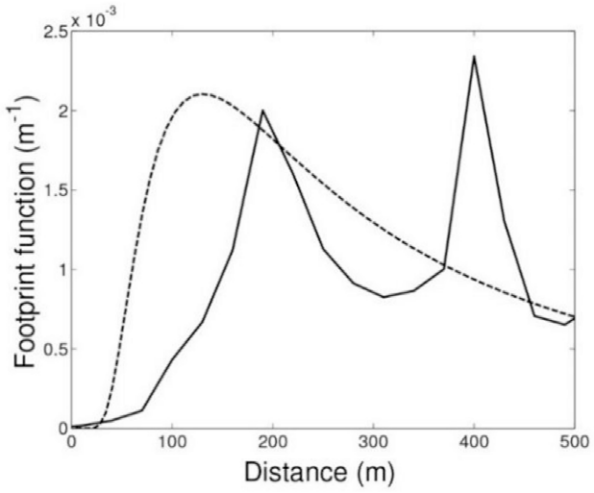

Fig. 11. Cross-wind integrated flux footprint as estimated for surface sources. Analytical model (Horst and Weil [88]; dashed line) and numerical model (Sogachev and Lloyd, [151]; solid line) are presented. After Järvi et al. [90].

train stations might generate important heterogeneities under certain wind directions. Despite the degree of heterogeneity varies substantially among these studies, the four of them were classified by the authors as a *compact mid-rise* (LCZ 2), and all of them have used an analytical footprint model to contextualise their measurements. This tendency has been a constant among all the reviewed studies within this research.

Urban climate researchers should bear in mind that measuring above the *blending height* is not a sufficient condition to guarantee the use of analytical footprint models. Special attention should be given to the degree of heterogeneity of the footprint, and for that purpose the LCZ scheme might be very useful. Classifying the context according to the LCZ after defining the footprint and corroborating that it is suitable for that purpose, which follows the LCZ guidelines proposed by Stewart and Oke [14], would be a good practice for measurements within the ISL.

3.2.2. The roughness sublayer (RSL)

Uncertainties increase when approaching the theoretical limit of the blending height (z_R). Under it, the roughness sublayer (RSL) develops in two different scales: the bottom part, which in urban contexts is usually referred as the urban canopy layer (UCL), and the upper part, which is normally denoted as the RSL (see Fig. 7). The last one could be considered as a transition layer between the UCL, the microclimatic scale where most of the urban activities take place, and the ISL, where the effects of the land surface are already well mixed and representative of the local scale. In that sense, and contrary to the ISL, Monin-Obukhov Similarity theory does not apply at the RSL level. Within this layer, turbulence dominates the flow and depends on the spatial characteristics underneath, which introduces many doubts about the source of the energy flux [44]. The wind aerodynamics and the footprint modelling at this scale have been roughly investigated, mainly through scale models placed within wind tunnels and CFD computation [199,202–204], normally assuming homogeneous 3D layouts.

All these considerations bring the difficulties that urban climate researchers might have to deal with to the fore, in case their measurements are carried out within this layer. To avoid these uncertainties, urban climate researchers usually try to avoid this scale when placing their instruments, therefore situating them as high as possible and trying to reach the ISL. There are many different methods to establish the depth of the RSL, which determines the height of z_R or *blending height*. The general consensus among researchers is that it should be somewhere between 1.5 and 5 times the average height of the roughness elements (h_b), and closer to $2{\cdot}h_b$ the most part of the time [193,205,206]. However, this limit is not static and might change its position within the day. In urban environments, where buildings easily rise tens of meters tall, reaching such heights might be a complicated task, particularly if there are legal constraints for erecting towers above the urban canopy [163]. These arguments are reflected in most of the RSL studies found in this review (see Fig. 14), which measurements are placed near the blending height limit $z_m/z_R = 1$ (where $z_R = 2{\cdot}z_B$).

Despite these limitations, authors frequently implicitly *assume* to be within the ISL [48,83,94,121,145,146,183,207] or explicitly *state* that they are measuring within the ISL [100,109,112,133,137,140], even though some doubts might arise about it. Not many urban climate researchers recognise they struggle to justify the climatic context of some of their measurements [113,128,139] and, in a similar way, not many studies have focused in the RSL *on purpose* [84,96,98,138]. Previous studies have pointed out the uncertainties these RSL-ISL measurements might introduce in the source area estimation [70].

Authors normally discuss the convenience of using analytical footprint models within the RSL, which poses a question regarding how biased these estimations are. In that sense, Hellsten et al. [127] have

Fig. 12. LCZ description at the measurement site and its surroundings. After Alexander et al. [201].

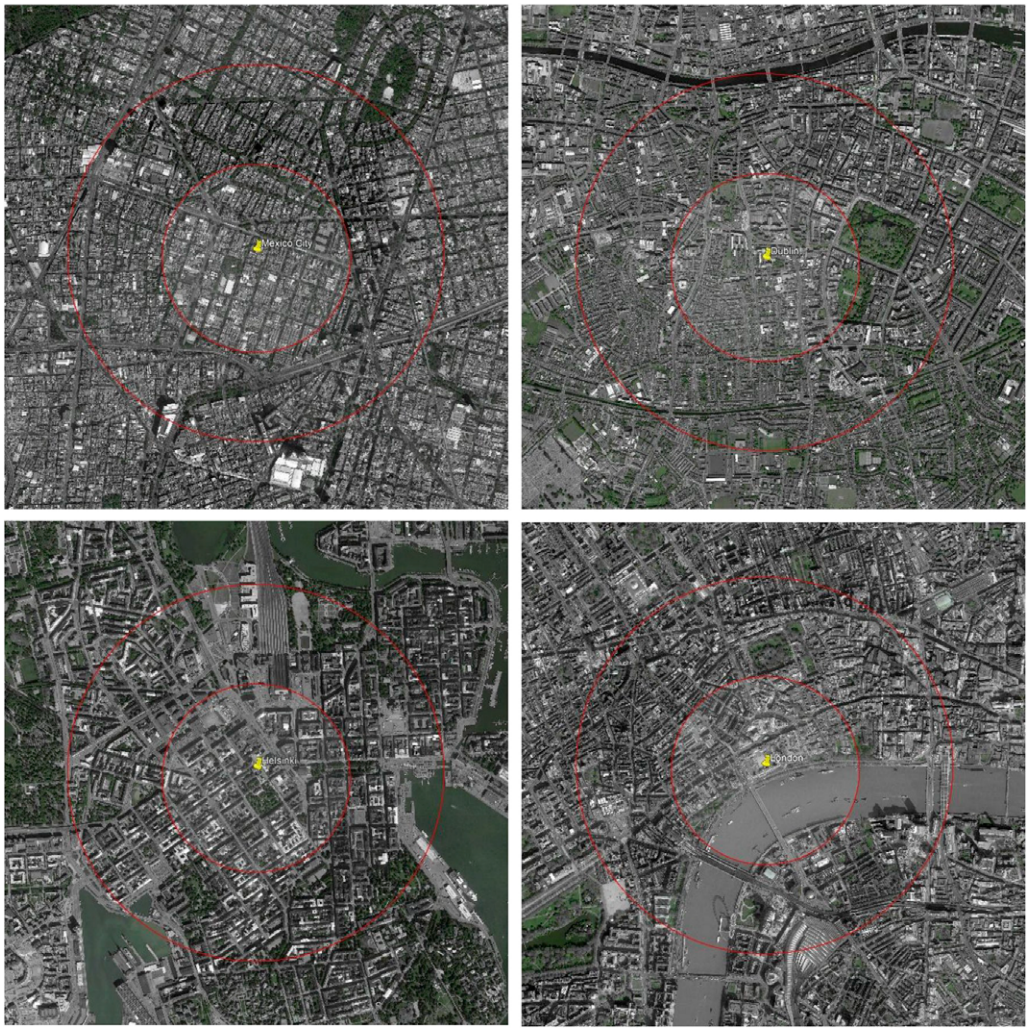

Fig. 13. Satellite image of the urban sites and location of the measurement equipment according to different studies. Top left: Mexico City, Mexico [116]. Top right: Dublin, Ireland [201]. Bottom left: Helsinki, Finland [132]. Bottom right: London, UK [131].

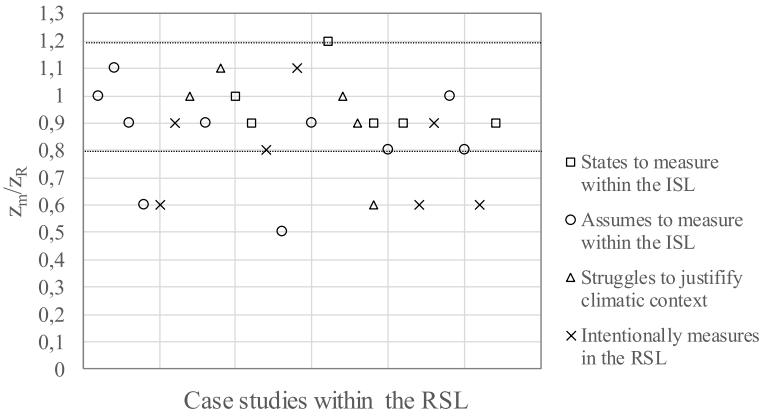

Fig. 14. Relative height of the measurements classified as RSL case studies. Dotted line indicates the region where uncertainties might arise regarding the definition of the atmospheric context.

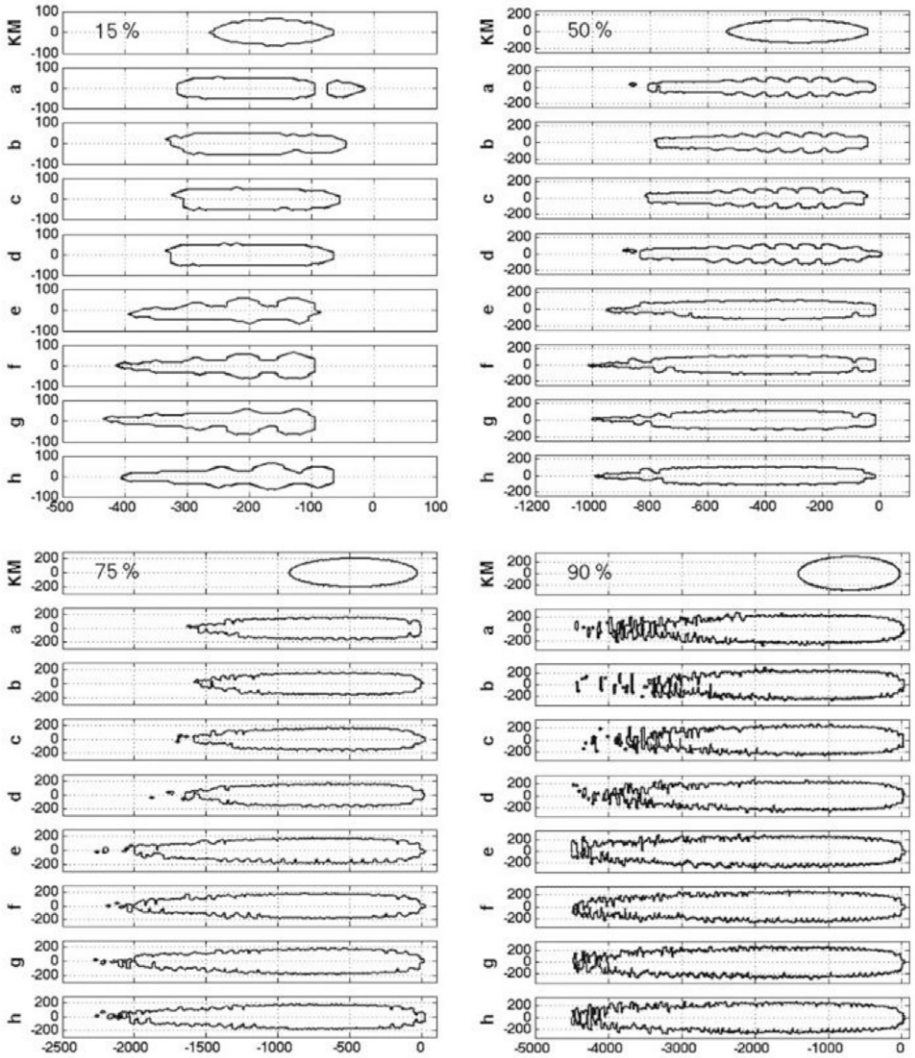

Fig. 15. Comparison of flux footprints evaluated using the Kormann-Meixner (KM01) and the LES-LS model from Steinfeld et al. (ST08) for measurements at height $1.8 \cdot z_b$. After Hellsten et al. [127].

used a LES-LS model to show how the footprint might look like at different heights over an urban canopy. They have demonstrated that at $1.8 \cdot h_B$ the source area of a measurement might resemble the shape of the footprint derived from an analytical model, while its extension might be overestimated (Fig. 15). This bias might be overcome if the input parameters for the analytical model are locally estimated [208,209], and particularly if some boundary conditions are fulfilled. For example, Zou et al. [142,210] have demonstrated that, closer to the top of the RSL, the classical relations that govern the ISL might be applicable. They also coincide with Yusup and Lim [211] and Yusup and Anis [212], when they say that under unstable (daytime) conditions local turbulent effects might be negligible. In those cases, filtering the measured data according to weather stability (u* filtering), which is a common practice when carrying out EC and scintillometer measurements [124,130,146,148], might reduce uncertainties regarding the source area definition within the RSL.

3.2.3. The urban canopy layer (UCL)

All the uncertainties that arise within the RSL increase exponentially when reaching the UCL, but in contrast to what urban climate researchers try to do when approaching the RSL, the UCL is normally not avoided. There is a strong interest about this climatic context, as it has many implications for the urban life: buildings exchange energy mostly at this scale, people live in and breath the air contained within the urban canyon, and most of the anthropogenic emissions are generated and emitted to this atmosphere [213–216]. Furthermore, many of the strategies that urban planners might be able to adopt happen at this scale, such as increasing the greenery of streets

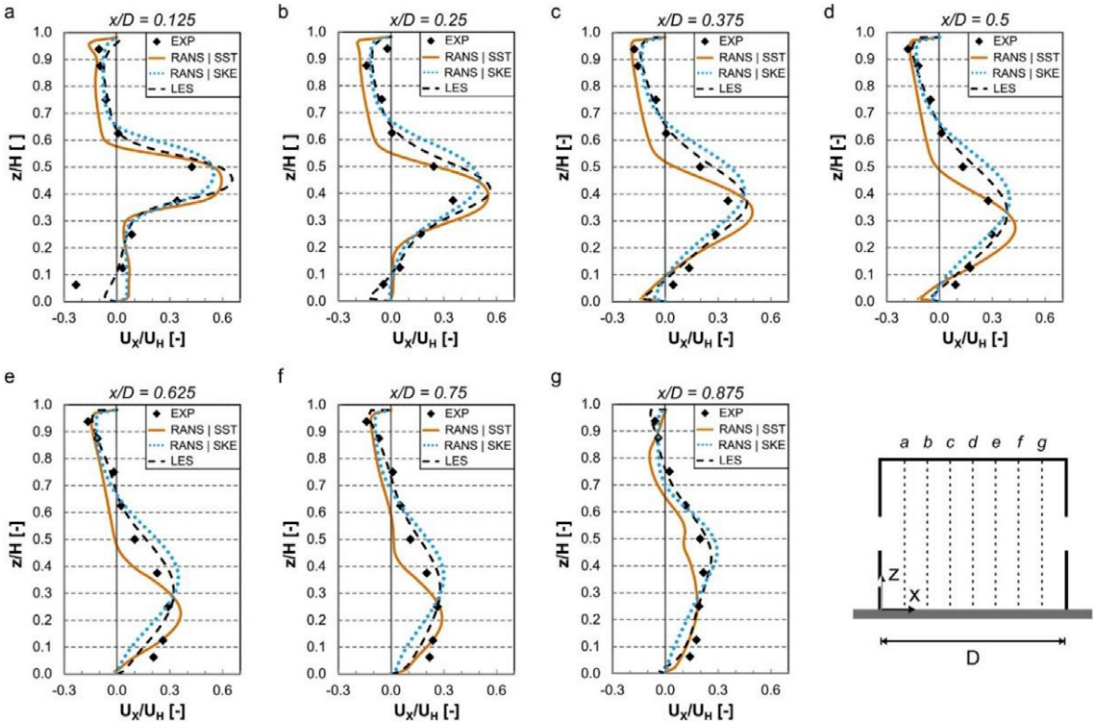

Fig. 16. Comparison of dimensionless mean x-velocity obtained with LES, RANS, and wind tunnel measurements within a simplified building geometry. It can be observed that LES fits better than RANS with the experimental data. After Van Hoff et al. [225].

and parks, smartly planning the traffic flow, or regulating the use of certain materials and equipment [35,217–220].

There are also no doubts that, within this scale, turbulence follows a different pattern than in the ISL and RSL [174,221–224], and therefore none of the classical assumptions might be adopted. Regarding the footprint modelling, very few authors have used analytical approaches for estimating the source area of their measurements. For instance, Häb et al. [95] developed a visualization framework for studying and contextualising measurements carried out using the transect methodology, using the model by Schmid [39,92] for estimating the source area. They underline the limitations of such modelling and point towards future improvement of the source area within their framework. Likewise, there are other authors who tend to use analytical models for comparison purposes, particularly when studying different scales simultaneously [138,207].

As mentioned above, the most accurate approach relies on Computer Fluid Dynamics. In last years it has been extensively used by urban climate researchers for modelling the microclimatic atmosphere [174,221,226]. Although most of these CFD models are based on RANS, it is commonly accepted that LES might be more reliable when simulating the UCL due to the higher resolution when modelling eddies [225,227,228] (see Fig. 16). In that sense, the model presented by Steinfeld et al. [155] has been applied to demonstrate how different footprints might be obtained at different sites within the urban canyon [127]. According to Fig. 17, the footprint near the ground ($z_m = 0.25 \cdot h_B$) is significantly less predictable than the footprint right above the urban canyon ($z_m = 1.25 \cdot h_B$), particularly when it is situated perpendicularly to the wind direction (cases *b, c, d*). Under those circumstances a strong vortex conditions the source area estimation, where measurements taken near the vertical boundaries might be represented by a strong positive (source) or negative (sink) footprint. On the other hand, measurements carried out in the crossing of two urban canyons (case *h*) might be characterised by a more homogeneous footprint, similar in shape with those obtained at $1.25 \cdot h_B$ heights.

Despite its high accuracy and the fact that LES-LS modelling significantly reduces CPU needs and expenses compared to other CFD approaches, it is still an unfordable solution for many research purposes. Due to these uncertainties and limitations, other authors have adopted different methods. One of the most common is to use correlations between surface cover and air temperatures to define the footprint that better *explains* the measured temperatures (see Fig. 18). Authors usually reference to the approximated source area for a screen-height sensor in urban contexts given by Oke [7] or Stewart and Oke [14] to test these correlations with radius of similar size, and which might range between 100 and 1000 m. Examples for mobile [229–231] and fixed measurements [74,232,233] that have used correlations to estimate the source area were identified within this systematic review.

Similarly, Wang et al. [141] have used and compared the correlation approach with the analytical footprint model by Kormann and Meixner [118]. They have found that both methods behave likewise and produce similar results when normalising correlations. Some questions might arise regarding the precision of the correlation process, as it does not seem to provide more accurate information than analytical models (see Fig. 19).

A different approach was presented by Erell et al. [234], who embraced a simplification of the footprint function concept (see section 1). These authors divided the source area derived from an analytical model into different sectors and weighted them according to their proximity to

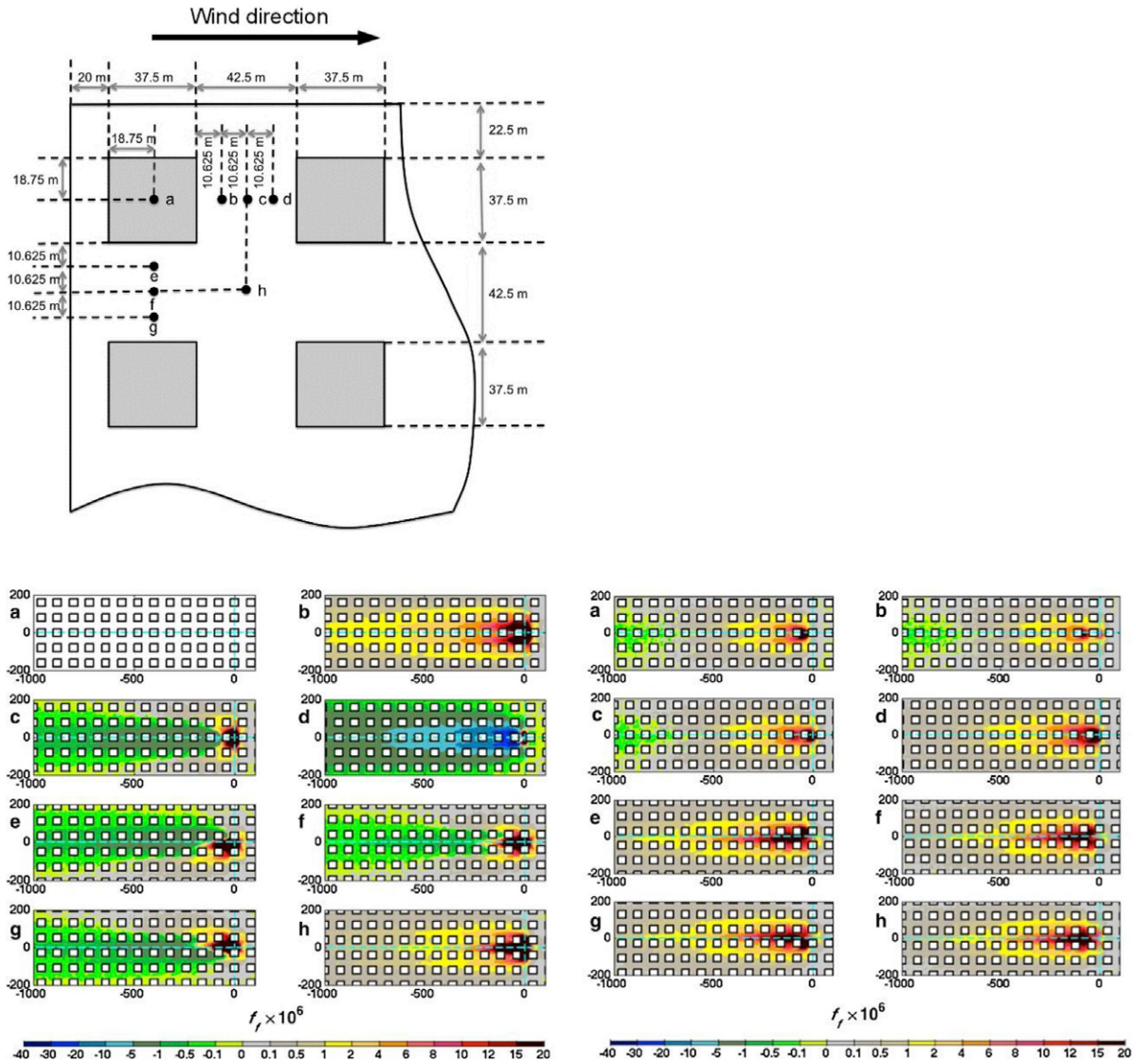

Fig. 17. Footprint prediction by a LES-LS coupled model, for different positions within ($0.25H_b$, left) and just above ($1.25H_b$, right) the urban canyon. The situation of each position is described at the top. After Hellsten et al. [127].

the measurement site. The same procedure was used some years after by Kaplan et al. [82], who took up these data and classified the source area sectors into local climate zones, linking microclimatic temperatures with the LCZ scheme. In that sense, and despite there are still not many local climate zones studies in the UCL, the LCZ could have a twofold purpose in this scale. Further from contextualising measurements, they might also be useful to assure a certain degree of homogeneity in the surroundings of the measurement context, following a similar approach as the one developed by Alexander et al. [201] for the ISL (see Fig. 12). In other words, if the source area cannot be certainly defined, LCZ might be a good manner to guarantee that the upwind surroundings have similar characteristics to the sensor site.

4. Discussion

The present study provides evidence that suggests that the thermal source area is not yet completely embraced by LCZ studies. The origin of such disassociation seems to be related with the wide use researchers make of the LCZ, particularly with those uses where the footprint definition might not be relevant or might be calculated differently, such as climatic urban planning with remote sensing techniques. Among in-situ turbulent measurements, the application of the LCZ scheme is not constraint to thermal studies, but also applied in many energy and CO_2 studies. However, while most turbulent flux studies embrace the source area estimation, thermal studies do not normally consider it. A possible reason for this might be found in the measurement capabilities of EC

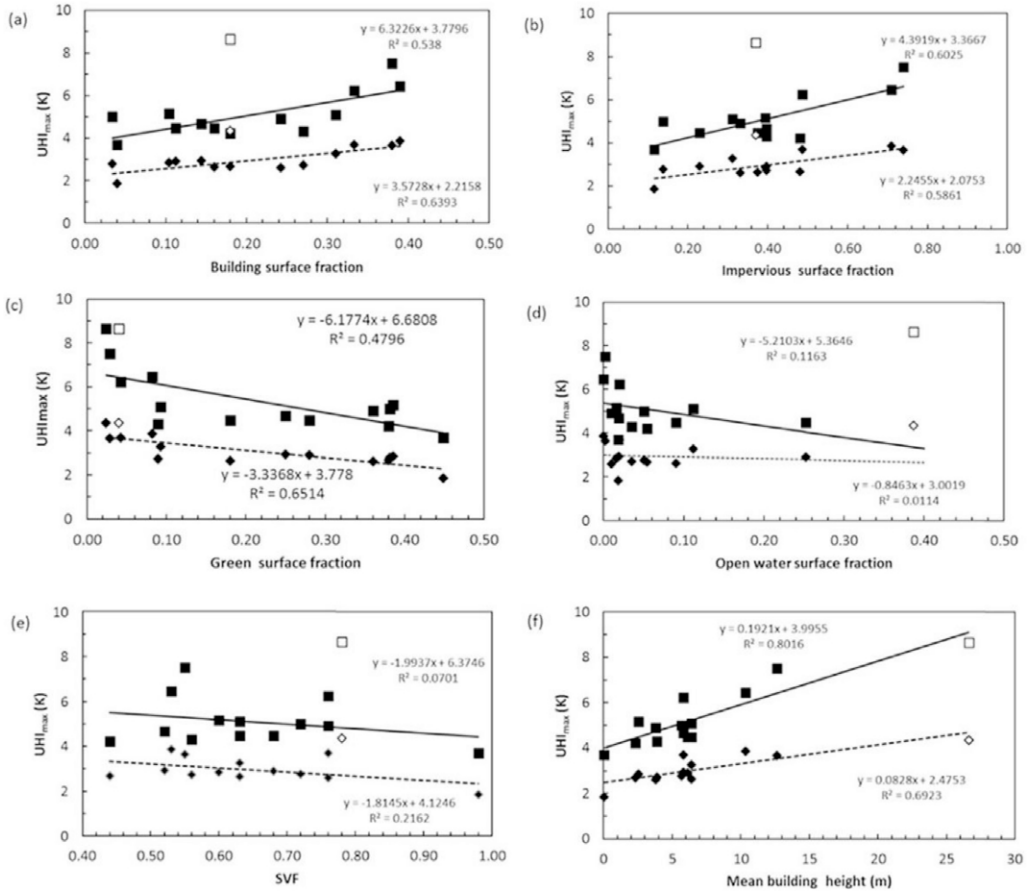

Fig. 18. Correlation between urban heat island intensity (median and 95 percentile) and urban parameters, and which could be found among the LCZ indicators. After Van Hove et al. [74].

systems, which are the most common technique among turbulent flux studies and are normally provided together with a software package that includes the footprint estimation. Another possible cause leading to differences in the footprint adoption might be related with the atmospheric scale. While flux measurements concentrate in the ISL, where assumptions and simplifications regarding the atmospheric physics can be made, thermal studies are mostly carried out in the UCL, thus encountering more barriers when trying to find a suitable source area model.

Results also found that urban researchers seem to seek easy-to-use

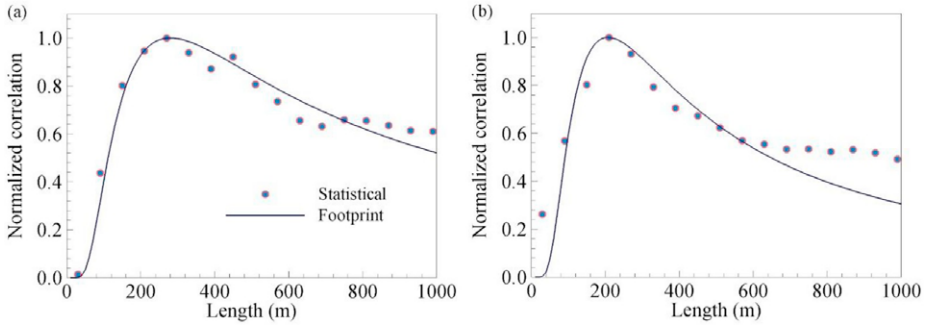

Fig. 19. Comparison of the normalised correlation between air temperature and land use, and the normalised footprint function with the K-M analytical model. (a) is for vegetation, and (b) for impervious surfaces. After Wang et al. [141].

tools that might be able to give a reasonable guess of what the source area might look like, while using a little amount of easy-to-collect inputs. This might explain why, despite the great advances in CFD's precision and efficiency, there is still a clear preference for one-dimension analytical solutions in the ISL and for qualitative approaches in the UCL. For example the three-dimension lagrangian model by Kljun et al. [143], albeit it might be more accurate than any other analytical solution, it has never been applied by any urban case study, while its analytical parameterisations into one- [144] and two-dimensions [157] is extensively used in the urban environment. Their appearing robustness [165] as well as the extended thought that there is not yet a suitable footprint solution for urban environments push urban climate researchers to work with such models. Even though CFDs alternatives, particularly coupled LES-LS solutions, seem to be the near-future of footprint modelling, they seem to be yet underdeveloped and are still rarely used.

The findings of this study reveal there is a need for standardisation and systematisation. Regardless the footprint approach, there are strong differences in the estimation of the inputs and the reporting of the outputs. Aerodynamic parameters, for example, have a critical relevance within analytical solutions and can be estimated in many ways, therefore introducing strong uncertainties within the modelling process. In a similar way, source areas are reported using different flux percentages, varying from 50 to 99%, thus making the comparison of results from different studies more difficult. The high number of variables that are involved and affect the source area size and shape, as well as its high variability with time, makes urgent to establish a common framework for all turbulent flux studies. Similarly to what happened with the definition of the LCZ scheme, further discussion is needed to determine the most appropriate process for choosing the footprint model, estimating the input parameters, and reporting the source area size within the urban context.

In regard to the limitations of this systematic review, improving the application of the PRISMA methodology would be advisable. Particularly, the identification process through the combination of keywords should be improved to guarantee a higher degree of returned relevant results, which in this review was roughly a 25% (2487 results out of 3214 were classified as 'not relevant'). In that sense there are already available methods and tools that could be implemented, such as contextual searching, and might therefore be taken into consideration in future reviews. The linearity of the screening and eligibility phases have also proven to be excessively resource and time consuming, although improving the identification phase would drastically reduce this issue.

5. Conclusions

This paper has systematically reviewed the knowledge on the source area definition within urban contexts and its application together with the Local Climate Zones scheme. It was found that, even though the estimation of the source area is rare among thermal studies, there is valuable knowledge regarding the footprint estimation within the measurement of other parameters, such as the energy flux or CO_2 observations. Hundreds of studies were found to be related with the source area concept and were used to identify the most common trends and limitations among different methodologies and the atmospheric scales near the ground: the inertial sublayer (ISL), the roughness sublayer (RSL), and the urban canopy layer (UCL). The following conclusions can be drawn:

- The source area within the ISL is well documented and studied. Analytical solutions are the prevailing choice due to their simplicity and relatively high accuracy. The estimation of the aerodynamic parameters was found to be an important source of uncertainties and a limitation for comparing results. Defining the LCZ of a measurement at this scale could be also problematic when obtaining large footprints, as strong horizontal heterogeneities usually appear.
- The RSL is usually considered a transition layer that should be avoided when placing measuring instruments. Few experiences have intentionally studied the source area at this atmospheric level, and no specific footprint solution has been developed. Analytical models might be valid when using local estimations of the aerodynamic parameters, and when filtering is applied to only evaluate measurements under unstable atmospheric conditions. These simplifications, however, are based on few experiences and should be confirmed in the future by other studies.
- In the UCL, which is the preferred scale among thermal studies, analytical approaches should be disregarded. In this context the footprint has been treated very heterogeneously, from the most precise and resource-consuming methods (CFD-based models) to the most extended qualitative approaches based on temperature-land cover correlations. To tackle uncertainties regarding the size of the footprint, the LCZs can be used to classify the surroundings of the measurement site, so a certain degree of homogeneity could be guaranteed.
- Finally, the degree of embracement of the source area by LCZ studies was proven to be low and very heterogeneous. The absence of a clear framework for estimating and reporting the source area, altogether with a lack of awareness among researchers on the relevance of the footprint, are found to be the main causes of this situation. Further research is needed to develop reliable and easy-to-use footprint tools for those scientists, particularly for measurements within the UCL.

Acknowledgements

The authors would like to thank Inês Costa Carrapiço and Alberto Vilches Such for their very detailed and helpful remarks on this manuscript. This research was supported by an FPU research grant (FPU15/05052) from the Spanish Ministry of Education, Culture and Sport, as well as by the MODIFICA research project (BIA2013-41732-R) funded by the Spanish Ministry of Economy and Competitiveness.

Appendix A.1. Case studies found within this systematic review

ID	Reference	Method. Reference[1]	City, Country	Measurement height [z_m] (m)	RSL height [z_R] (m)	z_m/z_R	Context[2]	Max. footprint distance [X] (m)	Measuring Conditions[3]	LCZ mentioned	LCZ applied
[201]	Alexander et al. (2016)	–	Dublin, IE	$z_{m,DU}$ = 48.0	$z_{R,DU} \approx 33^b$	1.1	ISL	X_{XX} = 500	-, -, -	Yes	LCZ 2
			Hamburg, DE	$z_{m,HA}$ = 50.0	$z_{R,HA} \approx 18^b$	2.8					LCZ 8
			Melbourne, AU	$z_{m,ME}$ = 40.0	$z_{R,ME} \approx 13^b$	3.1					LCZ 6
			Phoenix (AZ), US	$z_{m,PH}$ = 22.1	$z_{R,PH} \approx 9^b$	2.5					LCZ 6
[119]	Ando & Ueyama (2017)	KM01	Osaka, JP	z_m = 111.0	$z_R \approx 30^b$	3.7	ISL-ML	$X_{80} \approx$ 800–2400[d]	DT,AV,AV	Yes	LCZ 3_4
								$X_{80} \approx$ 1000–4400[d]	NT,AV,AV		
[120]	Auvinen et al. (2017)	ST08	Helsinki, FI	z_m = 60.0	$z_R \approx 48^b$	1.3	ISL	$X_{90,ST08} \approx$ 1200[d]	AV,NE,SU	No	No
		KM01						$X_{90,KM01} \approx$ 2000[d]			
[93]	Barlow et al. (2008)	SD94/97	Salford, UK	$z_{m,1}$ = 50.0	$z_R \approx 16^b$	3.1	ISL-ML	$X_{90,1} \approx$ 2200[d]	DT,NE,SP	–	–
				$z_{m,2}$ = 100.0		6.3		$X_{90,2} \approx$ 5000[d]			
[145]	Bergeron & Strachan (2011)	KN04	Montreal, CA	$z_{m,1}$ = 25.0	$z_{R,1} \approx 21^b$	1,2	RSL-ISL	$X_{80,1} \approx$ 500–1080[d]	DT,UN,SU	–	
				$z_{m,2}$ = 25.0	$z_{R,2} \approx 25^b$	1,0		$X_{80,1} \approx$ 640–1400[d]	NT,UN,SU		
								$X_{80,1} \approx$ 580–1120[d]	DT,UN,WI		
								$X_{80,1} \approx$ 520–1300[d]	NT,UN,WI		
								$X_{80,2} \approx$ 420–800[d]	DT,UN,SU		
								$X_{80,2} \approx$ 520–1320[d]	NT,UN,SU		
								$X_{80,2} \approx$ 460–1920[d]	DT,UN,WI		
								$X_{80,2} \approx$ 500–1120[d]	NT,UN,WI		
[72]	Björkegren & Grimmond (2016)	KM01	London, UK	z_m = 46.4	$z_R \approx 42^b$	1.1	ISL	$X_{50} \approx$ 250–1000[d]	-,UN,AV	No	No
								$X_{80} \approx$ 700–1700[d]			
								$X_{95} \approx$ 1500–3000[d]			
[122] [184]	Christen et al. (2011); Crawford & Christen (2015)	KM01	Vancouver, CA	z_m = 28.8	$z_R \approx 17^b$	1.7	ISL	$X_{50} \approx$ 100–260[d]	AV,AV,AV	Yes	LCZ 9
								$X_{80} \approx$ 380–740[d]			
[94]	Contini et al. (2012)	SD94/97 HH00	Lecce, IT	z_m = 14.0	$z_R \approx 15^b$	0.9	RSL	$X_{50} \approx$ 60–200[d]	AV,UN-NE,WI-SP	No	No
[123]	Crawford et al. (2011)	KM01	Baltimore (MD), US	z_m = 41.2	$z_R \approx 20^b$	2.1	ISL	$X_{50} \approx$ 1400–2100[d]	AV,AV,AV	–	–
								$X_{60} \approx$ 2000–3000[d]			
								$X_{70} \approx$ 3200–4800[d]			
[124]	Crawford et al. (2017)	KM01	London, UK	$z_{m,EC}$ = 49.9	$z_{R,EC} \approx 35^b$	1.4	ISL	$X_{50,EC} \approx$ 350–650[d]	AV,UN-NE,AV	No	No
				$z_{m,LAS}$ = 124.0[e]	$z_{R,LAS} \approx 29^b$	4.3		$X_{75,EC} \approx$ 800–1400[d]			
								$X_{50,LAS} \approx$ 2500[d]			
								$X_{75,LAS} \approx$ 5000[d]			
[76]	Dorsey et al. (2002)	SP90	Edinburgh, UK	z_m = 67.0	–	–	ISL	$X_{XX} \approx$ 3000	-,UN, –,ST, -	–	–
								$X_{XX} \approx$ 5000			
[234]	Erell et al. (2009)	CORREL.	Gothenburg, SE	–	–	–	UCL	X_{XX} = 100–1000	-, -, -	–	–
[125]	Feigenwinter et al. (2017)	KM01	Basel, CH	–	–	–	ISL	–	-, -, -	No	No
[108] [186]	Gioli et al. (2012; 2015)	HH00	Florence, IT	z_m = 35.0	$z_R \approx 28^b$	1.3	ISL	$X_{90} \approx$ 420–1700[d]	AV,UN,AV	No	No
[80]	Grimmond et al. (1991)	SO90	Vancouver, CA	z_m = 29.0	$z_R \approx 17^b$	1.7	ISL	–	-, -, -	–	–
[81]	Grimmond (1992)	SO90	Vancouver, CA	z_m = 20.5	–	–	ISL	–	-, -, -	–	–
[196]	Grimmond et al. (1998)	SD94/97	Chicago (IL), US	$z_{m,CH}$ = 31.0	–	5.9	ISL	–	-, -, -	–	–
			Los Ángeles (CA), US	$z_{m,LA}$ = 41.8		3.0					
			Miami (FL), US	$z_{m,MI}$ = 60.0		5.9					
			Vancouver, CA	$z_{m,VA}$ = 60.0		3.8					
[146]	Guidolotti et al. (2017)	KN04	Naples, IT	z_m = 26.0	$z_R \approx 44^b$	0.6	RSL	$X_{70} \approx$ 80–540[d]	AV, -,AV	No	No
								$X_{90} \approx$ 120–1780[d]			
[95]	Häb et al. (2015)	SD94/97	Gilbert (AZ), US	z_m = 1.0	–	–	UCL	–	-, -, -	No	No
[126] [72]	Helfter et al. (2011; 2016)	KM01	London, UK	z_m = 190.0	$z_R \approx 18^b$	10.6	ISL - ML	X_{90} = 13900	DT,NE,WI	No	No
								X_{90} = 10000	DT,UN,SP		
								X_{90} = 6900	DT,UN,SU		
								X_{90} = 13900	DT,NE,AU		

[127]	Hellsten et al. (2015)	ST08 KM01	idealised	$z_{m,1}$ = 10.0 $z_{m,2}$ = 50.0 $z_{m,3}$ = 78.0 $z_{m,4}$ = 100.0	$z_R \approx 80^b$	0.1 0.6 0.9 1.3	UCL RSL RSL ISL	$X_{75,2,ST08} \approx 580^d$ $X_{75,2,KM01} \approx 500^d$ $X_{90,2,ST08} \approx 1200^d$ $X_{90,2,KM01} \approx 950^d$ $X_{75,3,ST08} \approx X_{75,3,KM01} \approx 1700^d$ $\approx 900^d$ $X_{90,3,ST08} \approx 4000^d$ $X_{90,3,KM01} \approx 1400^d$	-,NE, -	No	No
[147]	Hiller et al. (2011)	KN04	Minneapolis-Saint Paul (MN), US	z_m = 1.35	–	–	UCL	$X_{80} \approx 75^d$ $X_{90} \approx 105^d$	-, -,AV	–	–
[77]	Jacobs et al. (2015)	SP90	Arnhem, NL	$z_{m,EC}$ = 41.0	$z_{R,EC} \approx 36^b$	1.1	ISL	$X_{80,EC} \approx 1000$	-, -, -	Yes	LCZ 2
[189]	Kleingeld et al. (2017)	HW92/94	Rotterdam, NL	$z_{m,LAS} = 64.0^e$	$z_{R,LAS} \approx 57^b$			$X_{80,LAS} \approx 1750$			
[90]	Järvi et al. (2009)	SL04 HW92/94	Helsinki, FI	z_m = 31.0	$z_R \approx 24^b$	1.3	ISL	$X_{64,SL04} = 500$	-,NE,AV	–	–
[96]	Kanda et al. (2002)	SD94/97	Tokyo, JP	$z_{m,EC}$ = 32.0 $z_{m,LAS} = 24.0^e$	$z_R \approx 17^b$	1.9 1.4	ISL	$X_{90,EC} = 1660$ $X_{90,LAS} = 1750$ $X_{90,EC} = 1240$ $X_{90,LAS} = 1250$ $X_{90,EC} = 304$ $X_{90,LAS} = 496$	DT,ST,AU DT,ST,AU DT,NE,AU DT,NE,AU DT,UN,AU DT,UN,AU	–	–
[82]	Kaplan et al. (2016)	SO90	Bat-Yam, IL	–	–	–	UCL	$X_{XX} = 1000^d$	-, -, -	Yes	Mix
[128]	Kent et al. (2017)	KM01	London, UK	$z_{m,1}$ = 50.3 $z_{m,2}$ = 48.9 $z_{m,3}$ = 38.8	$z_{R,1} \approx 43^b$ $z_{R,2} \approx 47^b$ $z_{R,3} \approx 47^b$	1.2 1.0 0.8	ISL RSL-ISL RSL	$X_{80,1,Mho} \approx 350–600^d$ $X_{80,1,Mac} \approx 950–1950^d$ $X_{80,2,Mho} \approx 250–450^d$ $X_{80,3,Mho} \approx 100–200^d$	DT,NE,AV	Yes	LCZ 2
[48]	Kordowski & Kuttler (2010)	SD94/97	Essen, DE	z_m = 26.0	$z_R \approx 24–32^b$	0,9	RSL	$X_{80} \approx 1000^d$	-,NE,AV	–	–
[129]	Kota et al. (2014)	KM01	Houston (TX), US	z_m = 60.0	$z_R \approx 16–40^b$	2.2	ISL	$X_{80} \approx 1500^d$	DT, -,SP-SU	No	No
[130]	Kotthaus & Grimmond (2012)	KM01	London, UK	z_m = 48.9	$z_R \approx 47^b$	1.0	RSL-ISL	$X_{50} \approx 100–220^d$ $X_{50} \approx 200–480^d$ $X_{70} \approx 320–800^d$ $X_{70} \approx 360–800^d$ $X_{80} \approx 480–1200^d$ $X_{80} \approx 500–1120^d$	-, -,SU -, -,WI -, -,SU -, -,WI -, -,SU -, -,WI	Yes	LCZ 2
[131]	Kotthaus & Grimmond (2014)	KM01	London, UK	z_m = 48.9	$z_R \approx 47^b$	1.0	RSL-ISL	$X_{50} \approx 140–280^d$ $X_{50} \approx 160–480^d$ $X_{70} \approx 260–480^d$ $X_{70} \approx 360–860^d$ $X_{80} \approx 360–720^d$ $X_{80} \approx 580–1300^d$	-,UN,AV -,NE,AV -,UN,AV -,NE,AV -,UN,AV -,NE,AV	Yes	LCZ 2
[132]	Kurppa et al. (2015)	KM01	Helsinki, FI	z_m = 60.9	$z_R \approx 48^b$	1.3	ISL	$X_{80} = 650–1150^d$ $X_{80} = 650–1000^d$	-,UN-NE,SU -,UN-NE,WI	Yes	LCZ 2
[148]	Langford et al. (2009)	KN04	Manchester, UK	z_m = 95.0	$z_R \approx 30^b$	3.2	ISL	$X_{80} = 1623$	-,AV,SP	–	–
[188]	JD Lee et al. (2015)	KM01	London, UK	z_m = 190.0	$z_R \approx 18^b$	10.6	ISL-ML	$X_{90} = 4695$	AV,AV,SP-SU	No	No
[91]	SH Lee et al. (2015)	HW92/94	Gongju, KR	$z_m = 48.5^e$	$z_R \approx 6^b$	8	ISL	$X_{60,LAS} \approx 350^d$ $X_{80,LAS} \approx 600^d$ $X_{90,LAS} \approx 900^d$	-,UN-NE,WI	No	No
[73]	Lietzke et al. (2015)	KM01	Basel, CH	z_m = 41.0	$z_R \approx 32^b$	1.3	ISL	$X_{50} \approx 80–240^d$ $X_{70} \approx 140–420^d$ $X_{80} \approx 200–560^d$ $X_{90} \approx 300–880^d$	-, -,AV	Yes	No
[235] [97]	Liu et al. (2009); Liu & Sun (2010)	SD94/97	Nanjing, CN	z_m = 24.2	$z_R \approx 39^b$	0.6	RSL	$X_{XX} = 500$	-, -,AV	–	–
[133]	Liu et al. (2012)	KM01	Beijing, CN	z_m = 47.0	$z_R \approx 47^b$	1.0	RSL-ISL	$X_{50} \approx 250–450^d$ $X_{70} \approx 450–800^d$ $X_{80} \approx 600–1200^d$ $X_{90} \approx 1000–2100^d$	-,UN-NE,AV	Yes	Mix
[83] [181]	Lemonsu et al. (2004); Henon et al. (2011)	SO90	Marseille, FR	z_m = 43.9	$z_R \approx 40^b$	1.1	RSL-ISL	$X_{90} \approx 500–1000^d$	-, -,SU	–	–
[232] [233]	Lindén (2011); Holmer et al. (2013)	CORREL.	Ouagadougou, BF	z_m = 1.7	–	–	UCL	$X_{XX} = 400$	AV,AV,AU	Yes	Mix

[149]	Mårtensson (2006)	KN04	Stockholm, SE	z_m = 118.0	$z_R \approx 30^b$	3,9	ISL-ML	X_{75} =	1700–2400	AV,AV,SP	–	–	
[150]	Menzer & McFadden (2015)	KN04	Minneapolis-Saint Paul (MN), US	z_m = 40.0	$z_R \approx 24^b$	1,7	ISL	X_{90} =	800	AV,UN-NE,AV	Yes	LCZ 6	
[49]	Middel et al. (2014)	–	Phoenix (AZ), US	z_m = 2.0	$z_R \approx 10^z$	–	UCL	X_{XX} =	200	-, -, -	Yes	Mix	
[109]	Morin et al. (2014)	HH00	Columbus (OH), US	$z_{m,1}$ = 9.6	$z_R \approx 16^b$	0.6	RSL	$X_{90,1}$ ≈	15–25[d]	DT, -,SU	No	No	
				$z_{m,2}$ = 15.0		0.9		$X_{90,1}$ ≈	20–40[d]	NT, -,SU			
								$X_{90,1}$ ≈	200–225[d]	DT, -,WI			
								$X_{90,1}$ ≈	90–125[d]	NT, -,WI			
								$X_{90,2}$ ≈	200–375[d]	DT, -,SU			
								$X_{90,2}$ ≈	225–425[d]	NT, -,SU			
								$X_{90,2}$ ≈	225–500[d]	DT, -,WI			
								$X_{90,2}$ ≈	250–550[d]	NT, -,WI			
[50]	Nichol & Hang (2012)	–	Hong Kong, CN	z_m = 1.0	–	–	UCL	X_{XX} =	10–100	AV, -,SU	No	No	
[134]	Nordbo et al. (2013)	KM01	Helsinki, FI	$z_{m,1}$ = 31.0	$z_{R,1} \approx 40^b$	0.8	RSL	$X_{50,1}$ ≈	100–450[d]	-,NE,AV	No	No	
				$z_{m,2}$ = 41.8	$z_{R,2} \approx 42^b$	1.0	RSL	$X_{50,2}$ ≈	300–450[d]				
				$z_{m,3}$ = 60.0	$z_{R,3} \approx 48^b$	1.3	ISL	$X_{50,3}$ ≈	500–750[d]				
								$X_{75,1}$ ≈	300–950[d]				
								$X_{75,2}$ ≈	600–950[d]				
								$X_{75,3}$ ≈	1000–1750[d]				
[179]	Oke et al. (1992)	SO90	Mexico city, MX	z_m = 28.0	z_R = 15-23	1.6	ISL	X_{90} =	900	DT, -,WI	–	–	
								X_{90} =	1800	NT, -,WI			
[98]	Oke et al. (1999)	SD94/97	Mexico city, MX	z_m = 28.0	z_R = 36.8	0,8	RSL	X_{90} ≈	200–400[d]	DT, -,AU	–	–	
								X_{90} ≈	400–700[d]	NT, -,AU			
[110]	Oliphant et al. (2017)	HH00	Black Rock (NV), US	z_m = 11.6	$z_R \approx 10^b$	1,2	ISL	–		-, -, -	No	No	
[135]	Park et al. (2011)	KN04	Houston (TX), US	z_m = 60.0	$z_R \approx 24^b$	2,5	ISL	$X_{90,KN04}$ =	900-1200	DT,NE, -DT, -,SU	–	–	
		KM01						$X_{50,KM01}$ ≈	900[d]				
								$X_{90,KM01}$ ≈	2300[d]	DT,-,SU			
[136]	Park et al. (2016)	KM01	Houston (TX), US	z_m = 60.0	$z_R \approx 24^b$	2,5	ISL	X_{60} ≈	400–1050[d]	AV,AV,SP	Yes	LCZ 6b	
								X_{90} ≈	750–1700[d]	AV,AV,SP		LCZ 5	
								X_{60} ≈	450–1000[d]	AV,AV,SU			
								X_{90} ≈	800–1650[d]	AV,AV,SU			
								X_{60} ≈	450–900[d]	AV,AV,AU			
								X_{90} ≈	800–1550[d]	AV,AV,AU			
								X_{60} ≈	450–1200[d]	AV,AV,WI			
								X_{90} ≈	800–1800[d]	AV,AV,WI			
[99]	Pawlak et al. (2016)	SD94/97	Łódz, PL	z_m = 37.0	$z_R \approx 22^b$	1.7	ISL	X_{50} ≈	125–200[d]	DT,UN,AV	Yes	LCZ 3	
								X_{75} ≈	175–400[d]				
								X_{90} ≈	300–750[d]				
[46]	Perera & Emmanuel (2016)	–	Colombo, LK	–	–	–	–	size of urban blocks		-, -, -	Yes	Mix	
[185]	Ramamurthy & Pardyjak (2011)	HH00	Saint Lake (UT), US	z_m = 36.0	$z_R \approx 13^b$	2,8	ISL	X_{90} ≈	600–850[d]	-,UN,SU	–	–	
								X_{90} ≈	4800–8800[d]	-,ST,SU			
[137] [236]	Rapsomanikis (2015); Loupa et al. (2016)	KM01	Athens, GR	z_m = 30,0	$z_R \approx 34^b$	0.9	RSL	X_{XX} ≈	560–1545[d]	-, -, -	No	No	
[183]	Rigby et al. (2008)	–	London, UK	z_m = 87.0	$z_R \approx 22^b$	4.0	ISL	X_{XX} =	1000	-, -,AV	–	–	
[84] [85]	Rooney (2001; 2005)	SO90 SD94/97	Birmingham, UK Salford, UK	$z_{m,1}$ = 45.0 $z_{m,2}$ = 30.0 $z_{m,3}$ = 20.0	–	–	RSL-ISL	–		-, -, -	–	–	
[187]	Roth et al. (2016)	HH00	Singapore, SG	$z_{m,1}$ = 20.7	$z_R \approx 17^b$	1.2	ISL	X_{80} ≈	400[d]	DT,AV,AV	Yes	LCZ 3	
								X_{80} ≈	1000[d]	NT,AV,AV			
[138]	Salmond et al. (2012)	KM01	Basel, CH	z_m = 31.7	$z_R \approx 29^b$	1.1	ISL	X_{80} ≈	800[d]	AV,AV,AV			
								X_{50} ≈	70–200[d]	DT,AV,SU	No	No	
								X_{60} ≈	110–240[d]	DT,AV,SU			
								X_{70} ≈	140–320[d]	DT,AV,SU			
								X_{80} ≈	190–460[d]	DT,AV,SU			
								X_{50} ≈	140–300[d]	NT,AV,SU			
								X_{60} ≈	200–390[d]	NT,AV,SU			
								X_{70} ≈	260–540[d]	NT,AV,SU			
								X_{80} ≈	400–800[d]	NT,AV,SU			
[86]	Schmid et al. (1991)	SO90	Vancouver, CA	z_m = 28.0	$z_R \approx 10^b$	2.8	ISL	X_{50} ≈	325–850[d]	DT,AV,SU	–	–	

[207]	Soegaard & Møller-Jensen (2003)	SD94/97	Copenhagen, DK	$z_{m,1}$ = 40.0 $z_{m,2}$ = 10.0	$z_R \approx$ 40–50[b]	0.9 0.2	RSL UCL	$X_{90,1} \approx$ 500 $X_{90,2} \approx$ 100	AV,NE,AV DT,NE,WI	–	–
[112]	Song & Wang (2012)	HH00	Beijing, CN	z_m = 47.0	$z_R \approx 50$[b]	1.0	RSL-ISL	$X_{90} \approx$ 220–450[d] $X_{90} \approx$ 200–750[d]	AV,UN,AV AV,ST,AV	Yes	Mix
[113]	Sparks & Toumi (2010)	HH00	London, UK	z_m = 50.0	$z_R \approx 50$[b]	1.0	RSL-ISL	$X_{90} \approx$ 1600	AV,AV,AV	–	–
[180]	Spronken-Smith (2002)	SD94/97	Christchurch, NZ	z_m = 20.0	$z_R \approx 12$[b]	1.7	ISL	$X_{50} \approx$ 90–100[d] $X_{50} \approx$ 250–800[d]	DT, -,SU DT, -,WI	–	–
[78]	Stabler et al. (2005)	SP90	Phoenix (AZ), US	z_m = 1.0	–	–	UCL	X_{XX} = 20–450	-, -, -	–	–
[237]	Szymanowski & Kryza (2011)	CORREL.	Wroclaw, PL	z_m = 2.0	–	–	UCL	X_{XX} = 550–600	DT,ST, -	–	–
[139]	Ueyama & Ando (2016)	KM01	Sakai, JP	$z_{m,1}$ = 111.0 $z_{m,2}$ = 30.0 $z_{m,3}$ = 16.2	$z_{R,1} \approx$ 22–72[b] $z_{R,2} \approx$ 25–42[b] $z_{R,3} \approx$ 22–34[b]	3.0 1.0 0.6	ISL RSL-ISL RSL	$X_{80,1} \approx$ 1300–3000[d] $X_{80,2} \approx$ 550–1000[d] $X_{80,3} \approx$ 80–200[d]	DT,AV,DT	No	No
[230]	Unger et al. (2010)	CORREL.	Szeged, HU	z_m = 1.5	–	–	UCL	X_{XX} = 500	NT,ST,SU	–	–
[140]	Valach et al. (2015)	KM01	London, UK	z_m = 50.3	$z_R \approx 53$[b]	0.9	RSL-ISL	X_{75} = 750 X_{90} = 1000 X_{99} = 2000	-,NE,AV	Yes	LCZ 2
[74]	van Hove et al. (2015)	CORREL.	Rotterdam, NL	$z_{m,1}$ = 20.0 $z_{m,2}$ = 18.0	–	–	UCL RSL	$X_{XX,1}$ = 500 $X_{XX,2}$ = 750	AV,AV,SU	Yes	LCZ 2
[114]	Velasco et al. (2005)	HH00	Mexico city, MX	z_m = 37.0	$z_R \approx 24$[b]	1.5	ISL	$X_{80} \approx$ 200–2100[d] $X_{80} \approx$ 1300–4000[d] $X_{80} \approx$ 500–2500[d]	DT, -,SP NT, -,SP AV, -,SP	–	–
[116]	Velasco et al. (2014)	HH00	Mexico city, MX	z_m = 37.0	$z_R \approx 19$[b]	1.9	ISL	$X_{60} \approx$ 100–1000[d] $X_{80} \approx$ 200–2100[d] $X_{60} \approx$ 500–1900[d] $X_{80} \approx$ 1300–4000[d]	DT, -,SP DT, -,SP NT, -,SP NT, -,SP	Yes	LCZ 2
[152]	Vesala et al. (2008)	SL04	Helsinki, FI	z_m = 31.0	$z_{R,1} \approx 39$[b] $z_{R,2} \approx 24$[b] $z_{R,3} \approx 18$[b]	0.8 1.3 1.7	RSL ISL ISL	–	-, -, -	–	–
[141]	Wang et al. (2016)	CORREL.	Phoenix (AZ), US	z_m = 2.0	–	< 0.5	UCL	X_{XX} = 300	DT,AV,SP	No	No
[182] [117] [195]	Ward et al. (2013; 2014; 2015)	HH00	Swindon, UK	$z_{m,EC}$ = 12.5 $z_{m,LAS}$ = 32.4[e] $z_{m,BLS}$ = 44.3[e]	$z_{R,EC} \approx 10$[b] $z_{R,LAS} \approx 12$[b] $z_{R,BLS} \approx 14$[b]	1.3 2.7 3.2	ISL	$X_{80,EC} \approx$ 400[d] $X_{95,EC} \approx$ 1300[d] $X_{80,LAS} \approx$ 700[d] $X_{95,LAS} \approx$ 2300[d] $X_{80,BLS} \approx$ 1000[d] $X_{95,BLS} \approx$ 2600[d]	-,UN,AV	No	No
[100]	Weber & Kordowski (2010)	SD94/97	Essen, DE	z_m = 35.0	$z_R \approx 34$[b]	1.0	RSL-ISL	X_{70} = 1000	-,NE,AV	–	
[212]	Yusup & Anis (2016)	–	Pulau Pinang, MY	z_m = 18.0	$z_R \approx$ 30–32[b]	0.6	RSL	X_{XX} = 450	NT, -,AV	Yes	LCZ 5b
[101]	Zielinski et al. (2017)	SD94/97	Łódz, PL	$z_{m,LAS}$ = 35.1[e]	$z_R \approx$ 22–31[b]	2.7	ISL	$X_{60,LAS}$ = 250–450[d] $X_{80,LAS}$ = 300–550[d] $X_{95,LAS}$ = 850–1250[d]	DT,UN,AV	No	No
[142]	Zou et al. (2017)	KM01	Nanjing, CN	$z_{m,1}$ = 33.5 $z_{m,2}$ = 48.5	$z_{R,SUP} \approx 39$[b] $z_{R,URB} \approx 43$[b]	0.9 1.1	RSL ISL (RSL)	$X_{75,1}$ = 500 $X_{75,2}$ = 800	-, -,AV	No	No

[1] Methodological reference abbreviations are described in Fig. 6.
[2] Context abbreviations: *ISL* is the Inertial Sublayer. *RSL* is Roughness Sublayer. *UCL* is the Urban Canopy Layer. X_{XX} is the distance from the receptor including a *XX%* of the area that influences the measurement.
[3] Measuring conditions abbreviations reference, in this order, to the time of the day (DT: Daytime, NT: Nighttime, AV: Average), the atmospheric stability (UN: Unstable, NE: Neutral, ST: Stable, AV: Average), and the season (WI: Winter, SP: Spring, SU: Summer, AU: Autumn, AV: Average).
[a] According to the description given by the authors.
[b] Approximated by $z_R = 2z_h$, where z_h is the average height of the surrounding buildings, which is given by the authors.
[c] z_h is derived from the LCZ class, which is defined by the authors.
[d] Graphically approximated from the representation that appears in the paper.
[e] Average of measurement heights for scintillometers.

References

[1] IPCC, Climate Change 2013: the Physical Science Basis. Contribution of Working Group I to the Fifth Assessment Report of the Intergovernmental Panel on Climate Change, Cambridge University Press, Cambridge, United Kingdom and New York, NY, USA, 2013.

[2] D. Baldocchi, E. Falge, L. Gu, R. Olson, D. Hollinger, S. Running, P. Anthoni, C. Bernhofer, K. Davis, R. Evans, J. Fuentes, A. Goldstein, G. Katul, B. Law, X. Lee, Y. Malhi, T. Meyers, W. Munger, W. Oechel, K.T. Paw U, K. Pilegaard, H.P. Schmid, R. Valentini, S. Verma, T. Vesala, K. Wilson, S. Wofsy, FLUXNET: a new tool to study the temporal and spatial variability of ecosystem-scale carbon dioxide, water vapor, and energy flux densities, Bull. Am. Meteorol. Soc. 82 (2001) 2415–2434 http://journals.ametsoc.org/doi/abs/10.1175/1520-0477(2001)082%3C2415%3AFANTTS%3E2.3.CO%3B2.

[3] National Aeronautics and Space Administration, NASA Plan for Increasing Access to the Results of Scientific Research: Digital Scientific Data and Peer-reviewed Publications, (2014) http://science.nasa.gov/media/medialibrary/2014/12/05/NASA_Plan_for_increasing_access_to_results_of_federally_funded_research.pdf.

[4] European Spatial Agency, Sentinel Data Access Annual Report, (2017) 2018 https://scihub.copernicus.eu/twiki/pub/SciHubWebPortal/AnnualReport2017/COPE-SERCO-RP-17-0186_-_Sentinel_Data_Access_Annual_Report_2017-Final_v1.4.1.pdf.

[5] E. Aguilar, I. Auer, M. Brunet, T.C. Peterson, J. Wieringa, Guidelines on Climate Metadata and Homogenization, (2003) http://www.wmo.int/pages/prog/wcp/wcdmp/wcdmp_series/documents/WCDMP-53.pdf.

[6] World Meteorological Organization, Guide to Meteorological Instruments and Methods of Observation, (2014) https://library.wmo.int/doc_num.php?explnum_id=4147.

[7] T.R. Oke, Initial Guidance to Obtain Representative Meteorological Observations at Urban Sites, (2006) https://library.wmo.int/pmb_ged/wmo-td_1250.pdf.

[8] I.D. Stewart, A systematic review and scientific critique of methodology in modern urban heat island literature, Int. J. Climatol. 31 (2011) 200–217, https://doi.org/10.1002/joc.2141.

[9] K. Knoch, Die Landesklimaaufnahme, Wesen und Methodik, Bad Kissinger, (1963) https://www.dwd.de/DE/leistungen/pbfb_verlag_berichte/pdf_einzelbaende/85_pdf.pdf?_blob=publicationFile&v=3.

[10] R. Ellefsen, Mapping and measuring buildings in the urban canopy boundary layer in ten US cities, Energy Build. 15–16 (1991) 1025–1049.

[11] T.R. Oke, Siting and exposure of meteorological instrument at urban sites, 27th NATO/CCMS, Int. Tech. Meet. Air Pollut. Model. Its Appl. 1 (2004) 615–631, https://doi.org/10.1007/978-0-387-68854-1_66.

[12] I.D. Stewart, T.R. Oke, Newly developed "Thermal Climate Zones" for defining and measuring urban heat island magnitude in the canopy layer, Eighth Symp. Urban Environ., Phoenix, AZ, 2009, pp. 1–2, , https://doi.org/10.1534/g3.114.014308.

[13] T. Loridan, C.S.B. Grimmond, Characterization of energy flux partitioning in urban environments: links with surface seasonal properties, J. Appl. Meteorol. Climatol. 51 (2012) 219–241, https://doi.org/10.1175/JAMC-D-11-038.1.

[14] I.D. Stewart, T.R. Oke, Local climate zones for urban temperature studies, Bull. Am. Meteorol. Soc. 93 (2012) 1879–1900, https://doi.org/10.1175/BAMS-D-11-00019.1.

[15] C. Ren, E.Y.Y. Ng, L. Katzschner, Urban climatic map studies: a review, Int. J. Climatol. 31 (2011) 2213–2233, https://doi.org/10.1002/joc.2237.

[16] B. Bechtel, P.J. Alexander, J. Böhner, J. Ching, O. Conrad, J. Feddema, G. Mills, L. See, I.D. Stewart, Mapping local climate zones for a worldwide database of the form and function of cities, ISPRS Int. J. Geo-Inf. 4 (2015) 199–219, https://doi.org/10.3390/ijgi4010199.

[17] Y.-C. Chen, T.-P. Lin, W.-Y. Shih, Modeling the urban thermal environment distributions in taipei basin using local climate zone (LCZ), 2017 Jt. Urban Remote Sens. Event, JURSE 2017, Institute of Electrical and Electronics Engineers Inc., 2017, , https://doi.org/10.1109/JURSE.2017.7924531.

[18] Y. Xu, C. Ren, M. Cai, N.Y.Y. Edward, T. Wu, Classification of local climate zones using ASTER and landsat data for high-density cities, IEEE J. Sel. Top. Appl. Earth Obs. Remote Sens. (2017), https://doi.org/10.1109/JSTARS.2017.2683484.

[19] M. Cai, C. Ren, Y. Xu, K.K.L. Lau, R. Wang, Investigating the Relationship between Local Climate Zone and Land Surface Temperature Using an Improved WUDAPT Methodology - a Case Study of Yangtze River Delta, China, Urban Clim, 2017, https://doi.org/10.1016/j.uclim.2017.05.010.

[20] J.A. Patz, D. Campbell-Lendrum, T. Holloway, J.A. Foley, Impact of regional climate change on human health, Nature 438 (2005) 310–317, https://doi.org/10.1038/nature04188.

[21] a. J. Arnfield, Two decades of urban climate research: a review of turbulence, exchanges of energy and water, and the urban heat island, Int. J. Climatol. 23 (2003) 1–26, https://doi.org/10.1002/joc.859.

[22] J. a. Voogt, T.R. Oke, Thermal remote sensing of urban climates, Remote Sens. Environ. 86 (2003) 370–384, https://doi.org/10.1016/S0034-4257(03)00079-8.

[23] T.R. Oke, The energetic basis of the urban heat island, Q. J. R. Meteorol. Soc. 108 (1982) 1–24, https://doi.org/10.1002/qj.49710845502.

[24] Q. Weng, D. Lu, J. Schubring, Estimation of land surface temperature-vegetation abundance relationship for urban heat island studies, Remote Sens. Environ. 89 (2004) 467–483, https://doi.org/10.1016/j.rse.2003.11.005.

[25] T.R. Oke, City size and the urban heat island, Atmos. Environ. 7 (1973) 769–779, https://doi.org/10.1016/0004-6981(73)90140-6.

[26] H. Akbari, M. Pomerantz, H. Taha, Cool surfaces and shade trees to reduce energy use and improve air quality in urban areas, Sol. Energy 70 (2001) 295–310, https://doi.org/10.1016/S0038-092X(00)00089-X.

[27] S.E. Gill, J.F. Handley, A.R. Ennos, S. Pauleit, Adapting cities for climate change: the role of the green infrastructure, Built. Environ. 33 (2007) 115–133, https://doi.org/10.2148/benv.33.1.115.

[28] V. Masson, A physically-based scheme for the urban energy budget in atmospheric models, Boundary-Layer Meteorol. 94 (2000) 357–397, https://doi.org/10.1023/A:1002463829265.

[29] F. Yuan, M.E. Bauer, Comparison of impervious surface area and normalized difference vegetation index as indicators of surface urban heat island effects in Landsat imagery, Remote Sens. Environ. 106 (2007) 375–386, https://doi.org/10.1016/j.rse.2006.09.003.

[30] H. Taha, Urban climates and heat islands: albedo, evapotranspiration, and anthropogenic heat, Energy Build. 25 (1997) 99–103, https://doi.org/10.1016/S0378-7788(96)00999-1.

[31] X.L. Chen, H.M. Zhao, P.X. Li, Z.Y. Yin, Remote sensing image-based analysis of the relationship between urban heat island and land use/cover changes, Remote Sens. Environ. 104 (2006) 133–146, https://doi.org/10.1016/j.rse.2005.11.016.

[32] C. Kennedy, J. Cuddihy, J. Engel-yan, Te changing metabolism of cities, J. Ind. Ecol. 11 (2007).

[33] H. Kusaka, H. Kondo, Y. Kikegawa, F. Kimura, A simple single-layer urban canopy model for atmospheric models: comparison with multi-layer and slab models, Boundary-Layer Meteorol. 101 (2001) 329–358, https://doi.org/10.1023/A:1019207923078.

[34] E. Oberndorfer, J. Lundholm, B. Bass, R.R. Coffman, H. Doshi, N. Dunnett, S. Gaffin, M. Köhler, K.K.Y. Liu, B. Rowe, Green roofs as urban ecosystems: ecological structures, functions, and services, Bioscience 57 (2007) 823–833, https://doi.org/10.1641/B571005.

[35] A.M. Rizwan, L.Y.C. Dennis, C. Liu, A review on the generation, determination and mitigation of Urban Heat Island, J. Environ. Sci. 20 (2008) 120–128, https://doi.org/10.1016/S1001-0742(08)60019-4.

[36] M. Santamouris, N. Papanikolaou, I. Livada, I. Koronakis, C. Georgakis, A. Argiriou, D. Assimakopoulos, On the impact of urban climate on the energy consumption of buildings, Sol. Energy 70 (2001) 201–216, https://doi.org/10.1016/S0038-092X(00)00095-5.

[37] S.L. Harlan, A.J. Brazel, L. Prashad, W.L. Stefanov, L. Larsen, Neighborhood microclimates and vulnerability to heat stress, Soc. Sci. Med. 63 (2006) 2847–2863, https://doi.org/10.1016/j.socscimed.2006.07.030.

[38] A. Matzarakis, H. Mayer, M.G. Iziomon, Application of a Universal Thermal Index: Physiological Equivalent Temperature, (1999), pp. 76–84.

[39] H.P. Schmid, Source areas for scalars and scalar fluxes, Boundary-Layer Meteorol. 67 (1994) 293–318, https://doi.org/10.1007/BF00713146.

[40] H.P. Schmid, Footprint modeling for vegetation atmosphere exchange studies: a review and perspective, Agric. For. Meteorol. 113 (2002) 159–183, https://doi.org/10.1016/S0168-1923(02)00107-7.

[41] F. Pasquill, Some aspects of boundary layer description, Q. J. R. Meteorol. Soc. 98 (1972) 469–494, https://doi.org/10.1002/qj.49709841702.

[42] A.P. van Ulden, Simple estimates for vertical diffusion from sources near the ground, Atmos. Environ. Times 12 (1978) 2125–2129, https://doi.org/10.1016/0004-6981(78)90167-1.

[43] J.H.C. Gash, A note on estimating the effect of a limited fetch on micrometeorological evaporation measurements, Boundary-Layer Meteorol. 35 (1986) 409–413, https://doi.org/10.1007/BF00118567.

[44] M.Y. Leclerc, T. Foken, Footprints in Micrometeorology and Ecology, Springer, 2014, https://doi.org/10.1007/978-3-642-54545-0.

[45] A. Christen, Atmospheric measurement techniques to quantify greenhouse gas emissions from cities, Urban Clim 10 (2014) 241–260, https://doi.org/10.1016/j.uclim.2014.04.006.

[46] N.G. Perera, R. Emmanuel, A "Local Climate Zone" Based Approach to Urban Planning in Colombo, Sri Lanka, Urban Clim., 2016, https://doi.org/10.1016/j.uclim.2016.11.006.

[47] B. Bechtel, S. Wiesner, K. Zakšek, Estimation of dense time series of urban air temperatures from multitemporal geostationary satellite data, IEEE J. Sel. Top. Appl. Earth Obs. Remote Sens. 7 (2014) 4129–4137, https://doi.org/10.1109/JSTARS.2014.2322449.

[48] K. Kordowski, W. Kuttler, Carbon dioxide fluxes over an urban park area, Atmos. Environ. 44 (2010) 2722–2730, https://doi.org/10.1016/j.atmosenv.2010.04.039.

[49] A. Middel, K. Häb, A.J. Brazel, C.A. Martin, S. Guhathakurta, Impact of urban form and design on mid-afternoon microclimate in Phoenix Local Climate Zones, Landsc. Urban Plann. 122 (2014) 16–28, https://doi.org/10.1016/j.landurbplan.2013.11.004.

[50] J.E. Nichol, T.P. Hang, ISPRS Journal of Photogrammetry and Remote Sensing Temporal characteristics of thermal satellite images for urban heat stress and heat island mapping, ISPRS J. Photogrammetry Remote Sens. 74 (2012) 153–162, https://doi.org/10.1016/j.isprsjprs.2012.09.007.

[51] M.J. Grant, A. Booth, A typology of reviews: an analysis of 14 review types and associated methodologies, Health Inf. Libr. J. 26 (2009) 91–108, https://doi.org/10.1111/j.1471-1842.2009.00848.x.

[52] A.L. Chapman, L.C. Morgan, G. Gartlehner, Semi-automating the manual literature search for systematic reviews increases efficiency, Health Inf. Libr. J. 27 (2010) 22–27, https://doi.org/10.1111/j.1471-1842.2009.00865.x.

[53] N.R. Haddaway, P. Woodcock, B. Macura, A. Collins, Making literature reviews more reliable through application of lessons from systematic reviews, Conserv. Biol. 29 (2015) 1596–1605, https://doi.org/10.1111/cobi.12541.

[54] K.A. Baker, S.M. Weeks, An overview of systematic review, J. PeriAnesthesia Nurs. 29 (2014) 454–458, https://doi.org/10.1016/j.jopan.2014.07.002.

[55] P.A. Mirzaei, F. Haghighat, Approaches to study urban heat island – abilities and

limitations, Build. Environ. 45 (2010) 2192–2201, https://doi.org/10.1016/j.buildenv.2010.04.001.
[56] M. Santamouris, Analyzing the heat island magnitude and characteristics in one hundred Asian and Australian cities and regions, Sci. Total Environ. 512–513 (2015) 582–598, https://doi.org/10.1016/j.scitotenv.2015.01.060.
[57] H. Akbari, D. Kolokotsa, Three decades of urban heat islands and mitigation technologies research, Energy Build. 133 (2016) 834–842, https://doi.org/10.1016/j.enbuild.2016.09.067.
[58] G.E. Marjaba, S.E. Chidiac, Sustainability and resiliency metrics for buildings - critical review, Build. Environ. 101 (2016) 116–125, https://doi.org/10.1016/j.buildenv.2016.03.002.
[59] H.B. Gunay, W. O'Brien, I. Beausoleil-Morrison, A critical review of observation studies, modeling, and simulation of adaptive occupant behaviors in offices, Build. Environ. 70 (2013) 31–47, https://doi.org/10.1016/j.buildenv.2013.07.020.
[60] J. Zuo, S. Pullen, J. Palmer, H. Bennetts, N. Chileshe, T. Ma, Impacts of heat waves and corresponding measures: a review, J. Clean. Prod. 92 (2015) 1–12, https://doi.org/10.1016/j.jclepro.2014.12.078.
[61] D.E. Bowler, L. Buyung-Ali, T.M. Knight, A.S. Pullin, Urban greening to cool towns and cities: a systematic review of the empirical evidence, Landsc. Urban Plann. 97 (2010) 147–155, https://doi.org/10.1016/j.landurbplan.2010.05.006.
[62] A.D. Oxman, G.H. Guyatt, The science of reviewing research, Ann. N. Y. Acad. Sci. 703 (1993) 125–134, https://doi.org/10.1111/j.1749-6632.1993.tb26342.x.
[63] D. Moher, A. Liberati, J. Tetzlaff, D.G. Altman, D. Altman, G. Antes, D. Atkins, V. Barbour, N. Barrowman, J.A. Berlin, J. Clark, M. Clarke, D. Cook, R. D'Amico, J.J. Deeks, P.J. Devereaux, K. Dickersin, M. Egger, E. Ernst, P.C. Gøtzsche, J. Grimshaw, G. Guyatt, J. Higgins, J.P.A. Ioannidis, J. Kleijnen, T. Lang, N. Magrini, D. McNamee, L. Moja, C. Mulrow, M. Napoli, A. Oxman, B. Pham, D. Rennie, M. Sampson, K.F. Schulz, P.G. Shekelle, D. Tovey, P. Tugwell, Preferred reporting items for systematic reviews and meta-analyses: the PRISMA statement, PLoS Med. 6 (2009), https://doi.org/10.1371/journal.pmed.1000097.
[64] J. Higgins, S. Green, Cochrane Handbook for Systematic Reviews of Interventions, (2011) http://community.cochrane.org/handbook-sri/chapter-1-introduction/11-cochrane/12-systematic-reviews/122-what-systematic-review.
[65] E. Aromataris, Z. Munn, Joanna Briggs Institute Reviewer's Manual, (2014) https://reviewersmanual.joannabriggs.org/.
[66] K. Hammerstrøm, A. Wade, A.K. Jørgensen, Searching for Studies: a Guide to Information Retrieval for Campbell Systematic Reviews, Oslo, (2017), https://doi.org/10.4073/cmg.2016.1.
[67] Y. Teng, K. Li, W. Pan, T. Ng, Reducing building life cycle carbon emissions through prefabrication: evidence from and gaps in empirical studies, Build. Environ. 132 (2018) 125–136, https://doi.org/10.1016/j.buildenv.2018.01.026.
[68] K.W. Ma, H.M. Wong, C.M. Mak, A systematic review of human perceptual dimensions of sound: meta-analysis of semantic differential method applications to indoor and outdoor sounds, Build. Environ. 133 (2018) 123–150, https://doi.org/10.1016/j.buildenv.2018.02.021.
[69] A. Asadzadeh, T. Kötter, P. Salehi, J. Birkmann, Operationalizing a concept: the systematic review of composite indicator building for measuring community disaster resilience, Int. J. Disaster Risk Reduct. 25 (2017) 147–162, https://doi.org/10.1016/j.ijdrr.2017.09.015.
[70] T. Vesala, N. Kljun, Ü. Rannik, J. Rinne, A. Sogachev, T. Markkanen, K. Sabelfeld, T. Foken, M.Y. Leclerc, Flux and concentration footprint modelling: state of the art, Environ. Pollut. 152 (2008) 653–666, https://doi.org/10.1016/j.envpol.2007.06.070.
[71] T. Foken, Micrometeorology, second ed., Springer Nature, 2017, https://doi.org/10.1007/978-3-642-25440-6.
[72] C. Helfter, A.H. Tremper, C.H. Halios, S. Kotthaus, A. Bjorkegren, C.S.B. Grimmond, J.F. Barlow, E. Nemitz, Spatial and temporal variability of urban fluxes of methane, carbon monoxide and carbon dioxide above London, UK, Atmos. Chem. Phys. 16 (2016) 10543–10557, https://doi.org/10.5194/acp-16-10543-2016.
[73] B. Lietzke, R. Vogt, C. Feigenwinter, E. Parlow, On the controlling factors for the variability of carbon dioxide flux in a heterogeneous urban environment, Int. J. Climatol. 35 (2015) 3921–3941, https://doi.org/10.1002/joc.4255.
[74] L.W.A. van Hove, C.M.J. Jacobs, B.G. Heusinkveld, J.A. Elbers, B.L. van Driel, A.A.M. Holtslag, Temporal and spatial variability of urban heat island and thermal comfort within the Rotterdam agglomeration, Build. Environ. 83 (2015) 91–103, https://doi.org/10.1016/j.buildenv.2014.08.029.
[75] P.H. Schuepp, M.Y. Leclerc, J.I. MacPherson, R.L. Desjardins, Footprint prediction of scalar fluxes from analytical solutions of the diffusion equation, Boundary-Layer Meteorol. 50 (1990) 355–373, https://doi.org/10.1007/BF00120530.
[76] J.R. Dorsey, E. Nemitz, M.W. Gallagher, D. Fowler, P.I. Williams, K.N. Bower, K.M. Beswick, Direct measurements and parameterization of aerosol flux, concentration and emissioin velocity above a city, Atmos. Environ. 36 (2002) 791–800.
[77] C. Jacobs, J. Elbers, R. Brolsma, O. Hartogensis, E. Moors, M.T. Rodríguez-Carretero Márquez, B. van Hove, Assessment of evaporative water loss from Dutch cities, Build. Environ. 83 (2015) 27–38, https://doi.org/10.1016/j.buildenv.2014.07.005.
[78] L.B. Stabler, C.A. Martin, A.J. Brazel, Microclimates in a desert city were related to land use and vegetation index, Urban For. Urban Green. 3 (2005) 137–147, https://doi.org/10.1016/j.ufug.2004.11.001.
[79] H.P. Schmid, T.R. Oke, A model to estimate the source area contributing to turbulent exchange in the surface layer over patchy terrain, Q. J. R. Meteorol. Soc. 116 (1990) 965–988, https://doi.org/10.1002/qj.49711649409.
[80] C.S.B.S.B. Grimmond, H.A. Cleugh, T.R.T.R. Oke, An objective urban heat storage model and its comparison with other schemes, Atmos. Environ. Part B Urban Atmos. 25 (1991) 311–326, https://doi.org/10.1016/0957-1272(91)90003-W.
[81] C.S.B. Grimmond, The suburban energy balance: methodological considerations and results for a mid-latitude west coast city under winter and spring conditions, Int. J. Climatol. 12 (1992) 481–497, https://doi.org/10.1002/joc.3370120506.
[82] S. Kaplan, A. Peeters, E. Erell, Predicting air temperature simultaneously for multiple locations in an urban environment: a bottom up approach, Appl. Geogr. 76 (2016) 62–74, https://doi.org/10.1016/j.apgeog.2016.09.015.
[83] A. Lemonsu, C.S.B. Grimmond, V. Masson, Modeling the surface energy balance of the core of an old mediterranean city: Marseille, J. Appl. Meteorol. 43 (2004) 312–327, https://doi.org/10.1175/1520-0450(2004)043<0312:MTSEBO>2.0.CO;2.
[84] G.G. Rooney, Comparıson of upwınd land use and roughness length measured in the urban boundary layer, Boundary-Layer Meteorol. 100 (2001) 469–486.
[85] G.G. Rooney, I.D. Longley, J.F. Barlow, Variation of urban momentum roughness length with land use in the upwind source area, as observed in two U.K. cities, Boundary-Layer Meteorol. 115 (2005) 69–84.
[86] H.P. Schmid, H.A. Cleugh, C.S.B. Grimmond, T.R. Oke, Spatial variability of energy fluxes in suburban terrain, Boundary-Layer Meteorol. 54 (1991) 249–276.
[87] M.Y. Leclerc, G.W. Thurtell, Footprint prediction of scalar fluxes using a Markovian analysis, Boundary-Layer Meteorol. 52 (1990) 247–258, https://doi.org/10.1007/BF00122089.
[88] T.W. Horst, J.C. Weil, Footprint estimation for scalar flux measurements in the atmospheric surface layer, Boundary-Layer Meteorol. 59 (1992) 279–296, https://doi.org/10.1007/BF00119817.
[89] T.W. Horst, J.C. Weil, How far is far enough?: the fetch requirements for micrometeorological measurement of surface fluxes, J. Atmos. Ocean. Technol. 11 (1994) 1018–1025, https://doi.org/10.1175/1520-0426(1994)011<1018:HFIFET>2.0.CO;2.
[90] L. Järvi, Ü. Rannik, I. Mammarella, A. Sogachev, P.P. Aalto, P. Keronen, E. Siivola, M. Kulmala, T. Vesala, Annual particle flux observations over a heterogeneous urban area, Atmos. Chem. Phys. 9 (2009) 7847–7856, https://doi.org/10.5194/acp-9-7847-2009.
[91] S.H. Lee, J.H. Lee, B.Y. Kim, Estimation of turbulent sensible heat and momentum fluxes over a heterogeneous urban area using a large aperture scintillometer, Adv. Atmos. Sci. 32 (2015) 1092–1105, https://doi.org/10.1007/s00376-015-4236-2.
[92] H.P. Schmid, Experimental design for flux measurements: matching scales of observations and fluxes, Agric. For. Meteorol. 87 (1997) 179–200, https://doi.org/10.1016/S0168-1923(97)00011-7.
[93] J.F. Barlow, G.G. Rooney, S. Hünerbein, S.G. Bradley, Relating urban surface-layer structure to upwind terrain for the Salford Experiment (Salfex), Boundary-Layer Meteorol. 127 (2008) 173–191, https://doi.org/10.1007/s10546-007-9261-y.
[94] D. Contini, A. Donateo, C. Elefante, F.M. Grasso, Analysis of particles and carbon dioxide concentrations and fluxes in an urban area: correlation with traffic rate and local micrometeorology, Atmos. Environ. 46 (2012) 25–35, https://doi.org/10.1016/j.atmosenv.2011.10.039.
[95] K. Häb, A. Middel, B.L. Ruddell, H. Hagen, TraVis - a visualization framework for mobile transect data sets in an urban microclimate context, IEEE Pacific Vis. Symp. (2015) 167–174, https://doi.org/10.1109/PACIFICVIS.2015.7156374 2015–July.
[96] M. Kanda, R.Y.O. Moriwaki, M. Roth, T.I.M. Oke, Area-averaged sensible heat flux and a new method to determine zero-plane displacement length over an urban surface using scintillometry, Boundary-Layer Meteorol. 105 (2002) 177–193.
[97] G. Liu, J. Sun, Impact of surface variations on the momentum flux above the urban canopy, Theor. Appl. Climatol. 101 (2010) 411–419, https://doi.org/10.1007/s00704-009-0219-5.
[98] T.R. Oke, R. Spronken-Smith, E. Jáuregui, C.S.D. Grimmond, The energy balance of central Mexico City during the dry season, Atmos. Environ. 33 (1999) 3919–3930.
[99] W. Pawlak, K. Fortuniak, M. Siedlecki, M. Zieliński, Urban – wetland contrast in turbulent exchange of methane, Atmos. Environ. 145 (2016) 176–191, https://doi.org/10.1016/j.atmosenv.2016.09.036.
[100] S. Weber, K. Kordowski, Comparison of atmospheric turbulence characteristics and turbulent fluxes from two urban sites in Essen, Germany, Theor. Appl. Climatol. 102 (2010) 61–74, https://doi.org/10.1007/s00704-009-0240-8.
[101] M. Zieliński, K. Fortuniak, W. Pawlak, M. Siedlecki, Influence of mean rooftop-level estimation method on sensible heat flux retrieved from a large-aperture scintillometer over a city centre, Boundary-Layer Meteorol. 164 (2017) 281–301, https://doi.org/10.1007/s10546-017-0254-1.
[102] S.K. Kaharabata, P.H. Schuepp, S. Ogunjemiyo, S. Shen, M.Y. Leclerc, R.L. Desjardins, J.I. MacPherson, Footprint considerations in BOREAS, J. Geophys. Res. Atmos. 102 (1997) 29113–29124, https://doi.org/10.1029/97JD02559.
[103] M.Y. Leclerc, S. Shen, B. Lamb, Observations and large-eddy simulation modeling of footprints in the lower convective boundary layer, J. Geophys. Res. 102 (1997) 9323–9334.
[104] D. Baldocchi, Flux footprints within and over forest canopies, Boundary-Layer Meteorol. 85 (1997) 273–292, https://doi.org/10.1023/A:1000472717236.
[105] U. Rannik, M. Aubinet, O. Kurbanmuradov, K.K. Sabelfeld, T. Markkanen, T. Vesala, Footprint analysis for measurements over a heterogeneous forest, Boundary-Layer Meteorol. 97 (2000) 137–166, https://doi.org/10.1023/A:1002702810929.
[106] U. ¨ Rannik, T. Markkanen, J. Raittila, P. Hari, T. Vesala, Turbulence statistics inside and over forest: influence on footprint prediction, Boundary-Layer Meteorol. 109 (2003) 163–189, https://doi.org/10.1023/A:1025404923169.
[107] C.I. Hsieh, G. Katul, T.W. Chi, An approximate analytical model for footprint estimation of scalar fluxes in thermally stratified atmospheric flows, Adv. Water Resour. 23 (2000) 765–772, https://doi.org/10.1016/S0309-1708(99)00042-1.
[108] B. Gioli, P. Toscano, E. Lugato, A. Matese, F. Miglietta, A. Zaldei, F.P. Vaccari,

Methane and carbon dioxide fluxes and source partitioning in urban areas: the case study of Florence, Italy, Environ. Pollut. 164 (2012) 125–131, https://doi.org/10.1016/j.envpol.2012.01.019.
[109] T.H. Morin, G. Bohrer, R.P. d. M. Frasson, L. Naor-Azreli, S. Mesi, K.C. Stefanik, K.V.R. Schäfer, Environmental drivers of methane fluxes from an urban temperate wetland park, J. Geophys. Res. Biogeosciences. (2014) 2188–2208, https://doi.org/10.1002/2014JG002750.Received.
[110] A.J. Oliphant, S. Stein, G. Bradford, Micrometeorology of an ephemeral desert city, the Burning Man experiment, Urban Clim 23 (2017) 53–70, https://doi.org/10.1016/j.uclim.2017.03.001.
[111] M. Roth, J.A. Salmond, A.N.V. Satyanarayana, Methodological considerations regarding the measurement of turbulent fluxes in the urban roughness sublayer: the role of scintillometery, Boundary-Layer Meteorol. 121 (2006) 351–375, https://doi.org/10.1007/s10546-006-9074-4.
[112] T. Song, Y. Wang, Carbon dioxide fluxes from an urban area in Beijing, Atmos. Res. 106 (2012) 139–149, https://doi.org/10.1016/j.atmosres.2011.12.001.
[113] N. Sparks, R. Toumi, Remote sampling of a CO2 point source in an urban setting, Atmos. Environ. 44 (2010) 5287–5294, https://doi.org/10.1016/j.atmosenv.2010.07.048.
[114] E. Velasco, S. Pressley, E. Allwine, H. Westberg, B. Lamb, Measurements of CO2 fluxes from the Mexico City urban landscape, Atmos. Environ. 39 (2005) 7433–7446, https://doi.org/10.1016/j.atmosenv.2005.08.038.
[115] E. Velasco, B. Lamb, S. Pressley, E. Allwine, H. Westberg, B.T. Jobson, M. Alexander, P. Prazeller, L. Molina, M. Molina, Flux measurements of volatile organic compounds from an urban landscape, Geophys. Res. Lett. 32 (2005) 1–4, https://doi.org/10.1029/2005GL023356.
[116] E. Velasco, R. Perrusquia, E. Jiménez, F. Hernández, P. Camacho, S. Rodríguez, A. Retama, L.T. Molina, Sources and sinks of carbon dioxide in a neighborhood of Mexico City, Atmos. Environ. Times 97 (2014) 226–238, https://doi.org/10.1016/j.atmosenv.2014.08.018.
[117] H.C. Ward, J.G. Evans, C.S.B. Grimmond, Multi-scale sensible heat fluxes in the suburban environment from large-aperture scintillometry and eddy covariance, Boundary-Layer Meteorol. 152 (2014) 65–89, https://doi.org/10.1007/s10546-014-9916-4.
[118] R. Kormann, F.X. Meixner, An analytical footprint model for non-neutral stratification, Boundary-Layer Meteorol. 99 (2001) 207–224, https://doi.org/10.1023/A:1018991015119.
[119] T. Ando, M. Ueyama, Surface energy exchange in a dense urban built-up area based on two-year eddy covariance measurements in Sakai, Japan, Urban Clim. 19 (2017) 155–169, https://doi.org/10.1016/j.uclim.2017.01.005.
[120] M. Auvinen, L. Järvi, A. Hellsten, Ü. Rannik, T. Vesala, Numerical framework for the computation of urban flux footprints employing large-eddy simulation and Lagrangian stochastic modeling, Geosci. Model Dev. (GMD) 10 (2017) 4187–4205, https://doi.org/10.5194/gmd-10-4187-2017.
[121] A. Björkegren, C.S.B. Grimmond, Net carbon dioxide emissions from central London, Urban Clim. 23 (2018), https://doi.org/10.1016/j.uclim.2016.10.002.
[122] A. Christen, N.C. Coops, B.R. Crawford, R. Kellett, K.N. Liss, I. Olchovski, T.R. Tooke, M. Van Der Laan, J.A. Voogt, Validation of modeled carbon-dioxide emissions from an urban neighborhood with direct eddy-covariance measurements, Atmos. Environ. 45 (2011) 6057–6069, https://doi.org/10.1016/j.atmosenv.2011.07.040.
[123] B. Crawford, C.S.B. Grimmond, A. Christen, Five years of carbon dioxide fluxes measurements in a highly vegetated suburban area, Atmos. Environ. 45 (2011) 896–905, https://doi.org/10.1016/j.atmosenv.2010.11.017.
[124] B. Crawford, C.S.B. Grimmond, H.C. Ward, W. Morrison, S. Kotthaus, Spatial and temporal patterns of surface-atmosphere energy exchange in a dense urban environment using scintillometry, Q. J. R. Meteorol. Soc. 143 (2017) 817–833, https://doi.org/10.1002/qj.2967.
[125] C. Feigenwinter, E. Parlow, R. Vogt, M. Schmutz, N. Chrysoulakis, F. Lindberg, M. Marconcini, F. del Frate, Spatial distribution of sensible and latent heat flux in the URBANFLUXES case study city Basel (Switzerland), 2017 Jt, Urban Remote Sens. Event (2017) 1–4, https://doi.org/10.1109/JURSE.2017.7924594.
[126] C. Helfter, D. Famulari, G.J. Phillips, J.F. Barlow, C.R. Wood, C.S.B. Grimmond, E. Nemitz, Controls of carbon dioxide concentrations and fluxes above central London, Atmos. Chem. Phys. 11 (2011) 1913–1928, https://doi.org/10.5194/acp-11-1913-2011.
[127] A. Hellsten, S.M. Luukkonen, G. Steinfeld, F. Kanani-Sühring, T. Markkanen, L. Järvi, J. Lento, T. Vesala, S. Raasch, Footprint evaluation for flux and concentration measurements for an urban-like canopy with coupled Lagrangian stochastic and large-eddy simulation models, Boundary-Layer Meteorol. 157 (2015) 191–217, https://doi.org/10.1007/s10546-015-0062-4.
[128] C.W. Kent, S. Grimmond, J. Barlow, D. Gatey, S. Kotthaus, F. Lindberg, C.H. Halios, Evaluation of urban local-scale Aerodynamic parameters: implications for the vertical profile of wind speed and for source areas, Boundary-Layer Meteorol. 164 (2) (2017) 183–213, https://doi.org/10.1007/s10546-017-0267-9 10.1007/s10546-017-0248-z), Boundary-Layer Meteorol. 164 (2017) 215.
[129] S.H. Kota, C. Park, M.C. Hale, N.D. Werner, G.W. Schade, Q. Ying, Estimation of VOC emission factors from flux measurements using a receptor model and footprint analysis, Atmos. Environ. 82 (2014) 24–35, https://doi.org/10.1016/j.atmosenv.2013.09.052.
[130] S. Kotthaus, C.S.B. Grimmond, Identification of Micro-scale Anthropogenic CO2, heat and moisture sources - processing eddy covariance fluxes for a dense urban environment, Atmos. Environ. 57 (2012) 301–316, https://doi.org/10.1016/j.atmosenv.2012.04.024.
[131] S. Kotthaus, C.S.B. Grimmond, Energy exchange in a dense urban environment – Part II: impact of spatial heterogeneity of the surface, Urban Clim 10 (2014) 281–307, https://doi.org/10.1016/j.uclim.2013.10.001.
[132] M. Kurppa, A. Nordbo, S. Haapanala, L. Järvi, Effect of seasonal variability and land use on particle number and CO_2 exchange in Helsinki, Finland, Urban Clim 13 (2015) 94–109, https://doi.org/10.1016/j.uclim.2015.07.006.
[133] H.Z. Liu, J.W. Feng, L. Järvi, T. Vesala, Four-year (2006-2009) eddy covariance measurements of CO 2 flux over an urban area in Beijing, Atmos. Chem. Phys. 12 (2012) 7881–7892, https://doi.org/10.5194/acp-12-7881-2012.
[134] A. Nordbo, L. Järvi, S. Haapanala, J. Moilanen, T. Vesala, Intra-city variation in urban morphology and turbulence structure in Helsinki, Finland, Boundary-Layer Meteorol. 146 (2013) 469–496, https://doi.org/10.1007/s10546-012-9773-y.
[135] C. Park, G.W. Schade, I. Boedeker, Characteristics of the flux of isoprene and its oxidation products in an urban area, J. Geophys. Res. Atmos. 116 (2011) 1–13, https://doi.org/10.1029/2011JD015856.
[136] C. Park, G.W. Schade, N.D. Werner, D.J. Sailor, C.H. Kim, Comparative estimates of anthropogenic heat emission in relation to surface energy balance of a subtropical urban neighborhood, Atmos. Environ. 126 (2016) 182–191, https://doi.org/10.1016/j.atmosenv.2015.11.038.
[137] S. Rapsomanikis, A. Trepekli, G. Loupa, C. Polyzou, Vertical energy and momentum fluxes in the centre of athens, Greece during a heatwave period (thermopolis 2009 campaign), Boundary-Layer Meteorol. 154 (2015) 497–512, https://doi.org/10.1007/s10546-014-9979-2.
[138] J.A. Salmond, M. Roth, T.R. Oke, A. Christen, J.A. Voogt, Can surface-cover tiles be summed to give neighborhood fluxes in cities? J. Appl. Meteorol. Climatol. 51 (2012) 133–149, https://doi.org/10.1175/JAMC-D-11-078.1.
[139] M. Ueyama, T. Ando, Diurnal, weekly, seasonal, and spatial variabilities in carbon dioxide flux in different urban landscapes in Sakai, Japan, Atmos. Chem. Phys. 16 (2016) 14727–14740, https://doi.org/10.5194/acp-16-14727-2016.
[140] A.C. Valach, B. Langford, E. Nemitz, A.R. Mackenzie, C.N. Hewitt, Seasonal and diurnal trends in concentrations and fluxes of volatile organic compounds in central London, Atmos. Chem. Phys. 15 (2015) 7777–7796, https://doi.org/10.5194/acp-15-7777-2015.
[141] Z.-H. Wang, C. Fan, S.W. Myint, C. Wang, Size matters: what are the characteristic source areas for urban planning strategies? PloS One 11 (2016) e0165726, , https://doi.org/10.1371/journal.pone.0165726.
[142] J. Zou, B. Zhou, J. Sun, Impact of eddy characteristics on turbulent heat and momentum fluxes in the urban roughness sublayer, Boundary-Layer Meteorol. 164 (2017) 39–62, https://doi.org/10.1007/s10546-017-0244-3.
[143] N. Kljun, M.W. Rotach, H.P. Schmid, A three-dimensional backward Lagrangian footprint model for a wide range of boundary-layer stratifications, Boundary-Layer Meteorol. 103 (2002) 205–226.
[144] N. Kljun, P. Calanca, M.W. Rotach, H.P. Schmid, A simple parameterisation for flux footprint predictions, Boundary-Layer Metorology 112 (2004) 503–523 https://doi.org/10.1023/B:BOUN.0000030653.71031.96.
[145] O. Bergeron, I.B. Strachan, CO2 sources and sinks in urban and suburban areas of a northern mid-latitude city, Atmos. Environ. 45 (2011) 1564–1573, https://doi.org/10.1016/j.atmosenv.2010.12.043.
[146] G. Guidolotti, C. Calfapietra, E. Pallozzi, G. De Simoni, R. Esposito, M. Mattioni, G. Nicolini, G. Matteucci, E. Brugnoli, Promoting the potential of flux-measuring stations in urban parks: an innovative case study in Naples, Italy, Agric. For. Meteorol. 233 (2017) 153–162, https://doi.org/10.1016/j.agrformet.2016.11.004.
[147] R.V. Hiller, J.P. McFadden, N. Kljun, Interpreting CO2 fluxes over a suburban lawn: the influence of traffic emissions, Boundary-Layer Meteorol. 138 (2011) 215–230, https://doi.org/10.1007/s10546-010-9558-0.
[148] B. Langford, B. Davison, E. Nemitz, C.N.N. Hewitt, Mixing ratios and eddy covariance flux measurements of volatile organic compounds from an urban canopy (Manchester, UK), Atmos. Chem. Phys. 9 (2009) 1971–1987, https://doi.org/10.5194/acpd-8-245-2008.
[149] E.M. Mårtensson, E.D. Nilsson, G. Buzorius, C. Johansson, Eddy covariance measurements and parameterisation of traffic related particle emissions in an urban environment, Atmos. Chem. Phys. 6 (2006) 769–785, https://doi.org/10.5194/acp-6-769-2006.
[150] O. Menzer, J.P. McFadden, Statistical partitioning of a three-year time series of direct urban net CO2flux measurements into biogenic and anthropogenic components, Atmos. Environ. 170 (2017) 319–333, https://doi.org/10.1016/j.atmosenv.2017.09.049.
[151] A. Sogachev, J. Lloyd, Using a one-and-a-half order closure model of the atmospheric boundary layer for surface flux footprint estimation, Boundary-Layer Meteorol. 112 (2004) 467–502, https://doi.org/10.1023/B:BOUN.0000030664.52282.ee.
[152] T. Vesala, L. Järvi, S. Launiainen, A. Sogachev, Ü. Rannik, I. Mammarella, E. Siivola, P. Keronen, J. Rinne, A. Riikonen, E. Nikinmaa, Surface-atmosphere interactions over complex urban terrain in Helsinki, Finland, Tellus Ser. B Chem. Phys. Meteorol. 60 B (2008) 188–199, https://doi.org/10.1111/j.1600-0889.2007.00312.x.
[153] X. Cai, M.Y. Leclerc, Forward-in-time and backward-in-time dispersion in the convective boundary layer: the concentration footprint, Boundary-Layer Meteorol. 123 (2007) 201–218, https://doi.org/10.1007/s10546-006-9141-x.
[154] T.V. Prabha, M.Y. Leclerc, D. Baldocchi, Comparison of in-canopy flux footprints between large-eddy simulation and the Lagrangian simulation, J. Appl. Meteorol. Climatol. 47 (2008) 2115–2128, https://doi.org/10.1175/2008JAMC1814.1.
[155] G. Steinfeld, S. Raasch, T. Markkanen, Footprints in homogeneously and heterogeneously driven boundary layers derived from a Lagrangian stochastic particle model embedded into large-eddy simulation, Boundary-Layer Meteorol. 129 (2008) 225–248, https://doi.org/10.1007/s10546-008-9317-7.
[156] C.I. Hsieh, G. Katul, The Lagrangian stochastic model for estimating footprint and

water vapor fluxes over inhomogeneous surfaces, Int. J. Biometeorol. 53 (2009) 87–100, https://doi.org/10.1007/s00484-008-0193-0.
[157] N. Kljun, P. Calanca, M.W. Rotach, H.P. Schmid, A simple two-dimensional parameterisation for flux footprint prediction (FFP), geosci, Model Dev 8 (2015) 3695–3713, https://doi.org/10.5194/gmd-8-3695-2015.
[158] A. Inagaki, M. Kanda, N.H. Ahmad, A. Yagi, N. Onodera, T. Aoki, A numerical study of turbulence statistics and the structure of a spatially-developing boundary layer over a realistic urban geometry, Boundary-Layer Meteorol. 164 (2017) 161–181, https://doi.org/10.1007/s10546-017-0249-y.
[159] R.B. Stull, An Introduction to Boundary Layer Meteorology, Kluwer Academic Publisher, 1988, https://doi.org/10.1007/978-94-009-3027-8.
[160] T.K. Flesch, The footprint for flux measurements, from backward Lagrangian stochastic models, Boundary-Layer Meteorol. 78 (1996) 399–404.
[161] L. Mahrt, The bulk aerodynamic formulation over heterogeneous surfaces, Boundary-Layer Meteorol. 78 (1996) 87–119.
[162] M. Aubinet, Comparison between different methods of measurement of momentum and sensible heat fluxes over canopies, Biotechnol. Agron. Soc. Environ. 1 (1997) 17–25.
[163] M. Roth, Review of atmospheric turbulence over cities.pdf, Q. J. R. Meteorol. Soc. 126 (2000) 941–990.
[164] J.F. Barlow, Progress in observing and modelling the urban boundary layer, Urban Clim 10 (2014) 216–240, https://doi.org/10.1016/j.uclim.2014.03.011.
[165] T. Vesala, Ü. Rannik, M. Leclerc, T. Foken, K. Sabelfeld, Flux and concentration footprints, Agric. For. Meteorol. 127 (2004) 111–116, https://doi.org/10.1016/j.agrformet.2004.07.007.
[166] M. Göckede, C. Thomas, T. Markkanen, M. Mauder, J. Ruppert, T. Foken, Sensitivity of Lagrangian Stochastic footprints to turbulence statistics, Tellus Ser. B Chem. Phys. Meteorol. 59 (2007) 577–586, https://doi.org/10.1111/j.1600-0889.2007.00275.x.
[167] M. Roth, Review of urban climate research in (sub)tropical regions, Int. J. Climatol. 27 (2007) 1859–1873, https://doi.org/10.1002/joc.1591.
[168] C.S.B. Grimmond, M. Roth, T.R. Oke, Y.C. Au, M. Best, R. Betts, G. Carmichael, H. Cleugh, W. Dabberdt, R. Emmanuel, E. Freitas, K. Fortuniak, S. Hanna, P. Klein, L.S. Kalkstein, C.H. Liu, A. Nickson, D. Pearlmutter, D. Sailor, J. Voogt, Climate and more sustainable cities: climate information for improved planning and management of cities (Producers/Capabilities Perspective), Procedia Environ. Sci. 1 (2010) 247–274, https://doi.org/10.1016/j.proenv.2010.09.016.
[169] L. Mahrt, Computing turbulent fluxes near the surface: needed improvements, Agric. For. Meteorol. 150 (2010) 501–509, https://doi.org/10.1016/j.agrformet.2010.01.015.
[170] E. Velasco, M. Roth, Cities as net sources of CO2: review of atmospheric CO2 exchange in urban environments measured by eddy covariance technique, Geogr. Compass. 4 (2010) 1238–1259, https://doi.org/10.1111/j.1749-8198.2010.00384.x.
[171] T. Vesala, N. Kljun, Ü. Rannik, J. Rinne, A. Sogachev, T. Markkanen, K. Sabelfeld, T. Foken, M.Y. Leclerc, Flux and concentration footprint modeling, in: G. Hanrahan (Ed.), Model. Pollut. Complex Environ. Syst. ILM Publications, 2010, pp. 339–355.
[172] C. Feigenwinter, R. Vogt, A. Christen, Eddy covariance measurements over urban areas, in: M. Aubinet, T. Vesala, D. Papale (Eds.), Eddy Covariance a Pract. Guid. To Meas. Data, Springer Science and Business Media, 2012, pp. 377–397, , https://doi.org/10.1007/978-94-007-2351-1.
[173] Ü. Rannik, A. Sogachev, T. Foken, G. Mathias, N. Kljun, M.Y. Leclerc, T. Vesala, Eddy covariance, in: M. Aubinet, T. Vesala, D. Papale (Eds.), Eddy Covariance a Pract. Guid. To Meas. Data, Springer Science and Business Media, 2012, pp. 211–261, , https://doi.org/10.1007/978-94-007-2351-1.
[174] Y. Toparlar, B. Blocken, B. Maiheu, G.J.F. van Heijst, A review on the CFD analysis of urban microclimate, Renew. Sustain. Energy Rev. 80 (2017) 1613–1640, https://doi.org/10.1016/j.rser.2017.05.248.
[175] C. Park, G.W. Schade, I. Boedeker, Flux measurements of volatile organic compounds by the relaxed eddy accumulation method combined with a GC-FID system in urban Houston, Texas, Atmos. Environ. Times 44 (2010) 2605–2614, https://doi.org/10.1016/j.atmosenv.2010.04.016.
[176] T.R. Oke, Towards better scientific communication in urban climate, Theor. Appl. Climatol. 84 (2006) 179–190, https://doi.org/10.1007/s00704-005-0153-0.
[177] H. Tennekes, The logarithmic wind profile, J. Atmos. Sci. 30 (1973) 234–238, https://doi.org/10.1175/1520-0469(1973)030<0234:TLWP>2.0.CO;2.
[178] A.S. Monin, A.M. Obukhov, Basic laws of turbulent mixing in the surface layer of the atmosphere, Contrib. Geophys. Inst. Acad. Sci. USSR. 24 (1954) 163–187.
[179] T.R. Oke, G. Zeuner, E. Jauregui, The surface energy balance in Mexico City, Atmos. Environ. 26B (1992) 433–444.
[180] R.A. Spronken-Smith, Comparison of summer- and winter-time suburban energy fluxes in Christchurch, New Zealand, Int. J. Climatol. 22 (2002) 979–992, https://doi.org/10.1002/joc.767.
[181] A. Hénon, P.G. Mestayer, D. Groleau, J. Voogt, High resolution thermo-radiative modeling of an urban fragment in Marseilles city center during the UBL-ESCOMPTE campaign, Build. Environ. 46 (2011) 1747–1764, https://doi.org/10.1016/j.buildenv.2011.02.001.
[182] H.C. Ward, J.G. Evans, C.S.B. Grimmond, Multi-season eddy covariance observations of energy, water and carbon fluxes over a suburban area in Swindon, UK, Atmos. Chem. Phys. 13 (2013) 4645–4666, https://doi.org/10.5194/acp-13-4645-2013.
[183] M. Rigby, R. Toumi, R. Fisher, D. Lowry, E.G. Nisbet, First continuous measurements of CO2 mixing ratio in central London using a compact diffusion probe, Atmos. Environ. 42 (2008) 8943–8953, https://doi.org/10.1016/j.atmosenv.2008.06.040.
[184] B. Crawford, A. Christen, Spatial source attribution of measured urban eddy covariance CO2 fluxes, Theor. Appl. Climatol. 119 (2015) 733–755, https://doi.org/10.1007/s00704-014-1124-0.
[185] P. Ramamurthy, E.R. Pardyjak, Toward understanding the behavior of carbon dioxide and surface energy fluxes in the urbanized semi-arid Salt Lake Valley, Utah, USA, Atmos. Environ. Times 45 (2011) 73–84, https://doi.org/10.1016/j.atmosenv.2010.09.049.
[186] B. Gioli, G. Gualtieri, C. Busillo, F. Calastrini, A. Zaldei, P. Toscano, Improving high resolution emission inventories with local proxies and urban eddy covariance flux measurements, Atmos. Environ. 115 (2015) 246–256, https://doi.org/10.1016/j.atmosenv.2015.05.068.
[187] M. Roth, C. Jansson, E. Velasco, Multi-year energy balance and carbon dioxide fluxes over a residential neighbourhood in a tropical city, Int. J. Climatol. 37 (2016) 2679–2698, https://doi.org/10.1002/joc.4873.
[188] J.D. Lee, C. Helfter, R.M. Purvis, S.D. Beevers, D.C. Carslaw, A.C. Lewis, S.J. Møller, A. Tremper, A. Vaughan, E.G. Nemitz, Measurement of NOx fluxes from a tall tower in central London, UK and comparison with emissions inventories, Environ. Sci. Technol. 49 (2015) 1025–1034, https://doi.org/10.1021/es5049072.
[189] E. Kleingeld, B. van Hove, J. Elbers, C. Jacobs, Carbon Dioxide Fluxes in the City Centre of Arnhem, a Middle-sized Dutch City, Urban Clim, 2017, https://doi.org/10.1016/j.uclim.2017.12.003.
[190] S. Grimmond, A. Christen, Flux measurements in urban ecosystems, Fluxletter - Newsl. FLUXNET. 5 (2012) 25–31.
[191] A. Neftel, C. Spirig, C. Ammann, Application and test of a simple tool for operational footprint evaluations, Environ. Pollut. 152 (2008) 644–652, https://doi.org/10.1016/j.envpol.2007.06.062.
[192] T.R. Oke, G. Mills, A. Christen, J.A. Voogt, 4 airflow, Urban Clim, Cambridge University Press, 2017, pp. 77–121, , https://doi.org/10.1017/9781139016476.005.
[193] C.S.B. Grimmond, T.R. Oke, Aerodynamic properties of urban areas derived from analysis of surface form, J. Appl. Meteorol. 38 (1999) 1262–1292, https://doi.org/10.1175/1520-0450(1999)038<1262:APOUAD>2.0.CO;2.
[194] H.C. Ward, J.G. Evans, C.S.B. Grimmond, J. Bradford, Infrared and millimetre-wave scintillometry in the suburban environment-Part 1: structure parameters, Atmos. Meas. Tech. 8 (2015) 1385–1405, https://doi.org/10.5194/amt-8-1385-2015.
[195] H.C. Ward, J.G. Evans, C.S.B. Grimmond, Infrared and millimetre-wave scintillometry in the suburban environment -Part 2: large-area sensible and latent heat fluxes, Atmos. Meas. Tech. 8 (2015) 1407–1424, https://doi.org/10.5194/amt-8-1407-2015.
[196] C.S.B. Grimmond, T.S. King, M. Roth, T.R. Oke, Aerodynamic roughness of urban areas derived from wind observations, Boundary-Layer Meteorol. 89 (1998) 1–24, https://doi.org/10.1023/A:1001525622213.
[197] H.P. Schmid, C.R. Lloyd, Spatial representativeness and the location bias of flux footprints over inhomogeneous areas, Agric. For. Meteorol. 93 (1999) 195–209, https://doi.org/10.1016/S0168-1923(98)00119-1.
[198] R.W. Macdonald, R.F. Griffiths, D.J. Hall, An improved method for the estimation of surface roughness of obstacle arrays, Atmos. Environ. 32 (1998) 1857–1864, https://doi.org/10.1016/S1352-2310(97)00403-2.
[199] J.T. Millward-Hopkins, A.S. Tomlin, L. Ma, D. Ingham, M. Pourkashanian, Estimating aerodynamic parameters of urban-like surfaces with heterogeneous building heights, Boundary-Layer Meteorol. 141 (2011) 443–465, https://doi.org/10.1007/s10546-011-9640-2.
[200] M. Kanda, A. Inagaki, T. Miyamoto, M. Gryschka, S. Raasch, A new aerodynamic parametrization for real urban surfaces, Boundary-Layer Meteorol. 148 (2013) 357–377, https://doi.org/10.1007/s10546-013-9818-x.
[201] P.J. Alexander, B. Bechtel, W.T.L. Chow, R. Fealy, G. Mills, Linking urban climate classification with an urban energy and water budget model: multi-site and multi-seasonal evaluation, Urban Clim 17 (2016) 196–215, https://doi.org/10.1016/j.uclim.2016.08.003.
[202] J.T. Millward-Hopkins, A.S. Tomlin, L. Ma, D. Ingham, M. Pourkashanian, The predictability of above roof wind resource in the urban roughness sublayer, Wind Energy 15 (2012) 225–243, https://doi.org/10.1002/we.463.
[203] F. Pascheke, J.F. Barlow, A. Robins, Wind-tunnel modelling of dispersion from a scalar area source in urban-like roughness, Boundary-Layer Meteorol. 126 (2008) 103–124, https://doi.org/10.1007/s10546-007-9222-5.
[204] P. Kastner-Klein, M.W. Rotach, Mean flow and turbulence characteristics in an urban roughness sublayer, Bound, Layer Meteorol 111 (2004) 55–84, https://doi.org/10.1023/B:BOUN.0000010994.32240.b1.
[205] P.J. Mason, The formation of areally-average roughness lengths, Q. J. R. Meteorol. Soc. 114 (1988) 399–420.
[206] M.W. Rotach, On the influence of the urban roughness sublayer on turbulence and dispersion, Atmos. Environ. 33 (1999) 4001–4008, https://doi.org/10.1016/S1352-2310(99)00141-7.
[207] H. Soegaard, L. Møller-Jensen, Towards a spatial CO2 budget of a metropolitan region based on textural image classification and flux measurements, Remote Sens. Environ. 87 (2003) 283–294, https://doi.org/10.1016/S0034-4257(03)00185-8.
[208] M.W. Rotach, Turbulence close to a rough urban surface. Part I: Reynolds stress, Boundary-Layer Meteorol. 65 (1993) 1–28.
[209] M.W. Rotach, Turbulence close to a rough urban surface. Part II: variances and gradients, Boundary-Layer Meteorol. 66 (1993) 75–92.
[210] J. Zou, G. Liu, J. Sun, H. Zhang, R. Yuan, J. Geophys. Res.: Atmospheres, J. Geophys. Res. Atmos. 120 (2015) 10797–10809, https://doi.org/10.1002/2015JD023909.
[211] Y. Yusup, J.F. Lim, Turbulence variances in the convective urban roughness

sublayer: an application of similarity theory using local scales, Meteorol. Appl. 21 (2014) 149–160, https://doi.org/10.1002/met.1316.
[212] Y. Yusup, S.I. Anis, Similarity theory and nocturnal locally scaled turbulence variances in the tropical urban roughness sublayer, Atmos. Pollut. Res. 7 (2016) 454–468, https://doi.org/10.1016/j.apr.2015.11.002.
[213] J. Taylor, M. Davies, A. Mavrogianni, Z. Chalabi, P. Biddulph, E. Oikonomou, P. Das, B. Jones, The relative importance of input weather data for indoor overheating risk assessment in dwellings, Build. Environ. 76 (2014) 81–91, https://doi.org/10.1016/j.buildenv.2014.03.010.
[214] R. Giridharan, S.S.Y. Lau, S. Ganesan, B. Givoni, Lowering the outdoor temperature in high-rise high-density residential developments of coastal Hong Kong: the vegetation influence, Build. Environ. 43 (2008) 1583–1595, https://doi.org/10.1016/j.buildenv.2007.10.003.
[215] L. Chen, J. Hang, M. Sandberg, L. Claesson, S. Di Sabatino, H. Wigo, The impacts of building height variations and building packing densities on flow adjustment and city breathability in idealized urban models, Build. Environ. 118 (2017) 344–361, https://doi.org/10.1016/j.buildenv.2017.03.042.
[216] L. Shashua-Bar, M.E. Hoffman, Y. Tzamir, Integrated thermal effects of generic built forms and vegetation on the UCL microclimate, Build. Environ. 41 (2006) 343–354, https://doi.org/10.1016/j.buildenv.2005.01.032.
[217] J.K. Page, Application of Building Climatology to the Problems of Housing and Building for Human Settlements, (1976).
[218] T.R. Oke, Street design and urban canopy layer climate, Energy Build. 11 (1988) 103–113, https://doi.org/10.1016/0378-7788(88)90026-6.
[219] G. Mills, Progress toward sustainable settlements: a role for urban climatology, Theor. Appl. Climatol. 84 (2006) 69–76, https://doi.org/10.1007/s00704-005-0145-0.
[220] L. Kleerekoper, M. van Esch, T.B. Salcedo, How to make a city climate-proof, addressing the urban heat island effect, Resour. Conserv. Recycl. 64 (2012) 30–38, https://doi.org/10.1016/j.resconrec.2011.06.004.
[221] B. Blocken, T. Stathopoulos, J.P.A.J. van Beeck, Pedestrian-level wind conditions around buildings: review of wind-tunnel and CFD techniques and their accuracy for wind comfort assessment, Build. Environ. Times 100 (2016) 50–81, https://doi.org/10.1016/j.buildenv.2016.02.004.
[222] C.W. Tsang, K.C.S. Kwok, P.A. Hitchcock, Wind tunnel study of pedestrian level wind environment around tall buildings: effects of building dimensions, separation and podium, Build. Environ. 49 (2012) 167–181, https://doi.org/10.1016/j.buildenv.2011.08.014.
[223] K.T. Tse, A.U. Weerasuriya, X. Zhang, S. Li, K.C.S. Kwok, Pedestrian-level wind environment around isolated buildings under the influence of twisted wind flows, J. Wind Eng. Ind. Aerod. 162 (2017) 12–23, https://doi.org/10.1016/j.jweia.2017.01.002.
[224] Q.M. Zahid Iqbal, A.L.S. Chan, Pedestrian level wind environment assessment around group of high-rise cross-shaped buildings: effect of building shape, separation and orientation, Build. Environ. 101 (2016) 45–63, https://doi.org/10.1016/j.buildenv.2016.02.015.
[225] T. van Hooff, B. Blocken, Y. Tominaga, On the accuracy of CFD simulations of cross-ventilation flows for a generic isolated building: comparison of RANS, LES and experiments, Build. Environ. 114 (2017) 148–165, https://doi.org/10.1016/j.buildenv.2016.12.019.
[226] B. Blocken, Computational Fluid Dynamics for urban physics: importance, scales, possibilities, limitations and ten tips and tricks towards accurate and reliable simulations, Build. Environ. 91 (2015) 219–245, https://doi.org/10.1016/j.buildenv.2015.02.015.
[227] J.F. Barlow, O. Coceal, A Review of Urban Roughness Sublayer Turbulence, (2009).
[228] K. Hanjalic, Will RANS survive LES? A view of perspectives, J. Fluid Eng. 127 (2005) 831, https://doi.org/10.1115/1.2037084.
[229] M. Mizuno, Y. Nakamura, H. Murakami, S. Yamamoto, Effects of land use on urban horizontal atmospheric temperature distributions, Energy Build. 16 (1991) 165–176.
[230] J. Unger, T. Gál, J. Rakonczai, L. Mucsi, J. Szatmári, Z. Tobak, B. van Leeuwen, K. Fiala, Modeling of the urban heat island pattern based on the relationship between surface and air temperatures, Idojaras 114 (2010) 287–302.
[231] M. Szymanowski, M. Kryza, Local regression models for spatial interpolation of urban heat island-an example from Wroc??aw, SW Poland, Theor. Appl. Climatol. 108 (2012) 53–71, https://doi.org/10.1007/s00704-011-0517-6.
[232] J. Lindén, Nocturnal cool island in the sahelian city of ouagadougou, Burkina Faso, Int. J. Climatol. 31 (2011) 605–620, https://doi.org/10.1002/joc.2069.
[233] B. Holmer, S. Thorsson, J. Lindén, Evening evapotranspirative cooling in relation to vegetation and urban geometry in the city of Ouagadougou, Burkina Faso, Int. J. Climatol. 33 (2013) 3089–3105, https://doi.org/10.1002/joc.3561.
[234] E. Erell, I. Eliasson, S. Grimmond, B. Offerle, T. Williamson, Incorporating spatial and temporal variations of advected moisture in the canyon air temperature (cat) model, Seventh Int. Conf. Urban Clim. (2009) 29–32.
[235] G. Liu, J. Sun, W. Jiang, Observational verification of urban surface roughness parameters derived from morphological models, R. Meteorol. Soc. 16 (2009) 205–213, https://doi.org/10.1002/met.109.
[236] G. Loupa, S. Rapsomanikis, A. Trepekli, K. Kourtidis, Energy flux parametrization as an opportunity to get urban heat island insights: the case of athens, Greece (thermopolis 2009 campaign), Sci. Total Environ. 542 (2016) 136–143, https://doi.org/10.1016/j.scitotenv.2015.10.056.
[237] M. Szymanowski, M. Kryza, Application of remotely sensed data for spatial approximation of urban heat island in the city of Wroc??aw, Poland, 2011 Jt. Urban Remote Sens. Event, JURSE 2011 - Proc (2011) 353–356, https://doi.org/10.1109/JURSE.2011.5764792.

7. Artículo 2 Research paper 2

Hourly evolution of intra-urban temperature variability across the local climate zones. The case of Madrid

Núñez-Peiró, M., Sánchez-Guevara Sánchez, C., Neila González, F.J. (2021)

Urban Climate, 39, 100921.

doi: 10.1016/j.uclim.2021.100921

Índice de impacto:

JIF = 5.731 (**JCR Q1**, *Environmental Sciences*)

SJR = 1.151 (**SJR Q1,** *Environmental Science*)

Urban Climate 39 (2021) 100921

Contents lists available at ScienceDirect

Urban Climate

journal homepage: www.elsevier.com/locate/uclim

Hourly evolution of intra-urban temperature variability across the local climate zones. The case of Madrid

Miguel Núñez-Peiró *, Carmen Sánchez-Guevara Sánchez, F. Javier Neila González

Escuela Técnica Superior de Arquitectura, Universidad Politécnica de Madrid, Avda. Juan de Herrera 4, 28040 Madrid, Spain

ARTICLE INFO

Keywords:
Urban heat Island
Urban canopy layer
Local climate zones (LCZs)
Intra-urban temperature variability
Air temperature measurements
Urban meteorological network

ABSTRACT

Field measurement campaigns have grown exponentially in recent years, stemming from the need for reliable data to validate urban climate models and obtain a better understanding of urban climate features. Also contributing to this growth is the Local Climate Zone (LCZ) scheme, firstly developed to enhance the accuracy in the contextualisation of urban measurements, and lately used for characterising urban areas. Due to its relative novelty, researchers are still investigating the potential of LCZs and its indicators for urban temperature variability detection. In this respect, the present study introduces the results of an extensive monitoring campaign carried out in the city of Madrid over a two-year period (2016–2018). The aim of this work is to further examine the relationships between LCZs and air temperature differences, with emphasis on their hourly and seasonal evolution. A graphical and statistical analysis to identify temperature variability trends for each LCZ is performed. Results support the existing evidence suggesting a high level of effectiveness in capturing the heat island (UHI) profile of different urban areas, while underperforming when it comes to capturing diurnal temperature variability. The incorporation of indicators that explain the daytime temperature variation phenomenon into the LCZ scheme is therefore recommended, warranting further research.

1. Introduction

Climate and cities are deeply interconnected. For centuries, cities have adapted to the climatic conditions of their environment. The way in which climate influences cities can be easily noticed through adaptive morphological actions such as street narrowing or roof pitch increases. Today, climate change is urging cities to adapt and adopt new strategies for facing global warming from an integrated urban perspective (Reckien et al., 2018). Similarly, the effect of cities on climate conditions is also well known: not only do they contribute to global warming (Dodman, 2009), but they also modify meso- and micro-climatic conditions (Oke, 1982; Oke et al., 2017a).

From a historical perspective (e.g. Hebbert, 2014; Mills, 2014; Stewart, 2019), the roots of urban climatology go back to the 19th century, when the first studies on air pollution and urban temperature differences were published (Howard, 1833; Renou, 1858; Rusel, 1888). Since then, urban climate studies evolved from urban-rural comparisons of multiple meteorological variables (e.g. Chandler, 1965; Geiger, 1950; Kratzer, 1937) to complex urban land surface models that can be coupled with meso-climatic (Ching, 2013; Jandaghian and Berardi, 2020) and building energy models (Lauzet et al., 2019; Mirzaei, 2015). Nowadays, the latter are also being used for in-depth exploration and unravelling of the most complex climatic processes at the urban scale, which would otherwise be

* Corresponding author.
E-mail address: miguel.nunez@upm.es (M. Núñez-Peiró).

https://doi.org/10.1016/j.uclim.2021.100921
Received 8 October 2020; Received in revised form 1 May 2021; Accepted 8 July 2021
Available online 18 July 2021

Table 1
Previous cities in which urban temperature variability across different LCZs was compared. It includes the background climate, the source used to obtain air temperature data, and the length of the dataset.

City	K-G Climate[1]	Reference	On-site air temperature measurements				Air temp. modelling	Length of the dataset[4]
			Fixed official[2]	Fixed non-official[2]	CWS[3]	Transects		
Delhi (India)	Cwa – BSh	Budhiraja et al. (2020)	■					5 days (CH, May 2018)
Nancy (France)	Cfb	Leconte et al. (2020, 2015, 2017)				■		2 days (D, Aug 2013)
Nanjing (China)	Cfa	Yang et al. (2020b, 2018)		■				3 years (CH, Aug 2016 – Jul 2019)
Sendai (Japan)	Cfa	Zhou et al. (2020)		■				11 days (CH, Aug 2018)
- (France)[5]	Csa – Cfb	Gardes et al. (2020)					■	6 days (CH)
Nagpur (India)	Aw – As	Kotharkar et al. (2019)		■		■		6 days (CH, D, Apr 2016, Mar – Apr 2017)
		Kotharkar and Bagade (2018)		■		■		5 days (CH, D, Dec 2015 – Feb 2016)
Novi Sad (Serbia)	Cfa	Šećerov et al. (2019)		■				2 months (CH, Jun – Aug 2015)
Toulouse (France)	Cfa	Kwok et al. (2019)		■			■	18 days (CH, Jun – Aug 2004)
Vienna (Austria)	Cfb	Hammerberg et al. (2018)	■		■		■	10 days (CH, Jan – Jul 2015)
Antwerp (Belgium)	Cfb	Verdonck et al. (2018)					■	82 days (D, Jun – Aug 2014, 2015)
Brussels (Belgium)	Cfb	Verdonck et al. (2018)					■	101 days (D, Jun - Aug 2014, 2015)
Ghent (Belgium)	Cfb	Verdonck et al. (2018)					■	76 days (D, Jun – Aug 2014, 2015)
Augsburg (Germany)	Cfb	Beck et al. (2018)		■				~3 years (CH, Dec 2014 – Oct 2017)
		Verdonck et al. (2018)		■			■	~8 months (CH, Jun – Sep 2014, 2015)
Dijon (France)	Cfb	Richard et al. (2018)		■			■	3 weeks (CH, Jul 2015)
Berlin (Germany)	Cfb	Fenner et al. (2017)	■	■	■			12 months (CH, Jan – Dec 2015)
		Fenner et al. (2014)		■				10 years (CH, 2001–2010)
Hamburg (Germany)	Cfb	Arnds et al. (2017)	■	■				27 years (CD, 1985–2012)
Matsuyama (Japan)	Cfa	Thapa Chhetri et al. (2017)		■				6 days (CH, Aug)
Szeged (Hungary)	Cfa	Skarbit et al. (2017)		■				1 year (CH, Jun 2014 – May 2015)
		Unger et al. (2015)		■				2 days (CH, Mar 2014)
		Lelovics et al. (2014)				■		4 days (D, Apr 2002 – Mar 2003)
Olomouc (Czech Rep)	Cfb	Lehnert et al. (2015)		■				15 days (CH, Jul 2010 – Oct 2011)
Dublin (Ireland)	Cfb	Alexander and Mills (2014)		■		■		7 days (CH, D, Aug – Sep 2010)
Kochi (India)	Am	Thomas et al. (2014)				■		7 days (D, Jan 2011 – Mar 2013)
Nagano (Japan)	Cfa – Dfb	Stewart et al. (2014)				■		32 days (D, Dec 2001 – Nov 2002)
Uppsala (Sweden)	Cfb	Stewart et al. (2014)		■		■		31 days (D, ~1950); 3 days (CH, Sep 1976)
Vancouver (Canada)	Cfb – Csb	Stewart et al. (2014)				■		5 days (D, Nov 1999, March 2008, 2010)
Hong Kong (China)	Cwa	Siu and Hart (2013)	■					20 years (CD, 1989–2008; CH, 2004–2008)
Mendoza (Argentina)	BWk – BWh	Puliafito et al. (2013)				■		~5 days (D, Dec 2004 – Feb 2005)
Glasgow (UK)	Cfb	Emmanuel and Krüger (2012)	■					50 years (CH, 1959–2009)

[1] According to the updated version of the Köppen-Geiger climatic maps shown in (Kottek et al., 2006; Rubel et al., 2017).
[2] "Official" refers to those measurements derived from official meteorological or air quality networks.
[3] CWS: Citizen Weather Stations.
[4] CH: Continuous Hourly observations; CD: Continuous Daily observations; D: Discrete observations.
[5] Includes several urban areas.

impossible to discern in a real urban environment. Some recent examples are the study of the anthropogenic heat dispersion (Doan et al., 2019; Yuan et al., 2020), the effect of water bodies on the environment (Ampatzidis and Kershaw, 2020), or the relationship between heat loads and social inequalities (Zuvela-Aloise, 2017).

Despite the shift in focus from observation to modelling, measurements remain pivotal in urban climate research. Urban climate models still present a high level of uncertainty, as well as significant heterogeneity between them (Grimmond et al., 2011; Grimmond et al., 2010). They have yet to be tested under different urban contexts, in particular at the micro-climatic scale, to prove their reliability (Best and Grimmmmond, 2015; Toparlar et al., 2017). Measurement campaigns are, therefore, required for validating their performance (Velasco, 2018). On-site observations might also provide an improved understanding of the dynamic processes that govern the urban climate, leading to novel theoretical and modelling approaches, or the improvement of the existing ones (Barlow, 2014; Karl et al., 2020). On top of this, experimental urban climatic data can be used for a variety of multidisciplinary purposes, such as evaluating population vulnerability towards high temperatures (Jänicke et al., 2018; López-Bueno et al., 2019, 2020; Sánchez-Guevara et al., 2019; Willers et al., 2016), assessing buildings' energy consumption (Kolokotroni et al., 2012; Pyrgou et al., 2017), or investigating urban phenological patterns (i.e. pollen production, Jianan et al., 2007; Jochner et al., 2011).

1.1. Using Local Climate Zones for contextualising and characterising urban areas

The Local Climate Zone (LCZ) scheme is a climate classification system for urban environments proposed by Stewart and Oke (2012). LCZs aim at clustering urban (and rural) contexts into 17 conceptual units (10 built-up and 7 land cover types), each one representing their unique local thermal characteristics. A set of 10 quantitative parameters linked to their morphology (sky view factor, aspect ratio, height of roughness elements, terrain roughness class), the surface cover (building, impervious and pervious surface fraction) and their thermal, radiative and metabolic properties (surface admittance, surface albedo, anthropogenic heat output) differentiate each unit.

Although the original purpose of the LCZs was to strengthen the contextualisation and inter-comparability of urban temperature measurements, their use has extended to contextualising other measured parameters, such as $PM_{2,5}$ (Shi et al., 2019), VOCs (Valach et al., 2015), CH_4 (Pawlak and Fortuniak, 2016), CO_2 (Christen, 2014; Crawford and Christen, 2015; Kurppa et al., 2015; Menzer and McFadden, 2017; Roth et al., 2016; Velasco et al., 2014), and energy fluxes (Ando and Ueyama, 2017; Feigenwinter et al., 2012; Kotthaus and Grimmond, 2014). LCZs have demonstrated to be useful for other purposes as well, namely providing climatic guidance for urban planning (Alexander et al., 2016; Perera and Emmanuel, 2016) and modelling weather conditions in urban environments (Brousse et al., 2016; Hammerberg et al., 2018). In just a few years, the LCZs have been rapidly and intensively adopted, becoming the standard scheme in urban climate description.

Regarding the scheme's performance in urban micro-climatic characteristics detection, several studies have shown that its different classes tend to exhibit distinctive temperature profiles (see Table 1). In previous studies, the preferred methodology for obtaining temperature data is in-situ monitoring campaigns, both fixed and mobile. Data from urban models and Citizen Weather Stations (CWS) are also popular, although concerns over their reliability remain (Bell et al., 2015; Chapman et al., 2017; Gardes et al., 2020; Kwok et al., 2019). Some of these studies have also pointed out the need for assessing the performance of the LCZs, rather than just confirming that they display different trends. More specifically, they have focused on evaluating whether the differences between LCZs are statistically significant (Beck et al., 2018; Fenner et al., 2017; Leconte et al., 2020; Richard et al., 2018), if they concentrate at certain times of the year or under specific meteorological conditions (Arnds et al., 2017; Thomas et al., 2014; Yang et al., 2018), or if other parameters might affect the LCZs inter- and intra-variability (Kotharkar et al., 2019; Kwok et al., 2019; Leconte et al., 2017). However, research on the topic is still scarce and limited to a specific climatic context (mostly Cf, humid and warm temperate climates), and in some cases is based on short datasets. It thus seems necessary to continue investigating these links and expand the scope to include other climatic contexts.

1.2. Aim of the study

This study presents the results of an extensive monitoring campaign carried out in the city of Madrid over a two-year period (2016–2018). This work aims to further examine the relationships between LCZs and ambient temperature differences, with emphasis on their hourly and seasonal evolution. For that purpose, a comprehensive overview of the collected data and its associated metadata is firstly provided, describing the pre-processing techniques (i.e. Quality Control (QC) procedures) and the LCZs' contextualisation of the urban measurements. Then, a graphical analysis to identify the trends of the air temperature, Urban Heat Island (UHI) intensity, and cooling rate profiles, is performed for each LCZ. Finally, differences between the LCZs, as well as the ability of the LCZ indicators to capture urban temperature differences, are statistically evaluated on an hourly basis and at different times of the year.

2. Materials and methods

2.1. Study area

The present study focuses on the city of Madrid, located in the centre of Spain (40.42 N, 3.70 W). According to the Köppen-Geiger classification (Kottek et al., 2006; Rubel et al., 2017), Madrid has a Mediterranean climate bordering the semi-arid class (*Csa – BSk*), with hot summers and cold winters. Precipitation tends to concentrate in spring and autumn, while cloudless days are mostly observed in summer. Regionally, its climate is slightly influenced by the presence of the Central System, a mountain range that divides the inner

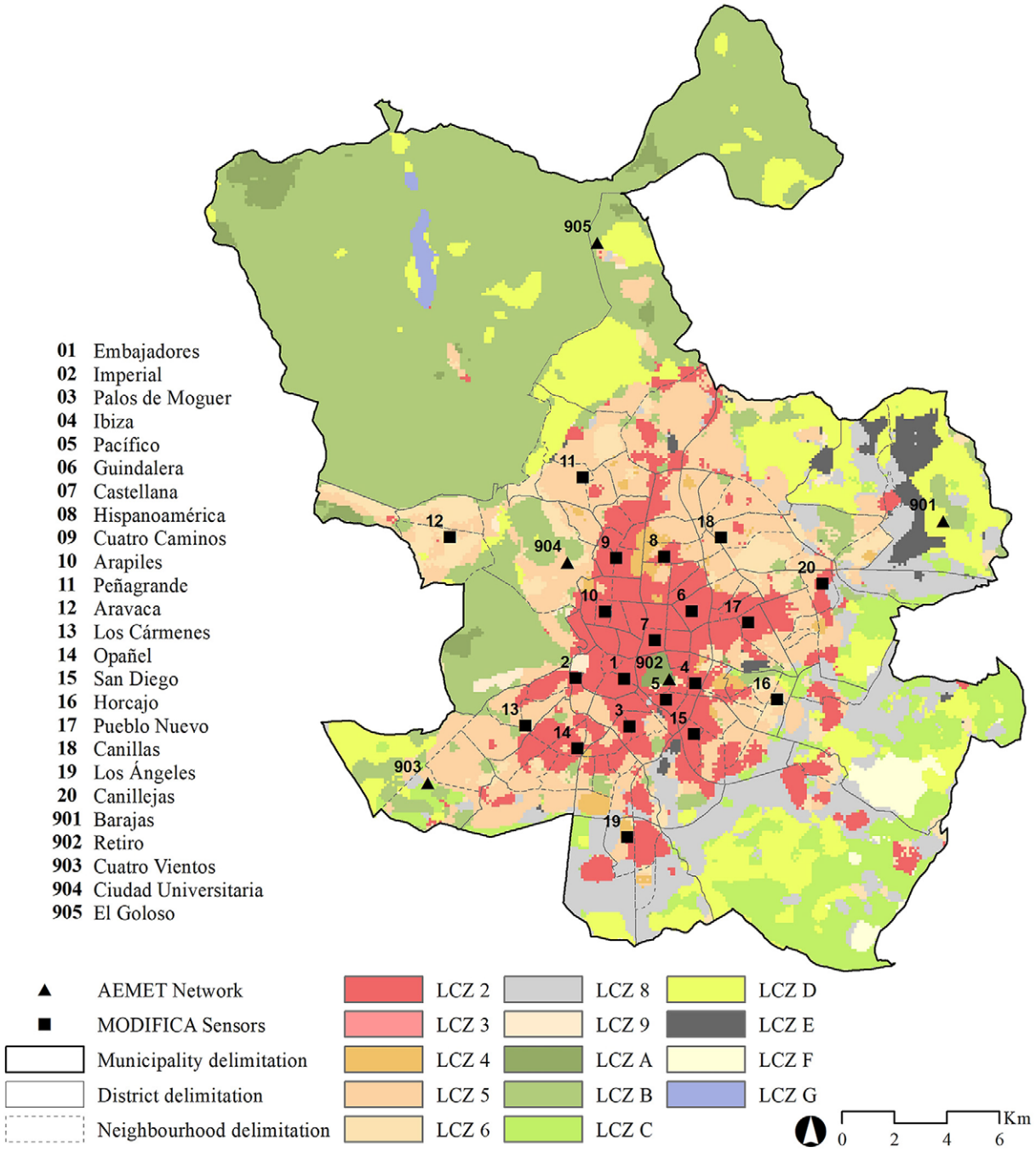

Fig. 1. Location of the MODIFICA sensors and the AEMET meteorological stations within the city of Madrid. The World Urban Database and Access Portal Tools (WUDAPT) LCZs (Brousse et al., 2016) are presented as a background layer.

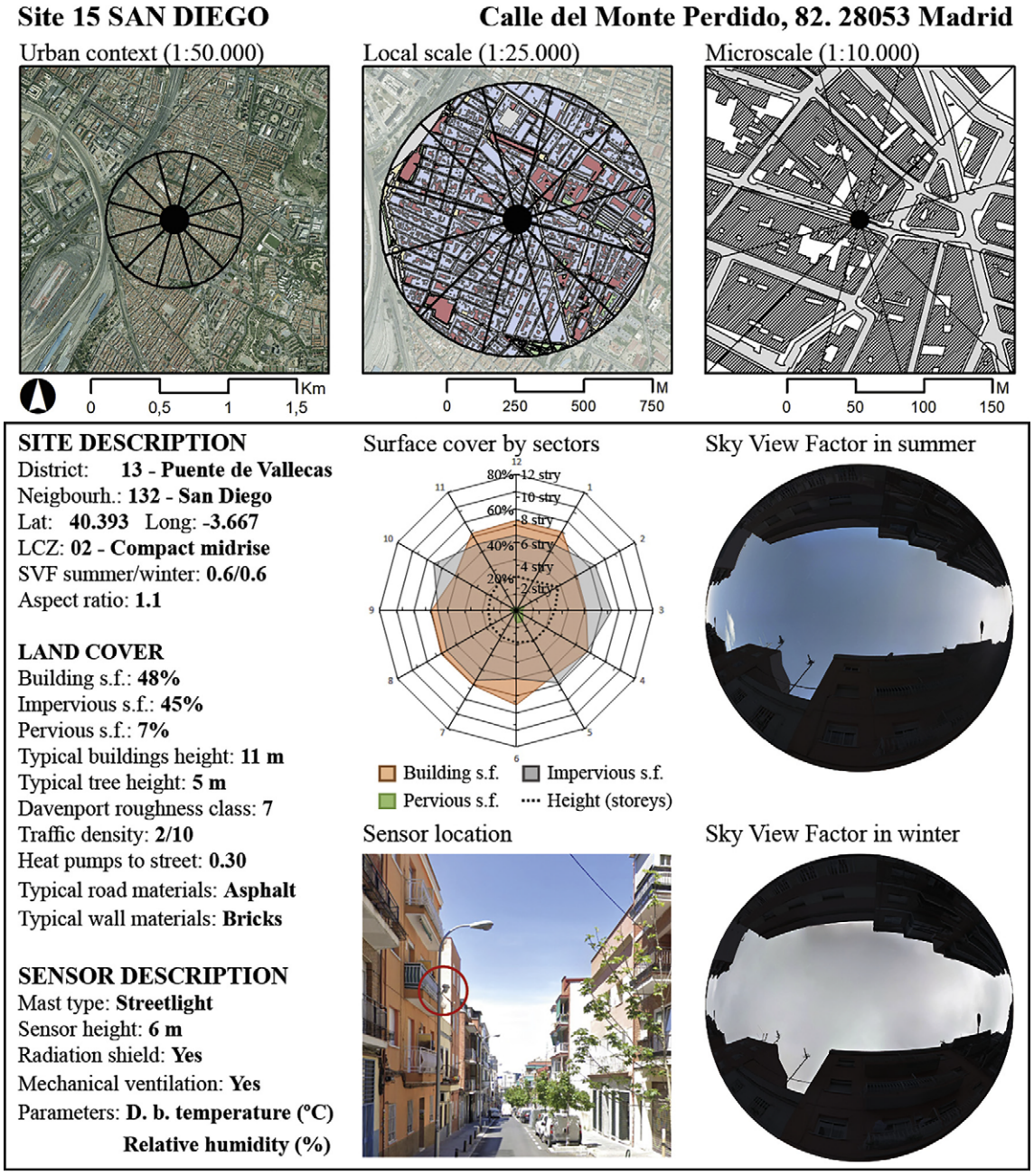

Fig. 2. Example of the metadata associated to each MODIFICA sensor, describing both the local scale and the micro-scale of the sensor located at the site #15 (San Diego), and including information of the measurement site and its surroundings. The metadata associated to the other sensors can be found in the Appendix.

Table 2
Classification of the measurement sites using the LCZ scheme. A manual classification based on the data summarised in the Appendix is compared with the WUDAPT classification.

Classif. method	Site ID																				
	01	03	04	05	06	07	08	09	10	11	12	14	15	16	17	18	19	20	901	902	903	904	905
Manual	2	2	4	2	2	2	2	2	2	4	6	5	2	9	2	6	5	5	D	A	D	9	C
WUDAPT	2	2	2	2	2	2	2	2	2	5	6	2	2	5	2	5	4	2	D	A	C	5	C

plateau of the Iberian Peninsula into two parts and influences the wind direction (mostly NE-SW), creating a north-south temperature gradient from colder to warmer conditions. The *Manzanares* river, which crosses the city from north to south, further contributes to this effect, channelling cold air from the mountains into the city (Fernández García et al., 1996).

With a population of 3.3 M inhabitants, 6.9 M if we consider the functional urban area (Eurostat, 2020), Madrid is the largest city of the country. It experienced an intense urban development during the 1960s and 1970s, when nearly 40% of the existing housing stock was built. Nowadays, Madrid presents a concentric radial distribution with a predominant north-south axis. The eastern border of the city is delimited by the metropolitan park *Casa de Campo* and the Mediterranean forest *Monte de El Pardo*, while the western side of the city gathers the bulk of the new urban developments. Overall, there is a prevalence of compact midrise (LCZ 2) and open midrise (LCZ 5) climatic zones. The large low-rise urban class (LCZ 8) is also substantially present in the south-western periphery (see Fig. 1).

2.2. Equipment and location

In cooperation with the municipality, 20 sensor units were deployed across the city of Madrid during the MODIFICA Project (Universidad Politécnica de Madrid, 2014, see Fig. 1). The distribution of the equipment followed a gradient approach (Muller et al., 2013), with a denser concentration of sensors in the city centre, taking into account the temperature gradient found in a previous study based on urban transects (Núñez Peiró et al., 2017). The campaign complied with the World Meteorological Organization (WMO) guidelines for carrying out measurements within urban environments, in terms of sensor siting and metadata documentation (WMO, 2017). This information is included in the Appendix, and an example can be seen in Fig. 2. Regarding the sensors siting, these were placed on lampposts 5–6 m above the ground. East-west streets were preferred for the sensors' location, to avoid daytime temperature peaks during the summer. In the absence of a standardised method to calculate source areas within the Urban Canopy Layer (UCL), an estimation based on a circumference of 500 m radius was used to analyse the urban structure homogeneity and guarantee the measurement representativeness (Núñez Peiró et al., 2019). Two locations, *Imperial* (site 2) and *Los Cármenes* (site 13) failed to meet the representativeness requirement since the surface cover varied significantly among sectors, and were therefore excluded from this paper. This data was complemented with the official temperature data from 5 meteorological observatories belonging to the State Meteorological Agency (AEMET). The metadata associated to these observatories can be found at the WIGOS metadata repository (WMO, 2020).

The measurements were made with HOBO U23–001 temperature and relative humidity dataloggers. These have an accuracy of ±0.2 °C and ±2.5% for the temperature and the relative humidity, respectively. Many researchers have previously employed this equipment in UHI studies, using predominantly naturally ventilated radiation shields (e.g. Beck et al., 2018; Borbora and Das, 2014; Coseo and Larsen, 2014; Kotharkar and Bagade, 2018; Kourtidis et al., 2015; Richard et al., 2018; Schatz and Kucharik, 2014; Suomi, 2018; Yang et al., 2020b). In the present study, a bespoke mechanically ventilated, low-cost radiation shield was developed to improve

Table 3
Summary of the records obtained from the MODIFICA campaign and the AEMET observatories. Records were flagged as missing, suspect, erroneous or correct according to QC procedures.

Sensor		Total data	Missing values	Flagged as suspect			Flagged as erroneous	Flagged as correct
ID	Site name			Plausible value	Time consist.	Space consist.		
MODIFICA campaign								
01	Embajadores	17,452	68	0	40	24	3	17,449
02	Imperial	17,452	68	0	851	69	10	17,442
03	La Chopera	17,452	68	0	252	30	5	17,447
04	Estrella	17,452	68	0	56	22	5	17,447
05	Pacífico	17,453	67	0	29	13	2	17,450
06	Guindalera	17,452	68	0	40	24	3	17,449
07	Recoletos	17,452	68	0	36	18	2	17,450
08	Hispanoamérica	17,452	68	0	45	22	3	17,449
09	Cuatro Caminos	17,452	68	0	36	22	2	17,450
10	Arapiles	17,452	68	0	31	15	2	17,450
11	Peñagrande	17,451	69	0	53	14	2	17,450
12	Aravaca	17,452	68	0	771	71	18	17,434
13	Los Cármenes	17,452	68	0	380	56	8	17,444
14	Opañel	17,452	68	0	101	40	7	17,445
15	San Diego	17,452	68	0	42	26	4	17,448
16	Horcajo	17,452	68	0	59	12	3	17,449
17	Pueblo Nuevo	17,452	68	0	34	27	5	17,447
18	Canillas	17,452	68	0	124	35	7	17,445
19	Los Ángeles	17,452	68	0	71	25	9	17,443
20	Canillejas	17,452	68	0	39	11	2	17,450
AEMET Network								
901	Barajas (reference)	17,516	4	–	–	–	–	–
902	Retiro	17,428	92	–	–	–	–	–
903	Cuatro Vientos	17,507	13	–	–	–	–	–
904	*C. universitaria*	17,132	388	–	–	–	–	–
905	El Goloso	16,983	537	–	–	–	–	–

the accuracy of the temperature measurements within the UCL during the daytime (Núñez Peiró et al., 2018; see the Appendix).

The classification of each sensor within the LCZs was estimated manually to contrast the WUDAPT information (Bechtel et al., 2019; Bechtel et al., 2015). The surface cover and geometric parameters for the source area of the sensors were determined using the municipal cartography Ayuntamiento de Madrid, 2015) and the national land registry (Ministerio de Hacienda, 2019). The aspect ratio (AR) was established for the street in which the sensor was located. The sky view factor (SVF) was calculated at the location of each sensor using Google Street View panorama images (Li et al., 2017; Miao et al., 2020). Since the changes in foliage were meaningful in most streets, SVFs were computed for both summer (SVFS) and winter (SVFW). The values for thermal, radiative, and metabolic properties could not be drawn due to the lack of available and reliable data sources. Instead, values for traffic density (Ayuntamiento de Madrid, 2013), the ratio of heat pumps per dwelling overlooking the street, which was established as the number of heat pumps overlooking the street over the total number of dwellings, and the typical road and wall materials data were included in the metadata. The MODIFICA network sites were classified as LCZ 2 (10), LCZ 4 (2), LCZ 5 (3), LCZ 6 (2), and LCZ 9 (1). The AEMET sites were classified as LCZ 9 (1), LCZ A (1), LCZ C (1), and LCZ D (2). Table 2 shows a comparison between the estimated LCZs classification according to the manual classification procedure and the WUDAPT database. Overall, the manual classification revealed a higher LCZ variability than the WUDAPT, particularly on the city's periphery. Even though the discrepancies were not negligible, they mostly occurred with adjacent classes (e.g. LCZ 4 and 5). The LCZs estimated from urban data were used in the further analysis.

2.3. Data and quality control procedures

Two years of screen-height air temperature were collected between August 2016 and July 2018 on an hourly basis. The temperature series of the MODIFICA campaign were, for all sites, mostly complete. Only one significant discontinuity of 68 h, due to technical issues, was registered in October 2017. Quality Control (QC) procedures were also applied to this dataset. These were derived from the WMO Guidelines for Level II data (WMO, 2017b; WMO, 2017a; Zahumensky, 2004), and included plausible value and time consistency checks. Additionally, a test for evaluating spatial consistency was conducted, analysing whether the gap between a specific record and its surrounding data was too large when compared to the average. If it remained within 4 standard deviations, it was not considered suspect data. Records were marked as erroneous when flagged as suspect data twice. Regarding the temperature records provided by the AEMET, these only presented small discontinuities (<2 consecutive hours) and, since these records are subject to regular QC analysis before publishing, they were not included in the QC analysis. Neither erroneous nor missing records were replaced but were removed from the series. Table 3 summarises the aforementioned process.

3. Methods

The relationship between LCZs and intra-urban temperature variability was appraised from two perspectives: statistical and graphical. The latter was used to explore the evolution of the intra-urban and intra-daily temperature differences, mostly in terms of the UHI intensity. In that sense, the UHI intensity was defined as the temperature difference between two LCZs (Stewart and Oke,

Table 4
Mean daily temperature and UHI intensity registered for each location during 2017. The highest values are highlighted in bold type.

Sensor		LCZ	Dist. to centroid[1] (km)	Temperature (°C)			UHI intensity (°C)[2]			Ranking UHI intensity
ID	Site name			Mean	Min	Max	Mean	Min	Max	
MODIFICA Network										
01	Embajadores	2	2.0	**17.9**	**13.3**	22.5	**2.2**	−0.7	**5.2**	**1**
03	La Chopera	2	3.5	17.5	12.3	22.7	1.8	**−0.6**	4.3	4
04	Estrella	4	2.1	17.3	12.5	22.1	1.6	−1.0	4.3	7
05	Pacífico	2	2.3	17.6	13.1	22.3	1.9	−1.0	4.9	2
06	Guindalera	2	1.6	17.0	12.4	22.6	1.3	−1.4	4.3	9
07	Recoletos	2	0.3	17.4	12.9	21.9	1.7	−1.3	4.9	5
08	Hispanoamérica	2	3.2	17.0	12.4	21.8	1.3	−1.6	4.4	9
09	Cuatro Caminos	2	3.6	17.4	12.9	21.9	1.7	−1.3	5.0	5
10	Arapiles	2	2.5	17.2	13.0	21.4	1.4	−1.7	4.9	8
11	Peñagrande	4	6.9	16.5	11.7	22.6	0.8	−1.8	3.6	15
12	Aravaca	6	9.0	16.1	9.9	23.1	0.4	−1.7	2.5	18
14	Opañel	5	5.2	17.0	11.7	**23.1**	1.3	−1.0	3.6	9
15	San Diego	2	3.8	17.6	12.7	22.6	1.9	−0.6	4.7	2
16	Horcajo	9	4.9	16.2	11.1	21.9	0.5	−1.9	3.2	17
17	Pueblo Nuevo	2	3.4	17.0	12.1	22.4	1.3	−1.1	4.0	9
18	Canillas	6	4.5	16.9	11.6	23.0	1.2	−1.0	3.4	13
19	Los Ángeles	5	7.6	16.3	11.1	22.3	0.6	−1.7	3.2	16
20	Canillejas	5	6.5	16.9	11.7	23.0	1.2	−0.9	3.5	13
AEMET Network										
901	Barajas (reference)	D	11.6	15.7	8.8	22.6	0.0	0.0	0.0	–

[1] Centroid of the city of Madrid, considering only the built area.
[2] UHI intensity estimated as the difference of temperature between each site and Barajas, for the average daily mean, minimum and maximum temperatures.

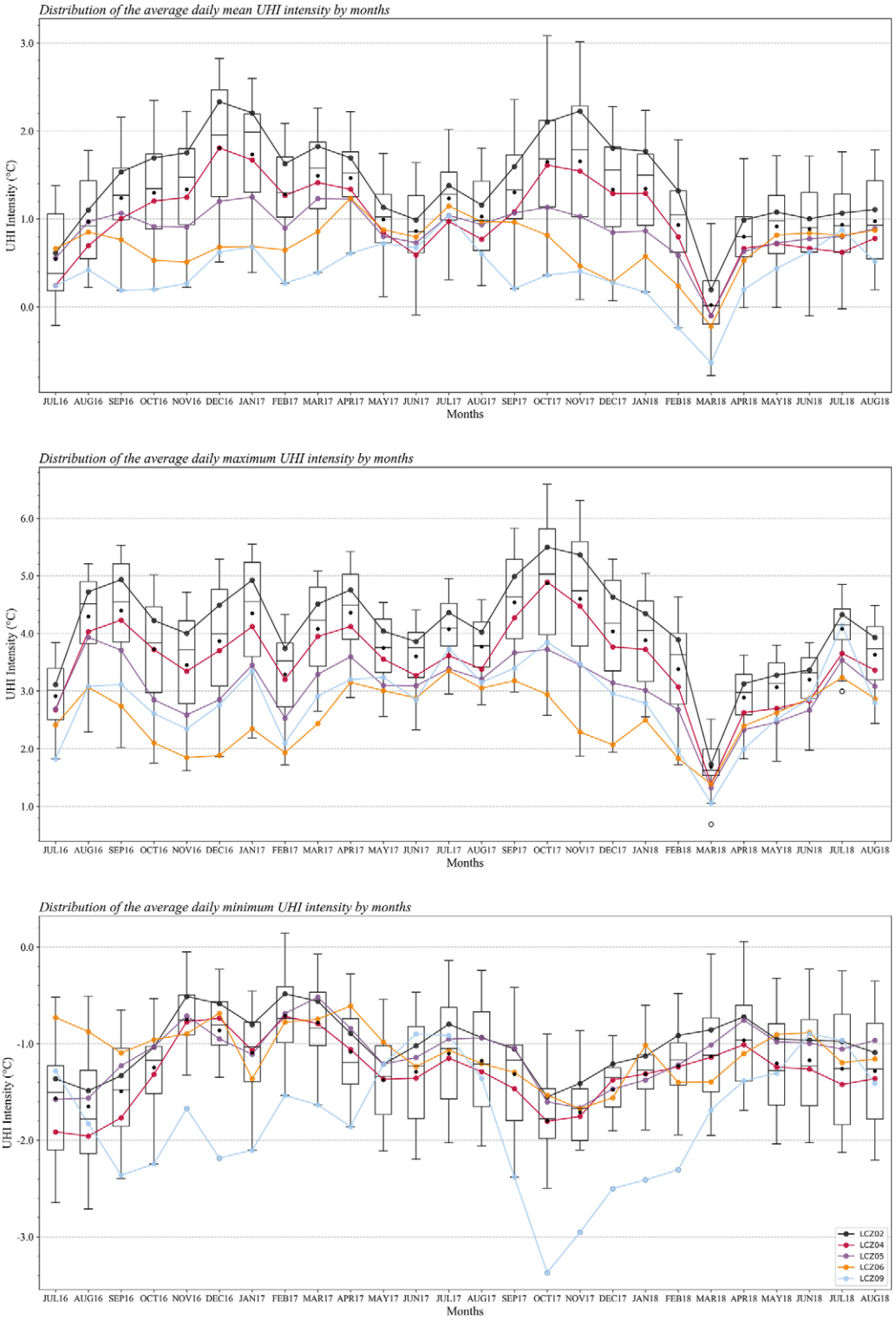

Fig. 3. Monthly mean (top), maximum (middle) and minimum (bottom) UHI intensity for all urban sites, between 2016 and 2018. The UHI intensity is expressed as $\Delta T_{LCZ\ X,\ LCZ\ D}$, where LCZ X represents each of the built-up LCZs and LCZ D refers to the AEMET Barajas observatory.

2012). As in previous studies (e.g. Budhiraja et al., 2020; Kwok et al., 2019; Skarbit et al., 2017; Yang et al., 2020b), we used a LCZ D site placed on the outskirts of the city as the reference for estimating the UHI intensity in all urban sites (Barajas AEMET Observatory). Therefore, the UHI intensity was estimated as $\Delta T_{LCZ\ X,\ LCZ\ D}$, where the LCZ X represents each of the built-up LCZs. Temperatures at each LCZ were spatially averaged to obtain a representative value for each one (Stewart et al., 2014). Only in the case of the LCZ 9 was the temperature derived from a single measurement site. Regarding the cooling rates, these were estimated as the temperature difference between two consecutive hours, $T_t - T_{t-1}$.

Within the statistical approach, correlation coefficients (Spearman and Pearson, depending on the type of parameter) were used to quantify and numerically compare the LCZ scheme's ability to capture daily, diurnal and nocturnal, temperature disparities. They were also applied to analyse the relevance of each LCZ indicator on an hourly basis. Then, the authors employed Analysis of Variance (ANOVA) models to assess whether the average UHI intensities at each LCZ were statistically different ($p < 0.05$). It should be mentioned that each LCZ had equal-sized samples with a quasi-normal distribution, leading the authors to consider parametric approaches. However, since the Levene's variance check revealed that our LCZs presented different variances for the mean and minimum UHI intensities, a Welch ANOVA was used instead of the classical one-way ANOVA. Together with the Welch ANOVA, the Games-Howell post-hoc test was applied to evaluate if the divergences between each LCZ pair were statistically significant. In this respect, previous studies have also reported the use of non-parametric methods (i.e. Kruskal Wallis) together with other post-hoc tests, such as the Conover-Iman (Leconte et al., 2017) or the Wilcoxon Rank-sum (Chapman et al., 2017; Fenner et al., 2017) tests. While these present the advantage of not having to comply with any specific distribution, their statistical power might be diminished compared to parametric approaches.

The statistical differences between the LCZs were determined based on days under ideal conditions on an hourly basis. These were defined using the weather factor, Φ_w, introduced by Oke (Oke, 1998, as found in Runnalls and Oke, 2006):

$$\Phi_w = \frac{1 - kn^2}{\sqrt{u}} \quad where\, u \geq 1m \Big/ s$$

Φ_w depends on the wind speed in m/s (u) and the cloud cover, which in turn is computed based on the amount of clouds in tenths (n) and a correction coefficient depending on the clouds' height (k). This way, the lower the cloud cover and the wind speed (i.e. the closer Φ_w is to 1), the more favourable might weather conditions be. Following the example of previous studies (Skarbit et al., 2017; Stewart et al., 2014; Yang et al., 2018), days were tagged as ideal when $\Phi_w > 0.7$, which was estimated as a daily average. Since temperature differences are sharper during the nighttime and might depend on the preceding hours' conditions, the daily average was estimated

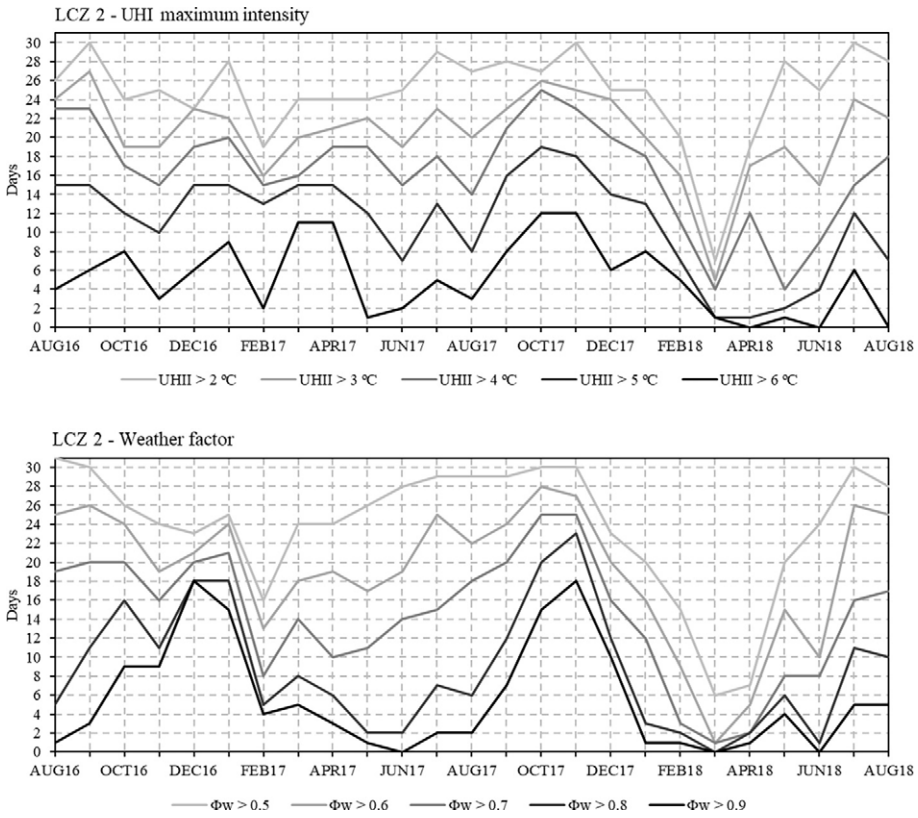

Fig. 4. Frequency of days for LCZ 2 in which the UHI maximum intensity (top) and the weather factor (bottom) were above certain values.

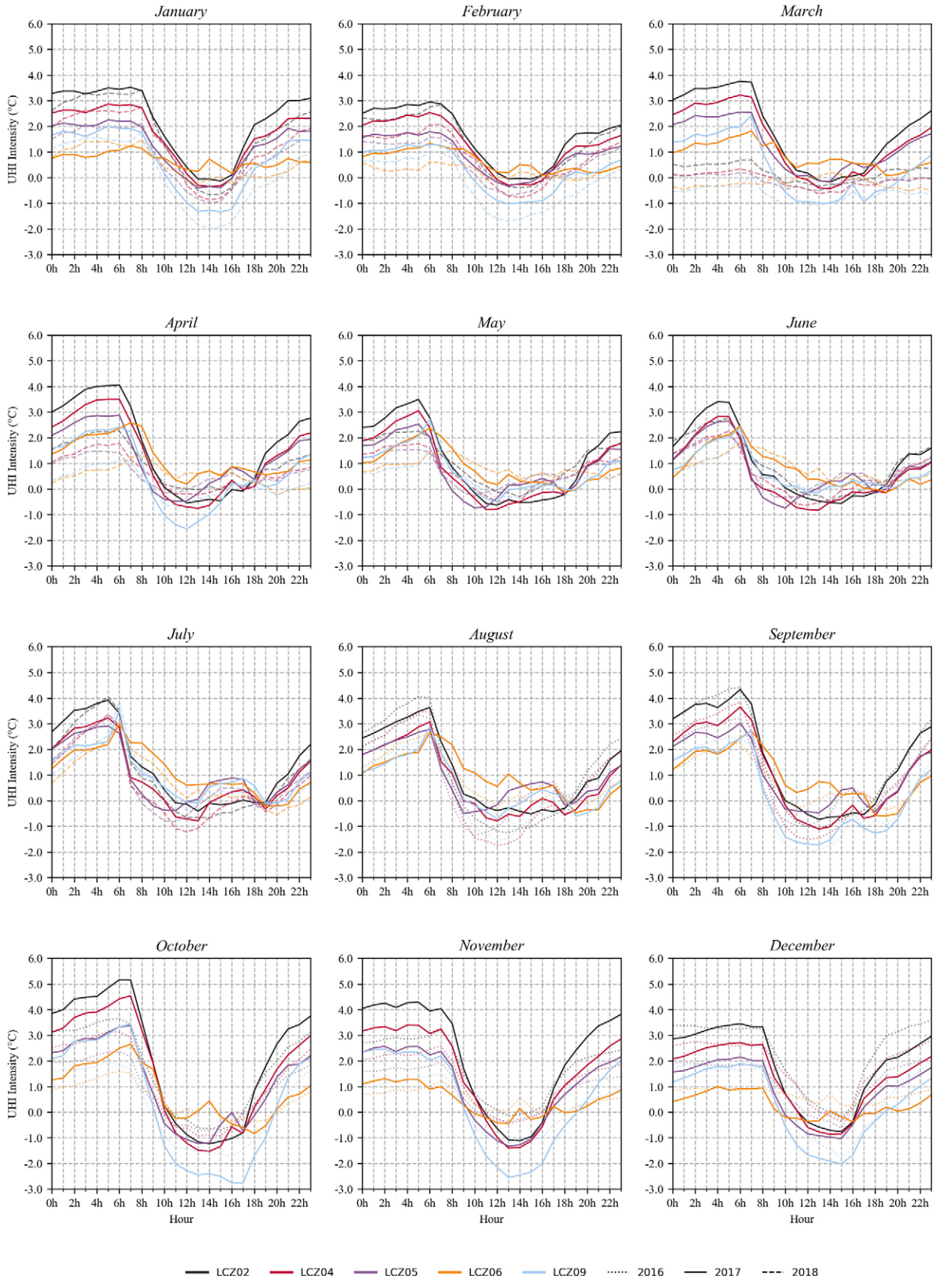

(caption on next page)

Fig. 5. Average hourly UHI intensity from January to December for each LCZ. The data corresponding to the year 2017 are shown in the foreground (solid lines). Measurements corresponding to 2016 and 2018 complete the 2-year series and are displayed in the background (dashed lines). All the data correspond to the average hourly UHI intensity for each of the LCZ included in this study.

between middays (12:00 UTC).

4. Results

4.1. Global overview of the UHI of Madrid

Table 4 displays the annual averages regarding temperature and UHI intensity at each location during 2017, which was the only full calendar year of the series. In Spain, 2017 was the hottest year since 1965. During this year, all urban sites were mostly warmer than the AEMET Barajas observatory. On average, temperature differences of up to 2.2 °C can be expected between sites. This variation rises

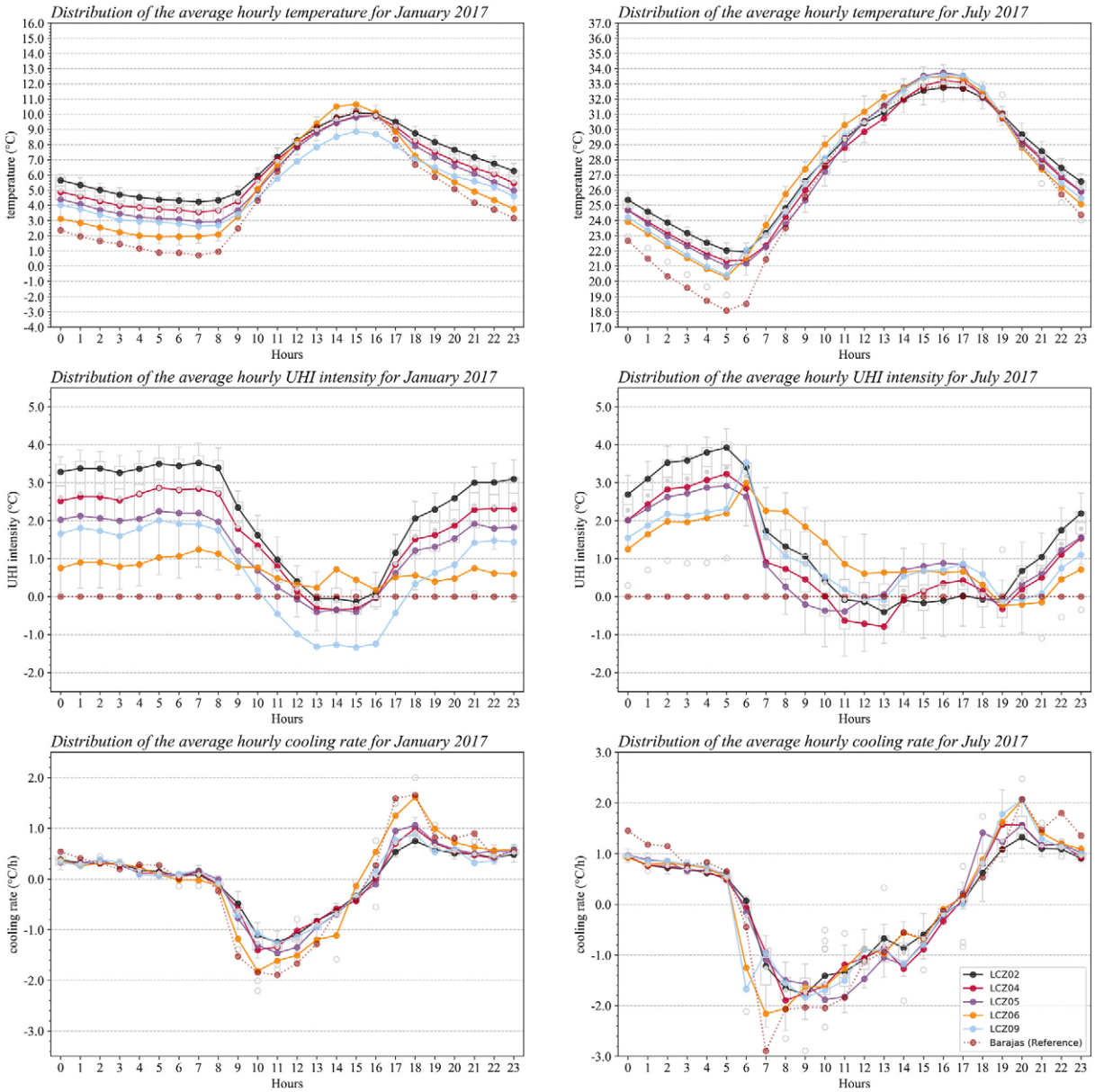

Fig. 6. Average hourly temperature (top), UHI intensity (centre) and cooling rates (bottom) for January (left) and July 2017 (right). The different LCZs and the reference site are outlined. The hourly ranges from all measuring sites are displayed as a boxplot in the background.

to 4.5 °C when looking at minimum temperatures and drops to 1.7 °C for maximum temperatures. Despite not being completed, the 2016 and 2018 series follow the same trend.

A high correlation between the sites registering the highest minimum temperatures and those with the highest maximum UHI intensity was observed. As expected, the UHI presented a clear nighttime pattern, typically registering maximum UHI intensities above 4 °C. Overall, an Urban Cool Island could be observed as well, although its intensity usually remained below 2 °C.

As illustrated in Fig. 3, the mean, maximum and minimum UHI intensities (herein after referred to as "$UHII_{mean}$", "$UHII_{max}$", "$UHII_{min}$") also exhibit different behaviour when analysed monthly. Since the UHI is a nighttime phenomenon and nights grow longer close to the winter solstice, it is not surprising to find higher means and medians near the winter solstice, while yielding lower means and medians near the summer solstice. Anthropogenic heat, which has shown to be higher during the winter months in other cities (Molnár et al., 2020; Varentsov et al., 2018), should also be considered as a key factor. Nevertheless, this trend seems to be clearly influenced by meteorological conditions. For instance, the daily $UHII_{mean}$ in March 2018 was 0 °C, a far cry from what could be expected for this month, but in line with the aggregation of weather instability shown in Fig. 4 (bottom). The accumulated precipitation in March 2018 was, in fact, the highest ever recorded since 1965 (AEMET, 2019).

As expected, the daily $UHII_{max}$ also manifested a high sensitivity level to meteorological stability. Yet, it did not seem to follow a seasonal pattern, which contrasts with previous evidence (e.g. Arnds et al., 2017; Fenner et al., 2014; Schatz and Kucharik, 2014). Fig. 4 reveals that the cluster of days above certain UHI intensities thresholds reflects a homogeneous distribution throughout the year, reaching its highest values mostly with higher atmospheric stability. Nevertheless, it should be underlined that the weather factor (Φ_w) did not seem fully reliable for identifying ideal days. Of all days reaching a $\Phi_w \geq 0.7$ (see section 2.4), only 77.7% had temperature differences exceeding 4 °C and from those, 32.2% remained undetected. It is therefore not surprising that, even though the Φ_w exhibited a noticeable tendency towards higher values in winter (also found in Yang et al., 2018), the daily $UHII_{max}$ did not replicate this seasonal pattern.

The daily $UHII_{min}$ displayed a different behaviour, with no clear seasonal pattern or discernible effects derived from atmospheric instability. All months showed similar dispersion characteristics, with the exception of the interquartile ranges standing out for appearing larger during the summer months. The latter could be linked to the increase in solar radiation, but this relationship should be further explored.

4.2. Temperature variability across LCZs on an hourly basis

The temperature variability was subsequently explored in relation to each LCZ on an hourly basis. The findings from this hourly analysis supported the yearly patterns discussed in the previous section. According to the results presented in Fig. 5, temperature differences are sharper during the nighttime regardless of the time of year, thus making the months with longer nights more prone to a higher daily $UHII_{mean}$. The effect of meteorological instability is also evident, as observed in March 2018 (dashed lines). Otherwise, temperature differences appear to be quite similar throughout the year for all LCZs. Once more, no seasonal pattern was observed, in line with the overall trend observed in the previous section.

It is noteworthy that all LCZs share a similar trend, which is undoubtedly related to the traditional UHI profile: temperatures start to greatly differ just after sunset (between 17:00 and 20:00 UTC, depending on the time of year) and reach their maximum disparity just before sunrise (between 5:00 and 8:00 UTC). During the daytime, the UHI seems to fade away and, under certain circumstances, even transform into an Urban Cool Island. It may be noted that, during the nighttime, variations between LCZs become more evident. LCZ 2 and LCZ 6 distinctly and consistently differ from the other LCZs, registering the highest and lowest UHI intensities throughout the year, respectively. LCZs 4 and 5, on the contrary, do not appear to significantly vary from each other: in fact, their UHI show a rather analogous hourly evolution, with differences rarely exceeding 0.2 °C (which concurs with the sensors' accuracy). In theory, LCZ 9 should have been registering the lowest nighttime UHI intensities, yet it matched the values registered for LCZ 4 and 5, above those for LCZ 6. Per contra, LCZ 9 tends to register lower temperatures during the daytime.

To better analyse LCZs particularities, Fig. 6 provides an in-depth look into two months of the year, presenting the hourly evolution of the temperature, the UHI intensity and the cooling rates across different LCZs. As would have been expected, temperature oscillations are greater during the summer than during the winter months. Stronger oscillations can be found in more open areas, i.e. LCZ 6 and the reference site (LCZ D). LCZ 9 shows a different tendency, with relatively marked oscillations in summer but somewhat weak in winter. No clear explanation is available for this behaviour, apart from representativeness issues associated with the location and source area of the measuring site, since this data came from a single site (#16, Horcajo).

Table 5
Spearman's rank correlation coefficient (r_s) between the annual average of the daily $UHII_{mean}$, $UHII_{max}$ and $UHII_{min}$, and the different classification methods. The LCZs were ranked from 1 to 10, and then from A to E. The sites classified within the same LCZ were attributed a random position (LCZ_{RAND}) or according to their distance to the urban centre (LCZ_{DIST}).

Class. method	$UHII_{mean}$	$UHII_{max}$	$UHII_{min}$
RAND classification	−0.03	0.00	0.02
DIST classification	0.72	0.79	0.25
LCZ_{RAND} classification	0.75	0.79	0.24
LCZ_{DIST} classification	0.75	0.85	0.19

During the daytime, temperature differences between most LCZs are blurred. Although inter-urban thermal differences average nearly 2 °C in winter (see Fig. 6 boxplots in the background), the temperature variation range between LCZs 2, 4, 5 and 6 seems to be within 0.2 °C. A similar pattern is observed in summer, with no clear differentiation between LCZs, despite average temperature variations of up to 2.5 °C. In summer, however, the average trend of the urban measurement sites unveils a slight overheating of some sensors between 14:00 and 18:00 UTC. This late afternoon overheating gains more prominence in the LCZs that are sparsely built and is especially noticeable close to the summer solstice only to disappear close the winter solstice (see Fig. 5). The remaining urban AEMET observatories did not replicate this trend, but the latter is consistent with the findings of previous studies (Fenner et al., 2014; Skarbit et al., 2017; Yang et al., 2020b). A discussion on this topic is included in the next section.

Sharper temperature oscillations also lead to steeper cooling rates (Fig. 6, bottom) during the hottest months. In July, the cooling and heating rates are nearly symmetric throughout the day, since each cycle takes about a half-day. In this sense, the cooling cycle starts 2–3 h before sunset (17:00 UTC) and ends at sunrise (5:00 UTC). In January, however, the cooling cycle takes place during two-thirds of the day, being, therefore, less intense than the heating cycle. It can be observed that during several hours of the night (2:00–7:00 UTC) the cooling rate remains very low (<0.2 °C/h), contributing to a higher UHI nighttime stability during the winter season.

The cooling rate analysis also confirms that a great part of the UHI intensity develops a few hours after sunset (Holmer et al., 2007; Leconte et al., 2017). During the first 3 h of nighttime, the densest LCZs (02, 04 and 05) reach up to 40–55% of the daily $UHII_{max,}$ with significant diversity between LCZs. As shown in Fig. 6, these differences then tend to fade away throughout the night. This effect was also observed in previous studies (e.g. Thomas et al., 2014; Yang et al., 2018).

4.3. Temperature differences across LCZs from a statistical perspective

In this section, the authors further investigate the previously identified trends from a statistical perspective. As a starting point, a Spearman's rank correlation coefficient (r_s) analysis between the LCZs and the UHI intensity is presented. Table 5 shows the results for the annual average of the daily $UHII_{mean}$, $UHII_{max}$ and $UHII_{min}$. Sites are ranked according to their LCZ class, from most compact areas (LCZ 2) to most sparsely built areas (LCZ 9). Within the LCZs, the sites were organised according to a random position scheme (LCZ_{RAND}), and alternatively via the criteria of distance from the city centre (LCZ_{DIST}). The findings reveal that, while there is a strong correlation between the LCZ_{RAND} and the $UHII_{max}$ (nighttime, $r_s = 0.79$), said correlation becomes very weak regarding the $UHII_{min}$ (daytime, $r_s = 0.24$). Including the criteria of distance from the city centre when ranking urban sites (LCZ_{DIST}) increases the contrast between night and day ($r_s = 0.85$ and $r_s = 0.19$, respectively). In regard to annual mean data, the LCZs seem to perform poorly at capturing the minimum urban temperature differences that take place during the daytime.

The Welch ANOVA models and post-hoc Games-Howell tests confirmed these results, revealing varying significant differences between the LCZs in reference to the $UHII_{mean}$, $UHII_{max}$, and the $UHII_{min}$ (Table 6). In that sense, LCZ 2 differs from all other LCZs in relation to both the $UHII_{max}$ and $UHII_{mean}$, but it does not for the $UHII_{min}$. LCZ 4 and 5 always group together, which is consistent with the trends observed in Fig. 5. LCZ 4 and 5 might also associate with other LCZ individually, depending on the moment of the day. LCZ 6 and 9 also group together in terms of the $UHII_{mean}$ and $UHII_{min}$, but they diverge as far as the $UHII_{max}$ is concerned.

Daytime differences found in LCZs should be, however, interpreted with caution. First, because most concentrate in the LCZ 9 class, which is characterised by a single measuring site and which did not conform to the expected behaviour associated with this type of LCZ class during the graphic analysis. And second, due to the high temperature variability during the daytime hours. Situations such as the late afternoon overheating identified in the previous section, where it is unclear if it is intrinsic to the LCZs characteristics, could be influencing these results.

This point is confirmed when looking at the ANOVAs and post-hoc tests on an hourly basis. The results are given for the months of January and July 2017 (see Table 7), for every day of the month and the days with ideal conditions. During the daytime, there are more

Table 6
Games-Howell post-hoc test between pairs of LCZs (significance level α = 0.05). Tested for the average monthly $UHII_{mean}$, $UHII_{max}$, and $UHII_{min}$.

	Significant difference between pairs		
LCZ pairs	$UHII_{mean}$	$UHII_{max}$	$UHII_{min}$
2–4	■	■	
2–5	■	■	
2–6	■	■	■
2–9	■	■	■
4–5			
4–6	■	■	
4–9	■	■	■
5–6	■	■	■
5–9	■		■
6–9		■	■

Table 7
Hourly Games-Howell post-hoc test between pairs of LCZs for January and July 2017. This analysis is presented for every day of each month and for the days with ideal conditions ($\Phi_w > 0.7$, no precipitations in the last 24 h and an UHI intensity >5 °C). Notice how, within ideal days, significant differences concentrated at different times of the night, depending on the time of the year (dashed square).

LCZ pairs	Significant difference between pairs																							
	0h	1h	2h	3h	4h	5h	6h	7h	8h	9h	10h	11h	12h	13h	14h	15h	16h	17h	18h	19h	20h	21h	22h	23h
EVERY DAY																								
January 2017 (n = 31 days)																								
2 - 4																								
2 - 5	■				■	■	■	■	■	■									■	■	■	■	■	■
2 - 6	■	■	■	■	■	■	■	■	■	■								■	■	■	■	■	■	■
2 - 9	■	■		■	■	■	■	■	■	■	■	■	■	■	■	■	■	■	■	■	■	■	■	■
4 - 5																								
4 - 6	■				■	■	■	■	■									■	■	■	■	■	■	■
4 - 9											■	■	■	■	■	■	■	■	■					
5 - 6																				■	■			
5 - 9													■	■	■	■	■	■	■					
6 - 9													■	■	■	■	■	■						
July 2017 (n = 31 days)																								
2 - 4								■	■	■		■	■				■							
2 - 5			■			■		■	■	■	■				■	■	■	■						
2 - 6	■	■	■	■	■	■			■	■	■	■				■	■			■	■	■	■	■
2 - 9	■	■	■	■	■	■									■	■	■	■	■		■	■	■	■
4 - 5										■			■		■	■	■							
4 - 6	■	■	■	■	■	■															■	■	■	■
4 - 9											■	■	■		■	■		■	■					
5 - 6	■	■	■	■	■	■									■	■	■	■		■	■	■	■	■
5 - 9								■	■	■	■	■							■					
6 - 9										■	■	■			■	■	■	■	■	■		■		
IDEAL DAYS																								
January 2017 (n = 12-13 days)																								
2 - 4	■	■	■	■	■	■																		
2 - 5	■	■	■	■	■	■	■	■	■	■	■									■	■	■	■	■
2 - 6	■	■	■	■	■	■	■	■	■	■										■	■	■	■	■
2 - 9	■	■	■	■	■	■	■	■	■	■	■	■	■	■	■	■	■	■	■	■	■	■	■	■
4 - 5		■	■	■	■																			
4 - 6	■	■	■	■	■	■	■	■	■						■		■			■	■	■	■	■
4 - 9		■	■	■							■	■	■	■	■	■	■	■						
5 - 6	■	■	■	■	■										■					■				
5 - 9														■	■	■	■	■						
6 - 9	■	■	■	■	■								■	■	■	■	■	■						
July 2017 (n = 10 days)																								
2 - 4	■			■		■						■	■											
2 - 5	■		■	■	■	■	■	■	■	■	■			■	■	■	■	■						
2 - 6	■	■	■	■	■	■	■										■			■	■	■	■	■
2 - 9	■		■	■	■	■									■	■	■	■	■					■
4 - 5													■	■	■	■								
4 - 6	■	■	■	■	■	■							■											■
4 - 9						■						■	■	■	■	■			■					
5 - 6	■	■	■	■	■	■								■	■		■	■				■		■
5 - 9							■	■	■	■	■	■							■					
6 - 9		■		■		■	■					■		■	■	■	■	■	■	■				■

Table 8
Pearson's correlation coefficient between the hourly $UHII_{mean}$ and six LCZ indicators for January and July of 2017.

LCZ indicator	Correlation coefficient (r_p)																							
	0 h	1 h	2 h	3 h	4 h	5 h	6 h	7 h	8 h	9 h	10 h	11 h	12 h	13 h	14 h	15 h	16 h	17 h	18 h	19 h	20 h	21 h	22 h	23 h
January 2017								Nighttime		Daytime						Daytime		Nighttime						
SVFS	−0.43	−0.42	−0.42	−0.40	−0.39	−0.37	−0.41	−0.45	−0.46	−0.48	−0.58	−0.52	−0.42	−0.35	−0.49	−0.49	−0.39	−0.61	−0.63	−0.58	−0.56	−0.52	−0.49	−0.49
SVFW	−0.77	−0.75	−0.76	−0.75	−0.75	−0.74	−0.76	−0.77	−0.78	−0.76	−0.70	−0.58	−0.46	−0.24	−0.11	−0.18	−0.29	−0.67	−0.79	−0.80	−0.80	−0.79	−0.79	−0.79
AR	0.77	0.75	0.75	0.74	0.73	0.73	0.74	0.77	0.78	0.79	0.73	0.64	0.60	0.43	0.32	0.38	0.54	0.81	0.86	0.85	0.84	0.82	0.81	0.81
BSF	0.74	0.72	0.72	0.73	0.73	0.72	0.72	0.75	0.76	0.76	0.69	0.60	0.56	0.42	0.25	0.27	0.35	0.67	0.75	0.77	0.76	0.74	0.74	0.76
ISF	−0.02	−0.02	−0.03	−0.04	−0.05	−0.03	−0.02	−0.08	−0.11	−0.17	−0.25	−0.31	−0.45	−0.50	−0.44	−0.38	−0.29	−0.18	−0.05	−0.02	−0.01	0.03	0.00	−0.02
PSF	−0.85	−0.83	−0.82	−0.82	−0.83	−0.82	−0.82	−0.84	−0.84	−0.82	−0.70	−0.57	−0.47	−0.29	−0.12	−0.17	−0.29	−0.71	−0.85	−0.88	−0.88	−0.87	−0.86	−0.87
HRE	0.27	0.27	0.26	0.26	0.28	0.29	0.29	0.28	0.28	0.25	0.25	0.16	−0.06	−0.18	−0.29	−0.20	−0.01	0.15	0.25	0.27	0.28	0.30	0.31	0.28
DIST	−0.85	−0.84	−0.84	−0.82	−0.82	−0.82	−0.84	−0.85	−0.85	−0.84	−0.66	−0.51	−0.32	−0.12	−0.06	−0.09	−0.13	−0.59	−0.79	−0.83	−0.86	−0.88	−0.88	−0.87
July 2017																								
SVFS	−0.63	−0.65	−0.67	−0.67	−0.69	−0.69	−0.51	−0.28	−0.45	−0.58	−0.54	−0.46	−0.40	−0.10	0.17	0.20	0.24	0.30	−0.02	−0.34	−0.58	−0.61	−0.63	−0.64
SVFW	−0.75	−0.77	−0.80	−0.80	−0.81	−0.81	−0.53	−0.09	−0.16	−0.24	−0.19	−0.05	0.02	0.25	0.36	0.33	0.36	0.38	0.11	−0.26	−0.60	−0.66	−0.68	−0.73
AR	0.76	0.77	0.79	0.80	0.81	0.82	0.52	0.09	0.15	0.29	0.26	0.21	0.15	−0.07	−0.22	−0.25	−0.26	−0.43	−0.31	0.25	0.65	0.70	0.72	0.74
BSF	0.75	0.78	0.77	0.76	0.76	0.77	0.64	0.38	0.26	0.32	0.13	0.12	0.12	−0.05	−0.25	−0.37	−0.41	−0.48	−0.19	0.29	0.60	0.64	0.68	0.71
ISF	−0.05	−0.07	−0.07	−0.04	−0.03	−0.06	−0.40	−0.64	−0.50	−0.46	−0.24	−0.25	−0.22	−0.16	0.09	0.18	0.28	0.24	0.01	−0.06	0.00	0.03	0.00	0.01
PSF	−0.85	−0.87	−0.87	−0.87	−0.86	−0.86	−0.58	−0.19	−0.11	−0.19	−0.06	−0.04	−0.05	0.12	0.25	0.36	0.36	0.47	0.21	−0.31	−0.69	−0.75	−0.79	−0.83
HRE	0.09	0.11	0.14	0.15	0.15	0.17	−0.03	−0.36	−0.19	−0.06	−0.02	−0.15	−0.25	−0.41	−0.33	−0.25	−0.17	−0.28	−0.20	−0.11	0.03	0.08	0.08	0.11
DIST	−0.78	−0.80	−0.82	−0.82	−0.82	−0.82	−0.67	−0.33	−0.34	−0.39	−0.22	−0.11	−0.01	0.19	0.43	0.51	0.50	0.63	0.32	−0.21	−0.59	−0.67	−0.71	−0.75
					Nighttime		Daytime											Daytime			Nighttime			

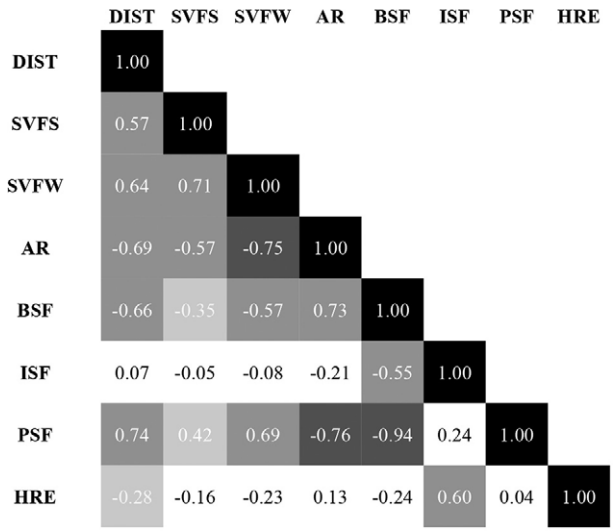

Fig. 7. Correlation matrix between the following LCZ parameters: sky view factor in summer (SVFS) and winter (SVFW), aspect ratio (AR), building surface fraction (BSF), impervious surface fraction (ISF), pervious surface fraction (PSF) and height of roughness elements (HRE). It also includes the distance to the city centre (DIST).

pairs of LCZs associated with LCZ 9. In July, significant differences are also found between other LCZs from 13:00 to 17:00 UTC, which coincides to a large extent with the late afternoon overheating hours. Contrariwise, the results suggest a much higher level of consistency and stability in the differences between LCZs during the nighttime. In January, these differences are more relevant between 1:00 and 3:00 UTC (middle of the night), while in July they intensify between 3:00 and 5:00 UTC (end of the night). These hour bands occur in both cases 7 to 8 h after sunset.

The results show that the LCZs' ability to illustrate differences in urban temperature varies throughout the day. This is examined in further depth via a correlation analysis between LCZ indicators and the UHI intensity. As shown in Table 8, none of the LCZ parameters are able to account for temperature differences during the daytime. While most of these parameters strongly correlate with nighttime temperature differences (i.e. previous surface fraction (PSF), aspect ratio (AR), building surface fraction (BSF) and sky view factor in winter (SVFW) show $r_p > \pm 0.7$), these correlations steadily weaken after sunrise until fading away. The impervious surface fraction indicator (ISF) stands out as an exception, linking with daytime urban temperatures only and exhibiting a relatively weak correlation ($r_p < -0.5$).

Most LCZ parameters showed similar correlations during summer and winter, except for the SVF. The annual cycle of deciduous trees, which are prevailing in the measuring sites, is somewhat detected by the SVFS and SVFW. Surprisingly, the SVFW showed slightly better performance during the summer nights, while this was true for the SVFS during the winter daytime.

While it is remarkable that all LCZs presented relevant correlations with the UHI at a certain point in time ($r_p > \pm 0.3$), it might be argued that additional indicators could be included into the scheme for better capturing the urban temperature variability, particularly during the daytime. One of the most discussed additional parameters is the distance to the city centre (DIST, e.g. Gardes et al., 2020; Kotharkar et al., 2019). As shown in Table 8, DIST follows the pattern of other LCZ indicators, with strong correlations during the nighttime that lessen during the daytime. In spite of failing to solve the issue of predicting of daytime temperature differences, its predictive power might be on the same level than that of the PSF, which discloses the highest correlations among LCZ parameters ($r_p > -0.8$). Moreover, one might consider that DIST shows strong linear relationships with other LCZs. For example, the PSF tends to be more prominent in the outskirts of the city. It is certainly true that DIST displays a relevant collinearity degree with most LCZ parameters ($r_p > \pm 0.5$, see Fig. 7), reaching its maximum with the PSF ($r_p = 0.74$). Nonetheless, its collinearity is akin to that found between LCZ parameters. In fact, the highest values are found between BSF-PSF ($r_p = -0.94$), AR-PSF ($r_p = -0.76$) and AR-SVFW ($r_p = -0.75$).

5. Discussion

The results presented in this paper support previous evidence suggesting that LCZs can correctly capture most of the intra-urban nighttime temperature variability. The hourly behaviour and expected cooling rates associated with each LCZ, which are primarily defined by the nighttime pattern of the UHI, are also in consonance with previous findings. However, LCZs fail to discern the daytime temperature variability to a large extent. LCZ indicators also exhibited much better correlations with temperature differences during the nighttime than during the daytime, with none providing a good estimate during the central hours of the day. There is no doubt that urban temperature differences are considerably wider during the nighttime than during the daytime, but the latter are still significant

(>2 °C). It would also be interesting to consider whether diurnal temperatures could be framed within a classification system like the LCZs, or if they are heavily dependent on the micro-climatic characteristics of urban areas. In either case, and regardless of the higher uncertainties introduced by solar radiation and the varying urban geometry, further research is warranted to better comprehend the determining factors behind the daytime thermal differences.

A limitation of this study lies in the fact that it only focuses on six out of ten LCZ parameters. The other four (the anthropogenic heat output, the terrain roughness, the surface albedo, and the surface admittance) were excluded due to the lack of robust data. Although these could be approximated based on the metadata included in the Appendix, these estimations would be subject to interpretation, which could include too many uncertainties. It could also be argued that these parameters might be similar across all the LCZs within the same city, or that they might strongly vary within each LCZ. In any case, the absence of some LCZ parameters is a common occurrence in most previous investigations and has not constituted an impediment to define and study the LCZs (Kwok et al., 2019; Yang et al., 2018). Furthermore, the high correlation between some of these indicators is also notable (Kotharkar et al., 2019; Leconte et al., 2020), removing the need to use them in their entirety for classifying urban areas into LCZs. The WUDAPT Project is an example of this procedure, in which a random forest classifier algorithm is trained to classify urban areas into LCZs based only in 2-D multi-spectral satellite imagery (Bechtel et al., 2019; Bechtel et al., 2015). When analysing their differences at the intra-urban and hourly level, however, including these other parameters might contribute to gaining a better insight into the climatic properties of each LCZ. In fact, they might be particularly relevant for representing diurnal temperature variations, since albedo and surface admittance are closely linked to heat storage from solar radiation.

This research used the weather factor proposed by Oke (1998) to identify the days with the most favourable conditions for the UHI formation. This indicator has been widely used in previous research (Eastin et al., 2018; Molnár et al., 2020; Skarbit et al., 2017; Stewart et al., 2014; Theeuwes et al., 2017; Yang et al., 2018) and, given its simplicity and readability, it appears to be adequate for promoting the cross-comparability among urban climate studies. However, in this study it has shown a clear seasonal bias, concentrating the identification of ideal days in winter while leaving undetected several of them in the summer months. To this respect, it might be worth investigating the use of other methods, such as the proposed by Hidalgo and Jougla (2018), which might offer an alternative way to cluster local weather conditions. These alternative methods, instead of using an algorithm to define the potentiality of a certain day to reach high UHI intensities, statistical methods are proposed to define the number and type of clusters that would determine the UHI potential characteristics of each day. These might be of interest for future studies due to their greater flexibility and better fit to local conditions.

The inclusion of the distance to the city centre (DIST) as an extra indicator within the LCZ scheme should also be discussed. This research has demonstrated that, when compared with the other LCZs parameters, DIST ranked among those with the highest correlation coefficients. Several previous studies have also emphasised its relevance for examining urban temperature differences (e.g. Gardes et al., 2020; Kotharkar et al., 2019; Kwok et al., 2019; Leconte et al., 2020; Leconte et al., 2017; Leconte et al., 2015). This might be particularly relevant during calm nights with clear skies, when the air temperature differences between the urban areas and their surroundings promote the entrance of cool air into the city (Oke et al., 2017b). This *country breeze* would cool down the outskirts of the urban areas, but its effect might progressively abate as we get close to the city centre. In like manner, this cooling effect can be observed at the intra-urban level with contrasting LCZs (e.g. green areas next to densely built-up areas), albeit in a localised and avoidable fashion by virtue of proper sensor siting. On the other hand, this same breeze might result in a rural-to-urban thermal gradient (i.e. from the outskirts to the city centre), affecting urban areas regardless of their LCZ class.

It should also be mentioned that this airflow behaves to a large extent independently of where the city is established, and should, therefore, be differentiated from other wind flows that only originate when the city is located in a specific place, such as the sea or valley breezes. The fact that the countryside breeze is an urban intrinsic phenomenon might be a determining factor for its inclusion as a parameter to classify and compare the climatic properties of an urban area. What is more, it might call into question the comparability of two built-up sections, classified in the same LCZ but positioned differently within an urban area. In addition, it could also help overcome the partial overlap between LCZs found in previous studies (Fenner et al., 2017). To this respect, it would be worth investigating if the need to divide LCZs into subclasses could be reduced when taking DIST into account, and how this could be extended to non-concentric urban areas.

In the present study, only a subtle seasonal pattern was noticed during winter for the $UHII_{mean}$, which could be linked to the night length during this period. Unlike previous studies, no clear seasonal pattern was identified for the $UHII_{max}$. It is worth mentioning that previous evidence suggests that the most severe temperature differences might appear during the warmer months of the year, as happens in Madison (Schatz and Kucharik, 2014), Szeged (Skarbit et al., 2017), Berlin (Fenner et al., 2017; Fenner et al., 2014), Hamburg (Arnds et al., 2017) or Lodz (Klysik and Fortuniak, 1999). However, other studies also point to pronounced UHI intensities during the winter (e.g. Glasgow, (Emmanuel and Krüger, 2012), Beijing (Yang et al., 2013), Nanjing (Yang et al., 2020a) or Buenos Aires (Figuerola and Mazzeo, 1998)). In the case of Madrid, previous investigations suggest that the widest thermal differences take place both in the winter (Fernández García et al., 2016) and the summer periods (Núñez Peiró et al., 2017; Yagüe et al., 1991).

The reasons for these seasonal discrepancies remain unclear. Multiple factors have been singled out for promoting seasonality. For example, some studies have related this occurrence to parameters presenting a clear annual cycle, such as solar irradiation (Arnds et al., 2017; Núñez Peiró et al., 2017) or the foliation and defoliation tree cycle (Stewart et al., 2014; Yang et al., 2018). Other works point towards the accumulation of favourable meteorological conditions during a specific time of the year, particularly wind,

cloudiness, and precipitation (Yang et al., 2020a). This is evident in subtropical areas affected by the monsoon (Thomas et al., 2014), as well as in mid-latitude cities in which certain meteorological conditions might concentrate on specific months (e.g. Berlin, Fenner et al., 2017). Our measurements outline the relevance of certain meteorological conditions in the formation of the UHI (e.g. March 2018, section 3.1), but these conditions do not seem to accumulate during any particular season. The concentration of ideal days with UHI intensities >5 °C was, in fact, slightly larger during January than during July 2017 (13 vs 10 days, respectively), and a similar pattern was found during the rest of the two-year measurement period. To this respect, although the meteorological instability in Madrid tends to aggravate during the spring and autumn, the cluster of unfavourable conditions in March 2018 seems more likely to result from transitory meteorological circumstances than from the seasonal climatic background of the city.

The accuracy level of the collected data concerning diurnal thermal disparities among LCZs is also worth discussing. As expected, temperatures within urban areas were mostly equal or below those registered at the reference site during the daytime, and significantly lower than during the nighttime. However, temperature differences at the more sparsely built areas (i.e. LCZ 4, 5, 6 and 9) suddenly swapped to positive values during the late afternoon of several months (12–18 GMT) only to turn back to negative values a few hours before sunset, when the nighttime UHI starts to form. This late afternoon overheating at urban sites exacerbates when approaching the summer solstice, when solar radiation is at its strongest and the sun is at its maximum altitude. A visual analysis of the data reported in previous investigations revealed similar trends (Fenner et al., 2014; Skarbit et al., 2017; Yang et al., 2020b). Erell and Williamson (2007) determined that urban-rural daytime temperature differences are heavily connected with solar radiation exposure. They also proved that significant thermal differences between urban sites should be expected due to the orientation of streets during the afternoon and late afternoon. Fenner et al. (2014) compared downward short-wave radiation within an urban canyon and on the rooftop, connecting the increase in temperature registered during the afternoon at the two urban sites with the orientation of the streets (N-S).

However, one might debate whether this daytime temperature anomaly is exclusively attributed to higher solar access in view of street orientation, or if it could be related to sensor overheating. The majority of the previous research on LCZs has used Stevenson-like, naturally-ventilated radiation shields (Beck et al., 2018; Fenner et al., 2014; Kotharkar and Bagade, 2018; Yang et al., 2018), possibly compromising ventilation when exposed to high levels of solar radiation. In this context, Erell et al. (2005) observed temperature differences of around +1 °C when comparing a Stevenson screen and a mechanically ventilated shield in the late afternoon of a sunny day. In like manner, the tests of Fenner et al. (2014), who checked their daytime urban measurements against a sensor housed within a mechanically ventilated radiation shield, found thermal differences of up to 0.4 (±0.5) °C. Although our equipment was designed to be ventilated mechanically and its correct functioning was continuously ensured during the measurement campaign, a similar overheating phenomenon took place. Consequently, studies in cities with high-intensity levels of solar radiation during the summertime, like Madrid, might require extra precautions to avoid sensor overheating. These observations might also put into question the daytime LCZ statistical analysis, since the significance found between LCZ pairs might be due not to the intrinsic climatic properties of each LCZ, but to the fact that some of them might provide enhanced solar radiation access and, therefore, account for stronger sensor overheating episodes.

Finally, it should be mentioned that it was surprising to find overheating sensors despite following the QC procedures derived from the WMO recommendations. It should be noted that other urban studies have made use of advanced filtering techniques to remove or correct their measurements, particularly those based on CWS, where the correct siting, housing and calibration of the sensor cannot be guaranteed (Chapman et al., 2017; Hammerberg et al., 2018; Meier et al., 2017). Others, such as Beck et al. (2018), designed spatial consistency tests based on reference time series derived from inverse distance weighting (IDW) spatial interpolations. Given that the WMO already provides recommendations for sensor siting and metadata collection within urban environments, it would be desirable to include specific guidelines on QC within urban areas, particularly considering the use of non-standard equipment. When using spatial consistency tests, it would be advisable to work with an official reference site, since using averages from the deployed sensors could mask overheating issues.

6. Conclusions

This study allowed for a deeper understanding of the UHI of Madrid, as well as the capacity of LCZs to portray these temperature differences within the urban environment. In relation to the former, relatively high UHI intensities were consistently observed in Madrid, reaching values above 5 °C in more than 35% of the total monitoring days. There was no clear seasonal pattern found for the maximum and minimum UHI intensities, while a slight seasonality towards higher daily means could be noted in winter.

For their part, the LCZs performed strongly concerning the detection of the UHI nighttime profile. They showed high levels of correspondence with the logical LCZs arrangement, confirming that compact urban settings (LCZ 2) systematically register higher UHI intensities than sparsely built ones (LCZ 6). During the night of ideal days, statistical differences proved to be significant among all the LCZs as well, particularly 7 to 8 h after sunset. During the day, however, the LCZs did not seem to be very effective. The correlation study between the LCZ parameters and the temperature differences corroborates this point, with all parameters failing to accurately represent midday temperature differences. Although diurnal temperature divergences might be closely linked with micro-climatic parameters, such as the street orientation or the sensor location within the urban canyon, more research is needed to identify relevant drivers of diurnal temperature differences and their possible incorporation into the LCZ classification scheme. It would also be

advisable to further explore the role of the distance to the city centre within the LCZs.

Overall, the instruments used for the monitoring campaign, as well as the tools adopted for the contextualisation and pre-processing, have shown a high level of reliability. Doubts have only arisen with temperature records during the central hours of the days with the strongest level of solar radiation. It is unclear whether the so-called late afternoon overheating was due to actual sensor overheating issues or to the increased solar radiation availability in the urban canyon. In any case, it would be advisable to continue investigating new ways of protecting the measuring devices as well as novel QC processes to detect anomalies within urban environments.

Funding

This research was funded by the FPU research grant FPU15/05052, from the Spanish Ministry of Science, Innovation and Universities. This research was also supported by the MODIFICA research project (BIA2013–41732-R), funded by the Spanish Ministry of Economy and Competitiveness.

Authorship

All persons who meet authorship criteria are listed as authors, and all authors certify that they have participated sufficiently in the work to take public responsibility for the content, including participation in the concept, design, analysis, writing, or revision of the manuscript. Furthermore, each author certifies that this material or similar material has not been and will not be submitted to or published in any other publication.

Declaration of Competing Interest

There is NO affiliations of authors with or involvement in any organization or entity with any financial interest, or non-financial interest in the subject matter or materials discussed in this manuscript.

Acknowledgements

The authors would like to thank the Spanish State Meteorological Agency (AEMET) for providing access to their meteorological data. The authors would like to extend their gratitude to Luis Tejero Encinas and Juan Azcárate Luxán, from the Madrid City Council' Subdivision of Energy and Climate Change, for their support with the urban measurements campaign. The authors would also like to thank Inês Costa Carrapiço for her valuable recommendations and inputs while proof-reading this manuscript.

Appendix A. Appendix

A.1. Physical characteristics, location and length of the MODIFICA measuring campaign

A.2. Metadata associated to each measuring site

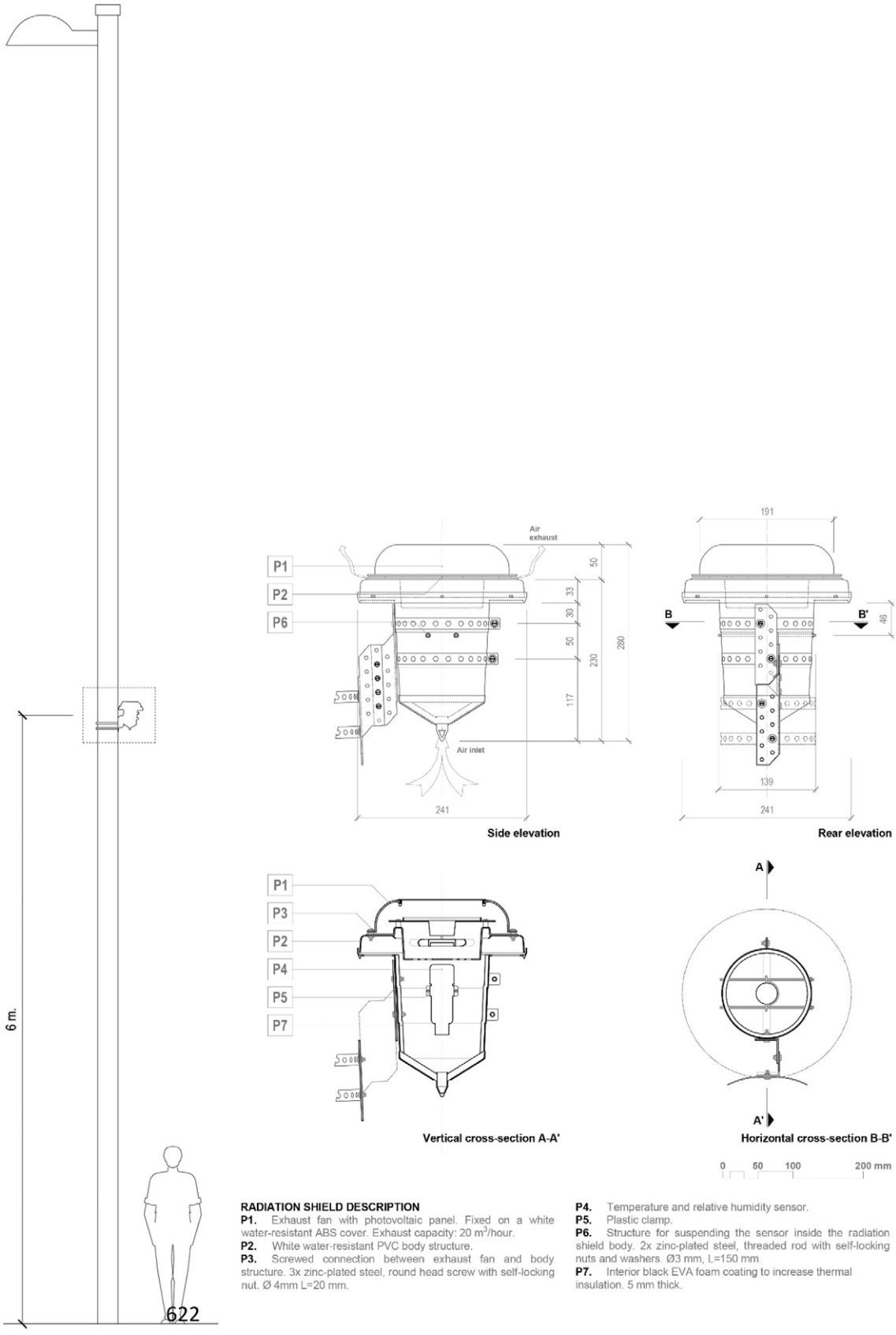

RADIATION SHIELD DESCRIPTION

P1. Exhaust fan with photovoltaic panel. Fixed on a white water-resistant ABS cover. Exhaust capacity: 20 m^3/hour.
P2. White water-resistant PVC body structure.
P3. Screwed connection between exhaust fan and body structure. 3x zinc-plated steel, round head screw with self-locking nut. Ø 4mm L=20 mm.
P4. Temperature and relative humidity sensor.
P5. Plastic clamp.
P6. Structure for suspending the sensor inside the radiation shield body. 2x zinc-plated steel, threaded rod with self-locking nuts and washers. Ø3 mm, L=150 mm.
P7. Interior black EVA foam coating to increase thermal insulation. 5 mm thick.

(caption on next page)

Site 01 EMBAJADORES **Calle de Atocha, 62. 28012 Madrid**

Urban context (1:50.000)

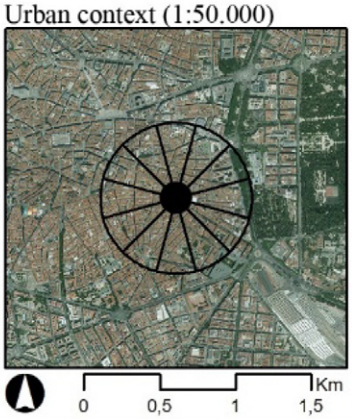

Local scale (1:25.000)

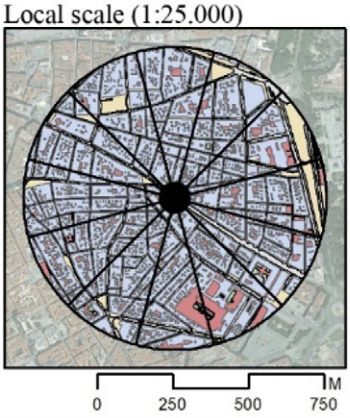

Microscale (1:10.000)

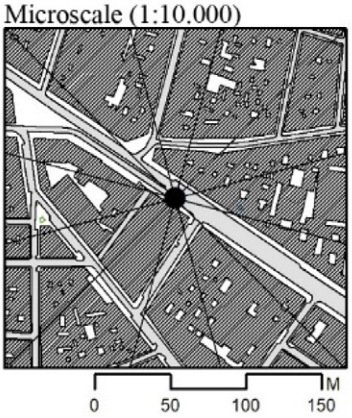

SITE DESCRIPTION
District: **01 - Centro**
Neigbourh.: **012 - Embajadores**
Lat: **40.412** Long: **-3.698**
LCZ: **02 - Compact midrise**
SVF summer/winter: **0.3/0.3**
Aspect ratio: **2.0**

LAND COVER
Building s.f.: **61%**
Impervious s.f.: **36%**
Pervious s.f.: **3%**
Typical buildings height: **15 m**
Typical tree height: **-**
Davenport roughness class: **7**
Traffic density: **8/10**
Heat pumps to street: **0.12**
Typical road materials: **Asphalt**
Typical wall materials: **Bricks**

SENSOR DESCRIPTION
Mast type: **Streetlight**
Sensor height: **6 m**
Radiation shield: **Yes**
Mechanical ventilation: **Yes**
Parameters: **D. b. temperature (ºC)**
Relative humidity (%)

Surface cover by sectors

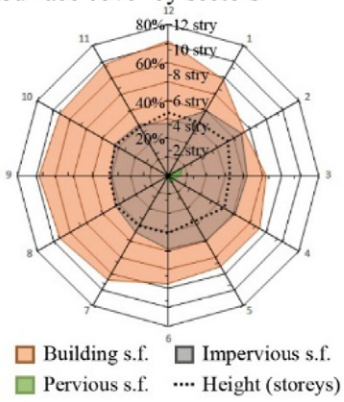

Sky View Factor in summer

Sensor location

Sky View Factor in winter

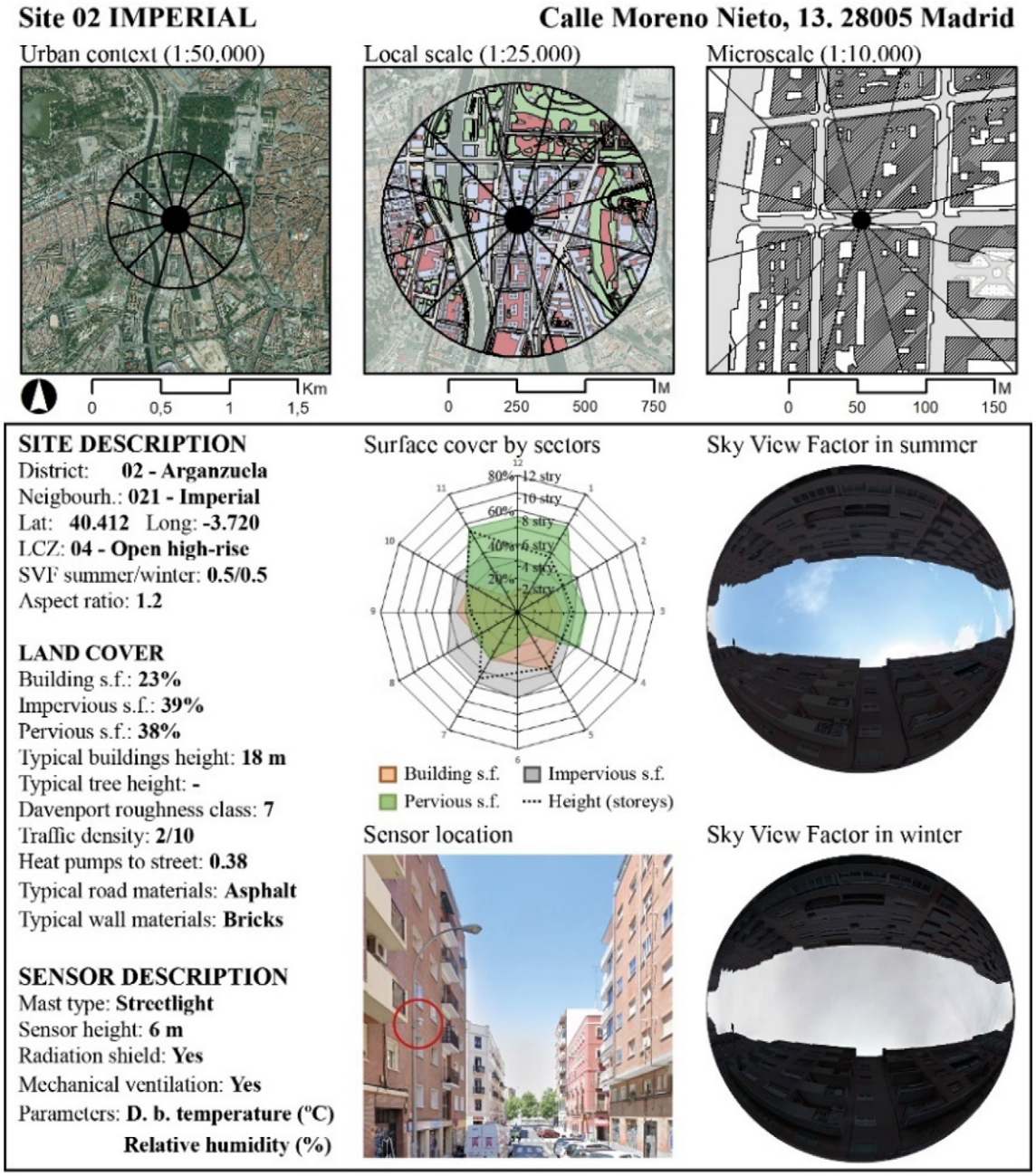
Site 02 IMPERIAL
Calle Moreno Nieto, 13. 28005 Madrid
Urban context (1:50.000)
Local scale (1:25.000)
Microscale (1:10.000)
0 0,5 1 1,5 Km
0 250 500 750 M
0 50 100 150 M
SITE DESCRIPTION
District: 02 - Arganzuela
Neigbourh.: 021 - Imperial
Lat: 40.412 Long: -3.720
LCZ: 04 - Open high-rise
SVF summer/winter: 0.5/0.5
Aspect ratio: 1.2
LAND COVER
Building s.f.: 23%
Impervious s.f.: 39%
Pervious s.f.: 38%
Typical buildings height: 18 m
Typical tree height: -
Davenport roughness class: 7
Traffic density: 2/10
Heat pumps to street: 0.38
Typical road materials: Asphalt
Typical wall materials: Bricks
SENSOR DESCRIPTION
Mast type: Streetlight
Sensor height: 6 m
Radiation shield: Yes
Mechanical ventilation: Yes
Parameters: D. b. temperature (ºC)
Relative humidity (%)
Surface cover by sectors
80% 12 stry
60% 10 stry
40% 6 stry
20% 2 stry
Building s.f.
Impervious s.f.
Pervious s.f.
Height (storeys)
Sky View Factor in summer
Sensor location
Sky View Factor in winter

Site 03 LA CHOPERA **Calle de Embajadores, 168. 28045 Madrid**

Urban context (1:50.000)

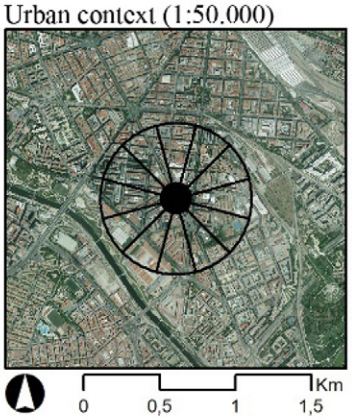

Local scale (1:25.000)

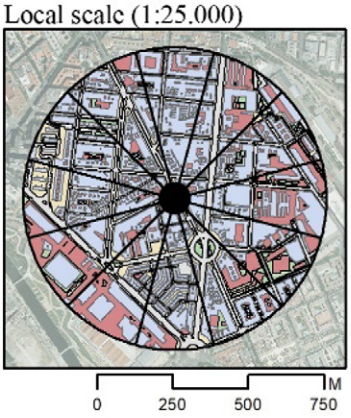

Microscale (1:10.000)

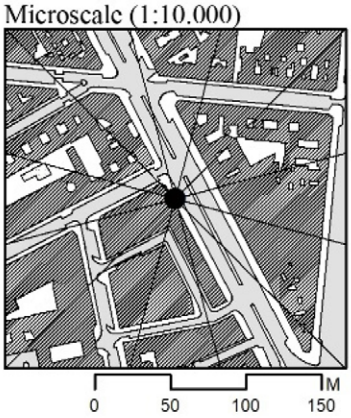

SITE DESCRIPTION
District: **02 - Arganzuela**
Neigbourh.: **023 - La Chopera**
Lat: **40.396** Long: **-3.696**
LCZ: **02 - Compact midrise**
SVF summer/winter: **0.4/0.6**
Aspect ratio: **1.3**

LAND COVER
Building s.f.: **44%**
Impervious s.f.: **47%**
Pervious s.f.: **9%**
Typical buildings height: **20 m**
Typical tree height: **6-12 m**
Davenport roughness class: **7**
Traffic density: **6/10**
Heat pumps to street: **0.67**
Typical road materials: **Asphalt**
Typical wall materials: **Bricks**

SENSOR DESCRIPTION
Mast type: **Streetlight**
Sensor height: **6 m**
Radiation shield: **Yes**
Mechanical ventilation: **Yes**
Parameters: **D. b. temperature (ºC)**
Relative humidity (%)

Surface cover by sectors

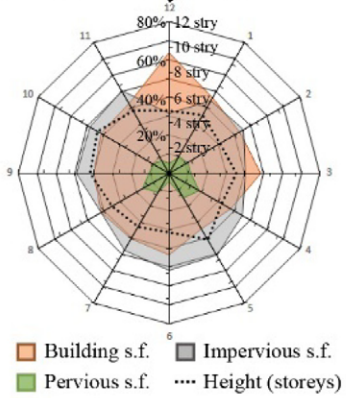

Sky View Factor in summer

Sensor location

Sky View Factor in winter

Site 04 ESTRELLA **Calle de la Estrella Polar, 8. 28007 Madrid**

Urban context (1:50.000)

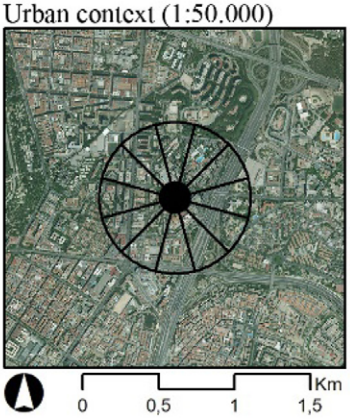

Local scale (1:25.000)

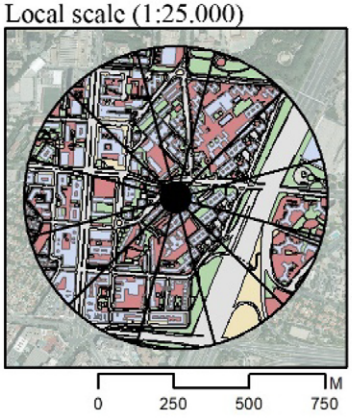

Microscale (1:10.000)

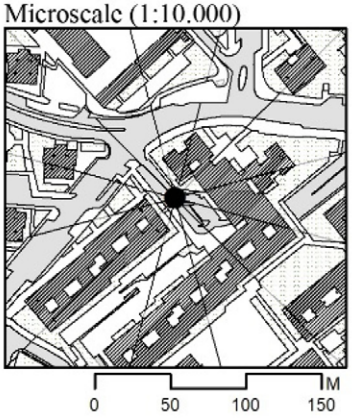

SITE DESCRIPTION
District: **03 - Retiro**
Neigbourh.: **033 - Estrella**
Lat: **40.411** Long: **-3.667**
LCZ: **04 - Open high-rise**
SVF summer/winter: **0.6/0.7**
Aspect ratio: **1.4**

LAND COVER
Building s.f.: **20%**
Impervious s.f.: **52%**
Pervious s.f.: **28%**
Typical buildings height: **28-52 m**
Typical tree height: **12 m**
Davenport roughness class: **8**
Traffic density: **1/10**
Heat pumps to street: **0.52**
Typical road materials: **Asphalt**
Typical wall materials: **Bricks**

SENSOR DESCRIPTION
Mast type: **Streetlight**
Sensor height: **6 m**
Radiation shield: **Yes**
Mechanical ventilation: **Yes**
Parameters: **D. b. temperature (ºC)**
Relative humidity (%)

Surface cover by sectors

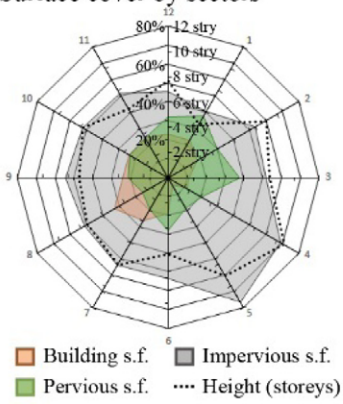

Sky View Factor in summer

Sensor location

Sky View Factor in winter

Site 05 PACÍFICO **Calle de Granada, 12. 28007 Madrid**

Urban context (1:50.000)

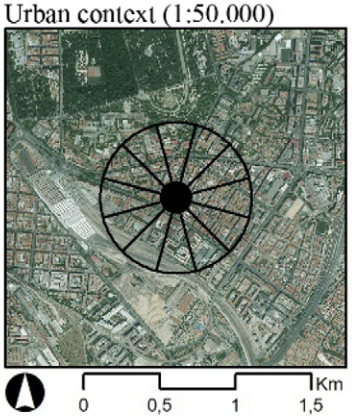

Local scale (1:25.000)

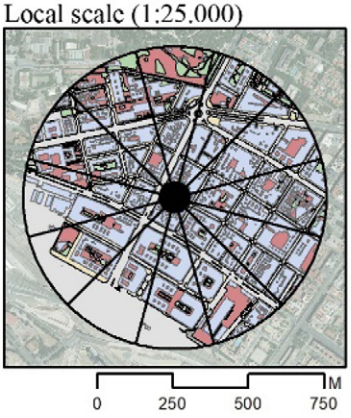

Microscale (1:10.000)

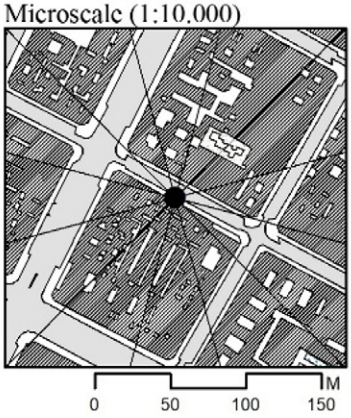

SITE DESCRIPTION
District: **03 - Retiro**
Neigbourh.: **031 - Pacífico**
Lat: **40.405** Long: **-3.680**
LCZ: **02 - Compact midrise**
SVF summer/winter: **0.4/0.5**
Aspect ratio: **1.7**

LAND COVER
Building s.f.: **39%**
Impervious s.f.: **51%**
Pervious s.f.: **10%**
Typical buildings height: **26 m**
Typical tree height: **8 m**
Davenport roughness class: **7**
Traffic density: **1/10**
Heat pumps to street: **0.50**
Typical road materials: **Asphalt**
Typical wall materials: **Bricks**

SENSOR DESCRIPTION
Mast type: **Streetlight**
Sensor height: **6 m**
Radiation shield: **Yes**
Mechanical ventilation: **Yes**
Parameters: **D. b. temperature (ºC)**
Relative humidity (%)

Surface cover by sectors

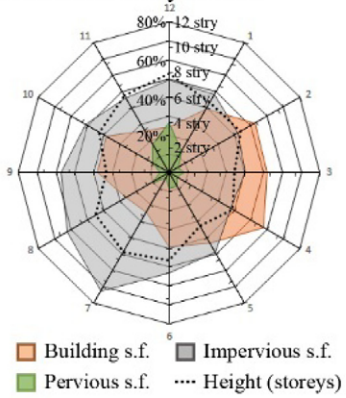

Sky View Factor in summer

Sensor location

Sky View Factor in winter

Site 06 GUINDALERA **Calle de Eraso, 34. 28028 Madrid**

Urban context (1:50.000)

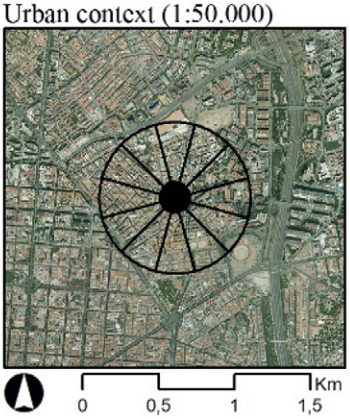

Local scale (1:25.000)

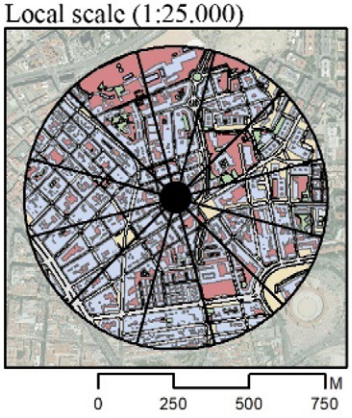

Microscale (1:10.000)

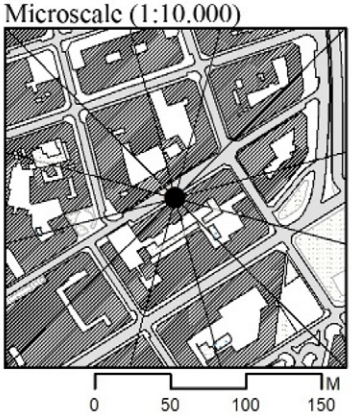

SITE DESCRIPTION
District: **04 - Salamanca**
Neigbourh.: **044 - Guindalera**
Lat: **40.435** Long: **-3.668**
LCZ: **02 - Compact midrise**
SVF summer/winter: **0.6/0.6**
Aspect ratio: **1.5**

LAND COVER
Building s.f.: **41%**
Impervious s.f.: **47%**
Pervious s.f.: **12%**
Typical buildings height: **15 m**
Typical tree height: **-**
Davenport roughness class: **7**
Traffic density: **3/10**
Heat pumps to street: **0.22**
Typical road materials: **Asphalt**
Typical wall materials: **Bricks**

SENSOR DESCRIPTION
Mast type: **Streetlight**
Sensor height: **6 m**
Radiation shield: **Yes**
Mechanical ventilation: **Yes**
Parameters: **D. b. temperature (ºC)**
Relative humidity (%)

Surface cover by sectors

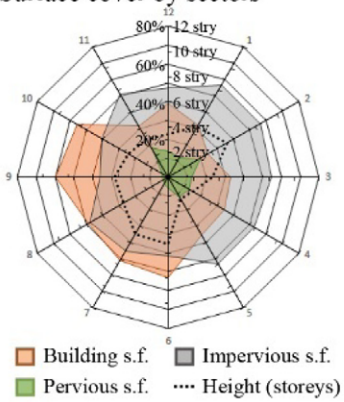

Sky View Factor in summer

Sensor location

Sky View Factor in winter

Site 07 RECOLETOS **Calle de Goya, 14. 28001 Madrid**

Urban context (1:50.000)

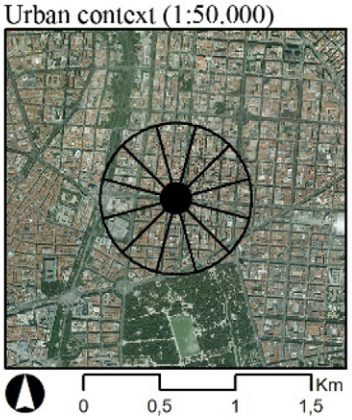

Local scale (1:25.000)

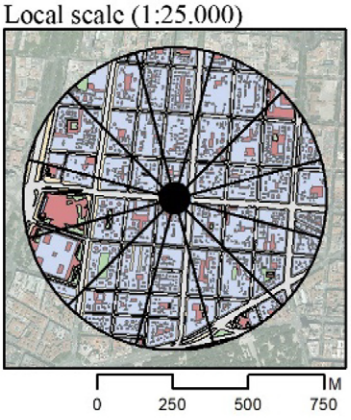

Microscale (1:10.000)

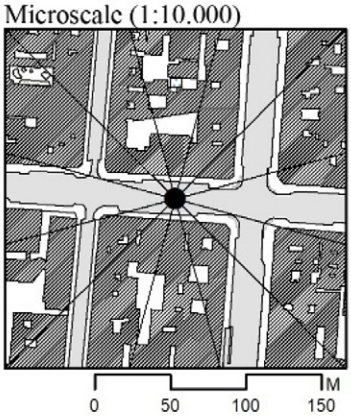

SITE DESCRIPTION
District: **04 - Salamanca**
Neigbourh.: **041 - Recoletos**
Lat: **40.425** Long: **-3.685**
LCZ: **02 - Compact midrise**
SVF summer/winter: **0.7/0.8**
Aspect ratio: **1.3**

LAND COVER
Building s.f.: **52%**
Impervious s.f.: **42%**
Pervious s.f.: **6%**
Typical buildings height: **20 m**
Typical tree height: **8-12 m**
Davenport roughness class: **7**
Traffic density: **9/10**
Heat pumps to street: **0.00**
Typical road materials: **Asphalt**
Typical wall materials: **Bricks**

SENSOR DESCRIPTION
Mast type: **Streetlight**
Sensor height: **6 m**
Radiation shield: **Yes**
Mechanical ventilation: **Yes**
Parameters: **D. b. temperature (ºC)**
Relative humidity (%)

Surface cover by sectors

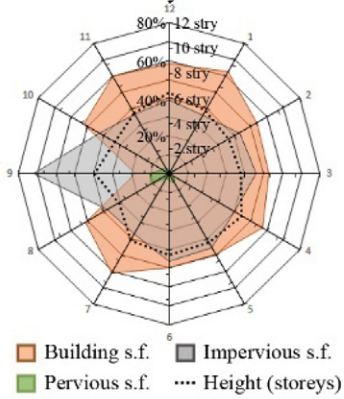

Sky View Factor in summer

Sensor location

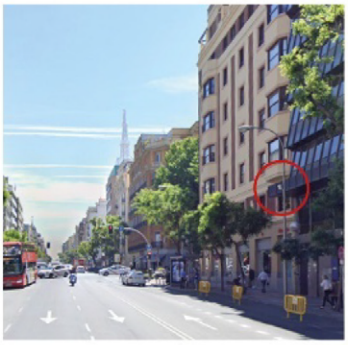

Sky View Factor in winter

Site 08 HISPANOAMÉRICA **Calle Infanta María Teresa, 12. 28016 Madrid**

Urban context (1:50.000)

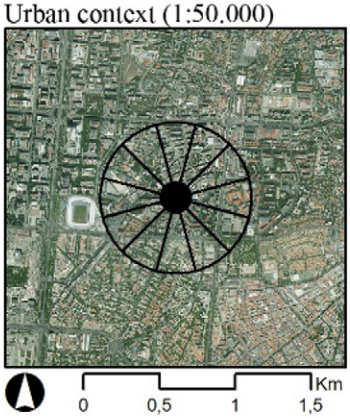

Local scale (1:25.000)

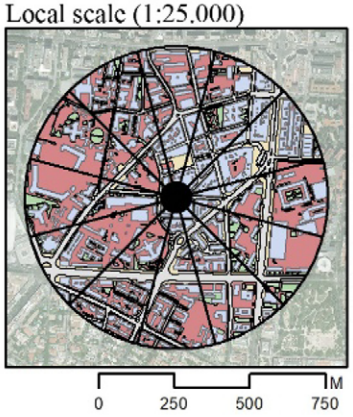

Microscale (1:10.000)

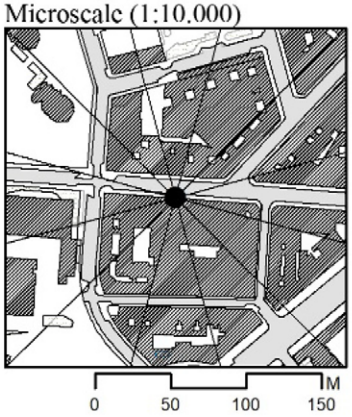

SITE DESCRIPTION
District: **05 - Chamartín**
Neigbourh.: **054 - Hispanoamérica**
Lat: **40.454** Long: **-3.681**
LCZ: **02 - Compact midrise**
SVF summer/winter: **0.6/0.6**
Aspect ratio: **1.1**

LAND COVER
Building s.f.: **29%**
Impervious s.f.: **49%**
Pervious s.f.: **22%**
Typical buildings height: **16 m**
Typical tree height: **12 m**
Davenport roughness class: **7**
Traffic density: **6/10**
Heat pumps to street: **0.18**
Typical road materials: **Asphalt**
Typical wall materials: **Bricks**

SENSOR DESCRIPTION
Mast type: **Streetlight**
Sensor height: **6 m**
Radiation shield: **Yes**
Mechanical ventilation: **Yes**
Parameters: **D. b. temperature (ºC)**
Relative humidity (%)

Surface cover by sectors

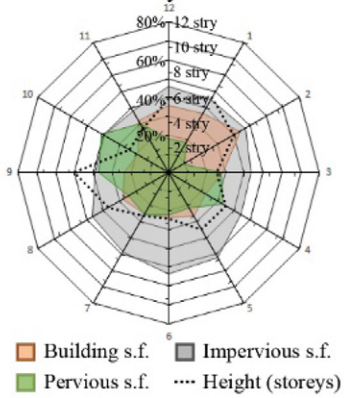

Sky View Factor in summer

Sensor location

Sky View Factor in winter

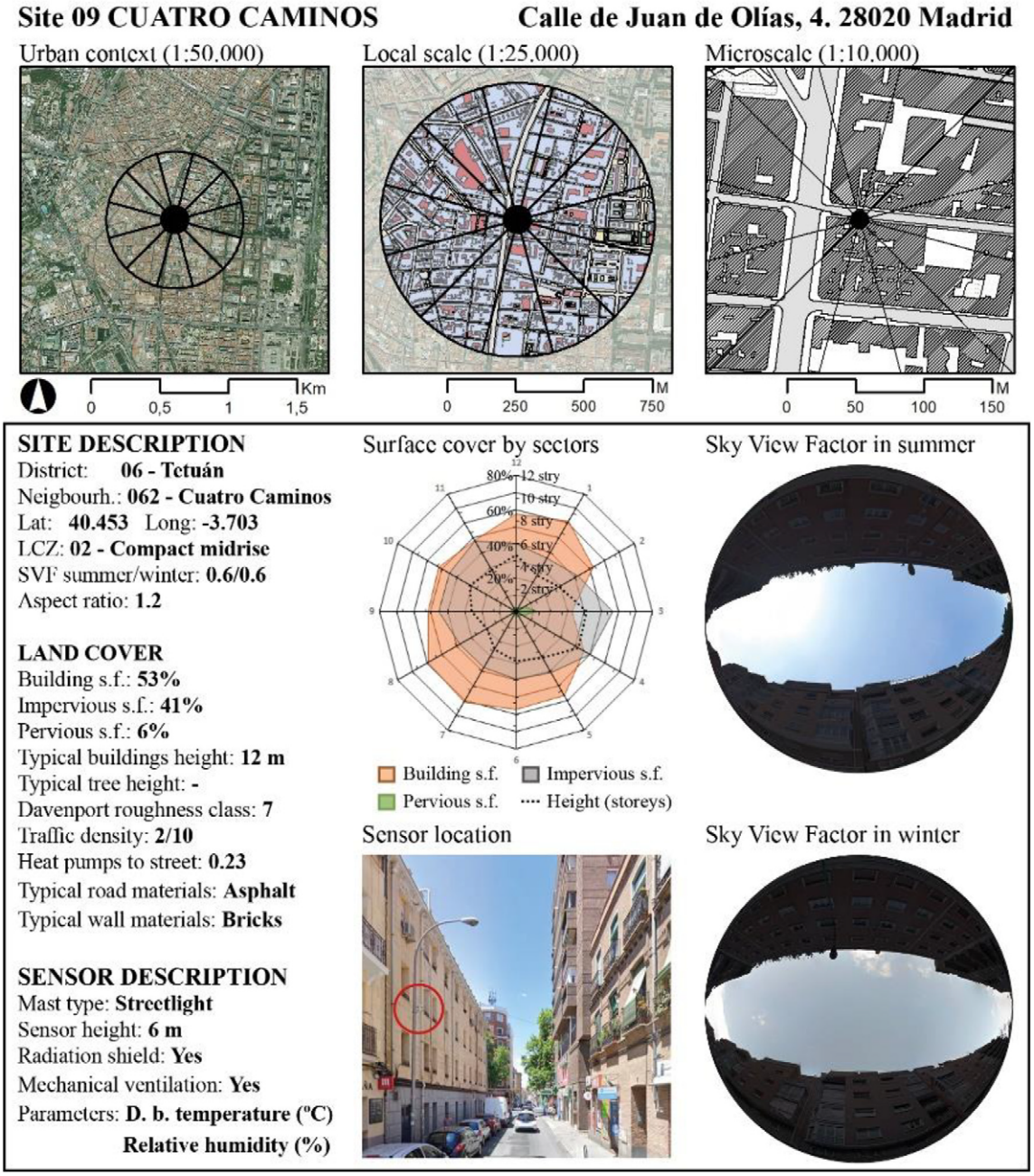
Site 09 CUATRO CAMINOS
Calle de Juan de Olías, 4. 28020 Madrid
Urban context (1:50.000)
Local scale (1:25.000)
Microscale (1:10.000)
0 0,5 1 1,5 Km
0 250 500 750 M
0 50 100 150 M
SITE DESCRIPTION
District: 06 - Tetuán
Neigbourh.: 062 - Cuatro Caminos
Lat: 40.453 Long: -3.703
LCZ: 02 - Compact midrise
SVF summer/winter: 0.6/0.6
Aspect ratio: 1.2
LAND COVER
Building s.f.: 53%
Impervious s.f.: 41%
Pervious s.f.: 6%
Typical buildings height: 12 m
Typical tree height: -
Davenport roughness class: 7
Traffic density: 2/10
Heat pumps to street: 0.23
Typical road materials: Asphalt
Typical wall materials: Bricks
SENSOR DESCRIPTION
Mast type: Streetlight
Sensor height: 6 m
Radiation shield: Yes
Mechanical ventilation: Yes
Parameters: D. b. temperature (ºC)
Relative humidity (%)
Surface cover by sectors
80%
60%
40%
20%
12 stry
10 stry
8 stry
6 stry
4 stry
2 stry
Building s.f.
Impervious s.f.
Pervious s.f.
Height (storeys)
Sky View Factor in summer
Sensor location
Sky View Factor in winter

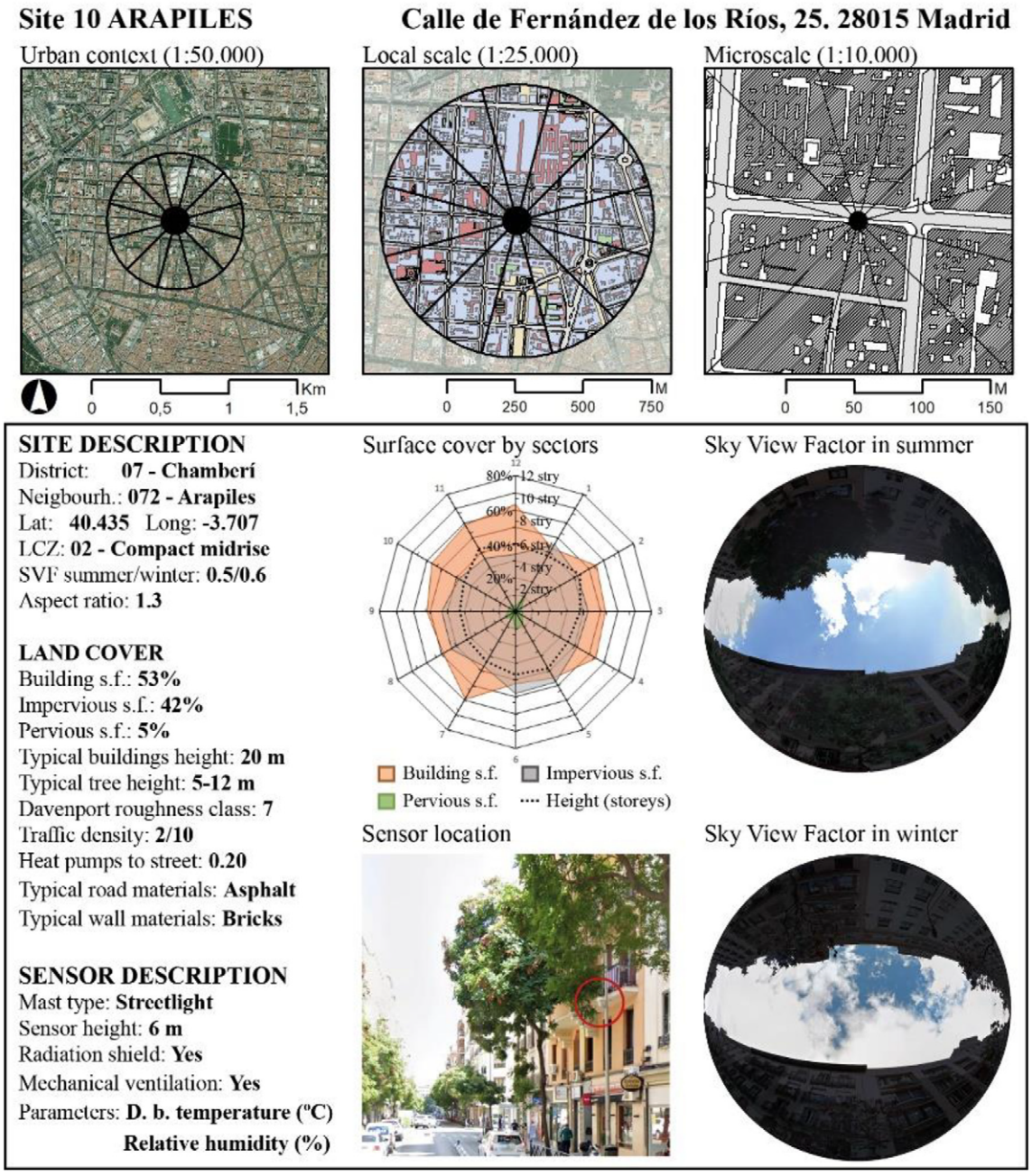
Site 10 ARAPILES
Calle de Fernández de los Ríos, 25. 28015 Madrid
Urban context (1:50.000)
Local scale (1:25.000)
Microscale (1:10.000)
Km
0 0,5 1 1,5
M
0 250 500 750
M
0 50 100 150
SITE DESCRIPTION
District: 07 - Chamberí
Neigbourh.: 072 - Arapiles
Lat: 40.435 Long: -3.707
LCZ: 02 - Compact midrise
SVF summer/winter: 0.5/0.6
Aspect ratio: 1.3
LAND COVER
Building s.f.: 53%
Impervious s.f.: 42%
Pervious s.f.: 5%
Typical buildings height: 20 m
Typical tree height: 5-12 m
Davenport roughness class: 7
Traffic density: 2/10
Heat pumps to street: 0.20
Typical road materials: Asphalt
Typical wall materials: Bricks
SENSOR DESCRIPTION
Mast type: Streetlight
Sensor height: 6 m
Radiation shield: Yes
Mechanical ventilation: Yes
Parameters: D. b. temperature (ºC)
Relative humidity (%)
Surface cover by sectors
80%
60%
40%
20%
12 stry
10 stry
8 stry
6 stry
4 stry
2 stry
Building s.f.
Impervious s.f.
Pervious s.f.
Height (storeys)
Sky View Factor in summer
Sensor location
Sky View Factor in winter

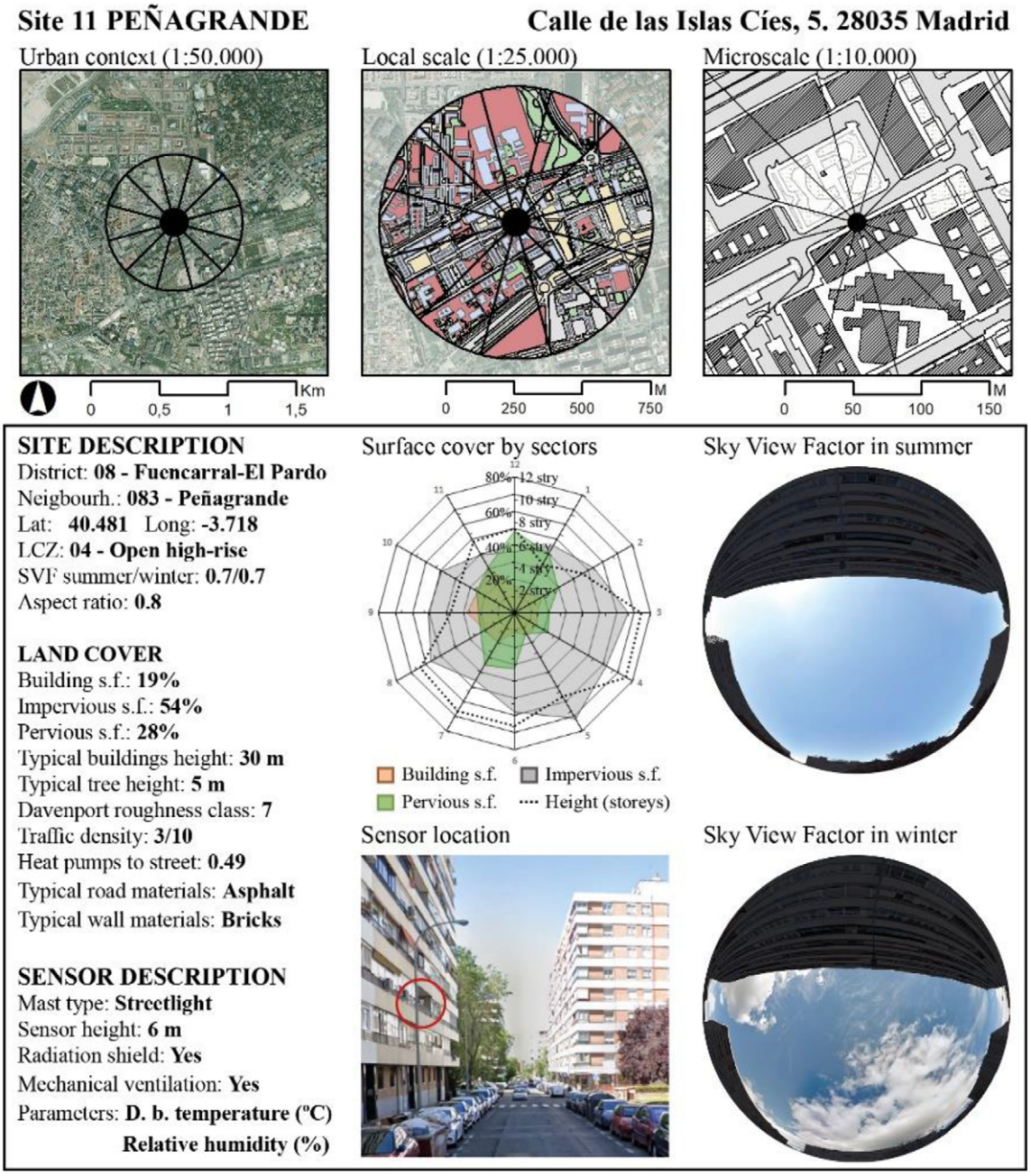
Site 11 PEÑAGRANDE
Calle de las Islas Cíes, 5. 28035 Madrid
Urban context (1:50.000)
Local scale (1:25.000)
Microscale (1:10.000)
0 0,5 1 1,5 Km
0 250 500 750 M
0 50 100 150 M
SITE DESCRIPTION
District: 08 - Fuencarral-El Pardo
Neigbourh.: 083 - Peñagrande
Lat: 40.481 Long: -3.718
LCZ: 04 - Open high-rise
SVF summer/winter: 0.7/0.7
Aspect ratio: 0.8
LAND COVER
Building s.f.: 19%
Impervious s.f.: 54%
Pervious s.f.: 28%
Typical buildings height: 30 m
Typical tree height: 5 m
Davenport roughness class: 7
Traffic density: 3/10
Heat pumps to street: 0.49
Typical road materials: Asphalt
Typical wall materials: Bricks
SENSOR DESCRIPTION
Mast type: Streetlight
Sensor height: 6 m
Radiation shield: Yes
Mechanical ventilation: Yes
Parameters: D. b. temperature (ºC)
Relative humidity (%)
Surface cover by sectors
80% 12 stry
60% 10 stry
40% 8 stry
20% 6 stry
4 stry
2 stry
Building s.f.
Impervious s.f.
Pervious s.f.
Height (storeys)
Sky View Factor in summer
Sensor location
Sky View Factor in winter

Site 12 ARAVACA **Avenida de la Osa Mayor, 15. 28023 Madrid**

Urban context (1:50.000)

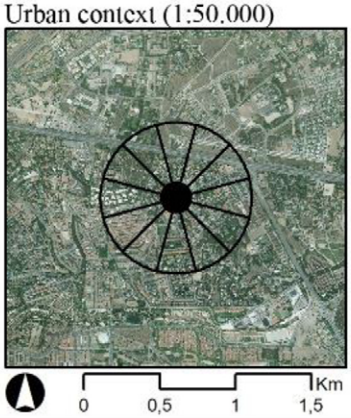

Local scale (1:25.000)

Microscale (1:10.000)

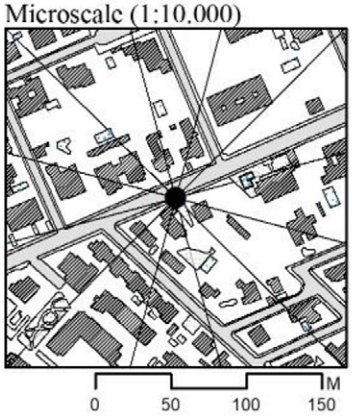

SITE DESCRIPTION
District: **09 - Moncloa-Aravaca**
Neigbourh.: **097 - Aravaca**
Lat: **40.460** Long: **-3.777**
LCZ: **06 - Open low-rise**
SVF summer/winter: **0.9/1.0**
Aspect ratio: **0.4**

LAND COVER
Building s.f.: **20%**
Impervious s.f.: **37%**
Pervious s.f.: **43%**
Typical buildings height: **8 m**
Typical tree height: **4-12 m**
Davenport roughness class: **5**
Traffic density: **1/10**
Heat pumps to street: **0.00**
Typical road materials: **Asphalt**
Typical wall materials: **Bricks**

SENSOR DESCRIPTION
Mast type: **Streetlight**
Sensor height: **6 m**
Radiation shield: **Yes**
Mechanical ventilation: **Yes**
Parameters: **D. b. temperature (ºC)**
Relative humidity (%)

Surface cover by sectors

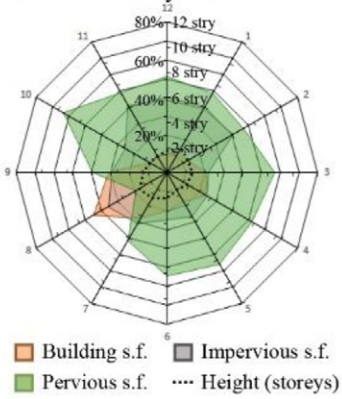

Sky View Factor in summer

Sensor location

Sky View Factor in winter

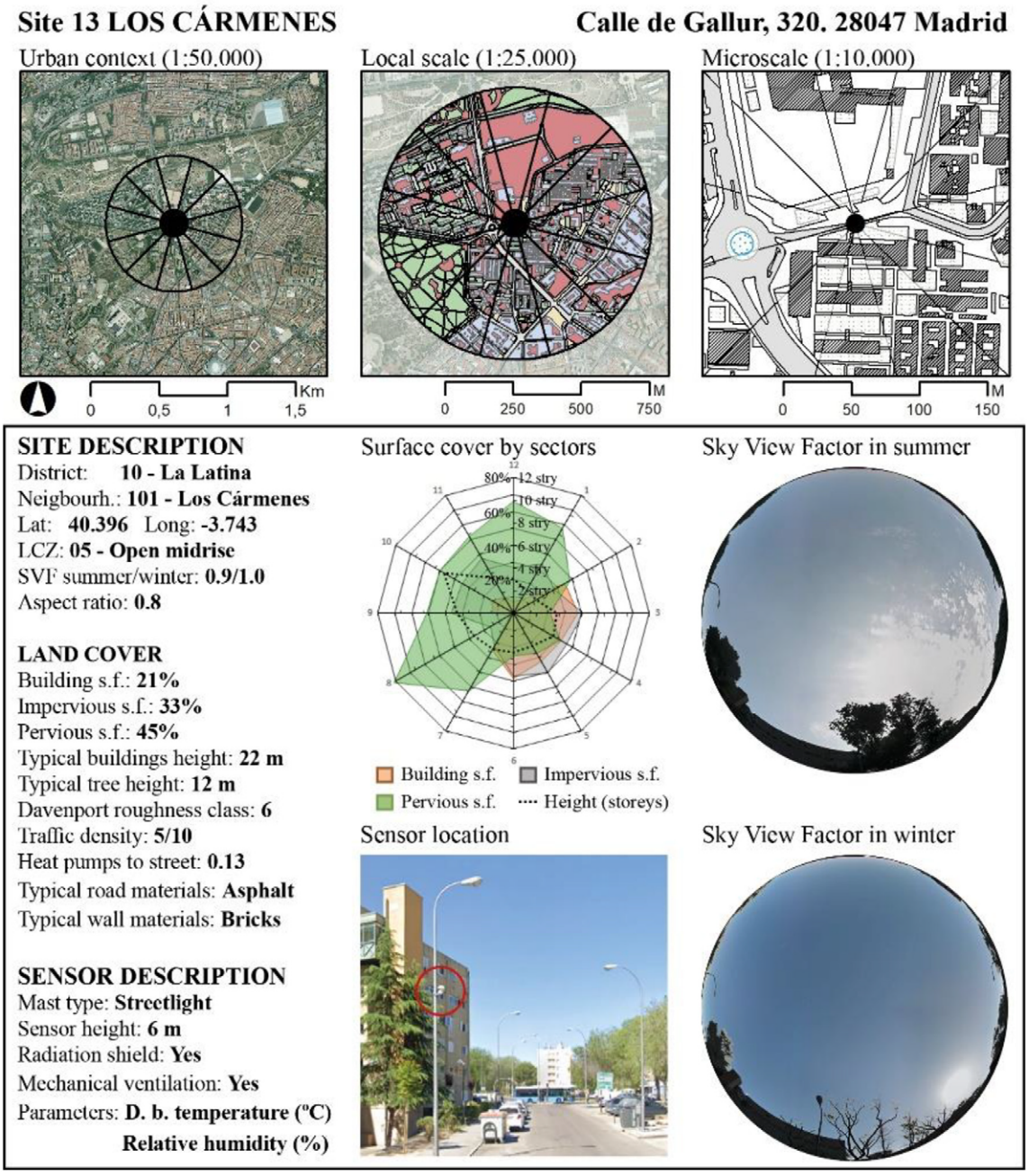
Site 13 LOS CÁRMENES
Calle de Gallur, 320. 28047 Madrid
Urban context (1:50.000)
Local scale (1:25.000)
Microscale (1:10.000)
0 0,5 1 1,5 Km
0 250 500 750 M
0 50 100 150 M
SITE DESCRIPTION
District: 10 - La Latina
Neigbourh.: 101 - Los Cármenes
Lat: 40.396 Long: -3.743
LCZ: 05 - Open midrise
SVF summer/winter: 0.9/1.0
Aspect ratio: 0.8
LAND COVER
Building s.f.: 21%
Impervious s.f.: 33%
Pervious s.f.: 45%
Typical buildings height: 22 m
Typical tree height: 12 m
Davenport roughness class: 6
Traffic density: 5/10
Heat pumps to street: 0.13
Typical road materials: Asphalt
Typical wall materials: Bricks
SENSOR DESCRIPTION
Mast type: Streetlight
Sensor height: 6 m
Radiation shield: Yes
Mechanical ventilation: Yes
Parameters: D. b. temperature (ºC)
Relative humidity (%)
Surface cover by sectors
80%
60%
40%
20%
12 stry
10 stry
8 stry
6 stry
4 stry
2 stry
Building s.f.
Impervious s.f.
Pervious s.f.
Height (storeys)
Sky View Factor in summer
Sensor location
Sky View Factor in winter

Site 14 OPAÑEL **Calle del Arroyo Opañel, 19. 28019 Madrid**

Urban context (1:50.000)

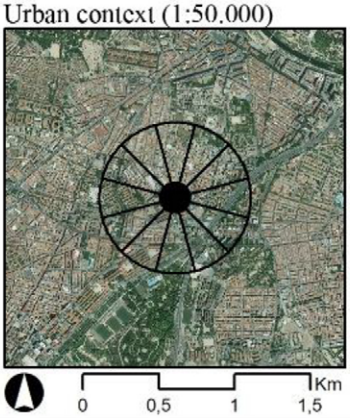

Local scale (1:25.000)

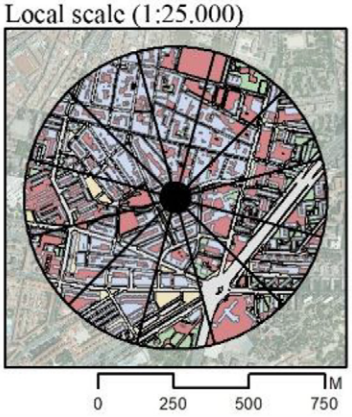

Microscale (1:10.000)

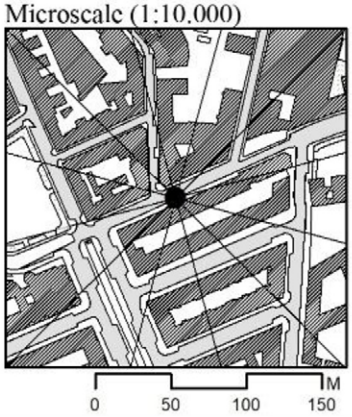

SITE DESCRIPTION
District: **11 - Carabanchel**
Neigbourh.: **112 - Opañel**
Lat: **40.388** Long: **-3.719**
LCZ: **05 - Open midrise**
SVF summer/winter: **0.8/0.8**
Aspect ratio: **1.1**

LAND COVER
Building s.f.: **31%**
Impervious s.f.: **48%**
Pervious s.f.: **21%**
Typical buildings height: **14 m**
Typical tree height: **-**
Davenport roughness class: **7**
Traffic density: **2/10**
Heat pumps to street: **0.64**
Typical road materials: **Asphalt**
Typical wall materials: **Bricks**

SENSOR DESCRIPTION
Mast type: **Streetlight**
Sensor height: **6 m**
Radiation shield: **Yes**
Mechanical ventilation: **Yes**
Parameters: **D. b. temperature (ºC)**
Relative humidity (%)

Surface cover by sectors

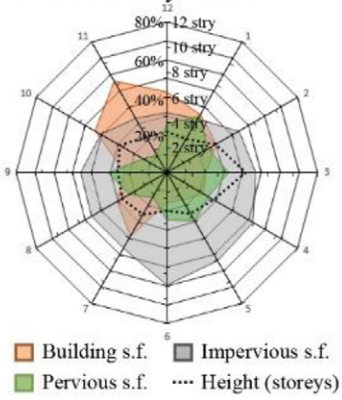

Sky View Factor in summer

Sensor location

Sky View Factor in winter

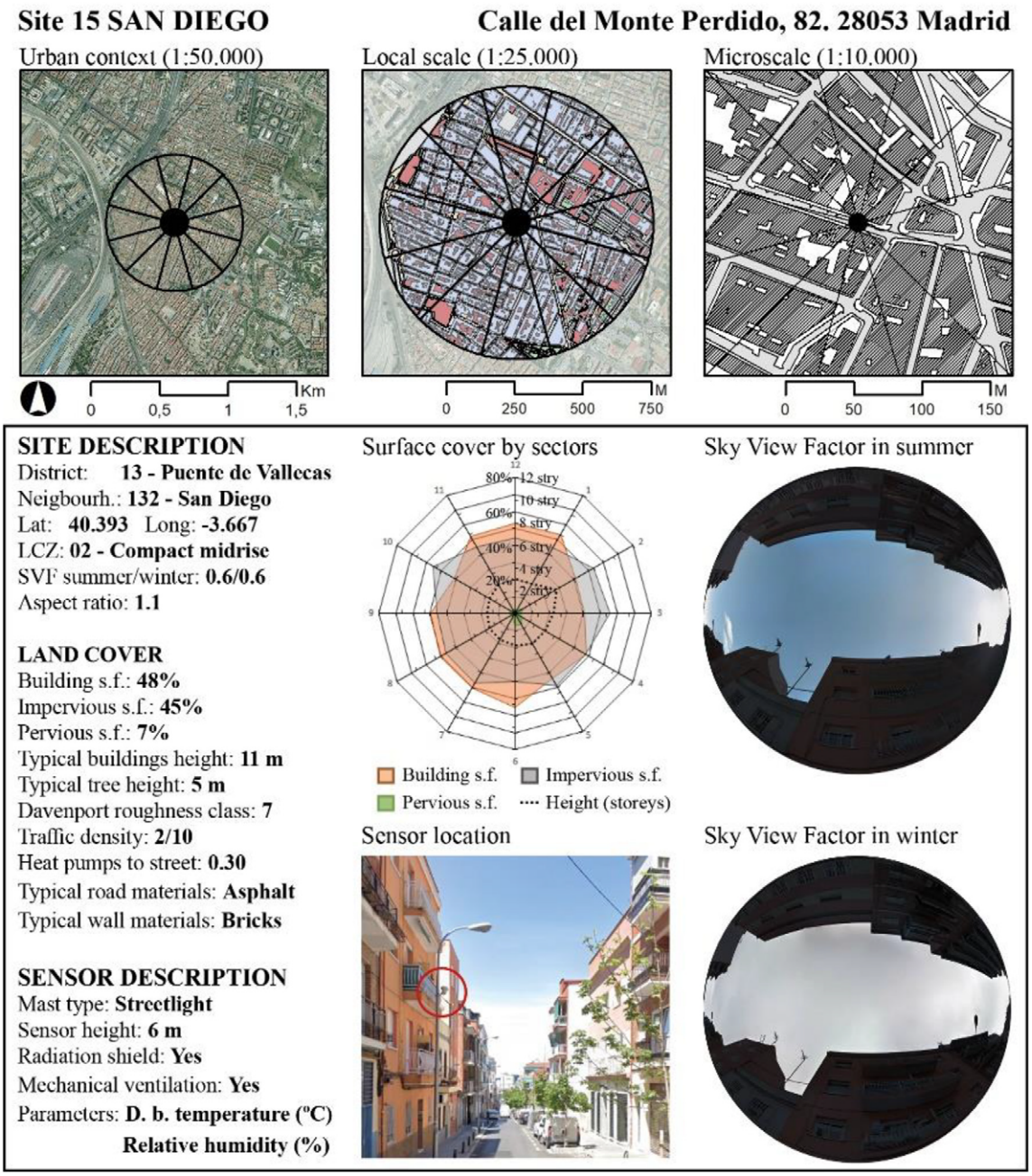
Site 15 SAN DIEGO
Calle del Monte Perdido, 82. 28053 Madrid
Urban context (1:50.000)
Local scale (1:25.000)
Microscale (1:10.000)
Km
0 0,5 1 1,5
M
0 250 500 750
M
0 50 100 150
SITE DESCRIPTION
District: 13 - Puente de Vallecas
Neigbourh.: 132 - San Diego
Lat: 40.393 Long: -3.667
LCZ: 02 - Compact midrise
SVF summer/winter: 0.6/0.6
Aspect ratio: 1.1
LAND COVER
Building s.f.: 48%
Impervious s.f.: 45%
Pervious s.f.: 7%
Typical buildings height: 11 m
Typical tree height: 5 m
Davenport roughness class: 7
Traffic density: 2/10
Heat pumps to street: 0.30
Typical road materials: Asphalt
Typical wall materials: Bricks
SENSOR DESCRIPTION
Mast type: Streetlight
Sensor height: 6 m
Radiation shield: Yes
Mechanical ventilation: Yes
Parameters: D. b. temperature (ºC)
Relative humidity (%)
Surface cover by sectors
80% 12 stry
60% 10 stry
40% 8 stry
20% 6 stry
4 stry
2 stry
Building s.f.
Impervious s.f.
Pervious s.f.
Height (storeys)
Sky View Factor in summer
Sensor location
Sky View Factor in winter

Site 16 HORCAJO **Calle de la Provenza, 13F. 28030 Madrid**

Urban context (1:50.000)

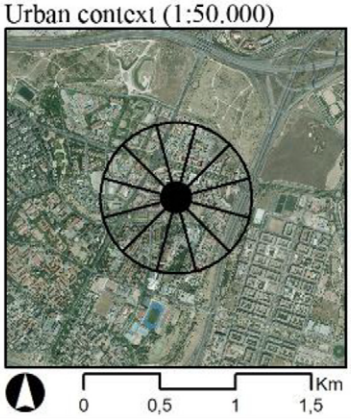

Local scale (1:25.000)

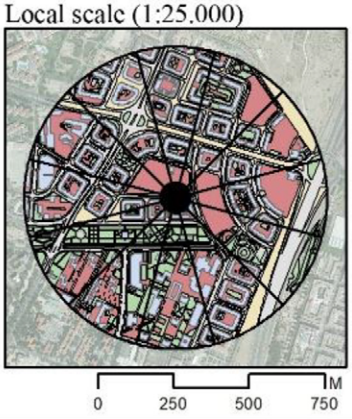

Microscale (1:10.000)

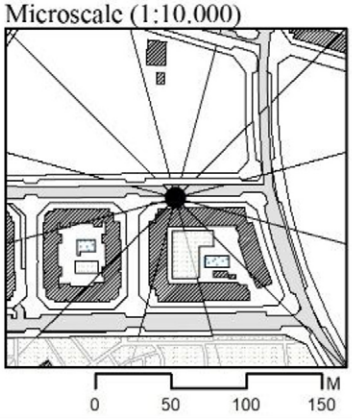

SITE DESCRIPTION
District: **14 - Moratalaz**
Neigbourh.: **142 - Horcajo**
Lat: **40.405** Long: **-3.630**
LCZ: **09 - Sparsely built**
SVF summer/winter: **0.9/0.9**
Aspect ratio: **0.2**

LAND COVER
Building s.f.: **17%**
Impervious s.f.: **49%**
Pervious s.f.: **35%**
Typical buildings height: **20 m**
Typical tree height: **7 m**
Davenport roughness class: **6**
Traffic density: **1/10**
Heat pumps to street: **0.00**
Typical road materials: **Asphalt**
Typical wall materials: **Bricks**

SENSOR DESCRIPTION
Mast type: **Streetlight**
Sensor height: **6 m**
Radiation shield: **Yes**
Mechanical ventilation: **Yes**
Parameters: **D. b. temperature (ºC)**
Relative humidity (%)

Surface cover by sectors

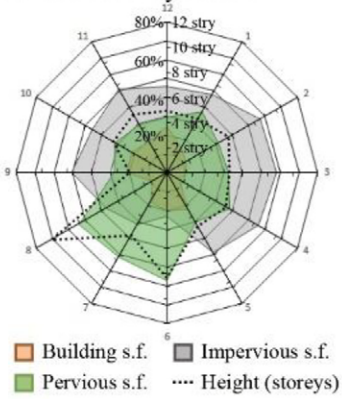

Sky View Factor in summer

Sensor location

Sky View Factor in winter

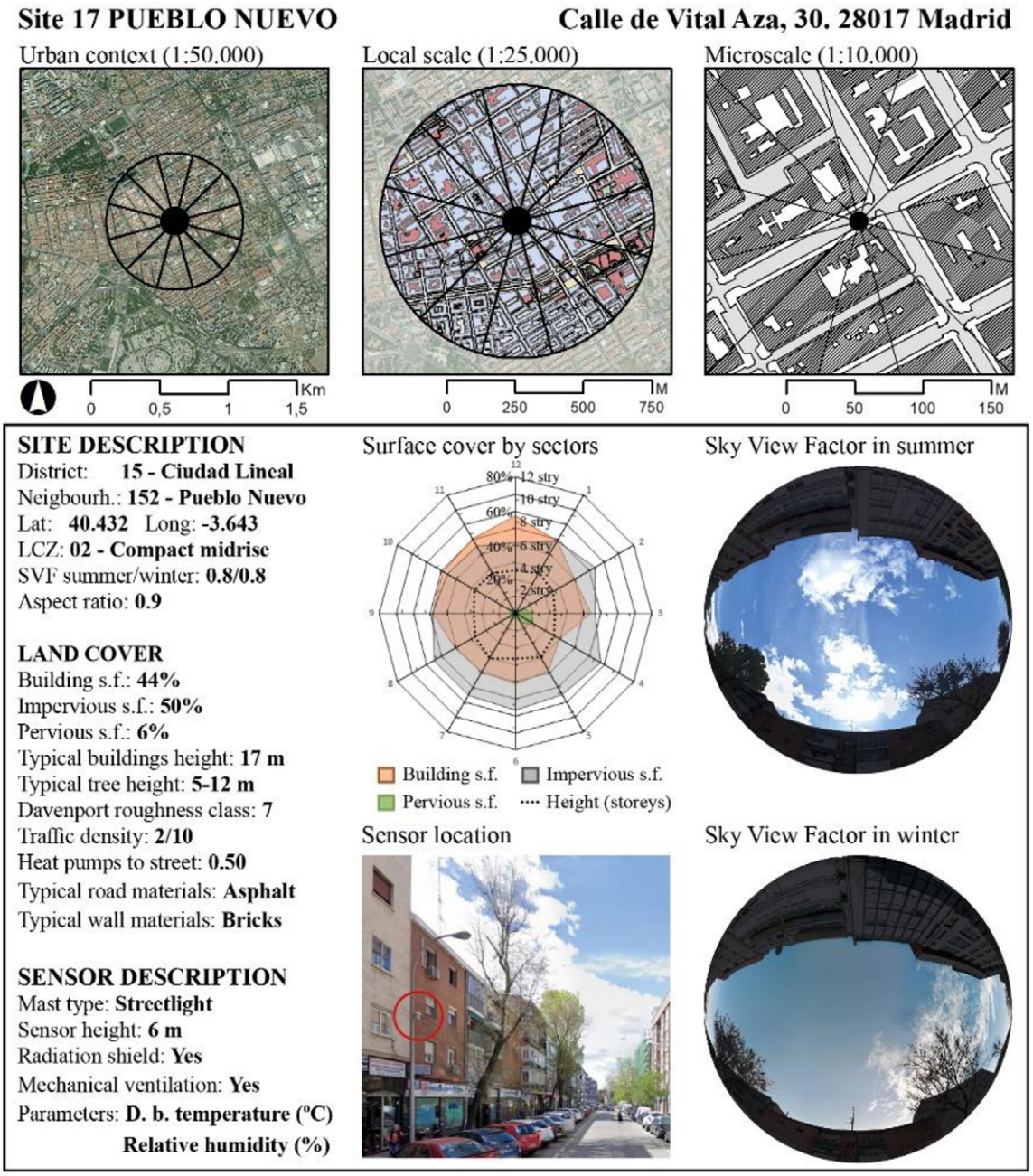
Site 17 PUEBLO NUEVO
Calle de Vital Aza, 30. 28017 Madrid
Urban context (1:50.000)
Local scale (1:25.000)
Microscale (1:10.000)
Km
0 0,5 1 1,5
M
0 250 500 750
M
0 50 100 150
SITE DESCRIPTION
District: 15 - Ciudad Lineal
Neigbourh.: 152 - Pueblo Nuevo
Lat: 40.432 Long: -3.643
LCZ: 02 - Compact midrise
SVF summer/winter: 0.8/0.8
Aspect ratio: 0.9
LAND COVER
Building s.f.: 44%
Impervious s.f.: 50%
Pervious s.f.: 6%
Typical buildings height: 17 m
Typical tree height: 5-12 m
Davenport roughness class: 7
Traffic density: 2/10
Heat pumps to street: 0.50
Typical road materials: Asphalt
Typical wall materials: Bricks
SENSOR DESCRIPTION
Mast type: Streetlight
Sensor height: 6 m
Radiation shield: Yes
Mechanical ventilation: Yes
Parameters: D. b. temperature (ºC)
Relative humidity (%)
Surface cover by sectors
80%
60%
40%
20%
12 stry
10 stry
8 stry
6 stry
4 stry
2 stry
Building s.f.
Impervious s.f.
Pervious s.f.
Height (storeys)
Sky View Factor in summer
Sensor location
Sky View Factor in winter

Site 18 CANILLAS **Calle de Santa Natalia, 5. 28043 Madrid**

Urban context (1:50.000)

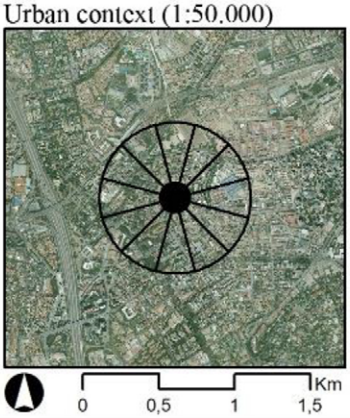

Local scale (1:25.000)

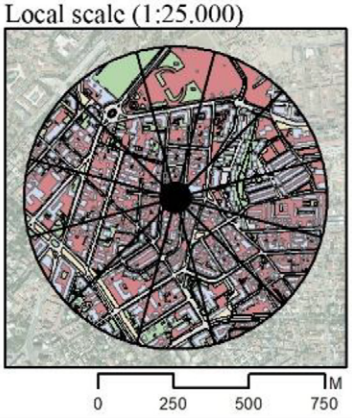

Microscale (1:10.000)

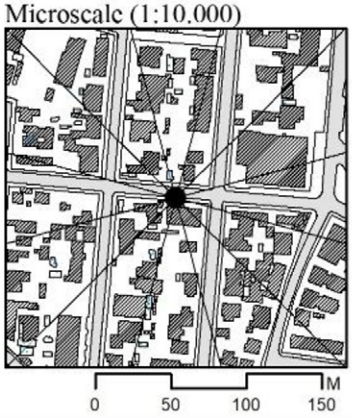

SITE DESCRIPTION
District: **16 - Hortaleza**
Neigbourh.: **163 - Canillas**
Lat: **40.461** Long: **-3.655**
LCZ: **06 - Open low-rise**
SVF summer/winter: **0.4/0.8**
Aspect ratio: **0.9**

LAND COVER
Building s.f.: **22%**
Impervious s.f.: **46%**
Pervious s.f.: **32%**
Typical buildings height: **10 m**
Typical tree height: **8-20 m**
Davenport roughness class: **7**
Traffic density: **1/10**
Heat pumps to street: **0.00**
Typical road materials: **Asphalt**
Typical wall materials: **Bricks**

SENSOR DESCRIPTION
Mast type: **Streetlight**
Sensor height: **6 m**
Radiation shield: **Yes**
Mechanical ventilation: **Yes**
Parameters: **D. b. temperature (ºC)**
Relative humidity (%)

Surface cover by sectors

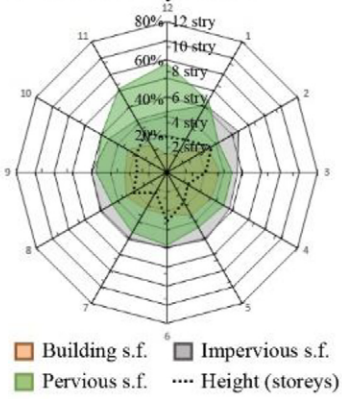

Sky View Factor in summer

Sensor location

Sky View Factor in winter

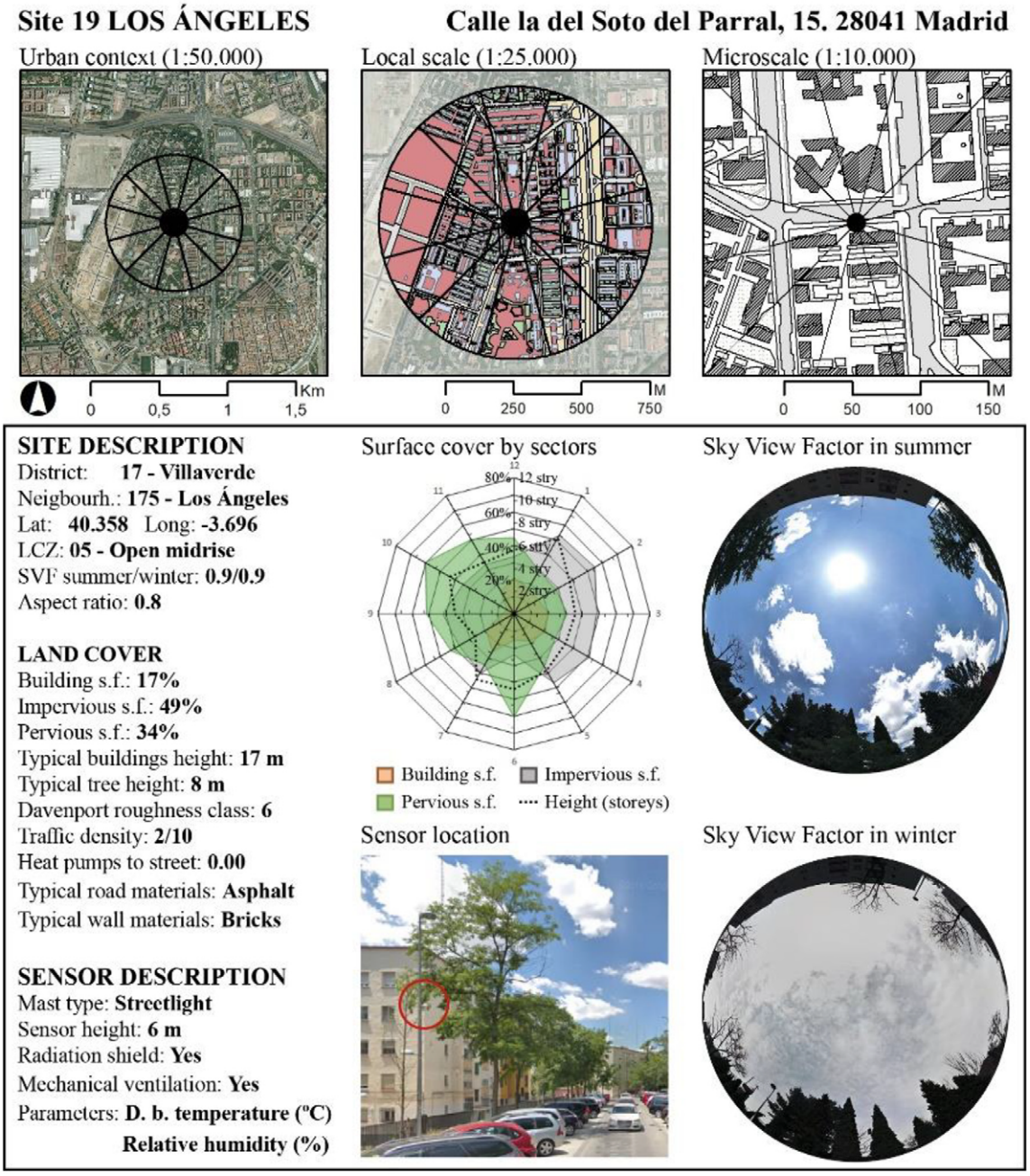
Site 19 LOS ÁNGELES
Calle la del Soto del Parral, 15. 28041 Madrid
Urban context (1:50.000)
Local scale (1:25.000)
Microscale (1:10.000)
Km
0 0,5 1 1,5
M
0 250 500 750
M
0 50 100 150
SITE DESCRIPTION
District: 17 - Villaverde
Neigbourh.: 175 - Los Ángeles
Lat: 40.358 Long: -3.696
LCZ: 05 - Open midrise
SVF summer/winter: 0.9/0.9
Aspect ratio: 0.8
LAND COVER
Building s.f.: 17%
Impervious s.f.: 49%
Pervious s.f.: 34%
Typical buildings height: 17 m
Typical tree height: 8 m
Davenport roughness class: 6
Traffic density: 2/10
Heat pumps to street: 0.00
Typical road materials: Asphalt
Typical wall materials: Bricks
SENSOR DESCRIPTION
Mast type: Streetlight
Sensor height: 6 m
Radiation shield: Yes
Mechanical ventilation: Yes
Parameters: D. b. temperature (ºC)
Relative humidity (%)
Surface cover by sectors
80%
60%
40%
20%
12 stry
10 stry
8 stry
6 stry
4 stry
2 stry
Building s.f.
Impervious s.f.
Pervious s.f.
Height (storeys)
Sky View Factor in summer
Sensor location
Sky View Factor in winter

Site 20 CANILLEJAS **Calle de San Narciso, 19. 28022 Madrid**

Urban context (1:50.000)

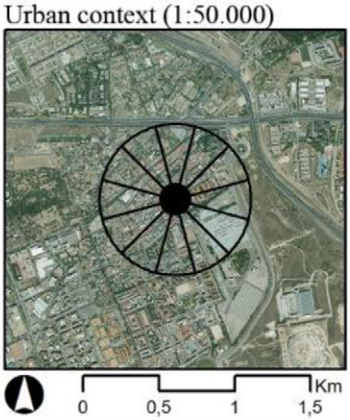

Local scale (1:25.000)

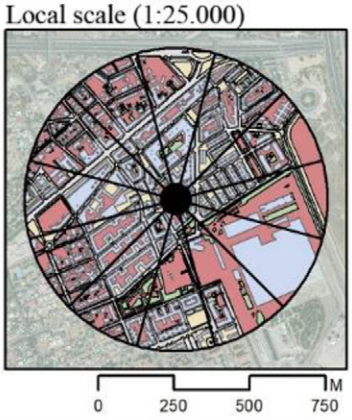

Microscale (1:10.000)

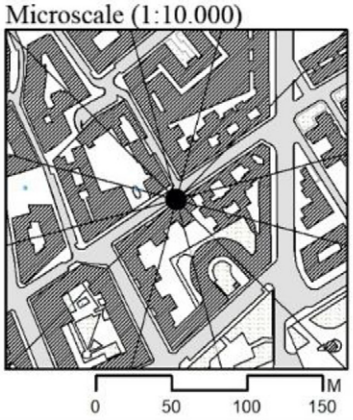

SITE DESCRIPTION
District: **20 - San Blas-Canillejas**
Neigbourh.: **207 - Canillejas**
Lat: **40.445** Long: **-3.610**
LCZ: **05 - Open midrise**
SVF summer/winter: **0.8/0.8**
Aspect ratio: **1.2**

LAND COVER
Building s.f.: **31%**
Impervious s.f.: **49%**
Pervious s.f.: **20%**
Typical buildings height: **14 m**
Typical tree height: -
Davenport roughness class: **7**
Traffic density: **2/10**
Heat pumps to street: **0.34**
Typical road materials: **Asphalt**
Typical wall materials: **Bricks**

SENSOR DESCRIPTION
Mast type: **Streetlight**
Sensor height: **6 m**
Radiation shield: **Yes**
Mechanical ventilation: **Yes**
Parameters: **D. b. temperature (ºC)**
Relative humidity (%)

Surface cover by sectors

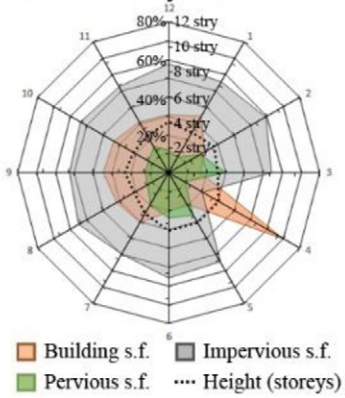

Sky View Factor in summer

Sensor location

Sky View Factor in winter

References

AEMET, 2019. Informe Anual 2018. Madrid, Spain.
Alexander, P.J., Mills, G., 2014. Local climate classification and Dublin's urban heat island. Atmosphere (Basel). 5, 755–774. https://doi.org/10.3390/atmos5040755.
Alexander, P.J., Bechtel, B., Chow, W.T.L., Fealy, R., Mills, G., 2016. Linking urban climate classification with an urban energy and water budget model: multi-site and multi-seasonal evaluation. Urban Clim. 17, 196–215. https://doi.org/10.1016/j.uclim.2016.08.003.
Ampatzidis, P., Kershaw, T., 2020. A review of the impact of blue space on the urban microclimate. Sci. Total Environ. 730, 139068. https://doi.org/10.1016/j.scitotenv.2020.139068.
Ando, T., Ueyama, M., 2017. Surface energy exchange in a dense urban built-up area based on two-year eddy covariance measurements in Sakai, Japan. Urban Clim. 19, 155–169. https://doi.org/10.1016/j.uclim.2017.01.005.
Arnds, D., Boehner, J., Bechtel, B., 2017. Spatio-temporal variance and meteorological drivers of the urban heat island in a European city. Theor. Appl. Climatol. 128, 43–61. https://doi.org/10.1007/s00704-015-1687-4.
Ayuntamiento de Madrid, 2013. Tráfico. Intensidad Media Diaria Anual por Tramos. Ayuntamiento de Madrid (Portal de datos abiertos).
Ayuntamiento de Madrid, 2015. Cartografía municipal por distritos a escala 1:1000. Ayuntamiento de Madrid (Portal de datos abiertos).
Barlow, J.F., 2014. Progress in observing and modelling the urban boundary layer. Urban Clim. 10, 216–240. https://doi.org/10.1016/j.uclim.2014.03.011.
Bechtel, B., Alexander, P.J., Böhner, J., Ching, J., Conrad, O., Feddema, J., Mills, G., See, L., Stewart, I.D., 2015. Mapping local climate zones for a worldwide database of the form and function of cities. ISPRS Int. J. Geo-Inform. 4, 199–219. https://doi.org/10.3390/ijgi4010199.
Bechtel, B., Alexander, P.J., Beck, C., Böhner, J., Brousse, O., Ching, J., Demuzere, M., Fonte, C., Gál, T., Hidalgo, J., Hoffmann, P., Middel, A., Mills, G., Ren, C., See, L., Sismanidis, P., Verdonck, M.L., Xu, G., Xu, Y., 2019. Generating WUDAPT level 0 data – current status of production and evaluation. Urban Clim. 27, 24–45. https://doi.org/10.1016/j.uclim.2018.10.001.
Beck, C., Straub, A., Breitner, S., Cyrys, J., Philipp, A., Rathmann, J., Schneider, A., Wolf, K., Jacobeit, J., 2018. Air temperature characteristics of local climate zones in the Augsburg urban area (Bavaria, southern Germany) under varying synoptic conditions. Urban Clim. 25, 152–166. https://doi.org/10.1016/j.uclim.2018.04.007.
Bell, S., Cornford, D., Bastin, L., 2015. How good are citizen weather stations? Addressing a biased opinion. Weather 70, 75–84. https://doi.org/10.1002/wea.2316.
Best, M.J., Grimmmmond, C.S.B., 2015. Key conclusions of the first international urban land surface model comparison project. Bull. Am. Meteorol. Soc. 96, 805–819. https://doi.org/10.1175/BAMS-D-14-00122.1.
Borbora, J., Das, A.K., 2014. Summertime urban Heat Island study for Guwahati City, India. Sustain. Cities Soc. 11, 61–66. https://doi.org/10.1016/j.scs.2013.12.001.
Brousse, O., Martilli, A., Foley, M., Mills, G., Bechtel, B., 2016. WUDAPT, an efficient land use producing data tool for mesoscale models? Integration of urban LCZ in WRF over Madrid. Urban Clim. 17, 116–134. https://doi.org/10.1016/j.uclim.2016.04.001.
Budhiraja, B., Agrawal, G., Pathak, P., 2020. Urban heat island effect of a polynuclear megacity Delhi – compactness and thermal evaluation of four sub-cities. Urban Clim. 32, 100634. https://doi.org/10.1016/j.uclim.2020.100634.
Chandler, T.J., 1965. The Climate of London. Hutchinson of London, London.
Chapman, L., Bell, C., Bell, S., 2017. Can the crowdsourcing data paradigm take atmospheric science to a new level? A case study of the urban heat island of London quantified using Netatmo weather stations. Int. J. Climatol. 37, 3597–3605. https://doi.org/10.1002/joc.4940.
Ching, J.K.S., 2013. A perspective on urban canopy layer modeling for weather, climate and air quality applications. Urban Clim. 3, 13–39. https://doi.org/10.1016/j.uclim.2013.02.001.
Christen, A., 2014. Atmospheric measurement techniques to quantify greenhouse gas emissions from cities. Urban Clim. 10, 241–260. https://doi.org/10.1016/j.uclim.2014.04.006.
Coseo, P., Larsen, L., 2014. How factors of land use/land cover, building configuration, and adjacent heat sources and sinks explain urban Heat Islands in Chicago. Landsc. Urban Plan. 125, 117–129. https://doi.org/10.1016/j.landurbplan.2014.02.019.
Crawford, B., Christen, A., 2015. Spatial source attribution of measured urban eddy covariance CO2 fluxes. Theor. Appl. Climatol. 119, 733–755. https://doi.org/10.1007/s00704-014-1124-0.
Doan, V.Q., Kusaka, H., Nguyen, T.M., 2019. Roles of past, present, and future land use and anthropogenic heat release changes on urban heat island effects in Hanoi, Vietnam: numerical experiments with a regional climate model. Sustain. Cities Soc. 47, 101479. https://doi.org/10.1016/j.scs.2019.101479.
Dodman, D., 2009. Blaming cities for climate change? An analysis of urban greenhouse gas emissions inventories. Environ. Urban. 21, 185–201. https://doi.org/10.1177/0956247809103016.
Eastin, M.D., Baber, M., Boucher, A., Di Bari, S., Hubler, R., Stimac-Spalding, B., Winesett, T., 2018. Temporal variability of the Charlotte (sub)urban heat island. J. Appl. Meteorol. Climatol. 57, 81–102. https://doi.org/10.1175/JAMC-D-17-0099.1.
Emmanuel, R., Krüger, E., 2012. Urban heat island and its impact on climate change resilience in a shrinking city: the case of Glasgow, UK. Build. Environ. 53, 137–149. https://doi.org/10.1016/j.buildenv.2012.01.020.
Erell, E., Williamson, T., 2007. Intra-urban differences in canopy layer air temperature at a mid-latitude city. Int. J. Climatol. 27, 1243–1255. https://doi.org/10.1002/joc.1469.
Erell, E., Leal, V., Maldonado, E., 2005. Measurement of air temperature in the presence of a large radiant flux: an assessment of passively ventilated thermometer screens. Boundary-Layer Meteorol. 114, 205–231. https://doi.org/10.1007/s10546-004-8946-8.
Eurostat, 2020. Population on 1 January by Age Groups and Sex - Functional Urban Areas (URB_LPOP1).
Feigenwinter, C., Vogt, R., Christen, A., 2012. Eddy covariance measurements over urban areas. In: Aubinet, M., Vesala, T., Papale, D. (Eds.), Eddy Covariance: A Practical Guide to Measurement and Data. Springer Science and Business Media, pp. 377–397. https://doi.org/10.1007/978-94-007-2351-1.
Fenner, D., Meier, F., Scherer, D., Polze, A., 2014. Spatial and temporal air temperature variability in Berlin, Germany, during the years 2001-2010. Urban Clim. 10, 308–331. https://doi.org/10.1016/j.uclim.2014.02.004.
Fenner, D., Meier, F., Bechtel, B., Otto, M., Scherer, D., 2017. Intra and inter "local climate zone" variability of air temperature as observed by crowdsourced citizen weather stations in Berlin, Germany. Meteorol. Z. 26, 525–547. https://doi.org/10.1127/metz/2017/0861.
Fernández García, F., Almendros Coca, M.Á., López Gómez, A., 1996. La influencia del relieve en la isla de calor de Madrid: las vaguadas del Manzanares y del Abroñigal. Estud. Geográficos 57, 473–494.
Fernández García, F., Allende Álvarez, F., Rasilla Álvarez, D., Martilli, A., Alcaide Muñoz, J., 2016. Estudio de Detalle Del Clima Urbano de Madrid. Madrid.
Figuerola, P.I., Mazzeo, N.a., 1998. Urban-rural temperature differences in Buenos Aires. Int. J. Climatol. 18, 1709–1723. https://doi.org/10.1002/(SICI)1097-0088(199812)18:15<1709::AID-JOC338>3.0.CO;2-I.
Gardes, T., Schoetter, R., Hidalgo, J., Long, N., Marquès, E., Masson, V., 2020. Statistical prediction of the nocturnal urban heat island intensity based on urban morphology and geographical factors - an investigation based on numerical model results for a large ensemble of French cities. Sci. Total Environ. 737, 139253. https://doi.org/10.1016/j.scitotenv.2020.139253.
Geiger, R., 1950. The Climate near the Ground. Blue Hill Meteorological Observatory, Harvard University, Cambridge.
Grimmond, C.S.D., Blackett, M., Best, M.J., Barlow, J., Baik, J.-J., Belcher, S.E., Bohnenstengel, S.I., Calmet, I., Chen, F., Dandou, A., Fortuniak, K., Gouvea, M.L., Hamdi, R., Hendry, M., Kawai, T., Kawamoto, Y., Kondo, H., Krayenhoff, E.S., Lee, S.-H., Loridan, T., Martilli, A., Masson, V., Miao, S., Oleson, K., Pigeon, G., Porson, A., Ryu, Y.-H., Salamanca, F., Shashua-Bar, L., Steeneveld, G.-J., Tombrou, M., Voogt, J., Young, D., Zhang, N., 2010. The international urban energy balance models comparison project: first results from phase 1. J. Appl. Meteorol. Climatol. 49, 1268–1292. https://doi.org/10.1175/2010JAMC2354.1.
Grimmond, C.S.D., Blackett, M., Best, M.J., Baik, J.-J., Belcher, S.E., Beringer, J., Bohnenstengel, S.I., Calmet, I., Chen, F., Coutts, A., Dandou, A., Fortuniak, K., Gouvea, M.L., Hamdi, R., Hendry, M., Kanda, M., Kawai, T., Kawamoto, Y., Kondo, H., Krayenhoff, E.S., Lee, S.-H., Loridan, T., Martilli, A., Masson, V., Miao, S., Oleson, K., Ooka, R., Pigeon, G., Porson, A., Ryu, Y.-H., Salamanca, F., Steeneveld, G.-J., Tombrou, M., Voogt, J.A., Young, D.T., Zhang, N., 2011. Initial results from phase 2 of the international urban energy balance model comparison. Int. J. Climatol. 31, 244–272. https://doi.org/10.1002/joc.2227.

Hammerberg, K., Brousse, O., Martilli, A., Mahdavi, A., 2018. Implications of employing detailed urban canopy parameters for mesoscale climate modelling: a comparison between WUDAPT and GIS databases over Vienna, Austria. Int. J. Climatol. 38, e1241–e1257. https://doi.org/10.1002/joc.5447.
Hebbert, M., 2014. Climatology for city planning in historical perspective. Urban Clim. 10, 204–215. https://doi.org/10.1016/j.uclim.2014.07.001.
Hidalgo, J., Jougla, R., 2018. On the use of local weather types classification to improve climate understanding: an application on the urban climate of Toulouse. PLoS One 13, 1–21. https://doi.org/10.1371/journal.pone.0208138.
Holmer, B., Thorsson, S., Eliasson, I., 2007. Cooling rates, sky view factors and the development of intra-urban air temperature difference. Geogr. Ann. Ser. A Phys. Geogr. 89 (A), 237–248. https://doi.org/10.1111/j.1468-0459.2007.00323.x.
Howard, L., 1833. The Climate of London. Harvey and Darton, London.
Jandaghian, Z., Berardi, U., 2020. Comparing urban canopy models for microclimate simulations in weather research and forecasting models. Sustain. Cities Soc. 55, 102025. https://doi.org/10.1016/j.scs.2020.102025.
Jänicke, B., Holtmann, A., Kim, K.R., Kang, M., Fehrenbach, U., Scherer, D., 2018. Quantification and evaluation of intra-urban heat-stress variability in Seoul, Korea. Int. J. Biometeorol. https://doi.org/10.1007/s00484-018-1631-2.
Jianan, X., Zhiyun, O., Hua, Z., Xiaoke, W., Hong, M., 2007. Allergenic pollen plants and their influential factors in urban areas. Acta Ecol. Sin. 27, 3820–3827. https://doi.org/10.1016/S1872-2032(07)60082-1.
Jochner, S.C., Beck, I., Behrendt, H., Traidl-Hoffmann, C., Menzel, A., 2011. Effects of extreme spring temperatures on urban phenology and pollen production: a case study in Munich and Ingolstadt. Clim. Res. 49, 101–112. https://doi.org/10.3354/cr01022.
Karl, T., Gohm, A., Rotach, M.W., Ward, H.C., Graus, M., Cede, A., Wohlfahrt, G., Hammerle, A., Haid, M., Tiefengraber, M., Lamprecht, C., Vergeiner, J., Kreuter, A., Wagner, J., Staudinger, M., 2020. Studying urban climate and air quality in the alps. Bull. Am. Meteorol. Soc. 101, E488–E507. https://doi.org/10.1175/BAMS-D-19-0270.1.
Klysik, K., Fortuniak, K., 1999. Temporal and spatial characteristics of the urban heat island of Lodz, Poland. Atmos. Environ. 33, 3885–3895. https://doi.org/10.1016/S1352-2310(99)00131-4.
Kolokotroni, M., Ren, X., Davies, M., Mavrogianni, A., 2012. London's urban heat island: impact on current and future energy consumption in office buildings. Energy Build. 47, 302–311. https://doi.org/10.1016/j.enbuild.2011.12.019.
Kotharkar, R., Bagade, A., 2018. Evaluating urban heat island in the critical local climate zones of an Indian city. Landsc. Urban Plan. 169, 92–104. https://doi.org/10.1016/j.landurbplan.2017.08.009.
Kotharkar, R., Bagade, A., Ramesh, A., 2019. Assessing urban drivers of canopy layer urban heat island: a numerical modeling approach. Landsc. Urban Plan. 190, 103586. https://doi.org/10.1016/j.landurbplan.2019.05.017.
Kottek, M., Grieser, J., Beck, C., Rudolf, B., Rubel, F., 2006. World map of the Köppen-Geiger climate classification updated. Meteorol. Z. 15, 259–263. https://doi.org/10.1127/0941-2948/2006/0130.
Kotthaus, S., Grimmond, C.S.B., 2014. Energy exchange in a dense urban environment - part I: temporal variability of long-term observations in Central London. Urban Clim. 10, 261–280. https://doi.org/10.1016/j.uclim.2013.10.002.
Kourtidis, K., Georgoulias, A.K., Rapsomanikis, S., Amiridis, V., Keramitsoglou, I., Hooyberghs, H., Maiheu, B., Melas, D., 2015. A study of the hourly variability of the urban heat island effect in the greater Athens area during summer. Sci. Total Environ. 517, 162–177. https://doi.org/10.1016/j.scitotenv.2015.02.062.
Kratzer, A., 1937. Das Stadtklima. Friedr. Vieweg and Sohn Braunschweig, Braunschweig.
Kurppa, M., Nordbo, A., Haapanala, S., Järvi, L., 2015. Effect of seasonal variability and land use on particle number and CO2 exchange in Helsinki, Finland. Urban Clim. 13, 94–109. https://doi.org/10.1016/j.uclim.2015.07.006.
Kwok, Y.T., Schoetter, R., Lau, K.K.L., Hidalgo, J., Ren, C., Pigeon, G., Masson, V., 2019. How well does the local climate zone scheme discern the thermal environment of Toulouse (France)? An analysis using numerical simulation data. Int. J. Climatol. 39, 5292–5315. https://doi.org/10.1002/joc.6140.
Lauzet, N., Rodler, A., Musy, M., Azam, M.H., Guernouti, S., Mauree, D., Colinart, T., 2019. How building energy models take the local climate into account in an urban context – a review. Renew. Sust. Energ. Rev. 116, 109390. https://doi.org/10.1016/j.rser.2019.109390.
Leconte, F., Bouyer, J., Claverie, R., Pétrissans, M., 2015. Using local climate zone scheme for UHI assessment: evaluation of the method using mobile measurements. Build. Environ. 83, 39–49. https://doi.org/10.1016/j.buildenv.2014.05.005.
Leconte, F., Bouyer, J., Claverie, R., Pétrissans, M., 2017. Analysis of nocturnal air temperature in districts using mobile measurements and a cooling indicator. Theor. Appl. Climatol. 130, 365–376. https://doi.org/10.1007/s00704-016-1886-7.
Leconte, F., Bouyer, J., Claverie, R., 2020. Nocturnal cooling in local climate zone: statistical approach using mobile measurements. Urban Clim. 33, 100629. https://doi.org/10.1016/j.uclim.2020.100629.
Lehnert, M., Geletič, J., Husák, J., Vysoudil, M., 2015. Urban field classification by "local climate zones" in a medium-sized central European city: the case of Olomouc (Czech Republic). Theor. Appl. Climatol. 122, 531–541. https://doi.org/10.1007/s00704-014-1309-6.
Lelovics, E., Unger, J., Gal, T., Gal, C.V., Gál, T., Gál, C.V., 2014. Design of an urban monitoring network based on local climate zone mapping and temperature pattern modelling. Clim. Res. 60, 51–62. https://doi.org/10.3354/cr01220.
Li, X., Ratti, C., Seiferling, I., 2017. Mapping urban landscapes along streets using Google street view. Adv. Cartogr. GIScience 341–356. https://doi.org/10.1007/978-3-319-57336-6_24.
López-Bueno, J., Díaz, J., Linares, C., 2019. Differences in the impact of heat waves according to urban and peri-urban factors in Madrid. Int. J. Biometeorol. https://doi.org/10.1007/s00484-019-01670-9.
López-Bueno, J.A., Díaz, J., Sánchez-Guevara, C., Sánchez-Martínez, G., Franco, M., Gullón, P., Núñez Peiró, M., Valero, I., Linares, C., 2020. The impact of heat waves on daily mortality in districts in Madrid: the effect of sociodemographic factors. Environ. Res. 190, 109993. https://doi.org/10.1016/j.envres.2020.109993.
Meier, F., Fenner, D., Grassmann, T., Otto, M., Scherer, D., 2017. Crowdsourcing air temperature from citizen weather stations for urban climate research. Urban Clim. 19, 170–191. https://doi.org/10.1016/j.uclim.2017.01.006.
Menzer, O., McFadden, J.P., 2017. Statistical partitioning of a three-year time series of direct urban net CO2flux measurements into biogenic and anthropogenic components. Atmos. Environ. 170, 319–333. https://doi.org/10.1016/j.atmosenv.2017.09.049.
Miao, C., Yu, S., Hu, Y., Zhang, H., He, X., Chen, W., 2020. Review of methods used to estimate the sky view factor in urban street canyons. Build. Environ. 168, 106497. https://doi.org/10.1016/j.buildenv.2019.106497.
Mills, G., 2014. Urban climatology: history, status and prospects. Urban Clim. 10, 479–489. https://doi.org/10.1016/j.uclim.2014.06.004.
Ministerio de Hacienda, 2019. Catastro inmobiliario. Gobierno de España (Dir. Gen. del Catastro).
Mirzaei, P.A., 2015. Recent challenges in modeling of urban heat island. Sustain. Cities Soc. 1–7. https://doi.org/10.1016/j.scs.2015.04.001.
Molnár, G., Kovács, A., Gál, T., 2020. How does anthropogenic heating affect the thermal environment in a medium-sized central European city? A case study in Szeged, Hungary. Urban Clim. 34, 100673. https://doi.org/10.1016/j.uclim.2020.100673.
Muller, C.L., Chapman, L., Grimmond, C.S.B., Young, D.T., Cai, X.M., 2013. Toward a standardized metadata protocol for urban meteorological networks. Bull. Am. Meteorol. Soc. 94, 1161–1185. https://doi.org/10.1175/BAMS-D-12-00096.1.
Núñez Peiró, M., Sánchez-Guevara, C., Neila González, F.J., 2017. Update of the urban heat island of Madrid and its influence on the building's energy simulation. In: Sustainable Development and Renovation in Architecture, Urbanism and Engineering, pp. 339–350. https://doi.org/10.1007/978-3-319-51442-0_28.
Núñez Peiró, M., Sánchez-Guevara Sánchez, C., Neila González, F.J., 2018. Abrigo Meteorológico Para Sensores Ambientales. ES-2642617-B2.
Núñez Peiró, M., Sánchez-Guevara Sánchez, C., Neila González, F.J., 2019. Source area definition for local climate zones studies. A systematic review. Build. Environ. 148, 258–285. https://doi.org/10.1016/j.buildenv.2018.10.050.
Oke, T.R., 1982. The energetic basis of the urban heat island. Q. J. R. Meteorol. Soc. 108, 1–24. https://doi.org/10.1002/qj.49710845502.
Oke, T.R., 1998. An algorithm scheme to estimate hourly heat island magnitude. In: The Second Symposium on Urban Environment. American Meteorological Society, Albuquerque.
Oke, T.R., Mills, G., Christen, A., Voogt, J.A., 2017a. 2 concepts. In: Urban Climates. Cambridge University Press, pp. 14–43. https://doi.org/10.1017/9781139016476.003.

Oke, T.R., Mills, G., Christen, A., Voogt, J.A., 2017b. 4 airflow. In: Urban Climates. Cambridge University Press, pp. 77–121. https://doi.org/10.1017/9781139016476.005.
Pawlak, W., Fortuniak, K., 2016. Eddy covariance measurements of the net turbulent methane flux in the city Centre-results of 2-year campaign in Lodz, Poland. Atmos. Chem. Phys. 16, 8281–8294. https://doi.org/10.5194/acp-16-8281-2016.
Perera, N.G., Emmanuel, R., 2016. A "local climate zone" based approach to urban planning in Colombo, Sri Lanka. Urban Clim. https://doi.org/10.1016/j.uclim.2016.11.006.
Puliafito, S.E., Bochaca, F.R., Allende, D.G., Fernandez, R., 2013. Green areas and microscale thermal comfort in arid environments: a case study in Mendoza, Argentina. Atmos. Clim. Sci. 03, 372–384. https://doi.org/10.4236/acs.2013.33039.
Pyrgou, A., Castaldo, V.L., Pisello, A.L., Cotana, F., Santamouris, M., 2017. Differentiating responses of weather files and local climate change to explain variations in building thermal-energy performance simulations. Sol. Energy 153, 224–237. https://doi.org/10.1016/j.solener.2017.05.040.
Reckien, D., Salvia, M., Heidrich, O., Church, J.M., Pietrapertosa, F., De Gregorio-Hurtado, S., D'Alonzo, V., Foley, A., Simoes, S.G., Krkoška Lorencová, E., Orru, H., Orru, K., Wejs, A., Flacke, J., Olazabal, M., Geneletti, D., Feliu, E., Vasilie, S., Nador, C., Krook-Riekkola, A., Matosović, M., Fokaides, P.A., Ioannou, B.I., Flamos, A., Spyridaki, N.A., Balzan, M.V., Fülöp, O., Paspaldzhiev, I., Grafakos, S., Dawson, R., 2018. How are cities planning to respond to climate change? Assessment of local climate plans from 885 cities in the EU-28. J. Clean. Prod. 191, 207–219. https://doi.org/10.1016/j.jclepro.2018.03.220.
Renou, P.M.E., 1858. Instructions Météorologiques et Tables Usuelles. Société Météorologique de France, Paris.
Richard, Y., Emery, J., Dudek, J., Pergaud, J., Chateau-Smith, C., Zito, S., Rega, M., Vairet, T., Castel, T., Thévenin, T., Pohl, B., 2018. How relevant are local climate zones and urban climate zones for urban climate research? Dijon (France) as a case study. Urban Clim. 26, 258–274. https://doi.org/10.1016/j.uclim.2018.10.002.
Roth, M., Jansson, C., Velasco, E., 2016. Multi-year energy balance and carbon dioxide fluxes over a residential neighbourhood in a tropical city. Int. J. Climatol. 37, 2679–2698. https://doi.org/10.1002/joc.4873.
Rubel, F., Brugger, K., Haslinger, K., Auer, I., 2017. The climate of the European Alps: shift of very high resolution Köppen-Geiger climate zones 1800-2100. Meteorol. Z. 26, 115–125. https://doi.org/10.1127/metz/2016/0816.
Runnalls, K.E., Oke, T.R., 2006. A techique to detect microclimatic inhomogeneities in historical records of screen-level air temperature. J. Clim. 19, 959–978. https://doi.org/10.1175/JCLI3663.1.
Rusel, F.A.R., 1888. Smoke in relation to fogs in London. Nature 39, 34–36. https://doi.org/10.1038/039034a0.
Sánchez-Guevara, C., Núñez Peiró, M., Taylor, J., Mavrogianni, A., Neila González, J., 2019. Assessing population vulnerability towards summer energy poverty: case studies of Madrid and London. Energy Build. 190, 132–143. https://doi.org/10.1016/j.enbuild.2019.02.024.
Schatz, J., Kucharik, C.J., 2014. Seasonality of the urban Heat Island effect in Madison, Wisconsin. J. Appl. Meteorol. Climatol. 53, 2371–2386. https://doi.org/10.1175/JAMC-D-14-0107.1.
Šećerov, I.B., Savić, S.M., Milošević, D.D., Arsenović, D.M., Dolinaj, D.M., Popov, S.B., 2019. Progressing urban climate research using a high-density monitoring network system. Environ. Monit. Assess. 191 https://doi.org/10.1007/s10661-019-7210-0.
Shi, Y., Ren, C., Lau, K.K.L., Ng, E., 2019. Investigating the influence of urban land use and landscape pattern on PM2.5 spatial variation using mobile monitoring and WUDAPT. Landsc. Urban Plan. 189, 15–26. https://doi.org/10.1016/j.landurbplan.2019.04.004.
Siu, L.W., Hart, M.A., 2013. Quantifying urban heat island intensity in Hong Kong SAR, China. Environ. Monit. Assess. 185, 4383–4398. https://doi.org/10.1007/s10661-012-2876-6.
Skarbit, N., Stewart, I.D., Unger, J., Gál, T., 2017. Employing an urban meteorological network to monitor air temperature conditions in the "local climate zones" of Szeged, Hungary. Int. J. Climatol. https://doi.org/10.1002/joc.5023.
Stewart, I.D., 2019. Why should urban heat island researchers study history? Urban Clim. 30, 100484. https://doi.org/10.1016/j.uclim.2019.100484.
Stewart, I.D., Oke, T.R., 2012. Local climate zones for urban temperature studies. Bull. Am. Meteorol. Soc. 93, 1879–1900. https://doi.org/10.1175/BAMS-D-11-00019.1.
Stewart, I.D., Oke, T.R., Krayenhoff, E.S., 2014. Evaluation of the "local climate zone" scheme using temperature observations and model simulations. Int. J. Climatol. 34, 1062–1080. https://doi.org/10.1002/joc.3746.
Suomi, J., 2018. Extreme temperature differences in the city of Lahti, southern Finland : intensity, seasonality and environmental drivers. Weather Clim. Extrem. 19, 20–28. https://doi.org/10.1016/j.wace.2017.12.001.
Thapa Chhetri, D.B., Fujimori, Y., Moriwaki, R., 2017. Local climate classification and urban heat/dry island in Matsuyama plain. J. Japan Soc. Civ. Eng. Ser. B1 (Hydraulic Eng.) 73. https://doi.org/10.2208/jscejhe.73.i_487. I_487-I_492.
Theeuwes, N.E., Steeneveld, G.J., Ronda, R.J., Holtslag, A.A.M., 2017. A diagnostic equation for the daily maximum urban heat island effect for cities in northwestern Europe. Int. J. Climatol. 37, 443–454. https://doi.org/10.1002/joc.4717.
Thomas, G., Sherin, A.P., Ansar, S., Zachariah, E.J., 2014. Analysis of urban Heat Island in Kochi, India, using a modified local climate zone classification. Procedia Environ. Sci. 21, 3–13. https://doi.org/10.1016/j.proenv.2014.09.002.
Toparlar, Y., Blocken, B., Maiheu, B., van Heijst, G.J.F., 2017. A review on the CFD analysis of urban microclimate. Renew. Sust. Energ. Rev. 80, 1613–1640. https://doi.org/10.1016/j.rser.2017.05.248.
Unger, J., Gál, T., Csépe, Z., Lelovics, E., Gulyás, Á., 2015. Development, data processing and preliminary results of an urban human comfort monitoring and information system. Idojaras 119, 337–354.
Universidad Politécnica de Madrid, 2014. MODIFICA Project: Predictive Model for Dwellings Energy Performance Under the Urban Heat Island Effect. Minist. Econ. Compet. BIA2013–41732-R.
Valach, A.C., Langford, B., Nemitz, E., Mackenzie, A.R., Hewitt, C.N., 2015. Seasonal and diurnal trends in concentrations and fluxes of volatile organic compounds in Central London. Atmos. Chem. Phys. 15, 7777–7796. https://doi.org/10.5194/acp-15-7777-2015.
Varentsov, M., Konstantinov, P., Baklanov, A., Esau, I., Miles, V., Davy, R., 2018. Anthropogenic and natural drivers of a strong winter urban heat island in a typical Arctic city. Atmos. Chem. Phys. 18, 17573–17587. https://doi.org/10.5194/acp-18-17573-2018.
Velasco, E., 2018. Go to field, look around, measure and then run models. Urban Clim. 24, 231–236. https://doi.org/10.1016/j.uclim.2018.04.001.
Velasco, E., Perrusquia, R., Jiménez, E., Hernández, F., Camacho, P., Rodríguez, S., Retama, A., Molina, L.T., 2014. Sources and sinks of carbon dioxide in a neighborhood of Mexico City. Atmos. Environ. 97, 226–238. https://doi.org/10.1016/j.atmosenv.2014.08.018.
Verdonck, M.L., Demuzere, M., Hooyberghs, H., Beck, C., Cyrys, J., Schneider, A., Dewulf, R., Van Coillie, F., 2018. The potential of local climate zones maps as a heat stress assessment tool, supported by simulated air temperature data. Landsc. Urban Plan. 178, 183–197. https://doi.org/10.1016/j.landurbplan.2018.06.004.
Willers, S.M., Jonker, M.F., Klok, L., Keuken, M.P., Odink, J., van den Elshout, S., Sabel, C.E., Mackenbach, J.P., Burdorf, A., 2016. High resolution exposure modelling of heat and air pollution and the impact on mortality. Environ. Int. 89–90, 102–109. https://doi.org/10.1016/j.envint.2016.01.013.
WMO, 2017a. Guide to Meteorological Instruments and Methods of Observation (WMO No. 8). World Meteorological Organization, Geneva, Switzerland.
WMO, 2017b. Guide to the Global Observing System (WMO No. 488). Geneva, Switzerland.
WMO, 2020. OSCAR - Observing Systems Capability Analysis and Review Tool [WWW Document]. URL. https://oscar.wmo.int/surface/ (accessed 4.28.21).
Yagüe, C., Zurita, E., Martinez, A., 1991. Statistical analysis of the Madrid urban heat island. Atmos. Environ. 25, 327–332. https://doi.org/10.1016/0957-1272(91)90004-X.
Yang, P., Ren, G., Liu, W., 2013. Spatial and temporal characteristics of Beijing urban Heat Island intensity. J. Appl. Meteorol. Climatol. 52, 1803–1816. https://doi.org/10.1175/JAMC-D-12-0125.1.
Yang, X., Yao, L., Jin, T., Peng, L.L.H., Jiang, Z., Hu, Z., Ye, Y., 2018. Assessing the thermal behavior of different local climate zones in the Nanjing metropolis, China. Build. Environ. 137, 171–184. https://doi.org/10.1016/j.buildenv.2018.04.009.
Yang, X., Chen, Y., Peng, L.L.H., Wang, Q., 2020a. Quantitative methods for identifying meteorological conditions conducive to the development of urban heat islands. Build. Environ. 178, 106953. https://doi.org/10.1016/j.buildenv.2020.106953.

Yang, X., Peng, L.L.H., Chen, Y., Yao, L., Wang, Q., 2020b. Air humidity characteristics of local climate zones: a three-year observational study in Nanjing. Build. Environ. 171, 106661. https://doi.org/10.1016/j.buildenv.2020.106661.
Yuan, C., Adelia, A.S., Mei, S., He, W., Li, X.X., Norford, L., 2020. Mitigating intensity of urban heat island by better understanding on urban morphology and anthropogenic heat dispersion. Build. Environ. 176, 106876. https://doi.org/10.1016/j.buildenv.2020.106876.
Zahumensky, I., 2004. Guidelines on Quality Control Procedures for Data from Automatic Weather Stations. Geneva, Switzerland.
Zhou, X., Okaze, T., Ren, C., Cai, M., Ishida, Y., Watanabe, H., Mochida, A., 2020. Evaluation of urban heat islands using local climate zones and the influence of sea-land breeze. Sustain. Cities Soc. 55, 102060. https://doi.org/10.1016/j.scs.2020.102060.
Zuvela-Aloise, M., 2017. Enhancement of urban heat load through social inequalities on an example of a fictional city King's landing. Int. J. Biometeorol. 61, 527–539. https://doi.org/10.1007/s00484-016-1230-z.

8. Artículo 3 Research paper 3

Modelling long-term urban temperatures with less training data: A comparative study using neural networks in the city of Madrid

Núñez-Peiró, M., Mavrogianni, A., Symonds, P., Sánchez-Guevara Sánchez, C., Neila González, F.J. (2021)

Sustainability, 13(15), 8143.

doi: 10.3390/su13158143

Índice de impacto:

JIF = 3.251 (**JCR Q2**, *Environmental Sciences*)

SJR = 0.612 (**SJR Q1**, *Geography, Planning and Development*)

PARTE III
PART III

sustainability

MDPI

Article

Modelling Long-Term Urban Temperatures with Less Training Data: A Comparative Study Using Neural Networks in the City of Madrid

Miguel Núñez-Peiró [1,*], Anna Mavrogianni [2], Phil Symonds [2], Carmen Sánchez-Guevara Sánchez [1] and F. Javier Neila González [1]

[1] School of Architecture, Universidad Politécnica de Madrid, Avda. Juan de Herrera 4, 28040 Madrid, Spain; carmen.sanchezguevara@upm.es (C.S.-G.S.); fjavier.neila@upm.es (F.J.N.G.)
[2] Institute of Environmental Design and Engineering, University College London, Central House, 14 Woburn Place, London WC1H 0NN, UK; a.mavrogianni@ucl.ac.uk (A.M.); p.symonds@ucl.ac.uk (P.S.)
* Correspondence: miguel.nunez@upm.es

Abstract: In the last decades, urban climate researchers have highlighted the need for a reliable provision of meteorological data in the local urban context. Several efforts have been made in this direction using Artificial Neural Networks (ANN), demonstrating that they are an accurate alternative to numerical approaches when modelling large time series. However, existing approaches are varied, and it is unclear how much data are needed to train them. This study explores whether the need for training data can be reduced without overly compromising model accuracy, and if model reliability can be increased by selecting the UHI intensity as the main model output instead of air temperature. These two approaches were compared using a common ANN configuration and under different data availability scenarios. Results show that reducing the training dataset from 12 to 9 or even 6 months would still produce reliable results, particularly if the UHI intensity is used. The latter proved to be more effective than the temperature approach under most training scenarios, with an average RMSE improvement of 16.4% when using only 3 months of data. These findings have important implications for urban climate research as they can potentially reduce the duration and cost of field measurement campaigns.

Keywords: urban heat island; microclimate; feed-forward neural networks; air temperature measurements; in-situ measurements; urban models; urban environment; climate change

Citation: Núñez-Peiró, M.; Mavrogianni, A.; Symonds, P.; Sánchez-Guevara Sánchez, C.; Neila González, F.J. Modelling Long-Term Urban Temperatures with Less Training Data: A Comparative Study Using Neural Networks in the City of Madrid. *Sustainability* **2021**, *13*, 8143. https://doi.org/10.3390/su13158143

Academic Editor: Roberto Alonso González Lezcano

Received: 17 June 2021
Accepted: 13 July 2021
Published: 21 July 2021

1. Introduction

In the context of raising awareness on climate change, a good understanding of urban climate phenomena is a key milestone in order to mitigate and adapt to thermal extremes within urban environments [1,2]. Cities are not only one of the main contributors to the greenhouse effect [3], but also places where many inequalities and therefore potential vulnerabilities accumulate [4–6]. Moreover, recent studies, such as those developed by Grimm et al. [7] and Youngsteadt [8], suggest that cities could provide important insights into the socio-ecological dynamics of our near future at a global scale, thus increasing the interest for reliable urban climatic data and expanding its applications to many other disciplines.

However, obtaining reliable climatic data within urban areas is still a challenging task due to the complexity of the urban climate. Nowadays, some of the most important advances concentrate on the modelling field [9]. Examples can be found evaluating the inter-relation between some parameters and the urban climate, such as the presence of water-bodies [10] or the emission of anthropogenic heat [11,12]. Regarding the accuracy of these numerical models, recent advances coupling urban canopy models with meso-climatic ones have also proved their overall reliability [13,14]. However, there are still some barriers that limit their applications in other fields. For example, Computational Fluid

Dynamics (CFD) has proved to be reliable for both building-scale models and relatively small urban areas (i.e., within a few hundred meters, [15,16]) but too computing intensive for larger domains [17,18]. Other authors, such as a Lauzet et al. [19], have highlighted that the high computational needs of high-resolution urban climate models pose a significant challenge in obtaining long-term datasets, therefore hindering their more widespread use of urban models within building energy simulations.

Conducting on-site measurement campaigns is also one of the most widespread practices towards improving urban climate knowledge [20,21]. They are still an essential component of numerical model validation processes [22]. Regarding meteorological parameters, experimental data is primarily derived from urban networks consisting of multiple sensors distributed across the city [23]. Several examples can be found in the literature for cities all around the globe, such as in Athens [24], London [25,26], Sendai [27], Szeged [28], Guangzhou [29], Kaohsiung [30], Guwahati [31], Augsburg [32], Nanjing [33,34], Rotterdam [35] or Berlin [36]. However, these urban networks are expensive to deploy and maintain, thus their use is usually constrained in time and space, limiting their suitability in long-term studies.

Other sources of experimental data might also present important drawbacks. Citizen Weather Stations (CWS) have grown exponentially in recent years [37,38] and are being used in a variety of ways, from studying the intra-urban temperature patterns [39] to complementing weather forecasts [40]. However, they require sophisticated filtering techniques and quality control procedures to manage their calibration bias, instrument errors and representativeness issues [41,42]. Mobile measurements, another widely adopted practice to study the spatial distribution of the UHI in detail, has expanded in recent years from the traditional approach of car transects [43–45] to bicycle transects [46–49] or even drone transects [50]. Despite their versatility, mobile measurements are very demanding in terms of human resources and can hardly be used to obtain time series at a fine scale (i.e., hourly). The latter is also one of the main drawbacks of remote sensing techniques, which depend on the timing of the satellite overpass, and require post-processing to address the presence of clouds and limited view angles [51].

1.1. Data-Driven Approaches for Modelling Outdoor Urban Temperatures

A widespread alternative technique for obtaining reliable and affordable long-term datasets of urban air temperatures is the development of empirical models. These models use pre-existing statistical correlations among available data to generate accurate projections without compromising their computational efficiency. Consequently, these data-driven approaches represent bespoke alternatives to more complex numerical models.

Several algorithms can be used for this purpose. A widely used technique for modelling urban temperatures is using Multiple Linear Regression (MLR), which has been tested for both temporal [52–55] and spatial predictions [56–60]. However, the increasing availability of machine learning and big data solutions is boosting the widespread use of other algorithms which, although potentially harder to interpret, are likely to improve their accuracy. Popular machine learning techniques include Support Vector Machines [61–64], Random Forest [58,60,62,65,66], or Artificial Neural Networks (ANN).

ANN seem to stand as the most popular approach for modelling the hourly evolution of outdoor urban temperatures. To the authors' knowledge, Mihalakakou et al. [67] presented the first attempt to model the outdoor temperature at an urban site using ANNs. They used the dry-bulb temperature data available from two existing meteorological stations in Athens: one located within the city (the target), and one at the outskirts (the reference site). In a follow-up study, the model was adapted for other urban sites in the same city, where they deployed a network of 23 temperature sensors across the city for 2 years [68,69].

In these early attempts to model urban temperatures using ANNs, the authors only used the air temperature from the reference site as the input. However, other researchers have explored the inclusion of additional predictors to increase model performance. The

most common ones are meteorological parameters linked with the UHI formation. Kim and Baik [70], for example, used the maximum UHI intensity of the previous day in Seoul together with wind speed, cloud cover, and relative humidity. In London, Kolokotroni et al. [71–73] used hourly air temperature, relative humidity, wind speed, cloud cover and global solar radiation. More recently, in Ontario, Demirezen et al. [74,75] used the air temperature, humidity, solar radiation, wind speed and wind direction. Other researchers have also included a time reference as an input to better capture the hourly evolution of urban temperatures. For example, Gobakis et al. [24] and Papantoniou and Kolokotsa [76] used the date in conjunction with air temperature and global solar radiation. Similarly, Heijden et al. [35] and Erdemir and Ayata [77] used the hour of the day together with other meteorological parameters. Table 1 summarizes these and other ANN studies that focused on outdoor urban temperatures and their modelling characteristics, such as the length of their datasets.

Table 1. Previous studies using ANN to model the outdoor air temperature in urban areas, in chronological order.

Reference	City, Country [a]	Training and Testing Dataset			ANN Target [b]	ANN Type
		Initial Date	Final Date	Duration		
Mihalakakou et al. [67]	Athens, GR	1986	1995	10 years	Temperature	FNN
Santamouris et al. [69]	Athens, GR	Jun 1996 Jun 1997	Sep 1996 Sep 1997	8 months	Temperature	FNN
Kim and Baik [70]	Seoul, KR	1973	1996	24 years	UHI intensity	FNN
Mihalakakou et al. [68,78]	Athens, GR	Jan 1996	Dec 1998	2 years	UHI intensity	FNN
Jang et al. [79]	Québec [1], CA	Jun 2000	Sep 2000	4 months	Temperature	FNN
Kolokotroni et al. [71–73]	London, GB	Jul 1999 2007	Sep 2000 2007	15 months	Temperature	FNN, CNN, ENN
Zhao [80]	Quinling [1], CN	-	-	-	Temperature	FNN
Beccali et al. [81]; Cellura et al. [82]	Palermo, IT	-	-	-	Temperature	NNARX, NNARMAX
Gobakis et al. [24]	Athens, GR	Apr 2009	May 2010	13 months	Temperature	FNN, CNN, ENN
Shao et al. [83]	Hangzhou, CN	Jan 1995	Dec 1996	2 years	Temperature	FNN
Heijden et al. [35]	Rotterdam, NL	Apr 2011	Oct 2012	19 months	UHI intensity	FNN
Lee et al. [84]	Seoul, KR	Jan 2012	Dec 2012	1 year	UHI intensity	FNN
Papantoniou and Kolokotsa [76]	Ancona, IT Chania, GR Granada, ES Mollet, ES	Jan [3]	Dec [3]	1 year	Temperature	FNN, CNN, ENN
Erdemir and Ayata [77]	Istanbul [2], TR	May [3]	Sept [3]	5 months	Temperature	FNN
Schuch et al. [85]	Abu Dhabi, AE	Mar 2016	Dec 2016	10 months	Temperature	FNN
Demirezen et al. [74,75]	Ontario, CA	Feb 2018	Nov 2018	9 months	Temperature	FNN
Han et al. [86]	Cambridge, US	Jan, 2019	Jun, 2019	6 months	Temperature	FNN, RNN

[a] ISO Country codes [87]. [b] Output of the ANN model, as declared or shown by the authors. [1] Extends further from the limits of the city, covering the surrounding regional areas. [2] Includes other cities of the same country. [3] Year not specified.

In most of these studies, the modelling of outdoor urban air temperature time series is addressed from a common perspective: using the temperatures collected during a monitoring campaign at the urban level to train a Feed-forward Neural Network (FNN, a relatively simple type of ANN). This modelling is usually performed using data from one or several reference points, in many cases well-established meteorological observatories providing detailed and robust information on a wide range of parameters. Although this process is quite extended, it could be discussed whether other ANN topologies might

be more suitable for this purpose. Cascade Neural Networks (CNN) or Elman Neural Networks (ENN) have also been widely applied [24,72,76], the latter being simplified versions of Recurrent Neural Networks (RNN). RNNs have proved to be very effective when it comes to make forecasts, especially when Long Short-Term Memory (LSTM) is used [88]. In that sense, the work of Han et al. [86] has recently demonstrated the superiority of RNNs over FNNs for predicting outdoor urban temperatures.

However, it should be noted that the aim of most of these studies is not to make time predictions or forecasts, but to model an urban time series from a preexisting one. In other words, the purpose is to obtain an adapted version of a reference time series that already exists, being this new time series representative of a certain urban area and covering the exact same period as the data used as a reference. This simplifies the process by eliminating the time dependence of the outputs, and which justifies working with simpler neural networks, such as FNNs. In fact, and under this modelling scenario, Kolokotroni et al. [72] did not find any improvement when comparing ENNs and CNNs with FNNs.

Although empirical models are site-specific (predictions are always made for a particular urban location), they can be used to extend the temporal coverage of urban monitoring campaigns, thus potentially increasing their utility among other disciplines. And despite FNN-based models are not suitable for future projections, they are certainly useful to adapt historical records obtained outside the city to the reality of urban areas. However, there is currently a knowledge gap with regard to the amount of input data potentially needed to accurately model urban temperature time series using FNNs. Collecting experimental data is very time-consuming and resource-intensive and, while it seems a common practice to rely on one whole year of data for the training, there is no evidence that this should be a minimum requirement. This study, therefore, aims to quantify the degree to which the amount of input data needed to train FNNs can be reduced without sacrificing their accuracy. We also explore the use of the UHI intensity as an alternative output of the FNN models, instead of directly targeting the air temperature, to test the hypothesis that its lower seasonality and direct association with the input variables might help reduce the amount of required data for the training phase.

The present research is structured in three phases: first, we compared the performance of more than 5000 different FNN configurations for modelling the outdoor urban temperature (TEMP approach) and the UHI intensity (UHII approach) when trained with 12 months of data in the city of Madrid. An optimal configuration was then selected and analysed further in-depth for both approaches, including their sensitivity to input parameters. Finally, the amount of data provided during the training phase was reduced from the initial 12 months to 9, 6 and 3 months to evaluate the capacity of these models to continue producing accurate results with fewer input data.

2. Materials and Methods

2.1. Study Area: The City of Madrid

The present study focuses on the city of Madrid. Due to its size, location and climatic conditions, Madrid is characterised by a strong UHI, with nighttime UHI intensities up to 10 °C during calm and clear nights. During the last decades, this phenomenon has been intensively studied in the city by means of on-site measurements [89–92], remote sensing [93,94] and numerical models [95,96].

Between 2016 and 2019, a continuous monitoring campaign was carried out at 20 fixed urban sites with the aim to study the temporal patterns of the UHI in Madrid [97]. In the present study, we use part of that experimental data to define the outputs of our ANN models. More specifically, we use the hourly, dry-bulb temperature gathered at the city centre (Embajadores, see Figure 1), classified as compact midrise (LCZ 2) according to the Local Climate Zones (LCZ) scheme [98], and which registered the highest mean and nighttime UHI intensity. The data available for this study cover the period from July 2016 to September 2018 on an hourly basis (800 days or 19,200 h, in total).

All sensors used in this monitoring campaign were protected from the rain and solar radiation using a custom-made, mechanically ventilated radiation shield. They were installed in the Urban Canopy Layer (UCL) at 5–6 m above the ground, following the guidelines of the World Meteorological Organization (WMO) for urban sites [99,100]. The location of each sensor was also studied in terms of its thermal source area [101]. In that sense, the representativeness of each sensor was appraised in terms of its surroundings' homogeneity [102,103].

Quality Control (QC) procedures were also applied, consisting of a plausible value check, a time consistency check, and an internal-consistency check [104]. This analysis was complemented by a spatial consistency check [105], which analysed whether the difference between a measurement and its surroundings was too large compared to the average. For the City Centre sensor, 126 records were flagged as suspect and just three as erroneous. 72 missing values were identified due to a recording failure between the 17th and the 20th of October 2017. Both erroneous and missing values were left blank in the analysed dataset. Further details about the monitoring campaign and QC procedures can be found in [97].

In addition to the experimental data collected at the city centre, records from the nearby meteorological stations of Barajas Airport (LCZ D) and Ciudad Universitaria (LCZ 9) were used. Hourly values of dry bulb temperature, relative humidity, wind speed, wind direction and precipitation were extracted from the former, while global solar radiation was obtained from the latter. The data covered the same time period (July 2016–September 2018). Both stations are managed by the Spanish Meteorological Agency (AEMET), which complies with the requirements established by the WMO Integrated Global Observing System (WIGOS, [106,107]) regarding QC and sensor installation.

Three different types of datasets, the training, validation and the test datasets, were created. The former were used to fit and evaluate different ANN model configurations. Several training and validation datasets, which varied in length (12, 9, 6 and 3 months) and the months that they covered, were created based on almost 15 months of monitoring (July 2016–September 2017, 10,440 records/hourly measurements). All these datasets were continuous over time, and they were distributed as 80% training and 20% validation. These training and validation subsets were created by randomly sampling the data. This prevented the potential accumulation of specific events in any of these datasets (e.g., certain meteorological conditions), which could bias either the training or the validation of the models. Additionally, a test dataset was created based on the second year of recorded data (October 2017–September 2018, 8688 records/hourly measurements) to independently test the models and assess their accuracy over an entirely different year.

2.2. Designing the ANNs

Feed-forward Neural Networks (FNN) were used in this study. Although FNNs are at the baseline of supervised deep neural networks, their utility for modelling urban temperatures has been widely demonstrated in previous studies (see Section 1.1). Figure 2 outlines the two different approaches, based on two different outputs, that were adopted in this study to model urban temperatures. The first one consisted of directly targeting the air temperature at the urban site, validating its outputs with the measurements previously recorded at that location. This approach is aligned with the majority of similar studies found in the literature, and it is referred in this study as the temperature approach (TEMP approach). The second option aims at modelling the urban air temperature indirectly. In this case, the model targets the UHI intensity instead, computed as the temperature difference between the urban site (*Embajadores*) and the reference location (*Barajas Airport*, $\Delta T_{LCZ2,\ LCZD}$). The urban temperature is then derived indirectly by adding the airport temperature to the output of the model. This will be referred to as the UHII approach from this point onwards.

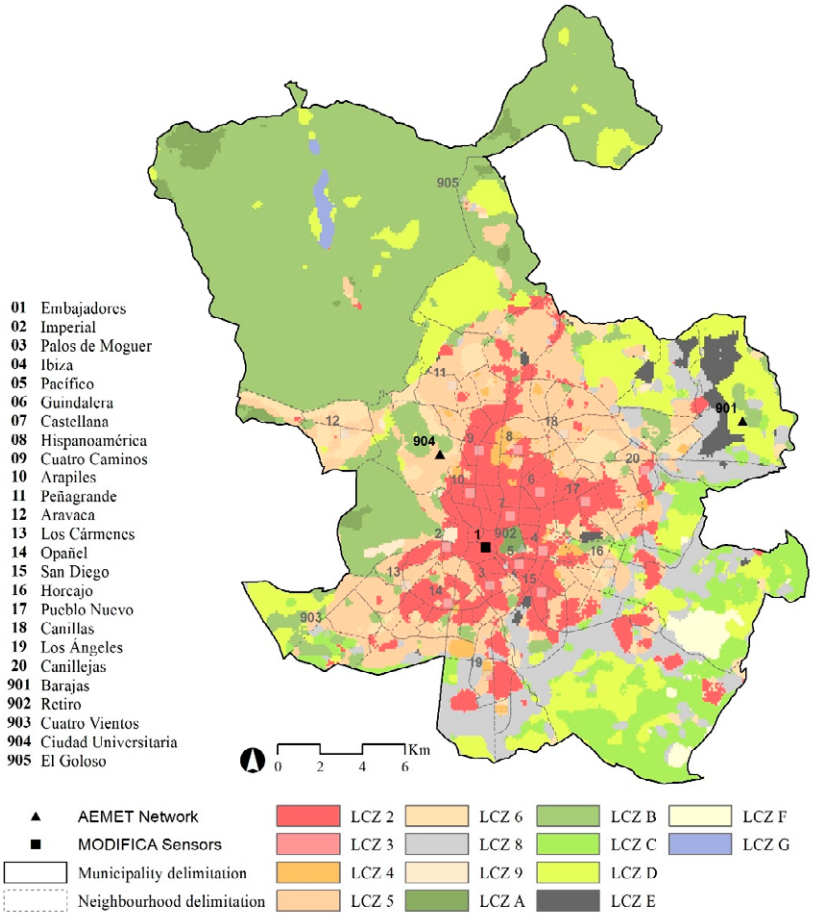

Figure 1. Distribution of the MODIFICA and AEMET networks across the city of Madrid. The data needed for the training, validation and test of the ANN model was extracted from the measurement sites in black. The classification of Madrid by Local Climate Zones, extracted from the WUDAPT database [108], is presented in the background.

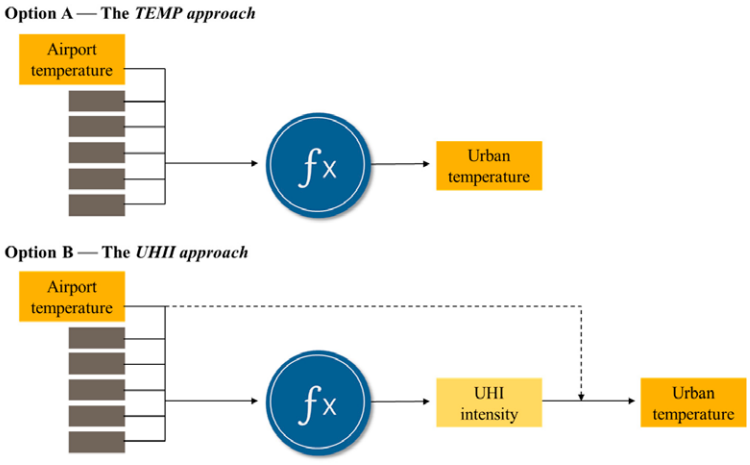

Figure 2. Schematic representation of the two approaches used for modelling the outdoor urban temperature.

The selection of the FNN model inputs of this study were informed by previous studies in Table 1, which have identified the variables that have a strong correlation with the formation of heat islands [109,110]. They consist of six meteorological variables: dry bulb temperature (°C), relative humidity (%), precipitation (mm), wind direction (degrees), wind speed (m/s) and global solar radiation (J/m^2). The time of the day was added to these six input parameters, which was expected to reflect the daily variability of the outputs, either the temperature or the UHI intensity. Cloud cover was not used as an input parameter because the available frequency (one record every eight hours) was incompatible with the hourly frequency for the outputs. The wind speed presented strong variations at an hourly level and introduced strong oscillations in the prediction. Thus, to help avoid abrupt changes in the output, a moving average (MA) filter was applied. The use of a MA filter is a common pre-processing technique when it comes to modelling time series from data with a high variability. Examples can be found in the field of urban traffic (applying a MA to the car's acceleration [111]), atmospheric pollution (MA applied to measured $PM_{2.5}$ concentration [112]) or urban climate modelling [113], the latter using a MA of order 8 (i.e., 8 h) to reduce the presence of wind gust peaks in the dataset prior feeding their model. In this study, a MA of order 4 (4 h) was found to be sufficient to reduce the noise of the wind speed while preserving the time series trend.

All the inputs were standardized prior the FNN feeding, meaning that all variables were transformed in order to have a mean = 0 and a standard deviation = 1 [114,115]. A diagram of the FNN structure for both approaches can be seen in Figure 3.

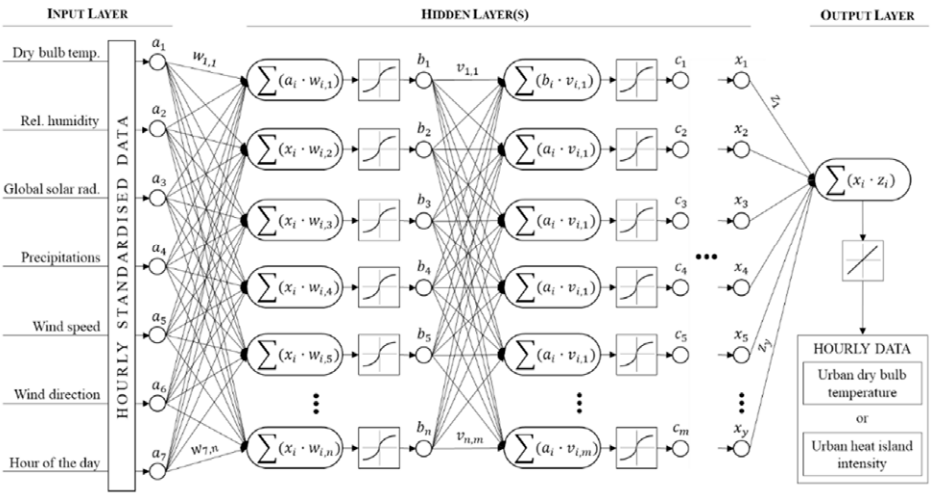

Figure 3. Base structure of the Feed-forward Neural Network (FNN) used in this study.

2.3. Comparing and Evaluating the FNNs

Several FNN structures with different configurations were trained during the first phase of this research. Hyperparameters, such as the number of neurons per hidden layer, the activation functions, or the number of epochs, were thoroughly iterated in order to find a common, optimal configuration for both the TEMP and the UHII approach. Despite some of the tested activation functions are commonly applied for classification tasks and were not likely to give the best performance (i.e., sigmoid-like functions), they were included in the iterative process since preceding similar works made use of them [24,67]. To streamline the process and reduce the complexity of the iteration, each subsequent hidden layer adopted half the neurons of the previous one. All models initialized their weights randomly and were initially trained using 12 months of data. Each configuration was compared by iterating just one parameter (e.g., the activation functions) and leaving the others fixed, while increasing the number of neurons per hidden layer. Those parameters

that reached the best overall accuracy with the lowest number of neurons were selected. After this iterative process 5478 FNNs were trained. Table 2 summarizes the parameters used to test these configurations, as well as the ones that were finally selected. The task outlined above was performed using Python and Keras, a deep-learning library based on Tensorflow [116,117].

Once a common structure and configuration were defined, a comparative analysis of these models was carried out. First, the contribution of each input to the model output was assessed using a sensitivity analysis [114,118,119]. The 5th, 25th, 50th, 75th and 95th percentiles were used to run the sensitivity analysis for each input, while fixing the rest on their means. The time of the day was excluded from the sensitivity analysis and fixed at two different moments: noon and midnight. Next, their overall accuracy was compared for the TEMP and the UHII approach using several error metrics, such as the root mean squared error (RMSE), the median absolute deviation (MAD) or the coefficient of determination (R^2). Modelled results were then plotted for three different weeks to visually assess whether the modelling ability of any of these two approaches could be compromised under certain scenarios. These corresponded to a week of high atmospheric stability (and thus, strong UHI intensity), a week of high atmospheric instability (weak UHI intensity), and a week under both of these conditions.

Table 2. Parameters used to train and evaluate different FNNs configurations. It includes the configuration that was finally selected for both the temperature and the UHII approach.

Parameters		Tested	Selected
Number of hidden layers		1–5	2
Number of neurons	Input layer	7	7
	Hidden layers [1]	3–85	18
	Output layer	1	1
Activation functions	Hidden layers	Linear, ELU, SELU, ReLU, Sigmoid, Hard sigmoid, Hyperbolic tangent, Exponential, Softmax, Softplus, Softsign	ELU
	Output layers	Linear, ELU, SELU, ReLU, Sigmoid, Hard sigmoid, Hyperbolic tangent, Exponential, Softmax, Softplus, Softsign	Linear
Optimizer		SGD, Adam, RMSProp, Adagrad, Adadelta, Nadam	Adam
Epochs		100, 200, 500	200
Batch size		2, 5, 10	10
Dataset length		12 months	12 months [2]
Train/Validation size		80%/20%	80%/20%

[1] The value here presented corresponds to the number of neurons contained in the first hidden layer. Each subsequent hidden layer adopts half of the value of the previous one. [2] Maximum length of the dataset. Results with shorter lengths are also presented (Table 4).

The last step of the evaluation process consisted of modifying the amount of data provided to the neural networks during the training phase. To this end, FNN models for both the TEMP and the UHII approach were trained using 12, 9, 6 and 3 months of data, and were used to model the outdoor air temperatures for one complete year using the test dataset. The accuracy was estimated, as in the previous cases, using common error metrics. The loss of accuracy of the models trained with shorter datasets was addressed by comparing their performance with the models trained on more data, obtaining a percentage indicating the increase of error for each metric. In the case of models trained with just 3 months of data, the Mean Absolute Error (MAE) was estimated on a monthly basis to further explore its distribution along one year of modelling.

3. Results

A comparison between several FNN configurations is first shown in Figure 4. Each graph represents the overall accuracy of a certain FNN when iterating just one of its parameters, and while increasing the number of neurons in the hidden layers. From this iterative process, a common, optimal FNN configuration for both the TEMP and the UHII approach was established. The optimal structure was defined as a neural network with seven inputs, two hidden layers of 18 and 9 neurons respectively, and one output. In that sense, it was found that increasing from one to two hidden layers produced a significant improvement in the models' accuracy, while increasing the number of hidden layers further did not. Similarly, moving from 100 to 200 epochs during the training phase could reduce the error of the FNN, while the computational expense of using 500 epochs instead of 200 did not seem justified. This was particularly evident when having tens of neurons in the hidden layers.

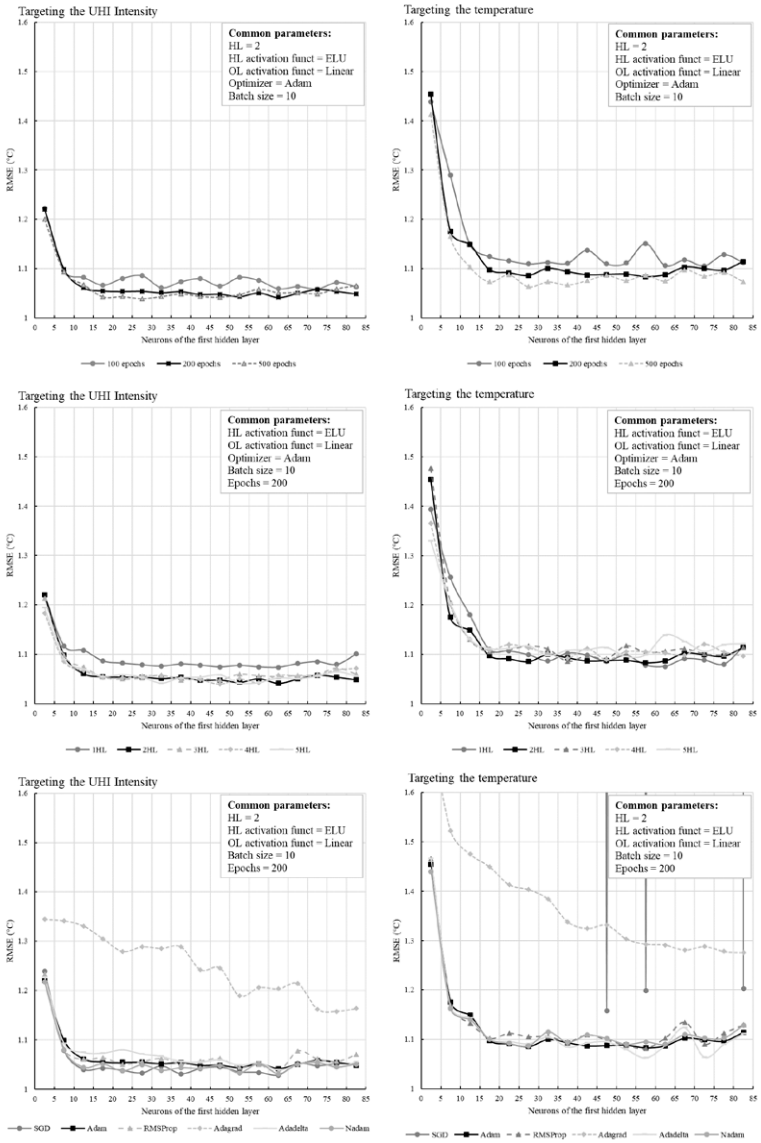

Figure 4. Average Root Mean Squared Error for different FNN configurations using Table 2. Results

obtained with the models derived from the TEMP and the UHII approach for the site Embajadores. Three weeks were selected, each one representing a different atmospheric stability scenario. The timeframe used to train these models extends from July 2016 to September 2017.

In some cases, due to the performance differences between the TEMP and the UHII approach, a common ground had to be reached in terms of the optimal configuration. That was the case of the activation functions, where the Stochastic Gradient Descent (SGD) seemed to produce the best results for those FNNs modelling the UHI intensity, but it led to exploding gradient problems when modelling the temperature. Thus, the Adaptive Moment Estimation (Adam) optimiser was used instead, which performed optimally in both scenarios. For the activation functions, a combination of the Exponential Linear Unit (ELU) for the hidden layers and the linear function for the output layer was used.

Overall, UHII models presented fewer converging problems than TEMP models, which seemed to have some difficulties with some activation functions and optimizers. Furthermore, the UHII approach usually outperformed the TEMP approach. The former did not only produce models with relatively smaller errors than the latter but required fewer neurons per hidden layer to reach a similar accuracy. This behaviour might be indicative of a clearer and more direct relationship between inputs and output, which in the case of the UHII approach links parameters such as wind speed, precipitation, or solar radiation with the UHI formation.

Differences between both modelling approaches also arise when looking at the inputs' relevance. In that sense, the sensitivity analyses presented in Figures 5 and 6 seem to reveal significant variations among them. The temperature from the reference site shifts from being the most relevant parameter of the entire FNN (TEMP approach) to being one of the least important (UHII approach). This is especially visible at night, when inter- and intra-urban temperature differences are most pronounced. The other parameters, albeit with different magnitude, seem to condition the outcome of both models in a similar way. In that sense, wind speed and direction seem to be two highly influential parameters during the night, while solar radiation and relative humidity seem to be key during the day.

Although the UHII approach appears to yield more balanced models, this apparent advantage does not seem to have a significant impact on their outputs when trained with 12 months of data. In this scenario, reasonably good results, and with similar error patterns, are obtained for both approaches. As it can be noted in Figure 7, modelled temperatures fit satisfactorily with the measured temperatures at the urban site and under a wide variety of circumstances, including different UHI scenarios: a rainy and windy week with generalised low UHI intensities (<2 °C); a week with varying meteorological conditions, during which a sudden weather change from calm to rainy was observed leading to a rapid change in the UHI intensities; or a calm week with strong UHI intensities (>5 °C), probably reinforced by temperature inversions. The greatest errors seem to accumulate on those nights when unusual conditions occur, such as when very high UHI intensities, close to 10 °C, are registered; or when the UHI intensity drops and rises abruptly, perhaps coinciding with occasional and localised weather events, such as rainfalls. Overall, models produced relatively smooth time series, without spikes or large variations from one hour to the next one, despite not having a built-in temporal dependence between consecutive outputs. Using a moving average for the wind speed seems to have contributed to reducing the noise in the models' output.

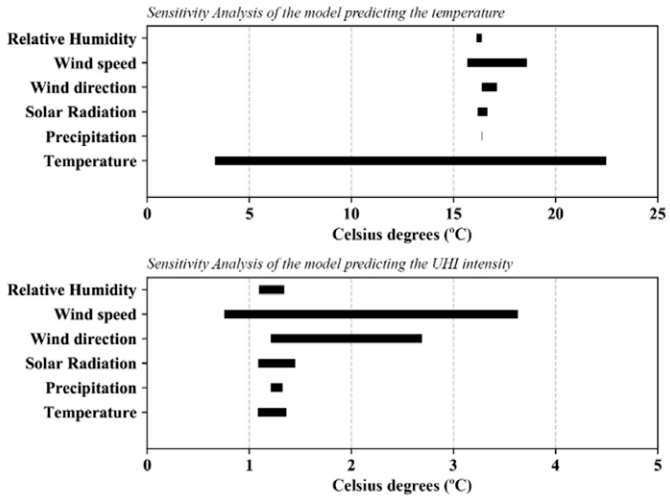

Figure 5. Sensitivity analysis of the inputs of the models. The same FNN configuration was used targeting the urban temperature (top) and the UHI intensity (bottom). The hour was fixed to 12 a.m. (Nighttime).

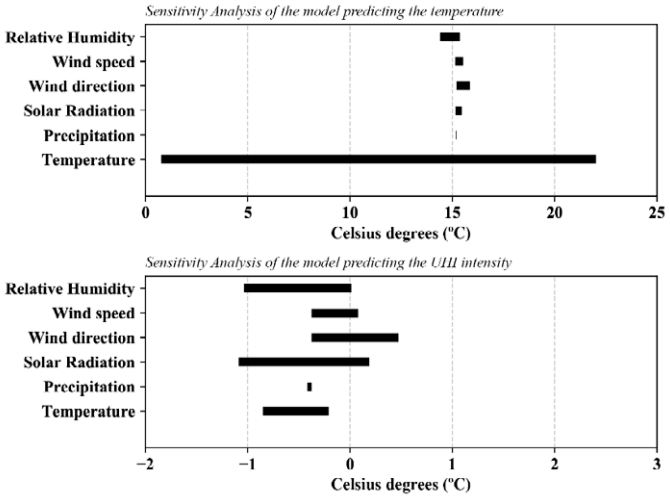

Figure 6. Sensitivity analysis of the inputs of the models. The same FNN configuration was used targeting the urban temperature (top) and the UHI intensity (bottom). The hour was fixed at 12 p.m. (Daytime).

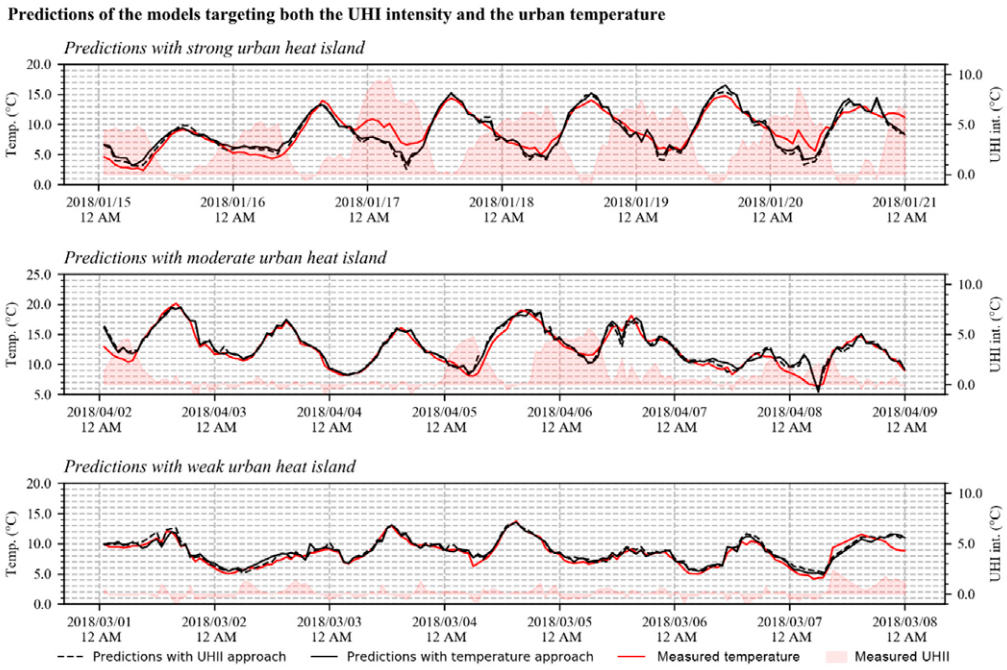

Figure 7. Results obtained with the models derived from the TEMP and the UHII approach for the site *Embajadores*. Three weeks were selected, each one representing a different atmospheric stability scenario. The timeframe used to train these models extends from July 2016 to September 2017.

Models targeting the UHI intensity got a slightly better score in the error metrics, with a reduction of the error between 6.4 and 11.7% (see Table 3). RMSE was 1.09 °C and 1.02 °C for the TEMP and the UHII approach, respectively. These results are in line with previous studies, such as in Kim and Baik (RMSE = 1.18 °C, [70]) or Demirezen et al. (RMSE = 1.29 °C, [75]), both modelling outdoor air temperature. The only exception is the coefficient of determination, which is extraordinarily high when targeting the temperature (R^2 = 0.99). This is also in line with previous studies (e.g., [75,77]) and it is further addressed in the discussion section.

Table 3. Metrics of the selected models targeting both the air temperature and the UHI intensity. Both models were trained using 12 months of data (July 2016–September 2017). The two variables regressed are modelled and monitored air temperatures.

Metrics		Model Targeting		Error Variation
		Temperature	UHI Intensity	
MAD	Median Absolute Deviation (°C)	0.60	0.53	−11.7%
MAE	Mean Absolute Error (°C)	0.81	0.74	−8.6%
RMSE	Root Mean Squared Error (°C)	1.09	1.02	−6.4%
R^2	Coefficient of Determination	0.99	0.79	+20.2%

Shortening the Training Dataset

The results presented above correspond to FNN models trained with one year of hourly data. So far, the TEMP and the UHII approach have proved to yield similar results. When training models with less data, however, differences started to arise. Results show that using 9 months instead of 12 months of data slightly increased the RMSE, with 0.9% and 2.4% for the TEMP and the UHII approach, respectively. When using 6 months of data the accuracy loss increased more markedly, especially in the case of the TEMP models (11.7% vs. 6.2%). The error kept growing exponentially when using 3 months of data,

although the tendency was more accentuated and led to significant differences between both approaches (63.1% vs. 40.7%). A similar trend was observed for the MAE and MAD metrics, which can be found in Table 4.

Table 4. Relative accuracy loss when reducing the size of the training dataset for both the TEMP and the UHII approach. The number of months in each column establish the baseline of accuracy. The accuracy was obtained using the evaluation dataset.

	TEMP Approach				**UHII Approach**			
	RMSE				**RMSE**			
	12 months	9 months	6 months	3 months	12 months	9 months	6 months	3 months
12 months	0.0%				0.0%			
9 months	0.9%	0.0%			2.4%	0.0%		
6 months	11.7%	10.6%	0.0%		6.2%	3.8%	0.0%	
3 months	63.1%	61.6%	46.1%	0.0%	40.7%	37.5%	32.5%	0.0%
	MAE				**MAE**			
	12 months	9 months	6 months	3 months	12 months	9 months	6 months	3 months
12 months	0.0%				0.0%			
9 months	3.2%	0.0%			4.8%	0.0%		
6 months	14.0%	10.4%	0.0%		8.9%	4.0%	0.0%	
3 months	66.1%	60.9%	45.7%	0.0%	40.0%	33.7%	28.5%	0.0%
	MAD				**MAD**			
	12 months	9 months	6 months	3 months	12 months	9 months	6 months	3 months
12 months	0.0%				0.0%			
9 months	7.6%	0.0%			10.6%	0.0%		
6 months	17.7%	9.4%	0.0%		14.5%	3.5%	0.0%	
3 months	70.7%	58.7%	45.0%	0.0%	42.7%	29.0%	24.6%	0.0%

These results are the average error yielded by several models trained with shortened datasets and are relative to the accuracy of the models trained with 12 months of data. Figure 8 presents the models' accuracy absolute levels, including the accuracy of all models trained with each shortened dataset. As already noted, differences arise not only when reducing the training datasets, but also when changing from one approach to another. The large variability of error between the models trained with 3 months of data is noticeable, being more accentuated in the case of the TEMP approach. It seems that, depending on the data used during training, it is possible to obtain models with an acceptable overall accuracy (RMSE < 1.5 °C, in line with previously developed models) to others that it is not clear that they could be used to make a reasonable modelling (RMSE > 2 °C).

Yet, these results represent the average cumulative error over a year. A more detailed analysis of the accuracy of the models showed that their error is unevenly distributed over the months, losing accuracy outside the months for which they were trained. It was also observed that their results do not suffer excessively within the months for which they were trained, being comparable with models trained on more data. In that sense, Figure 9 shows the additional error yielded by models trained with only 3 months of data. For convenience purposes, these months were made coincident with the seasons of the year, and a model trained with all 12 months of data was used as a reference.

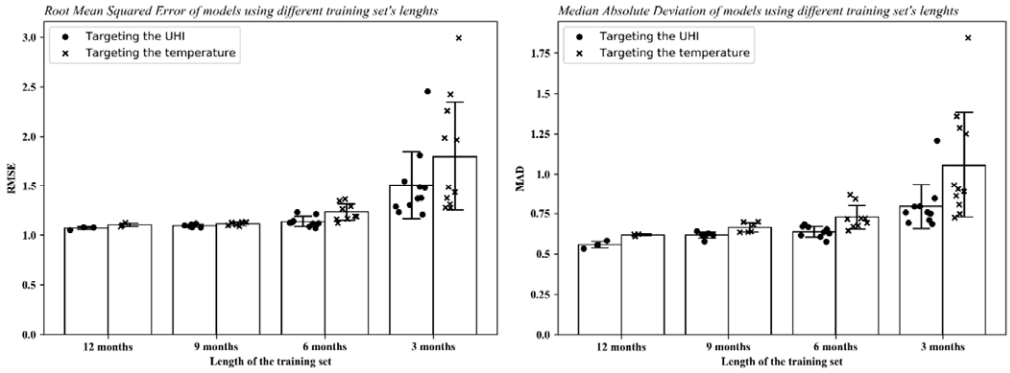

Figure 8. Comparison of the error obtained by several models, trained using different datasets of different length and differentiating between those targeting the air temperature and the UHI intensity. On the left is presented the RMSE. On the left is presented the RMSE. On the right is presented the MAD.

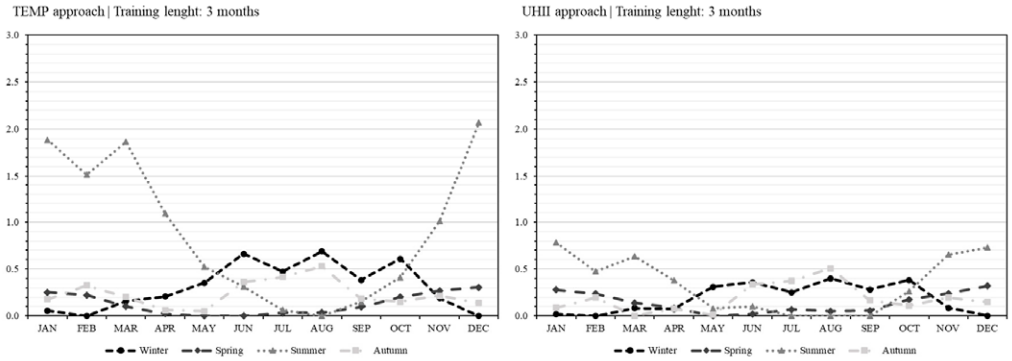

Figure 9. Additional error yielded by models trained with just 3 months of data, using both the TEMP and the UHII approach. These models are named according to the season they were trained on. The reference error baseline was established by the same ANN configuration trained with 12 months of data.

The results show that the models systematically tend to minimise their error within their season, with the RMSE gradually increasing as they move away from it. This is accentuated for models trained in winter and summer. The reason behind this could lie in the annual cyclical behaviour of temperatures: between solstices and equinoxes, temperatures remain at one extreme of the annual cycle, either at the high end of temperatures (summer) or at the low end (winter). Between the equinoxes and solstices (spring and autumn), though, the transition between the two extremes takes place. This could favour the training of the ANN, as it would extend pattern recognition to practically the entire annual temperature range, and where only the extremes would be at the expense of the neural network's ability to generalise and extrapolate its modelling capacity beyond what is known during its training.

This dynamic is noticeable in the case of the UHII approach as well, although it seems to be rather less pronounced. As it was pointed out in the introduction, Madrid's UHI does not seem to follow a seasonal pattern, which means it might reach its highest and lowest UHII intensities at any time during the year (see Figure A1). However, these UHI peaks depend on the meteorological conditions, thus the loss of accuracy registered by these UHII models seems to be likely related to the concentration of certain meteorological conditions during the training phase. In other words, these FNNs would have difficulties in refining the modelling if, within the three months of data used to train them, there is

not a sufficiently large record of the different meteorological conditions that favour the occurrence of UHI.

The performance differences between the TEMP and the UHII approach are now clearly noticeable when plotting the data. In this respect, Figure 10 shows how the results of a TEMP model trained from May to August would produce quite precise results for June of the next year, like the ones obtained by models trained with 12 months of data. However, when trying to obtain the temperature profile in February, that same model barely captures the global trend. In that scenario, the UHII model, trained with the same three months of data, was able to fit to observed values with higher accuracy. It accumulated the error at the same moment as the models trained with 12 months of data, in many cases amplifying it. Despite the unusual distribution of temperatures and UHI intensities for that week, the UHII model was able to capture most of it, which turned to be surprising due to the relatively low amount of data used for its training.

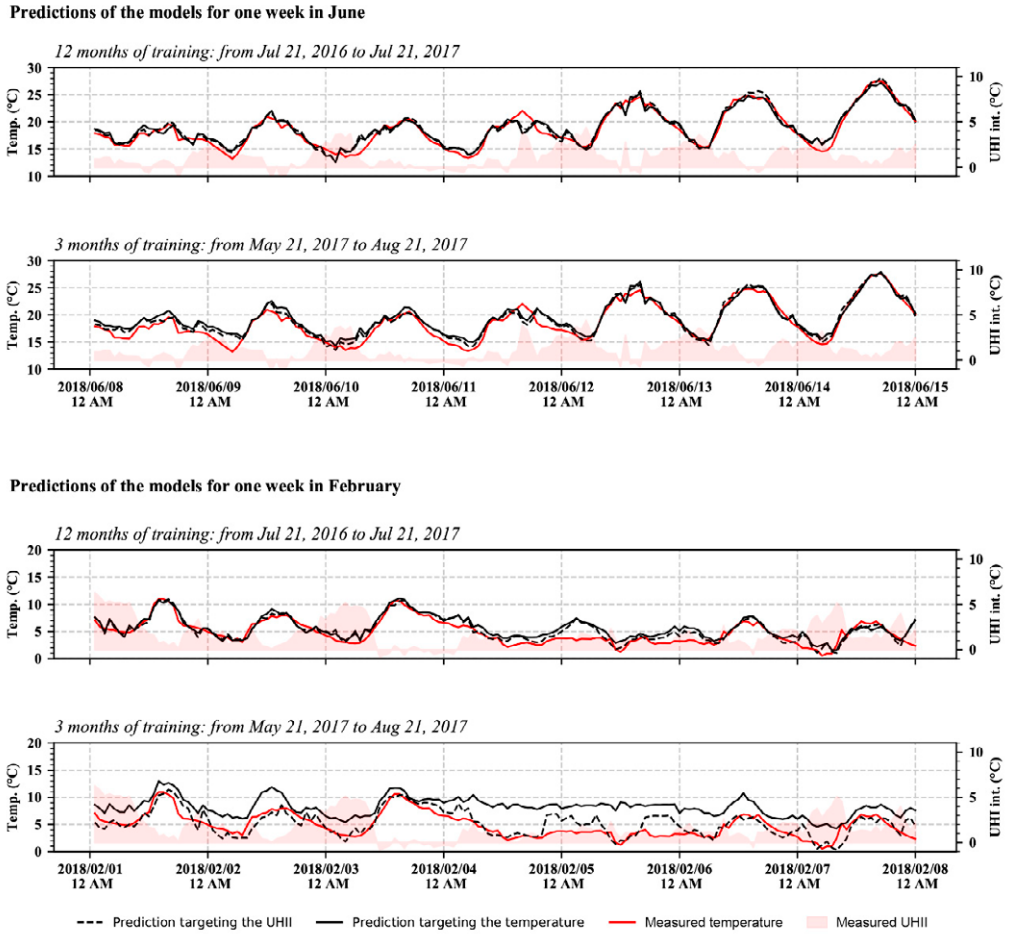

Figure 10. Comparison of TEMP and UHII models trained with 12 and 3 months of data for the site Embajadores. Results are presented for one week of June (top) and one week of February (bottom). The TEMP model trained on 3 months of data shows difficulties when modelling the temperatures further away from its training temporal range (i.e., February, bottom).

4. Discussion

The results of this research point towards the potential reduction of the training datasets without having a significant loss of accuracy. This could facilitate the work of urban climate researchers, thus promoting the development of shorter and simpler

monitoring campaigns. This does not mean that it is preferable to use smaller amounts of data to train ANN models, but that their accuracy might not be compromised when they are trained in this manner. Although using large amounts of high-quality data is always desirable, in some cases it is not possible due to varying circumstances, such as budget constraints or human resources limitations. In this context, knowing where the accuracy limits of the models are when trained with fewer data might help researchers explore their experimental data or design new measurement campaigns in an efficient manner.

In this study we propose the use of empirical, FNN-based models to extend the temporal coverage of urban monitoring campaigns. These models, although limited for carrying out temporal predictions into the future, they can be used to adjust long-term records gathered outside the city to the urban context. This approach, the generation of long-term datasets by looking backwards, might be potentially useful in many disciplines, including the generation of site-specific weather files for building energy modelling [120–123], the downscaling of heat-related epidemiological studies to evaluate the effect of urban temperatures in health [4,124–127], or the identification and characterization of energy poor households in urban environments [128–132].

It is worth noting that the use of UHI intensity instead of outdoor temperature as the output of the FNN models yielded significantly better results mainly when reducing the size of the training dataset. The accuracy improvement was limited when using 9 or more months of data during the training phase. The benefits of targeting the UHI intensity with the FNN model are, therefore, linked to the potential of using smaller datasets to model outdoor urban temperatures. However, using the UHI intensity instead of the temperature as the output, sustained on the lower seasonality of the former, could be arguable. ANN are universal function approximators [133] and, for that reason, using one parameter or the other should not produce significant differences. Although this was mathematically demonstrated, Curry [134] showed that to model the seasonality of a time series with FNN would require a very large structure. This structure would grow exponentially when increasing the length of the dataset, since more turning points are likely to appear. In fact, Zhang and Qi [135] recommended not only to deseasonalize the time series, but also to remove its trend (if any). Nowadays, pre-processing the dataset to make it stationary before feeding the ANN is a very extended practice and has demonstrated to be very effective with RNN as well [88,136]. This approach might be helpful in the future for other studies such as Han et al. [86], where the UHI intensity could be used instead of the outdoor air temperature to remove much of the seasonality from their temperature forecasts. However, it is unclear whether they could be extended to FNNs that use a reference site for modelling outdoor urban temperatures without any time dependence. Other reasons, such as the range of temperatures or the concentration of meteorological stability of the training dataset, might explain the varying accuracy results between the TEMP and the UHII approach when training these types of models, especially when using just 3 months of training data.

In line with the latter, it seems that the selection of days with different meteorological conditions and at different times of the year might be more relevant for the modelling than the continuity of the monitoring campaign. Thus, it may be more appropriate that future studies work with shorter, discontinuous monitoring campaigns covering a wider range of meteorological situations rather than a single, continuous-over-time campaign that might concentrate in a specific time of the year. Results may also support the use of data from sources whose long-term continuity may be compromised (i.e., CWS). In these cases, it would be relevant not only to apply filtering techniques to reduce the risks of introducing outliers, but also to carry out frequency distribution analyses to ensure that all meteorological conditions are being included into the modelling.

Some attention should be drawn to the pertinence of using certain error metrics. Despite being very extended (e.g., [75–77]), the use of R^2 as a performance indicator could be misleading [137,138]. As it can be seen in Equation (1), R^2 relies both on the size of the

residuals (SS_{res}, the actual deviation of the prediction from the observed values) and the total variance of the dependent variable (SS_{tot}):

$$R^2 = 1 - \frac{\sum(y_i - \hat{y}_i)^2}{\sum(y_i - \overline{y}_i)^2} = 1 - \frac{SS_{res}}{SS_{tot}} \quad (1)$$

Thus, obtaining a higher R^2 does not implicitly mean having less error (numerator), but might be the result of a higher variance of the output (denominator). This was observed in this study when comparing the two approaches. In the case of the TEMP approach, the variance of the output temperature (which ranges from −2 to 41 °C) is much higher that the variance of the UHI intensity (ranging from 0 to 8 °C). Furthermore, since the TEMP approach contains an input variable (airport temperature) that explains most of the variance of the output variable (urban temperature), the R^2 tends to be extremely high ($R^2 > 0.99$). This explains why significantly lower R^2 were obtained when using the UHII approach in spite of yielding better results with the rest of the performance indicators (RMSE, MAE, MAD).

Taking the above into consideration, it would be worthwhile to investigate whether the behaviour of the TEMP and the UHII models presented in this paper is only attributable to the case of Madrid or if, on the contrary, it might be common in other cities at different latitudes and climatic conditions. Some existing studies have identified strong seasonal differences in UHI intensities in other cities [139–142], while others have not found such differences [143–145]. In this respect, a strong annual seasonality of the UHI intensity would probably limit the capacity of the models to produce accurate results when trained with small datasets. On the contrary, in cities where air temperatures remain within a narrow range throughout the year, such as tropical regions, the TEMP approach might perform better.

5. Conclusions

Feed-forward neural networks were used in this study to model urban temperature time series from experimental data. The aim was to explore the reliability of these models in the context of low data availability, as well as the potential benefits from targeting the UHI intensity with these models. Results showed that, for the case study of Madrid, the training dataset could be reduced to 9 or even 6 months without compromising too much the accuracy of the FNN models, particularly when using the UHII approach (2.4% and 6.2% increase in RMSE, respectively).

Results showed that the UHII approach generally outperformed the TEMP approach. Overall, UHII models converged to lower error ratios with a smaller number of neurons, proving to be more effective at predicting the urban temperature of a reference site. When using the exact same configuration and structure, UHII models exhibited a significant increase in performance. TEMP models appeared to be quite seasonally dependent, thus facing more problems for modelling temperatures outside the training months. This was particularly relevant when trained on just 3 months of data, when the accuracy differences between UHII and TEMP models was at their highest. We argue that this could be related to the annual cyclical behaviour of temperatures. Targeting the UHI intensity with the FNNs instead, which in Madrid has shown to be almost stationary, seems to reduce uncertainty when modelling temperatures from a relatively small dataset.

The potential use of smaller datasets for training FNNs and still obtaining reliable results might benefit urban climate researchers since field measurements could be reduced in time and costs. Researchers might also take advantage of the accurate preliminary results that can be generated with relatively small datasets for speeding up their research, or for extending their measurements to other urban areas.

Author Contributions: Conceptualization, M.N.-P., A.M. and P.S.; methodology, M.N.-P., A.M. and P.S.; software, M.N.-P. and P.S.; validation, M.N.-P., A.M. and P.S.; formal analysis, M.N.-P., A.M. an P.S.; investigation, M.N.-P.; resources, M.N.-P. and C.S.-G.S.; data curation, M.N.-P.; writing—original

draft preparation, M.N.-P., A.M., P.S. and C.S.-G.S.; writing—review and editing, M.N.-P., A.M., P.S., C.S.-G.S. and F.J.N.G.; visualization, M.N.-P.; supervision, A.M. and P.S.; project administration, M.N.-P., C.S.-G.S. and F.J.N.G.; funding acquisition, M.N.-P., C.S.-G.S. and F.J.N.G. All authors have read and agreed to the published version of the manuscript.

Funding: This research was funded by an FPU research grant (FPU15/05052) and by a research visit grant (EST17/00825), both from the Spanish Ministry of Education, Culture and Sport. This research was also supported by the MODIFICA research project (BIA2013-41732-R), funded by the Spanish Ministry of Economy and Competitiveness.

Institutional Review Board Statement: Not applicable.

Informed Consent Statement: Not applicable.

Acknowledgments: The authors would like to thank the Spanish National Meteorological Agency (AEMET) for providing access to their meteorological data, and Luis Tejero Encinas and Juan Azcárate Luxán, from the Madrid City Council' Subdivision of Energy and Climate Change, for their support with the urban measurements.

Conflicts of Interest: The authors declare no conflict of interest.

Appendix A

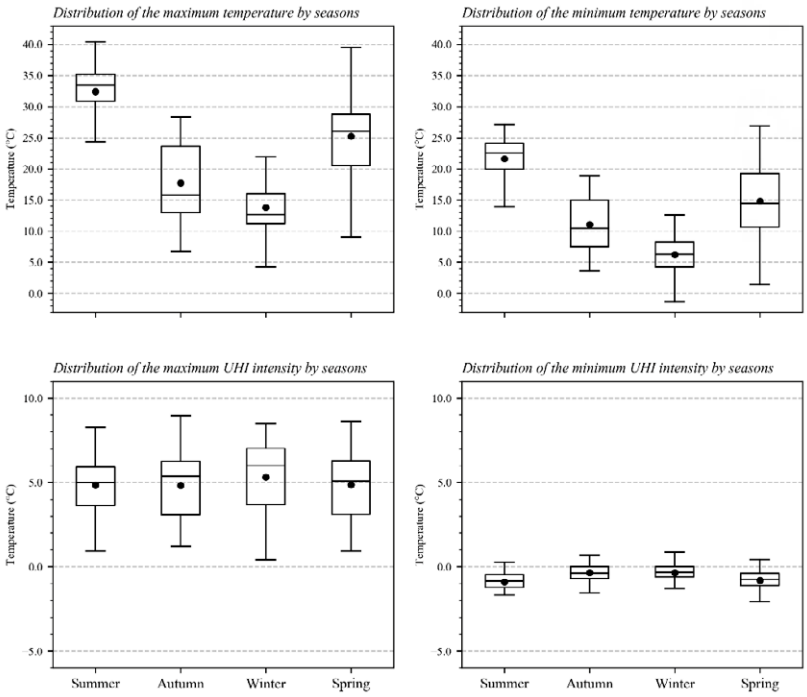

Figure A1. Seasonal fluctuations of the daily maximum and minimum temperature (top) and UHI intensity (bottom) between August 2016 and July 2018.

References

1. Reckien, D.; Salvia, M.; Heidrich, O.; Church, J.M.; Pietrapertosa, F.; De Gregorio-Hurtado, S.; D'Alonzo, V.; Foley, A.; Simoes, S.G.; Krkoška Lorencová, E.; et al. How are cities planning to respond to climate change? Assessment of local climate plans from 885 cities in the EU-28. *J. Clean. Prod.* **2018**, *191*, 207–219. [CrossRef]
2. Santamouris, M.; Cartalis, C.; Synnefa, A. Local urban warming, possible impacts and a resilience plan to climate change for the historical center of Athens, Greece. *Sustain. Cities Soc.* **2015**, *19*, 281–291. [CrossRef]
3. Moran, D.; Kanemoto, K.; Jiborn, M.; Wood, R.; Többen, J.; Seto, K.C. Carbon footprints of 13,000 cities. *Environ. Res. Lett.* **2018**, *13*. [CrossRef]

4. Macintyre, H.; Heaviside, C.; Cai, X.; Phalkey, R. Comparing temperature-related mortality impacts of cool roofs in winter and summer in a highly urbanized European region for present and future climate. *Environ. Int.* **2021**, *154*, 106606. [CrossRef]
5. Sánchez-Guevara, C.; Núñez Peiró, M.; Taylor, J.; Mavrogianni, A.; Neila González, J. Assessing population vulnerability towards summer energy poverty: Case studies of Madrid and London. *Energy Build.* **2019**, *190*, 132–143. [CrossRef]
6. Hsu, A.; Sheriff, G.; Chakraborty, T.; Manya, D. Disproportionate exposure to urban heat island intensity across major US cities. *Nat. Commun.* **2021**, *12*, 2721. [CrossRef]
7. Grimm, N.B.; Faeth, S.H.; Golubiewski, N.E.; Redman, C.L.; Wu, J.; Bai, X.; Briggs, J.M. Global change and the ecology of cities. *Science* **2008**, *319*, 756–760. [CrossRef] [PubMed]
8. Youngsteadt, E.; Dale, A.G.; Terando, A.J.; Dunn, R.R.; Frank, S.D. Do cities simulate climate change? A comparison of herbivore response to urban and global warming. *Glob. Chang. Biol.* **2015**, *21*, 97–105. [CrossRef]
9. Blocken, B. Computational Fluid Dynamics for urban physics: Importance, scales, possibilities, limitations and ten tips and tricks towards accurate and reliable simulations. *Build. Environ.* **2015**, *91*, 219–245. [CrossRef]
10. Doan, V.Q.; Kusaka, H.; Nguyen, T.M. Roles of past, present, and future land use and anthropogenic heat release changes on urban heat island effects in Hanoi, Vietnam: Numerical experiments with a regional climate model. *Sustain. Cities Soc.* **2019**, *47*, 101479. [CrossRef]
11. Ampatzidis, P.; Kershaw, T. A review of the impact of blue space on the urban microclimate. *Sci. Total Environ.* **2020**, *730*, 139068. [CrossRef]
12. Boehme, P.; Berger, M.; Massier, T. Estimating the building based energy consumption as an anthropogenic contribution to urban heat islands. *Sustain. Cities Soc.* **2015**, *19*, 373–384. [CrossRef]
13. Best, M.J.; Grimmmmond, C.S.B. Key conclusions of the first international urban land surface model comparison project. *Bull. Am. Meteorol. Soc.* **2015**, *96*, 805–819. [CrossRef]
14. Jandaghian, Z.; Berardi, U. Comparing urban canopy models for microclimate simulations in Weather Research and Forecasting Models. *Sustain. Cities Soc.* **2020**, *55*, 102025. [CrossRef]
15. Chen, Y.; Zheng, B.; Hu, Y. Numerical simulation of Local Climate Zone cooling achieved through modification of trees, albedo and green roofs-a case study of Changsha, China. *Sustainability* **2020**, *12*, 2752. [CrossRef]
16. Tsoka, S.; Tsikaloudaki, A.; Theodosiou, T. Analyzing the ENVI-met microclimate model's performance and assessing cool materials and urban vegetation applications—A review. *Sustain. Cities Soc.* **2018**, *43*, 55–76. [CrossRef]
17. Mirzaei, P.A. Recent challenges in modeling of urban heat island. *Sustain. Cities Soc.* **2015**, *19*, 200–206. [CrossRef]
18. Toparlar, Y.; Blocken, B.; Maiheu, B.; van Heijst, G.J.F. A review on the CFD analysis of urban microclimate. *Renew. Sustain. Energy Rev.* **2017**, *80*, 1613–1640. [CrossRef]
19. Lauzet, N.; Rodler, A.; Musy, M.; Azam, M.H.; Guernouti, S.; Mauree, D.; Colinart, T. How building energy models take the local climate into account in an urban context—A review. *Renew. Sustain. Energy Rev.* **2019**, *116*, 109390. [CrossRef]
20. Mirzaei, P.A.; Haghighat, F. Approaches to study Urban Heat Island—Abilities and limitations. *Build. Environ.* **2010**, *45*, 2192–2201. [CrossRef]
21. Stewart, I.D. Why should urban heat island researchers study history? *Urban Clim.* **2019**, *30*, 100484. [CrossRef]
22. Velasco, E. Go to field, look around, measure and then run models. *Urban Clim.* **2018**, *24*, 231–236. [CrossRef]
23. Muller, C.L.; Chapman, L.; Grimmond, C.S.B.; Young, D.T.; Cai, X. Sensors and the city: A review of urban meteorological networks. *Int. J. Climatol.* **2013**, *33*, 1585–1600. [CrossRef]
24. Gobakis, K.; Kolokotsa, D.; Synnefa, A.; Saliari, M.; Giannopoulou, K.; Santamouris, M. Development of a model for urban heat island prediction using neural network techniques. *Sustain. Cities Soc.* **2011**, *1*, 104–115. [CrossRef]
25. Giridharan, R.; Kolokotroni, M. Urban heat island characteristics in London during winter. *Sol. Energy* **2009**, *83*, 1668–1682. [CrossRef]
26. Kolokotroni, M.; Giridharan, R. Urban heat island intensity in London: An investigation of the impact of physical characteristics on changes in outdoor air temperature during summer. *Sol. Energy* **2008**, *82*, 986–998. [CrossRef]
27. Zhou, X.; Okaze, T.; Ren, C.; Cai, M.; Ishida, Y.; Watanabe, H.; Mochida, A. Evaluation of urban heat islands using local climate zones and the influence of sea-land breeze. *Sustain. Cities Soc.* **2020**, *55*, 102060. [CrossRef]
28. Skarbit, N.; Stewart, I.D.; Unger, J.; Gál, T. Employing an urban meteorological network to monitor air temperature conditions in the "local climate zones" of Szeged, Hungary. *Int. J. Climatol.* **2017**, *37*, 582–596. [CrossRef]
29. Chen, G.; He, M.; Li, N.; He, H.; Cai, Y.; Zheng, S. A method for selecting the typical days with full urban heat island development in hot and humid area, case study in Guangzhou, China. *Sustainability* **2021**, *13*, 320. [CrossRef]
30. Chao, C.C.; Hung, K.A.; Chen, S.Y.; Lin, F.Y.; Lin, T.P. Application of a high-density temperature measurement system for the management of the kaohsiung house project. *Sustainability* **2021**, *13*, 960. [CrossRef]
31. Borbora, J.; Das, A.K. Summertime Urban Heat Island study for Guwahati City, India. *Sustain. Cities Soc.* **2014**, *11*, 61–66. [CrossRef]
32. Beck, C.; Straub, A.; Breitner, S.; Cyrys, J.; Philipp, A.; Rathmann, J.; Schneider, A.; Wolf, K.; Jacobeit, J. Air temperature characteristics of local climate zones in the Augsburg urban area (Bavaria, southern Germany) under varying synoptic conditions. *Urban Clim.* **2018**, *25*, 152–166. [CrossRef]
33. Yang, X.; Yao, L.; Jin, T.; Peng, L.L.H.; Jiang, Z.; Hu, Z.; Ye, Y. Assessing the thermal behavior of different local climate zones in the Nanjing metropolis, China. *Build. Environ.* **2018**, *137*, 171–184. [CrossRef]

34. Yang, X.; Peng, L.L.H.; Chen, Y.; Yao, L.; Wang, Q. Air humidity characteristics of local climate zones: A three-year observational study in Nanjing. *Build. Environ.* **2020**, *171*, 106661. [CrossRef]
35. van der Heijden, M.G.M.; Blocken, B.; Hensen, J.L.M. Towards the integration of the urban heat island in building energy simulations. In Proceedings of the Building Simulation 2013: 13th Conference of the International Building Performance Simulation Association IBPSA, Chamberry, Ference, 25–28 August 2013; pp. 1006–1013.
36. Fenner, D.; Meier, F.; Scherer, D.; Polze, A. Spatial and temporal air temperature variability in Berlin, Germany, during the years 2001–2010. *Urban Clim.* **2014**, *10*, 308–331. [CrossRef]
37. Meier, F.; Fenner, D.; Grassmann, T.; Otto, M.; Scherer, D. Crowdsourcing air temperature from citizen weather stations for urban climate research. *Urban Clim.* **2017**, *19*, 170–191. [CrossRef]
38. Muller, C.L.; Chapman, L.; Johnston, S.; Kidd, C.; Illingworth, S.; Foody, G.; Overeem, A.; Leigh, R.R. Crowdsourcing for climate and atmospheric sciences: Current status and future potential. *Int. J. Climatol.* **2015**, *35*, 3185–3203. [CrossRef]
39. Fenner, D.; Meier, F.; Bechtel, B.; Otto, M.; Scherer, D. Intra and inter "local climate zone" variability of air temperature as observed by crowdsourced citizen weather stations in Berlin, Germany. *Meteorol. Z.* **2017**, *26*, 525–547. [CrossRef]
40. Nipen, T.N.; Seierstad, I.A.; Lussana, C.; Kristiansen, J.; Hov, Ø. Adopting citizen observations in operational weather prediction. *Bull. Am. Meteorol. Soc.* **2020**, *101*, E43–E57. [CrossRef]
41. Bell, S.; Cornford, D.; Bastin, L. How good are citizen weather stations? Addressing a biased opinion. *Weather* **2015**, *70*, 75–84. [CrossRef]
42. Chapman, L.; Bell, C.; Bell, S. Can the crowdsourcing data paradigm take atmospheric science to a new level? A case study of the urban heat island of London quantified using Netatmo weather stations. *Int. J. Climatol.* **2017**, *37*, 3597–3605. [CrossRef]
43. Kousis, I.; Pigliautile, I.; Pisello, A.L. Intra-urban microclimate investigation in urban heat island through a novel mobile monitoring system. *Nat. Sci. Rep.* **2021**, *11*, 9732. [CrossRef]
44. Yadav, N.; Sharma, C. Spatial variations of intra-city urban heat island in megacity Delhi. *Sustain. Cities Soc.* **2018**, *37*, 298–306. [CrossRef]
45. Schneider, R.; Taylor, J.; Davies, M.; Mavrogianni, A.; Milner, J.; Dos Santos, R.S.; Taylor, J.; Davies, M.; Mavrogianni, A.; Milner, J. The variation of air and surface temperatures in London within a 1 km grid using vehicle-transect and ASTER data. In *Proceedings of the 2017 Joint Urban Remote Sensing Event, JURSE 2017, Dubai, United Arab Emirates, 6–8 March 2017*; Institute of Electrical and Electronics Engineers Inc.: Manhattan, NY, USA, 2017; pp. 6–9.
46. Romero Rodríguez, L.; Sánchez Ramos, J.; Sánchez de la Flor, F.J.; Álvarez Domínguez, S. Analyzing the urban heat Island: Comprehensive methodology for data gathering and optimal design of mobile transects. *Sustain. Cities Soc.* **2020**, *55*, 102027. [CrossRef]
47. Heusinkveld, B.G.; Van Hove, L.W.A.; Jacobs, C.M.J.; Steeneveld, G.J.; El-Bers, J.A.; Moors, E.J.; Holtslag, A.A.M. Use of a mobile platform for assessing urban heat stress in Rotterdam. In Proceedings of the 7th Conference on Biometeorology, Freiburg, Germany, 12–14 April 2010; Volume 12, pp. 433–438.
48. Chow, W.T.L.; Pope, R.L.; Martin, C.A.; Brazel, A.J. Observing and modeling the nocturnal park cool island of an arid city: Horizontal and vertical impacts. *Theor. Appl. Climatol.* **2011**, *103*, 197–211. [CrossRef]
49. Brandsma, T.; Wolters, D. Measurement and statistical modeling of the urban heat island of the city of Utrecht (The Netherlands). *J. Appl. Meteorol. Climatol.* **2012**, *51*, 1046–1060. [CrossRef]
50. Fabbri, K.; Costanzo, V. Drone-assisted infrared thermography for calibration of outdoor microclimate simulation models. *Sustain. Cities Soc.* **2020**, *52*, 101855. [CrossRef]
51. Zhou, D.; Xiao, J.; Bonafoni, S.; Berger, C.; Deilami, K.; Zhou, Y.; Frolking, S.; Yao, R.; Qiao, Z.; Sobrino, J.A. Satellite remote sensing of surface urban heat islands: Progress, challenges, and perspectives. *Remote Sens.* **2019**, *11*, 48. [CrossRef]
52. László, E.; Szegedi, S. A multivariate linear regression model of mean maximum urban heat island: A case study of Beregszász (Berehove), Ukraine. *Idojaras* **2015**, *119*, 409–423.
53. Levermore, G.; Parkinson, J. The urban heat island of London, an empirical model. *Build. Serv. Eng. Res. Technol.* **2019**, *40*, 290–295. [CrossRef]
54. Levermore, G.J.; Parkinson, J.B. An empirical model for the urban heat island intensity for a site in Manchester. *Build. Serv. Eng. Res. Technol.* **2017**, *38*, 21–31. [CrossRef]
55. Romero Rodríguez, L.; Sánchez Ramos, J.; Molina Félix, J.L.; Álvarez Domínguez, S. Urban-scale air temperature estimation: Development of an empirical model based on mobile transects. *Sustain. Cities Soc.* **2020**, *63*, 102471. [CrossRef]
56. Bernard, J.; Musy, M.; Calmet, I.; Bocher, E.; Keravec, P. Urban heat island temporal and spatial variations: Empirical modeling from geographical and meteorological data. *Build. Environ.* **2017**, *125*, 423–438. [CrossRef]
57. Chun, B.; Guldmann, J.M. Spatial statistical analysis and simulation of the urban heat island in high-density central cities. *Landsc. Urban Plan.* **2014**, *125*, 76–88. [CrossRef]
58. Gardes, T.; Schoetter, R.; Hidalgo, J.; Long, N.; Marquès, E.; Masson, V. Statistical prediction of the nocturnal urban heat island intensity based on urban morphology and geographical factors—An investigation based on numerical model results for a large ensemble of French cities. *Sci. Total Environ.* **2020**, *737*, 139253. [CrossRef] [PubMed]
59. Jin, H.; Cui, P.; Wong, N.H.; Ignatius, M. Assessing the effects of urban morphology parameters on microclimate in Singapore to control the urban heat island effect. *Sustainability* **2018**, *10*, 206. [CrossRef]

60. Straub, A.; Berger, K.; Breitner, S.; Cyrys, J.; Geruschkat, U.; Jacobeit, J.; Kühlbach, B.; Kusch, T.; Philipp, A.; Schneider, A.; et al. Statistical modelling of spatial patterns of the urban heat island intensity in the urban environment of Augsburg, Germany. *Urban Clim.* **2019**, *29*, 100491. [CrossRef]
61. Chang, J.M.-H.; Lam, Y.F.; Lau, S.P.-W.; Wong, W.-K. Development of fine-scale spatiotemporal temperature forecast model with urban climatology and geomorphometry in Hong Kong. *Urban Clim.* **2021**, *37*, 100816. [CrossRef]
62. Ho, H.C.; Knudby, A.; Sirovyak, P.; Xu, Y.; Hodul, M.; Henderson, S.B. Mapping maximum urban air temperature on hot summer days. *Remote Sens. Environ.* **2014**, *154*, 38–45. [CrossRef]
63. Lai, J.; Zhan, W.; Quan, J.; Bechtel, B.; Wang, K.; Zhou, J.; Huang, F.; Chakraborty, T.; Liu, Z.; Lee, X. Statistical estimation of next-day nighttime surface urban heat islands. *ISPRS J. Photogramm. Remote Sens.* **2021**, *176*, 182–195. [CrossRef]
64. Zhou, J.; Zhou, J.; Chen, Y.; Wang, J.; Zhan, W.; Wang, J. Maximum Nighttime Urban Heat Island (UHI) Intensity Simulation by Integrating Remotely Sensed Data and Meteorological Observations. *IEEE J. Sel. Top. Appl. Earth Obs. Remote Sens.* **2011**, *4*, 138–146. [CrossRef]
65. Chen, Z.; Zhu, Z.; Jiang, H.; Sun, S. Estimating daily reference evapotranspiration based on limited meteorological data using deep learning and classical machine learning methods. *J. Hydrol.* **2020**, *591*, 125286. [CrossRef]
66. Venter, Z.S.; Brousse, O.; Esau, I.; Meier, F. Hyperlocal mapping of urban air temperature using remote sensing and crowdsourced weather data. *Remote Sens. Environ.* **2020**, *242*, 111791. [CrossRef]
67. Mihalakakou, G.; Santamouris, M.; Asimakopoulos, D. Modeling ambient air temperature time series using neural networks. *J. Geophys. Res.* **1998**, *103*, 19509–19517. [CrossRef]
68. Mihalakakou, G.; Flocas, H.A.; Santamouris, M.; Helmis, C.G. Application of Neural Networks to the Simulation of the Heat Island over Athens, Greece, Using Synoptic Types as a Predictor. *J. Appl. Meteorol.* **2002**, *41*, 519–527. [CrossRef]
69. Santamouris, M.; Mihalakakou, G.; Papanikolaou, N.; Asimakopoulos, D.N. A neural network approach for modeling the Heat Island phenomenon in urban areas during the summer period. *Geophys. Res. Lett.* **1999**, *26*, 337. [CrossRef]
70. Kim, Y.-H.; Baik, J.-J. Maximum Urban Heat Island Intensity in Seoul. *J. Appl. Meteorol.* **2002**, *41*, 651–659. [CrossRef]
71. Kolokotroni, M.; Davies, M.; Croxford, B.; Bhuiyan, S.; Mavrogianni, A. A validated methodology for the prediction of heating and cooling energy demand for buildings within the Urban Heat Island: Case-study of London. *Sol. Energy* **2010**, *84*, 2246–2255. [CrossRef]
72. Kolokotroni, M.; Zhang, Y.; Giridharan, R. Heating and cooling degree day prediction within the London urban heat island area. *Build. Serv. Eng. Res. Technol.* **2009**, *30*, 183–202. [CrossRef]
73. Kolokotroni, M.; Zhang, Y.; Watkins, R. The London Heat Island and building cooling design. *Sol. Energy* **2007**, *81*, 102–110. [CrossRef]
74. Demirezen, G.; Fung, A.S. Application of artificial neural network in the prediction of ambient temperature for a cloud-based smart dual fuel switching system. *Energy Procedia* **2019**, *158*, 3070–3075. [CrossRef]
75. Demirezen, G.; Fung, A.S.; Deprez, M. Development and optimization of artificial neural network algorithms for the prediction of building specific local temperature for HVAC control. *Int. J. Energy Res.* **2020**, *44*, 8513–8531. [CrossRef]
76. Papantoniou, S.; Kolokotsa, D. Prediction of outdoor air temperature using neural networks: Application in 4 European cities. *Energy Build.* **2016**, *114*, 72–79. [CrossRef]
77. Erdemir, D.; Ayata, T. Prediction of temperature decreasing on a green roof by using artificial neural network. *Appl. Therm. Eng.* **2017**, *112*, 1317–1325. [CrossRef]
78. Mihalakakou, G.; Santamouris, M.; Papanikolaou, N.; Cartalis, C.; Tsangrassoulis, A. Simulation of the Urban Heat Island Phenomenon in Mediterranean Climates. *Pure Appl. Geophys.* **2004**, *161*, 429–451. [CrossRef]
79. Jang, J.; Viau, A.A.; Anctil, F. Neural network estimation of air temperatures from AVHRR data. *Int. J. Remote Sens.* **2004**, *25*, 4541–4554. [CrossRef]
80. Zhao, D. Analysis of thermal environment and urban heat island using remotely sensed imagery over the north and south slope of the Qinling Mountain, China. In Proceedings of the 2007 IEEE International Geoscience and Remote Sensing Symposium, Barcelona, Spain, 23–27 July 2007; pp. 655–658.
81. Beccali, G.; Cellura, M.; Culotta, S.; Brano, V.L.; Marvuglia, A. A Web-Based Autonomous Weather Monitoring System of the Town of Palermo and Its Utilization for Temperature Nowcasting. In *Computational Science and Its Applications—ICCSA 2008*; Gervasi, O., Murgante, B., Laganà, A., Taniar, D., Mun, Y., Gavrilova, M.L., Eds.; Springer: Berlin, Germany, 2008; pp. 65–80.
82. Cellura, M.; Culotta, S.; Lo Brano, V.; Marvuglia, A.; Energetiche, R. Nonlinear Black-Box Models for Short-Term Forecasting of Air Temperature in the Town of Palermo. In *Geocomputation, Sustainability and Environmental Planning*; Murgante, B., Borruso, G., Lapucci, A., Eds.; Springer: Berlin, Germany, 2011; pp. 183–204.
83. Shao, B.; Zhang, M.; Mi, Q.; Xiang, N. Prediction and Visualization for Urban Heat Island. In *Transactions on Edutainment VI. Lecture Notes in Computer Science, Volume 6758*; Springer: Berlin, Germany, 2011; pp. 1–11.
84. Lee, Y.Y.; Kim, J.T.; Yun, G.Y. The neural network predictive model for heat island intensity in Seoul. *Energy Build.* **2016**, *110*, 353–361. [CrossRef]
85. Schuch, F.; Marpu, P.; Masri, D.; Afshari, A. Estimation of Urban Air Temperature from a Rural Station Using Remotely Sensed Thermal Infrared Data. *Energy Procedia* **2017**, *143*, 519–525. [CrossRef]
86. Han, J.M.; Ang, Y.Q.; Malkawi, A.; Samuelson, H.W. Using recurrent neural networks for localized weather prediction with combined use of public airport data and on-site measurements. *Build. Environ.* **2021**, *192*, 107601. [CrossRef]

87. ISO Online Browsing Platform. Available online: https://www.iso.org/obp/ui/#search (accessed on 14 January 2021).
88. Hewamalage, H.; Bergmeir, C.; Bandara, K. Recurrent Neural Networks for Time Series Forecasting: Current status and future directions. *Int. J. Forecast.* **2021**, *37*, 388–427. [CrossRef]
89. López Gómez, A.; López Gómez, J.; Fernández García, F.; Arroyo Ilera, F. *El Clima Urbano de Madrid: La Isla de Calor*; CSIC: Madrid, Spain, 1988; ISBN 978-84-00-07521-7.
90. Yagüe, C.; Zurita, E.; Martinez, A. Statistical analysis of the Madrid urban heat island. *Atmos. Environ.* **1991**, *25*, 327–332. [CrossRef]
91. Fernández García, F.; Montálvez, J.P.; González-Rouco, F.J.; Valero, F. A PCA Analysis of the UHI Form of Madrid. In Proceedings of the 5th International Conference on Urban Climate, Lodz, Poland, 1–5 September 2003; pp. 1–4.
92. Núñez Peiró, M.; Sánchez-Guevara Sánchez, C.; Neila González, F.J. *Update of the Urban Heat Island of Madrid and Its Influence on the Building's Energy Simulation*; Springer: New York, NY, USA, 2017; ISBN 9783319514420.
93. López Gómez, A.; López Gómez, J.; Fernández García, F.; Moreno Jiménez, A. *El Clima Urbano: Teledetección de la isla de Calor en Madrid*; MOPT: Madrid, Spain, 1993; ISBN 978-84-00-07521-7.
94. Sobrino, J.A.; Oltra-Carrió, R.; Sòria, G.; Jiménez-Muñoz, J.C.; Franch, B.; Hidalgo, V.; Mattar, C.; Julien, Y.; Cuenca, J.; Romaguera, M.; et al. Evaluation of the surface urban heat island effect in the city of Madrid by thermal remote sensing. *Int. J. Remote Sens.* **2013**, *34*, 3177–3192. [CrossRef]
95. Salamanca, F.; Martilli, A. A new Building Energy Model coupled with an Urban Canopy Parameterization for urban climate simulations-part II. Validation with one dimension off-line simulations. *Theor. Appl. Climatol.* **2010**, *99*, 345–356. [CrossRef]
96. Salamanca, F.; Martilli, A.; Yagüe, C. A numerical study of the Urban Heat Island over Madrid during the DESIREX (2008) campaign with WRF and an evaluation of simple mitigation strategies. *Int. J. Climatol.* **2011**, *32*, 2372–2386. [CrossRef]
97. Núñez-Peiró, M.; Sánchez-Guevara Sánchez, C.; Neila González, F.J. Hourly evolution of intra-urban temperature variability across the local climate zones. The case of Madrid. *Urban Clim.* **2021**, *39*, 100921. [CrossRef]
98. Stewart, I.D.; Oke, T.R. Local climate zones for urban temperature studies. *Bull. Am. Meteorol. Soc.* **2012**, *93*, 1879–1900. [CrossRef]
99. Oke, T.R. *Initial Guidance to Obtain Representative Meteorological Observations at Urban Sites (WMO/TD No. 1250)*; WMO: Geneva, Switzerland, 2006.
100. WMO. *Guide to Meteorological Instruments and Methods of Observation (WMO No. 8)*; WMO: Geneva, Switzerland, 2017. Available online: http://www.posmet.ufv.br/wp-content/uploads/2016/09/MET-474-WMO-Guide.pdf (accessed on 15 July 2021).
101. Núñez Peiró, M.; Sánchez-Guevara Sánchez, C.; Neila González, F.J. Source area definition for local climate zones studies. A systematic review. *Build. Environ.* **2019**, *148*, 258–285. [CrossRef]
102. Alexander, P.J.; Bechtel, B.; Chow, W.T.L.; Fealy, R.; Mills, G. Linking urban climate classification with an urban energy and water budget model: Multi-site and multi-seasonal evaluation. *Urban Clim.* **2016**, *17*, 196–215. [CrossRef]
103. Kaplan, S.; Peeters, A.; Erell, E. Predicting air temperature simultaneously for multiple locations in an urban environment: A bottom up approach. *Appl. Geogr.* **2016**, *76*, 62–74. [CrossRef]
104. WMO. *Guide to the Global Observing System (WMO No. 488)*; WMO: Geneva, Switzerland, 2017. Available online: https://library.wmo.int/doc_num.php?explnum_id=4236 (accessed on 15 July 2021).
105. Aguilar, E.; Auer, I.; Brunet, M.; Peterson, T.C.; Wieringa, J. *Guidelines on Climate Metadata and Homogenization (WMO/TD No. 1186)*; WMO: Geneva, Switzerland, 2003. Available online: https://library.wmo.int/doc_num.php?explnum_id=9252 (accessed on 15 July 2021).
106. WMO. *General Meteorological Standards and Recommended Practices (WMO No. 49)*; WMO: Geneva, Switzerland, 2018; Volume I. Available online: https://library.wmo.int/doc_num.php?explnum_id=10113 (accessed on 15 July 2021).
107. WMO. *WIGOS Metadata Standard 2019*; WMO: Geneva, Switzerland, 2019. Available online: https://library.wmo.int/doc_num.php?explnum_id=10109 (accessed on 15 July 2021).
108. Brousse, O.; Martilli, A.; Foley, M.; Mills, G.; Bechtel, B. WUDAPT, an efficient land use producing data tool for mesoscale models? Integration of urban LCZ in WRF over Madrid. *Urban Clim.* **2016**, *17*, 116–134. [CrossRef]
109. Oke, T.R.; Mills, G.; Christen, A.; Voogt, J.A. *Urban Climates*; Cambridge University Press: Cambridge, UK, 2017; ISBN 9781139016476.
110. Sundborg, A. Local Climatological Studies of the Temperature Conditions in an Urban Area. *Tellus* **1950**, *2*, 222–232. [CrossRef]
111. Zhou, M.; Qu, X.; Li, X. A recurrent neural network based microscopic car following model to predict traffic oscillation. *Transp. Res. Part C Emerg. Technol.* **2017**, *84*, 245–264. [CrossRef]
112. Shi, Y.; Ren, C.; Lau, K.K.L.; Ng, E. Investigating the influence of urban land use and landscape pattern on PM2.5 spatial variation using mobile monitoring and WUDAPT. *Landsc. Urban Plan.* **2019**, *189*, 15–26. [CrossRef]
113. Afshari, A.; Ramirez, N. Improving the accuracy of simplified urban canopy models for arid regions using site-specific prior information. *Urban Clim.* **2021**, *35*, 100722. [CrossRef]
114. Olden, J.D.; Jackson, D.A. Illuminating the "black box": Understanding variable contributions in artificial neural networks. *Ecol. Modell.* **2002**, *154*, 135–150. [CrossRef]
115. Shanker, M.S.; Hu, M.Y.; Hung, M.S. Effect of data standardization on neural network training. *Omega* **1996**, *24*, 385–397. [CrossRef]

116. Abadi, M.; Barham, P.; Chen, J.; Chen, Z.; Davis, A.; Dean, J.; Devin, M.; Ghemawat, S.; Irving, G.; Isard, M.; et al. TensorFlow: A System for Large-Scale Machine Learning. In Proceedings of the 12th USENIX Symposium on Operating Systems Design and Implementation (OSDI'16), Savannah, GA, USA, 2–4 November 2016.
117. Chollet, F. Keras. Available online: https://keras.io (accessed on 28 February 2021).
118. Cortez, P.; Embrechts, M.J. Using sensitivity analysis and visualization techniques to open black box data mining models. *Inf. Sci.* **2013**, *225*, 1–17. [CrossRef]
119. Gerald, W.; Davis, J. Sensitivity Analysis in Neural Net Solutions. *IEEE Trans. Syst. Man. Cybern.* **1989**, *19*, 1078–1082. [CrossRef]
120. Ferrando, M.; Causone, F.; Hong, T.; Chen, Y. Urban building energy modeling (UBEM) tools: A state-of-the-art review of bottom-up physics-based approaches. *Sustain. Cities Soc.* **2020**, *62*, 102408. [CrossRef]
121. Erba, S.; Causone, F.; Armani, R. The effect of weather datasets on building energy simulation outputs. *Energy Procedia* **2017**, *134*, 545–554. [CrossRef]
122. Taylor, J.; Davies, M.; Mavrogianni, A.; Chalabi, Z.; Biddulph, P.; Oikonomou, E.; Das, P.; Jones, B. The relative importance of input weather data for indoor overheating risk assessment in dwellings. *Build. Environ.* **2014**, *76*, 81–91. [CrossRef]
123. Bienvenido-Huertas, D.; Marín-García, D.; Carretero-Ayuso, M.J.; Rodríguez-Jiménez, C.E. Climate classification for new and restored buildings in Andalusia: Analysing the current regulation and a new approach based on k-means. *J. Build. Eng.* **2021**, *43*, 102829. [CrossRef]
124. López-Bueno, J.A.; Linares, C.; Sánchez-Guevara, C.; Sánchez-Martínez, G.; Mirón, I.J.; Núñez Peiró, M.; Valero, I.; Díaz, J. The effect of cold waves on daily mortality in districts in Madrid considering sociodemographic variables. *Sci. Total Environ.* **2020**, *749*, 142364. [CrossRef] [PubMed]
125. López-Bueno, J.A.; Díaz, J.; Sánchez-Guevara, C.; Sánchez-Martínez, G.; Franco, M.; Gullón, P.; Núñez Peiró, M.; Valero, I.; Linares, C. The impact of heat waves on daily mortality in districts in Madrid: The effect of sociodemographic factors. *Environ. Res.* **2020**, *190*, 109993. [CrossRef] [PubMed]
126. López-Bueno, J.A.; Navas-martín, M.A.; Linares, C.; Mirón, I.J.; Luna, M.Y.; Sánchez-Martínez, G.; Culqui, D.; Díaz, J. Analysis of the impact of heat waves on daily mortality in urban and rural areas in Madrid. *Environ. Res.* **2021**, *195*, 110892. [CrossRef] [PubMed]
127. Macintyre, H.; Heaviside, C.; Cai, X.; Phalkey, R. The winter urban heat island: Impacts on cold-related mortality in a highly urbanized European region for present and future climate. *Environ. Int.* **2021**, *154*, 106530. [CrossRef] [PubMed]
128. Gouveia, J.P.; Seixas, J. Unraveling electricity consumption profiles in households through clusters: Combining smart meters and door-to-door surveys. *Energy Build.* **2016**, *116*, 666–676. [CrossRef]
129. Pino-Mejías, R.; Pérez-Fargallo, A.; Rubio-Bellido, C.; Pulido-Arcas, J.A. Artificial neural networks and linear regression prediction models for social housing allocation: Fuel Poverty Potential Risk Index. *Energy* **2018**, *164*, 627–641. [CrossRef]
130. Bienvenido-Huertas, D.; Pérez-Fargallo, A.; Alvarado-Amador, R.; Rubio-Bellido, C. Influence of climate on the creation of multilayer perceptrons to analyse the risk of fuel poverty. *Energy Build.* **2019**, *198*, 38–60. [CrossRef]
131. Serrano-Jiménez, A.; Lizana, J.; Molina-Huelva, M.; Barrios-Padura, Á. Indoor environmental quality in social housing with elderly occupants in Spain: Measurement results and retrofit opportunities. *J. Build. Eng.* **2020**, *30*, 101264. [CrossRef]
132. Castaño-Rosa, R.; Barrella, R.; Sánchez-Guevara, C.; Barbosa, R.; Kyprianou, I.; Paschalidou, E.; Thomaidis, N.S.; Dokupilova, D.; Gouveia, J.P.; Kádár, J.; et al. Cooling degree models and future energy demand in the residential sector. A seven-country case study. *Sustainability* **2021**, *13*, 2987. [CrossRef]
133. Hornik, K.; Stinchcombe, M.; White, H. Multilayer feedforward networks are universal approximators. *Neural Netw.* **1989**, *2*, 359–366. [CrossRef]
134. Curry, B. Neural networks and seasonality: Some technical considerations. *Eur. J. Oper. Res.* **2007**, *179*, 267–274. [CrossRef]
135. Zhang, G.P.; Qi, M. Neural network forecasting for seasonal and trend time series. *Eur. J. Oper. Res.* **2005**, *160*, 501–514. [CrossRef]
136. Bandara, K.; Bergmeir, C.; Smyl, S. Forecasting across time series databases using recurrent neural networks on groups of similar series: A clustering approach. *Expert Syst. Appl.* **2020**, *140*, 112896. [CrossRef]
137. Alexander, D.L.J.; Tropsha, A.; Winkler, D.A. Beware of R2: Simple, unambiguous assessment of the prediction accuracy of QSAR and QSPR models. *J. Chem. Inf. Model.* **2015**, *55*, 1316–1322. [CrossRef] [PubMed]
138. Kvalseth, T.O. Cautionary note about r2. *Am. Stat.* **1985**, *39*, 279–285. [CrossRef]
139. Roth, M. Review of urban climate research in (sub)tropical regions. *Int. J. Climatol.* **2007**, *27*, 1859–1873. [CrossRef]
140. Schwarz, N.; Lautenbach, S.; Seppelt, R. Exploring indicators for quantifying surface urban heat islands of European cities with MODIS land surface temperatures. *Remote Sens. Environ.* **2011**, *115*, 3175–3186. [CrossRef]
141. Suomi, J. Extreme temperature differences in the city of Lahti, southern Finland: Intensity, seasonality and environmental drivers. *Weather Clim. Extrem.* **2018**, *19*, 20–28. [CrossRef]
142. Zhou, B.; Rybski, D.; Kropp, J.P. On the statistics of urban heat island intensity. *Geophys. Res. Lett.* **2013**, *40*, 5486–5491. [CrossRef]
143. Fu, P.; Weng, Q. Variability in annual temperature cycle in the urban areas of the United States as revealed by MODIS imagery. *ISPRS J. Photogramm. Remote Sens.* **2018**, *146*, 65–73. [CrossRef]
144. Lazzarini, M.; Molini, A.; Marpu, P.R.; Ouarda, T.B.M.J.; Ghedira, H. Urban climate modifications in hot desert cities: The role of land cover, local climate, and seasonality. *Geophys. Res. Lett.* **2015**, *42*, 9980–9989. [CrossRef]
145. Zhou, B.; Lauwaet, D.; Hooyberghs, H.; De Ridder, K.; Kropp, J.P.; Rybski, D. Assessing Seasonality in the Surface Urban Heat Island of London. *J. Appl. Meteorol. Climatol.* **2016**, *55*, 493–505. [CrossRef]

9. Comunicación en congreso internacional
Presentation at an international conference

Two decades of weather files in Spain. A comparison of their reliability for building energy modelling using the BESTEST method

Núñez Peiró, M., Sánchez-Guevara Sánchez, C., Neila González, F.J. (2021)

VI International Conference on Technological Innovation in Building, 62.64.

PARTE III
PART III

Two decades of weather files in Spain. A comparison of their reliability for building energy modelling using the BESTEST method

[1]Miguel Núñez Peiró; [2]Carmen Sánchez-Guevara Sánchez; [3]F. Javier Neila González

[1] School of Architecture, Universidad Politécnica de Madrid, Spain. miguel.nunez@upm.es
[2] School of Architecture, Universidad Politécnica de Madrid, Spain. carmen.sanchezguevara@upm.es
[2] School of Architecture, Universidad Politécnica de Madrid, Spain. fjavier.neila@upm.es

Keywords: *weather files, BESTEST, building energy modelling, energy simulation models, performance gap*

Abstract

In the last decades, several energy policies have been directed towards energy efficiency and the improvement of building's energy performance. Most of these rely on Building Energy Modelling (BEM) for testing the efficiency of both existing and new buildings, as well as for forecasting future scenarios and help guide policy changes. However, the complexity of dynamically simulating the building physics, the varying performance of energy systems, and the unpredictable occupants' behaviour patterns still introduce many uncertainties in their results [1]. Similarly, the reliability of weather data might be put into question as well [2]. A wide range of options are usually available for each location, most derived from hourly time series of meteorological data that are several decades old. These weather files might severely affect the outcomes of energy simulation. This becomes even more relevant in the actual context of climate change [3], and it might be aggravated for cities in which the heat island effect takes place [4].

Present research compiles existing weather files for Madrid, Spain. It explores whether they can still be considered representative of the actual climatic conditions of the region. We compare the accuracy of existing weather files using a brand-new weather file, created following the standard ISO 15927-4 [5] with 10 recent years of the nearby meteorological observatory of Barajas Airport. **Table 1** identifies all the weather files used in this research, including the period of record, the first time they were published, and the source from which they were extracted. All of these weather files were tested using the IEA Building Energy Simulation Test (BESTEST) procedure [6], a normalised set of models which is also used by the ANSI-ASHRAE Standard 140-2017 [7] for testing computer programs.

Table 1: *Weather files identified and used in this study.*

ID	Period of record	First published	Source
IWEC	1982-1993	2001	EnergyPlus [8]
SWEC	unknown	2002	EnergyPlus [8]
LIDER	unknown	2003	Spanish soft. [9]
MITECO	unknown	2006	MITECO [10]
IWEC2	1984-2008	2014	ASHRAE [11]
PVGIS	2007-2016	2017	PVGIS [12]
OB45	1973-2017	2018	OneBuilding [13]
OB15	2003-2017	2018	OneBuilding [13]
ISO10	2008-2017	-	ISO 15927-4 [5]

Figure 1 summarizes the results for the BESTEST 600 Heavyweight. It reveals that the energy demand could vary as high as 66% for heating and 86% for cooling when using different weather files. If compared with the standard weather file (ISO10), pre-existing weather files tend to underestimate either the heating or the cooling energy demand. Normative weather files (SWEC, LIDER and MITECO), produced the lowest cooling demands with a reduction of 32-45% compared to the ISO10. On the contrary, the OB45, OB15 and PVGIS weather files yielded heating demands 19-33% lower compared to the reference ISO10. The ASHRAE weather file IWEC threw the highest heating demands, although these decreased significantly (40%) with their most recent version (IWEC2), which included more recent years.

It is highlighted the strong divergence of outcomes obtained by these weather files, which are available for the same location. Including more recent climatic data in the weather files' period of record significantly increased the cooling energy demand and reduced the heating. The influence of climate change on the modelling outputs seems clear and strong, thus, putting into question the use of out-of-date meteorological datasets. Institutions in charge of energy regulations should consider regularly updating their weather files to help produce better energy consumption estimations of the building stock.

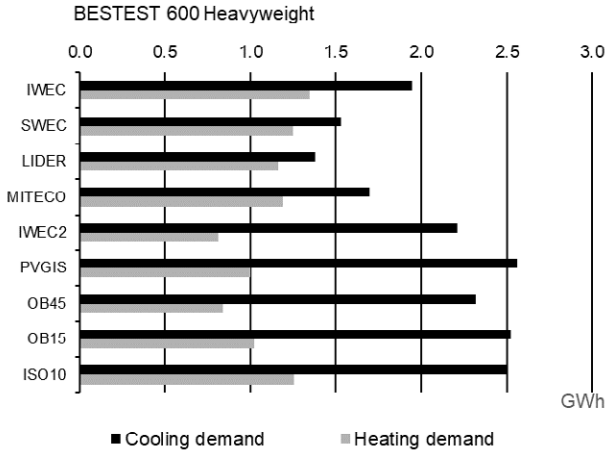

Figure 1: *Cooling and heating energy demand produced with each weather file of Madrid for the BESTEST 600.*

References

[1] N. Fumo, A review on the basics of building energy estimation, Renew. Sustain. Energy Rev. 31 (2014) 53–60. doi:10.1016/j.rser.2013.11.040.

[2] S. Erba, F. Causone, R. Armani, The effect of weather datasets on building energy simulation outputs, Energy Procedia. 134 (2017) 545–554. doi:10.1016/j.egypro.2017.09.561.

[3] A. Moazami, V.M. Nik, S. Carlucci, S. Geving, Impacts of future weather data typology on building energy performance – Investigating long-term patterns of climate change

and extreme weather conditions, Appl. Energy. 238 (2019) 696–720. doi:10.1016/j.apenergy.2019.01.085.

[4] N. Lauzet, A. Rodler, M. Musy, M.H. Azam, S. Guernouti, D. Mauree, T. Colinart, How building energy models take the local climate into account in an urban context – A review, Renew. Sustain. Energy Rev. 116 (2019) 109390. doi:10.1016/j.rser.2019.109390.

[5] International Organization for Standardization, Hygrothermal performance of buildings – Calculation and presentation of climatic data – Part 4: Hourly data for assessing the annual energy use for heating and cooling ISO 15927-4:2005, 2015. https://www.iso.org/standard/41371.html.

[6] R. Judkoff, J. Neymark, International Energy Agency Building Energy Simulation Test (BESTEST) and Diagnostic Method, 1995.

[7] ANSI-ASHRAE, Standard Method of Test for the Evaluation of Building Energy Analysis Computer Programs, (2017).

[8] U.S. Department of Energy, EnergyPlus Weather Data Sources, (2015). https://energyplus.net/weather (accessed January 9, 2020).

[9] Código Técnico de la Edificación, Herramienta unificada LIDER-CALENER (HULC), versiones anteriores, (2007). https://www.codigotecnico.org/Programas/HerramientaUnificadaLIDERCALENER.html (accessed March 1, 2021).

[10] Ministerio para la Transición Ecológica y el Reto Demográfico, Documentos reconocidos, (2021). https://energia.gob.es/desarrollo/EficienciaEnergetica/CertificacionEnergetica/DocumentosReconocidos/Paginas/documentosreconocidos.aspx (accessed March 1, 2021).

[11] ASHRAE, International Weather for Energy Calculations, v2.0, (2014). https://www.ashrae.org/technical-resources/bookstore/ashrae-international-weather-files-for-energy-calculations-2-0-iwec2.

[12] European Commission, Photovoltaic geographical information system, (2021). https://re.jrc.ec.europa.eu/pvg_tools/en/tools.html (accessed February 3, 2021).

[13] OneBuilding, Repository of free climate data for building performance simulation, (2018).